

# **Structural Chemistry and Biological Screening of Organotin(IV) Derivatives of Amide-based Carboxylates**



**Doctor of Philosophy**

**In**

**Inorganic/Analytical Chemistry**

**By**

**Iftikhar Ahmad**

**Department of Chemistry**

**Quaid-i-Azam University**

**Islamabad, Pakistan**

**(2021)**

# **Structural Chemistry and Biological Screening of Organotin(IV) Derivatives of Amide-based Carboxylates**



A dissertation submitted to the Department of Chemistry,  
Quaid-i-Azam University, Islamabad, in partial fulfilment of the  
requirements for the degree of

**Doctor of Philosophy**

In

**Inorganic/Analytical Chemistry**

By

**Iftikhar Ahmad**

**Department of Chemistry**

**Quaid-i-Azam University**

**Islamabad, Pakistan**

**(2021)**

This is to certify that this dissertation entitled “*Structural Chemistry and Biological Screening of Organotin(IV) Derivatives of Amide-based Carboxylates*” submitted by *Mr. Iftikhar Ahmad* is accepted in its present form by the Department of Chemistry, Quaid-i-Azam University, Islamabad, Pakistan, as satisfying the partial fulfillment for the degree of *Doctor of Philosophy in Inorganic/ Analytical Chemistry*.

**External Examiner (1):**

**External Examiner (2):**

**Head of Section:**

**Quaid-i-Azam University**

**Prof. Dr. Zareen Akhtar**  
*Department of Chemistry*

**Islamabad.**

**Supervisor**

**Prof. Dr. Amir Waseem**  
*Department of Chemistry*  
Quaid-i-Azam University  
**Islamabad.**

**Co-Supervisor**

**Prof. Dr. Zia-ur-Rehman**  
*Department of Chemistry*  
Quaid-i-Azam University  
**Islamabad**

**Chairman:**

**Prof. Dr. Aamer Saeed Bhatti**  
*Department of Chemistry*  
Quaid-i-Azam University  
**Islamabad.**



*In the Name of Allah, the Most Gracious, the Most Merciful*

SCIENCE

— *is the* —

P●ETRY

— *of* —

REALITY

*Dedicated To*  
*My Loving Mother and Father, Grandparents and*  
*Brothers*

## TABLE OF CONTENTS

---

Contents...	
Acknowledgement.....	i
Abstract.....	iii
List of Figures.....	vi
List of Tables.....	xvi
List of Schemes.....	xviii
List of Abbreviations.....	xix
Chapter 1.....	1
1. Introduction.....	1
1.1. Organotin(IV) carboxylates .....	1
1.2. Synthesis of organotin(IV) carboxylates .....	2
1.3. Structural diversity of organotin(IV) carboxylate Complexes.....	8
1.4. Oxygen donor ligands .....	10
1.4.1. Complexes of four coordination geometry.....	10
1.4.2. Complexes of five coordination geometry .....	12
1.4.3. Complexes of six coordination geometry.....	16
1.5. Biological Activity.....	18
1.5.1. Biological properties of organotin(IV) carboxylates.....	20
1.5.2. Cancer.....	21

1.5.3. Leishmaniasis .....	26
1.5.4. Computational Studies.....	27
Chapter 2.....	29
Materials and Methods/ Experimental.....	29
2. Introduction.....	30
2.1. Materials, Instrumentations and Techniques .....	30
2.2. Synthesis of Ligands .....	31
2.2.1. General procedures for the synthesis of ligands (scheme 1) IL(1-4) .....	31
2.2.2. Synthetic procedure for the salt of ligand IL(1-4).....	32
2.2.3. Synthetic procedure for the synthesis of ligands (Scheme 2) IL(5) .....	33
2.2.4. Synthetic procedure for the synthesis of ligands (Scheme 3) IL(6-8).....	34
2.2.5 General procedure for the synthesis of triorganotin(IV) amide-based carboxylates complexes .....	41
2.3. Biological Studies .....	65
2.3.1. Anticancer and Noncancerous Cell Activity .....	65
2.3.2. Antileishmanial Activity.....	65
2.3.3. Hemolysis Assay .....	66
2.3.4. Antibacterial Activity .....	67
2.3.5. Antifungal Activity.....	67
2.3.6. Brine Shrimp Lethality Assay .....	68
2.3.7. Antioxidant Activities.....	68



2.3.8. Computational Details .....	70
Chapter 3 .....	72
Results and Discussion .....	72
3. Spectroscopic Characterization.....	73
3.1 Infrared Spectroscopy .....	73
3.2. <sup>1</sup> H, <sup>13</sup> C, <sup>119</sup> Sn, and <sup>19</sup> F NMR studies .....	75
3.2.1. <sup>1</sup> H NMR studies.....	75
3.2.2. <sup>13</sup> C NMR spectroscopic studies.....	78
3.2.3. <sup>119</sup> Sn NMR studies.....	81
3.2.4. <sup>19</sup> F NMR studies .....	83
3.3 Biological Activities .....	85
3.3.1. Anticancer potential and cytotoxic activities of organotin(IV) amide-based carboxylate derivatives .....	85
3.3.2. Antileishmanial potency of the synthesized ligands and complexes.....	89
3.3.3. Hemolysis Assay .....	93
3.3.4. Antibacterial activities of the synthesized ligands and their complexes ....	97
3.3.5. Antifungal activities of the synthesized ligands and their complexes.....	101
3.3.6. Cytotoxicity .....	105
3.3.7. Antioxidant Activities.....	108
3.3.7.1. Total Antioxidant Capacity .....	108
3.3.7.2. Total Reducing Power .....	112

3.3.7.3. DPPH Free Radical Scavenging Assay .....	115
3.5. Computational Details .....	117
3.6. Computational Methods.....	122
Chapter 4.....	138
Crystallography.....	138
4.1. Crystal structure of the free ligand.....	139
4.2 Single Crystal XRD structures of triorganotin carboxylates .....	144
4.2.1 Five coordinated trigonal bipyramidal geometry .....	144
Conclusion/Future Perspectives.....	175
References.....	177
List of Publications .....	205
Appendices.....	207

## **Acknowledgements**

---

*I am very grateful to Almighty Allah.*

*I highly appreciate the efforts of **Prof. Dr. Amir Waseem (Supervisor)** Department of chemistry, Quaid-i-Azam University, Islamabad for being so motivating, thoroughly supporting, guiding and providing innovative ideas to me in my research work.*

*I would cordially like to acknowledge and very special thanks to **Dr. Zia-ur-Rehman (Co-Supervisor)** for introducing me this exciting field of medicinal chemistry and providing all technical support and guidance as well.*

*I will be always obliged to **Prof. Dr. Aamer Saeed Bhatti (Chairman)** for providing us all the necessary facilities in the department.*

*A very special thanks to **Prof. Dr. Cora Macbeth** for my 6 months stay in Emory University and providing all the lab facilities and guidance as well.*

*I am also very thankful to **Great Prof. Dr. Mehmet Karakus (Dean of Natural Sciences)** and **Rafet Kilincarslan Pamukkale** University for providing all the lab facilities and guidance as well.*

*I am highly grateful to **Prof. Dr. Saqib Ali, Prof. Dr. Muhammad Siddiq, Prof. Dr. Zareen Akhtar Prof. Dr. Afzal Shah, Prof. Dr. Muhammad Farman and Dr. Ali Haider** for their support and encouragement during my work and especially **Prof. Dr. Syed Ahmed Tirmizi (Late) and Dr. Syed Mujtaba Shah**, for help during my m.phil work.*

*Thanks to all respected Teachers of the department of chemistry.*

*I am very thankful to **Dr. John Bacs**a from Emory University for doing my single crystal XRD.*

*I am also obliged to my friends **Dr. Abdul Haleem Wazir, Dr. Usman Khan, Dr. Muhammad Wajid shah, Dr. Jehangir Patujo, Dr Ahmet Erdem, Dr Savita Sharma, Dr Noor Uddin, Dr Muhammad Zubair Marwat, Rana Waseem** and Lab fellows.*

*My special thanks to **Dr. Deepak Venkatraman, Dr. Saira Tabassum, Dr. Nazif ullah** and **Dr Altaf-ur-Rehman** for their help to do bio activities and computational studies as well.*

*Thanks to **Muhammad Amir, Ch.Amir Hassan, Abdur Rehman, Mr. Shabbir Sb, Mr Hanif Sb, Tayyib, Asam, Mustafa, Chaudhry Rizwan, Rana Matloob, Aitbar, Rizwan, Engr Nasir, Amjad, Saqib, Raza, Danish lala, Abid, Sajid** and all the technical and non-technical staff of chemistry department.*

*I would like to express my heartiest gratitude and regards to my **father, mother, brothers** and **uncle Saliheen Khan** for their love care, and continuous support during every moment of life. Their prayer, love and support over the years have enabled me to cross the finish line. Without their prayers, encouragement, excessive kindness and patience, I would have not been able to complete this task.*

*My special thanks and acknowledgement to **TUBITAK** (The Scientific and Technological Research Council of Turkey) for one-year financial support during my stay in Pamukkale University Denizli.*

*I highly acknowledge the participation of **Higher Education commission (HEC)** for providing funding to me for my IRSIP stay in Emory University.*

***Iftikhar Ahmad***

## Abstract

---

In the present study, twenty seven novel triorganotin(IV) amide-based carboxylates of general formula  $R_3SnL$  were synthesized by reacting triorganotin(IV) chloride with carboxylates ligands (1:1 ratio) in dry methanol. The ligands used were (Z)-4-(4-methoxyphenylamino)-4-oxobut-2-enoic acid (**IL**<sup>1</sup>), (Z)-4-(3,5-bis(trifluoromethyl)phenylamino)-4-oxobut-2-enoic acid (**IL**<sup>2</sup>), (Z)-4-(p-toluidino)-4-oxobut-2-enoic acid (**IL**<sup>3</sup>), (Z)-4-(4-fluorophenylamino)-4-oxobut-2-enoic acid (**IL**<sup>4</sup>), 4-(1,3-dioxoisindolin-2-yl)butanoic acid (**IL**<sup>5</sup>), 4-(4-methoxyphenylamino)-4-oxobutanoic acid (**IL**<sup>6</sup>), 4-(3,5-bis(trifluoromethyl)phenylamino)-4-oxobutanoic acid (**IL**<sup>7</sup>), 4-(p-toluidino)-4-oxobutanoic acid (**IL**<sup>8</sup>), 4-(4-fluorophenylamino)-4-oxobutanoic acid (**IL**<sup>9</sup>). The synthesized compounds were characterized by FT-IR, elemental analysis, NMR (<sup>1</sup>H, <sup>13</sup>C, <sup>119</sup>Sn & <sup>19</sup>F) and single crystal X-ray crystallography. The ligands coordinate to tin atom through oxygen (carboxylate and amide) showing distorted trigonal bipyramidal geometry with polymeric bridging behavior in solid state. However, the geometry is switched over from trigonal bipyramidal to tetrahedral upon dissolution as confirmed by multinuclear (<sup>1</sup>H, <sup>13</sup>C, <sup>19</sup>F and <sup>119</sup>Sn) NMR.

These synthesized organotin(IV) amide-based carboxylate complexes were selected for in vitro cytotoxic studies against various cell lines such as breast cancer cell lines (MCF-7) and human endometrial stromal cells (hESCs) by the MTT [Tetrazolium [3-(4,5-dimethylthiazol-2-yl)-2,5-diphenyltetrazolium bromide] method. The trimethyltin(IV) carboxylate was less active whereas tributyltin(IV) carboxylate and triphenyltin(IV) carboxylate complexes composed of carboxylate ligand having fluoro group were found to be most active against breast cancer cell lines as compared to

standard drug (cisplatin). Some of the complexes showed less cytotoxicity against normal cell lines as compared to cancer cell line which need to be further evaluated.

The prepared ligands and complexes were screened for antimicrobial activities against various strains of bacteria and fungi, and were found active. The tributyltin(IV) carboxylates unveiled the most active antimicrobial agents followed by triphenyltin (IV) carboxylates while trimethyltin(IV) carboxylates are the least active antimicrobial agents.

The antileishmanial activities were evaluated which showed that tributyltin(IV) carboxylates and triphenyltin carboxylates are the most active compound followed by trimethyltin(IV) carboxylates.

The synthesized ligands and their complexes were subjected to *in vitro* total antioxidant capacity, total reducing power and free radical scavenging activities. Some of the compounds were efficient and demonstrated their antioxidant strength equal to standard one (Ascorbic acid). Certain complexes were even much better antioxidant and near to the standard. However, a mix behavior was found among the three types of complexes. Additionally, hemolytic and shrimp assays were accomplished for the triorganotin(IV) carboxylates complexes so as to assess the cytotoxicity of the compounds.

The successful synthesis of these complexes also open the question of thermal stability and to find it's the electronic properties. Using DFT (Density-Functional Theory) we investigate the structural thermal stability and electronic structures of the complexes **1** & **4**. The structural optimization and low formation energies predict that these compounds **1** and **4** are thermodynamically stable. The electronic calculations show that these complexes are non-magnetic and direct band gap semiconductors. However, we found the band gaps of 1.87 eV for complex **1** and 2.73 eV for complex **4**. These values of the band-gaps are smaller by ~1 eV from experimentally observed values of

2.92 eV and 3.8 eV for Complex **1** and complex **4** respectively which were expected. The charge-density predicts that H-O2 bonding in both **1** and **4** complexes have van-der Waals nature of bonding. Finally, we also calculated the HOMO (highest-occupied molecular orbital), LUMO (lowest-unoccupied molecular orbital), Fermi level energy, and work function for **1** and **4** complexes to find its possible applications in electronic devices. Similarly we have also reported the DFT results on electronic structures and other properties of complexes **6**, **7**, **8**, **9**, **10**, **11** and **12** which is comparable with the experimental data. DFT studies also confirmed an excellent correlation with the structural parameters obtained from XRD crystallographic data for different complexes.

## List of Figures

---

Figure 1.1: Structure of triorganotin(IV)- benzamidomethionine complex.....	3
Figure 1.2: Structure of triorganotin(IV)- benzamidoglycin complex.....	3
Figure 1.3: Structure of triorganotin(IV)- benzamidoalanine complex.....	4
Figure 1.4: Structure of diorganotin(IV)- <i>N</i> -methyl- <i>m</i> -nitrobenzohydroxamic acid Complex.....	4
Figure 1.5: Structure of diorganotin(IV)- <i>N</i> -tolyl <i>m</i> -nitrobenzohydroxamic acid Complex.....	5
Figure 1.6: Structure of diorganotin(IV)- benzamidoacetic acid complex.....	6
Figure 1.7: Structure of diorganotin(IV)- 2-[(phenylcarbonyl)amino]propanoic acid Complex.....	6
Figure 1.8: Structure of diorganotin(IV)- 2-thioacetic-5-phenyl-1,3,4-oxadiazole Complex.....	7
Figure 1.9: Structure of diorganotin(IV)- <i>N</i> -methyl- <i>m</i> -methoxybenzohydroxamic acid Complex.....	7
Figure 1.10: Structure of diorganotin(IV)- benzamidocysteine complex.....	8
Figure 1.11: Different structural geometries of organotin(IV) complexes.....	9
Figure 1.12: Structure of triphenyltin(IV) [3-(3-fluoro-phenyl)-2-(4-chlorophenyl)-2- Propenoate.....	11
Figure 1.13: Structure of triphenyltin(IV)-(4-chloro-3,5-dinitrobenzoate.....	11
Figure 1.14: Structure of <i>catena</i> -poly[[tri-methyltin]- $\mu$ -2-phenyl-3-(4-chlorophenyl) propenoatoO:O`.....	13
Figure 1.15: Structure of tri- <i>n</i> -butyl( <i>N</i> -maleoyl- $\beta$ -alaninato)tin.....	14
Figure 1.16: Structure of <i>catena</i> -poly[[tri- <i>n</i> -butyltin(IV)]- $\mu$ -cyclopent-2-enylacetato-	



O:O` .....	14
Figure 1.17: Structure of <i>catena</i> -poly[[tri- <i>n</i> -butyltin(IV)]- $\mu$ -cyclopent-2-enylacetato-	
O:O` .....	15
Figure 1.18: Structure of tetrameric <i>catena</i> -poly[[tri- <i>n</i> -butyltin(IV)]- $\mu$ -cyclopent-2-	
enylacetato- O:O` .....	16
Figure 1.19: Structure of di- <i>n</i> -butyltin(IV) bis-[2,3-bis(4-chlorophenyl)propenoato-	
O,O` .....	17
Figure 1.20: Structure of dimethyltin(IV) bis[2,3-bis(4-chlorophenyl)propenoato-O,O`	
.....	18
Figure 1.21: Some of the biologically active Organotin compounds.....	19
Figure 1.22: Cancer and its treatment methodology by chemotherapy and radiations	
.....	22
Figure 1.23: Electrostatic interactions of metal complexes with cancerous cells DNA	
and gamma radiations.....	22
Figure 1.24: Intercalation interactions of metal complexes with cancerous DNA	
.....	23
Figure 1.25: Breast Cancer and different types of treatment.....	23-24
Figure 1.26: Organotin(IV) complexes in trial stages and metal complexes in cancer	
treatment.....	24
Figure 1.27: Cause and different types of drugs for Leishmania.....	27
Figure 3.1: Representative $^1\text{H}$ NMR spectrum of Ligand IL <sup>1</sup> .....	76
Figure 3.2: Representative $^1\text{H}$ NMR spectrum of Ligand IL <sup>5</sup> .....	76

Figure 3.3: Representative $^1\text{H}$ NMR spectrum of Complex 1 .....	77
Figure 3.4: Representative $^1\text{H}$ NMR spectrum of Complex 8 .....	77
Figure 3.5: Representative $^1\text{H}$ NMR spectrum of Complex 13 .....	78
Figure 3.6: Representative $^{13}\text{C}$ NMR spectrum of Ligand IL <sup>1</sup> .....	79
Figure 3.7: Representative $^{13}\text{C}$ NMR spectrum of Ligand IL <sup>5</sup> .....	79
Figure 3.8: Representative $^{13}\text{C}$ NMR spectrum of Complex 1 .....	80
Figure 3.9: Representative $^{13}\text{C}$ NMR spectrum of Complex 8 .....	80
Figure 3.10: Representative $^{13}\text{C}$ NMR spectrum of Complex 13 .....	81
Figure. 3.11: Representative $^{119}\text{Sn}$ NMR spectrum of Complex 1 .....	82
Figure. 3.12: Representative $^{119}\text{Sn}$ NMR spectrum of Complex 8 .....	82
Figure. 3.13: Representative $^{119}\text{Sn}$ NMR spectrum of Complex 13 .....	83
Figure. 3.14: Representative $^{19}\text{F}$ NMR spectrum of ligand IL <sup>2</sup> .....	84
Figure. 3.15: Representative $^{19}\text{F}$ NMR spectrum of complex 4 .....	84
Figure 3.16: IC <sub>50</sub> ( $\mu\text{M}$ ) values of synthesized Ligands (IL <sup>1</sup> & IL <sup>2</sup> ) and complexes (1-6) against breast cancer cell line (MCF-7) and and human endometrial stromal cells (hESCs).....	86
Figure 3.17: IC <sub>50</sub> ( $\mu\text{M}$ ) values of synthesized ligands (IL <sup>3</sup> & IL <sup>4</sup> ) and complexes (7-12) against breast cancer cell line (MCF-7) and and human endometrial stromal cells (hESCs).....	87
Figure. 3.18: IC <sub>50</sub> ( $\mu\text{M}$ ) values of synthesized ligand (IL <sup>5</sup> ) and complexes (13-15) against breast cancer cell line (MCF-7) and and human endometrial stromal cells (hESCs).....	88

Figure 3.19: Antileishmanial activities of ligand (IL <sup>1</sup> ) and complexes (1-3).....	90
Figure 3.20: Antileishmanial activities of ligand (IL <sup>2</sup> ) and complexes (4-6).....	91
Figure 3.21: Antileishmanial activities of ligand (IL <sup>3</sup> ) and complexes (7-9).....	91
Figure 3.22: Antileishmanial activities of ligand (IL <sup>4</sup> ) and complexes (10-12).....	92
Figure 3.23: Antileishmanial activities of ligand (IL <sup>5</sup> ) and complexes (13-15).....	93
Figure 3.24: Hemolytic assay activities of ligand (IL <sup>1</sup> ) and complexes (1-3).....	94
Figure 3.25: Hemolytic assay activities of ligand (IL <sup>2</sup> ) and complexes (4-6).....	95
Figure 3.26: Hemolytic assay activities of ligand (IL <sup>3</sup> ) and complexes (7-9).....	95
Figure 3.27: Hemolytic assay activities of ligand (IL <sup>4</sup> ) and complexes (10-12).....	96
Figure 3.28: Hemolytic assay activities of ligand (IL <sup>5</sup> ) and complexes (13-15).....	96
Figure 3.29: Antibacterial activity data of ligand (IL <sup>1</sup> and IL <sup>2</sup> ) and complexes (1-6).....	97
Figure 3.30: Antibacterial activity data of ligand (IL <sup>3</sup> and IL <sup>4</sup> ) and complexes (7-12).....	99
Figure 3.31: Antibacterial activity data of ligand (IL <sup>5</sup> ) and complexes (13-15).....	100
Figure 3.32: Antibacterial activity data of ligand (IL <sup>6</sup> and IL <sup>7</sup> ) and complexes (16-21).....	100
Figure 3.33: Antibacterial activity data of ligand (IL <sup>8</sup> and IL <sup>9</sup> ) and complexes (22-27).....	101
Figure 3.34: Antifungal activity data of ligand (IL <sup>1</sup> and IL <sup>2</sup> ) and complexes (1-6)....	102
Figure 3.35: Antifungal activity data of ligand (IL <sup>3</sup> and IL <sup>4</sup> ) and complexes (7-12)....	103

Figure 3.36: Antifungal activity data of ligand (IL <sup>5</sup> ) and complexes (13-15) .....	104
Figure 3.37: Antifungal activity data of ligand (IL <sup>6</sup> and IL <sup>7</sup> ) and complexes (16-21)..	104
Figure 3.38: Antifungal activity data of ligand (IL <sup>8</sup> and IL <sup>9</sup> ) and complexes (22-27) .....	105
Figure 3.39: Cytotoxicity data of ligand (IL <sup>1</sup> and IL <sup>2</sup> ) and complexes (1-6).....	106
Figure 3.40: Cytotoxicity data of ligand (IL <sup>3</sup> and IL <sup>4</sup> ) and complexes (7-12).....	107
Figure 3.41: Cytotoxicity data of ligand (IL <sup>5</sup> ) and complexes (13-15).....	107
Figure 3.42: Cytotoxicity data of ligand (IL <sup>6</sup> and IL <sup>7</sup> ) and complexes (16-21).....	108
Figure 3.43: Cytotoxicity data of ligand (IL <sup>8</sup> and IL <sup>9</sup> ) and complexes (22-27).....	108
Figure 3.44: Total antioxidant capacity of the synthesized ligands (IL <sup>1</sup> and IL <sup>2</sup> ) and complexes 1-6.....	109
Figure 3.45: Total antioxidant capacity of the synthesized ligands (IL <sup>3</sup> and IL <sup>4</sup> ) and complexes 7-12.....	110
Figure 3.46: Total antioxidant capacity of the synthesized ligands (IL <sup>5</sup> ) and complexes 13-15.....	110
Figure 3.47: Total antioxidant capacity of the synthesized ligands (IL <sup>6</sup> and IL <sup>7</sup> ) and complexes 16-21.....	111
Figure 3.48: Total antioxidant capacity of the synthesized ligands (IL <sup>8</sup> and IL <sup>9</sup> ) and complexes 22-27.....	111
Figure 3.49: Total reducing power of the synthesized ligands (IL <sup>1</sup> and IL <sup>2</sup> ) and complexes 1-6.....	112

Figure 3.50: Total Reducing Power of the synthesized ligands (IL <sup>3</sup> and IL <sup>4</sup> ) and complexes 7-12.....	113
Figure 3.51: Total reducing power of the synthesized ligands (IL <sup>5</sup> ) and complexes 13-15.....	113
Figure 3.52: Total reducing power of the synthesized ligands (IL <sup>6</sup> and IL <sup>7</sup> ) and complexes 16-21.....	114
Figure 3.53: Total reducing power of the synthesized ligands (IL <sup>8</sup> and IL <sup>9</sup> ) and complexes 22-27.....	114
Figure 3.54: Percentage scavenging of DPPH by the synthesized ligands (IL <sup>1</sup> and IL <sup>2</sup> ) and complexes 1-6.....	115
Figure 3.55: Percentage scavenging of DPPH by the synthesized ligands (IL <sup>3</sup> and IL <sup>4</sup> ) and complexes 7-12.....	116
Figure 3.56: Percentage scavenging of DPPH by the synthesized ligands (IL <sup>5</sup> ) and complexes 13-15.....	116
Figure 3.57: Percentage scavenging of DPPH by the synthesized ligands (IL <sup>6</sup> and IL <sup>7</sup> ) and complexes 16-21.....	117
Figure 3.58: Percentage scavenging of DPPH by the synthesized ligands (IL <sup>8</sup> and IL <sup>9</sup> ) and complexes 22-27.....	117
Figure 3.59: Side view of (A) compound 1 and (B) compound 4. In both figures, the yellow, blue, red, green, slate, and cyan balls represent C, N, O, F, Sn, and H atoms, respectively.....	118
Figure 3.60: (A) left side for compound 1 and (B) right side for compound 4. In both	

cases, (a) show GGA calculated band structures, the Fermi energy is set to zero as shown by the horizontal dashed red line. (b) The total density of states (TDOS) and (c-d) projected density of states (PDOS) of these compounds. The black line shows the TDOS, were green, blue, yellow, red, magenta lines and dark green show the PDOS of Sn, N, C, O, H and F respectively.....120

Figure 3.61: Top view of the charge-density plot (A) of compound 1, i.e., for a single monomer of compound 1. (B) Of compound 4. In both cases, we plot the charge density such that H and O2 lie in the same plane. In both cases, the dotted ellipse represents the van-der Waals interaction between the H-O2 bonds. The yellow, white-blue, dark-blue, gray red balls, green balls represent C, H, N, Sn, O, and F atoms, respectively.....121

Figure 3.62: Optical spectra calculated for (A) compound 1, (B) for compound 4....121

Figure 3.63: Electrostatic potential surfaces of the total SCF density (isovalue = 0.02) for the ligands (IL<sup>3</sup> and IL<sup>4</sup>) and organotin compounds (C7-C12). The color bars range from blue (electropositive) to green (neutral) to red (electronegative) potentials.....133-135

Figure 4.1: Outlook view of ligand IL<sup>3</sup> with intramolecular hydrogen bonding.....140

Figure 4.2: Outlook view of ligand IL<sup>3</sup> with intramolecular and intermolecular hydrogen bonding.....140

Figure 4.3: Outlook view of ligand IL<sup>3</sup> with packing diagram showing having hydrogen bonding and intermolecular secondary interactions.....141

Figure 4.4: Perspective view of monomeric structural unit of complex 1 .....	147
Figure 4.5: A perspective of one of the linear polymeric chains of compound 1. The translation ellipsoids are haggard at the probability level of 50% and hydrogen atoms are presented as trifling spheres of arbitrary radii.1 .....	148
Figure 4.6: Perspective outlook of complex 1 with packing structure having intramolecular and intermolecular hydrogen bonding and Van der Waals interactions.....	149
Figure 4.7: A perspective of the monomeric structural unit of compound 4.....	150
Figure 4.8: A perspective of one of the two crystallographically distinct one-dimensional polymeric chains of the crystal structure of compound 4.....	150
Figure 4.9: A perspective of one of the two crystallographically distinct monomeric structural units of compound 5.....	151
Figure 4.10: A perspective of one of the two crystallographically distinct one-dimensional polymeric chains of the crystal structure of complex 5.....	151
Figure 4.11: Perspective outlook of 1D monomeric structure of complex.....	152
Figure 4.12: Perspective outlook of complex 5 with packing structure having intramolecular and intermolecular hydrogen bonding and Van der Waals interactions.....	152

Figure 4.13: Perspective view of a monomeric structure of complex 7.....	158
Figure 4.14: Perspective outlook of 1D Polymeric structure of complex 7.....	158
Figure 4.15: Perspective outlook of the monomeric structure of complex 7.....	159
Figure 4.16: Perspective view of the dimeric structure of complex 10.....	159
Figure 4.17: Perspective view of 1D Polymeric structure of complex 10.....	160
Figure 4.18: Plot of the asymmetric unit of monomeric compound 13.....	164
Figure 4.19: A perspective of one of the linear polymeric chains of compound 13...164	
Figure 4.20: A perspective of one of the linear 2D polymeric chains of compound 13. The translation ellipsoids are haggard at the probability level of 50% and hydrogen atoms are presented as trifling spheres of Arbitrary radii.1.....	165
Figure 4.21: Packing diagram showing hydrogen bonding and secondary interactions of complex 13.....	166
Figure 4.22: Perspective view of the monomeric structure of complex 14.....	166
Figure 4.23: Perspective view of 2D Polymeric structure of complex 14.....	167
Figure 4.24: Outlook view of the monomeric structure of compound 8.....	170
Figure 4.25: Outlook view of 1D Polymeric structure of compound 8.....	171
Figure 4.26: Packing diagram showing hydrogen bonding and Van der Waals interactions of complex 8.....	171
Figure 4.27: Perspective view of the monomeric structure of compound 22.....	172



Figure 4.28: Perspective view of 2D Polymeric structure of compound 22.....172

## List of Tables

---

Table 3.1: Percent hemolysis and IC <sub>50</sub> values of ligand IL <sup>1</sup> and complexes (1-3).....	94
Table 3.2: Selected experimental and theoretical bond lengths (Å) for compound IL <sup>3</sup> , C7, C8, and C10. The theoretical bond lengths are calculated using DFT at the B3LYP/LANL2DZ level.....	124
Table 3.3: Selected experimental and theoretical bond angles (θ) for compound IL <sup>3</sup> , C7, C8, and C10. The theoretical bond angles are calculated using DFT at the B3LYP/LANL2DZ level.....	125
Table 3.4: Frontier molecular orbitals of ligands (IL <sup>3</sup> , IL <sup>4</sup> ) and the compounds (C-7, C-8, C-9, C-10, C-11, and C-12) compounds are depicted with the following color index of atoms: Red=O, Blue=N, Green=Sn, Yellow= F, Pink=C .....	127
Table 3.5: Frontier orbital energies, their band gap (E <sub>g</sub> ), and global reactivity parameters* of metal complexes obtained by B3LYP with a LANL2DZ basis set.....	130
Table 3.6: Mulliken charges were obtained using DFT (B3LYP) manner with a LANL2DZ basis set. The atom internal numbering is mentioned in parenthesis within each column along with the atomic charge.....	132
Table 4.1: Crystal data and structure refinement parameters for ligand IL <sup>3</sup> .....	142

Table 4.2: Selected Bond Lengths (Å) for compound IL <sup>3</sup> .....	143
Table 4.3: Selected Bond Angles (θ) for compound IL <sup>3</sup> .....	143
Table 4.4: Hydrogen bond information for ligand IL <sup>3</sup> .....	143
Table 4.5: Crystal data and structure refinement parameters for the complexes.....	153
Table 4.6: Selected Bond Lengths (Å) and Bond Angles (θ) for complexes 1, 4 and 5.....	154
Table 4.7: Crystal data and structure refinement parameters for complexes (7) and (10).....	161
Table 4.8: Selected bond lengths (Å) for compounds 7 and 10.....	162
Table 4.9: Selected Bond Angles (θ) for compounds 7 and 10.....	162
Table 4.10: Crystal data and structure refinement parameters for complexes (13) and (14).....	168
Table 4.11: Selected Bond Lengths (Å) and Bond Angles (θ) for compounds 13 and 14.....	169
Table 4.12: Crystal data and structure refinement parameters for complexes (8) and (22).....	173
Table 4.13: Selected Bond Lengths (Å) and Bond Angles (θ) for compounds 8 and 22.....	174

## List of Schemes

---

Scheme 1: Schematic representation of synthesis of ligands IL <sup>1</sup> -IL <sup>4</sup> and their sodium salts.....	32
Scheme 2: Synthesis of ligand IL <sup>5</sup> and sodium salt of the ligand.....	33
Scheme 3: Synthesis of ligands IL <sup>6</sup> -IL <sup>9</sup> and their sodium salts.....	35
Scheme 4: Synthesis procedure for the synthesis of organotin(IV) amide-based carboxylates.....	42

## List of Abbreviations

---

DPPH	1,1-diphenyl-2-picrylhydrazyl
DMSO	dimethyl sulphoxide
CDCL <sub>3</sub>	Chloroform
TMS	Tetramethyl silane
THF	Tetrahydrofuran
FT-IR	Fourier transform Infrared
NMR	Nuclear magnetic resonance
IC <sub>50</sub>	Concentration required to inhibit cell growth by 50 percent
LC <sub>50</sub>	Lethal dose 50 percent
LD <sub>50</sub>	Lethal concentration 50 percent
DFT	Density functional theory
GGA	Generalized gradient approximation
HOMO	Highest occupied molecular orbital
LUMO	Lowest unoccupied molecular orbital
VBM	Valence bond maximum
CBM	Conduction band minimum
TDOS	Total density of states
PDOS	Projected density of states
DOS	Density of states
HSAB	Hard soft acid base
XRD	X-ray diffraction
MEP	Molecular electrostatic potential
HESCs	Human endometrial stromal cells
MCF-7	Breast cancer cell lines
FBS	Fetal bovine serum
DMEM	Dulbecco's modified eagle's medium
MTT	3-(4,5-dimethylthiazol-2-yl)-2,5-diphenyl-2H-tetrazolium bromide
TAC	Total anti-oxidant assay

FRSA	Free radical scavenging activity
TRP	Total Reducing Power
PSB	Phosphate saline buffer

### 1. Introduction

This dissertation deals with the synthesis, characterization, anticancer, anti-leishmanial, biological, and computational details of novel Sn(IV) amide-based carboxylates complexes. It is important to know about the molecular basis of cancer to understand the metabolic pathway stimulated by metal-based anticancer drugs. The reason why this chapter presents core concepts in cancer biology and leishmanial disease as well. It also creates the present methodologies for treatment, including the single targeted therapy as a new trend whereas identifying the benefits of multi-targeted anticancer agents.

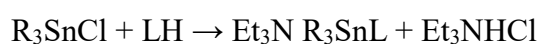
#### 1.1. Organotin(IV) carboxylates

Organotin(IV) carboxylates include one of the essential classes of metal complexes. Frankland and Ann are the earliest scientists who prepared the organotin(IV) based compounds in 1849 [1]. After the discovery of this innovation, scientists took interest in the synthesis and implementation of organotin(IV) based complexes in different fields. Such compounds are mainly used as heat stabilizers, biocides, and catalysts in agriculture and various industrial applications. Mono/di-substituted organotin(IV) based complexes are mainly used in pipes and packing materials as a stabilizing agent to reduce the dehydrochlorination of chlorine-based complexes, like polyvinyl chloride (PVC) and to foil oxygenolysis. Due to the low energy of the 5d orbital of the tin atom, organotin(IV) can be used as catalysts in esterification, transesterification, and cross-linking reactions [2, 3]. Organotin(IV) based complexes have many advantages such as the need for fewer reaction precursors, high proficiency, easy removal of the product, and non-corrosive for reactors. Organotin(IV) compounds are mainly implemented as biocides e.g., fungicides, insecticides, disinfectants, acaricides, molluscicides, marine antifoulants and wood preservatives [4]. However, there are many organotin biocides

that are banned because they are not environmentally friendly. Besides industrial and agricultural applications organotin(IV) carboxylates have also find importance in theoretical and structural chemistry [5]. In addition to these, researchers have also focused on the synthesis organotin compounds which may found good applications in health care especially for cancer treatments [6]. These compounds have potential as anticancer agents, but also revealed better anti-inflammatory, antileishmaniasis, anti-tuberculosis, antibacterial, antifungal and antioxidant activities etc. Here, we prepared triorganotin(IV) carboxylates based complexes for potential medicinal applications. Here it is also highlighted the significance of organotin(IV) based complexes toxic effect which co-occurs with the bioactive effectiveness and impact on their medicinal worth and implementation. One of the very important aspects is to develop such complexes for medicinal applications which generate solutions with low toxicity. New applications are likely to emerge shortly. The compounds containing – OCOR' groups bonded to tin are defined as organotin- esters which may be either monomeric or polymeric and of three general types, viz.  $R_3SnOOR'$ ,  $R_2Sn(OCOR')_2$  and  $RSn(OCOR')_3$ , where R and R' may be different or same groups [7].

## 1.2. Synthesis of organotin(IV) carboxylates

Organotin(IV) halides because of their hydrolyzable nature, which has been used as a starting material, and anhydrous organic solvents are such as acetone, methanol, ethanol, toluene, n-hexane, benzene is used as a medium to carry out the synthesis of these tin metal complexes with different types of ligands. Hameed *et al.* synthesized triorganotin(IV) based complexes like  $Ph_3SnL$ ,  $Bu_3SnL$ , and  $Me_3SnL$  of the ligand benzamidomethionine (HL). The typical reaction for the fabrication of the triorganotin(IV) based complexes is shown below.





From Fourier-Transform infrared spectroscopy (FT-IR) and multi-nuclear magnetic resonance (NMR) spectroscopy, the geometry of these synthesized complexes was proposed as the tetrahedral in nature as shown in **Figure 1.1**.

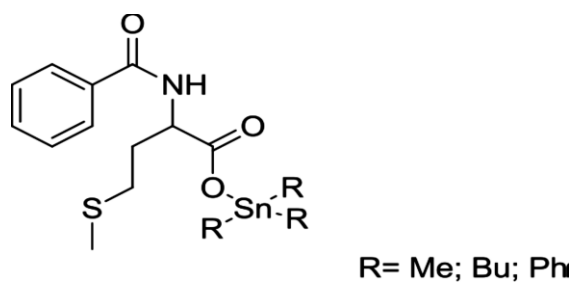


**Figure 1.1:** Structure of triorganotin(IV)- benzamidomethionine complex.

Yousif *et al.* prepared and studied the synthesis of triorganotin(IV) with benzamidoglycine. Ligand was made by the reaction of glycine with benzenecarbonyl chloride in basic media. The prepared metal amide based carboxylate complexes were analyzed using FT-IR, elemental analysis, NMR ( $^1\text{H}$ ,  $^{13}\text{C}$ , and  $^{119}\text{Sn}$ ) spectroscopy and conductance measurements. After the spectral analysis, the monodentate mode of binding of monomers, and tetrahedral geometry around Sn(IV) center were commended as shown in **Figure 1.2** [8].

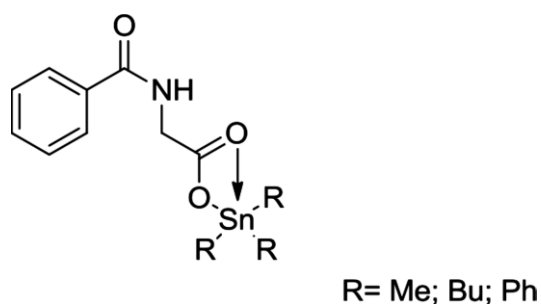


**Figure 1.2:** Structure of triorganotin(IV)- benzamidoglycine complex.

Yousif *et al.* also studied the preparation of triorganotin(IV) complexes with benzamidoalanine, which was synthesized by using reactant materials that includes

benzoyl chloride, and alanine in alkaline media. These compounds were analyzed by using FT-IR elemental analysis, UV-Vis Spectroscopy, conductance measurements, and NMR spectroscopy ( $^1\text{H}$ ,  $^{13}\text{C}$ , and  $^{119}\text{Sn}$ ). The proposed monomeric structure from the spectral analysis is shown in **Figure 1.3**, with a bidentate ligand [9].

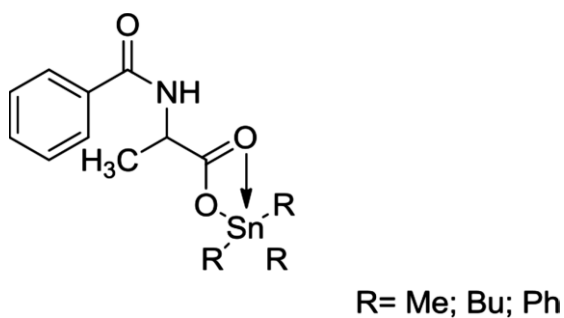


**Figure 1.3:** Structure of triorganotin(IV)- benzamidoalanine complex.

An important method of preparing diorganotin carboxylates is by refluxing of organotin derivatives and carboxylic acid. Farina *et al.* synthesized metal complexes like  $\text{R}_2\text{SnL}_2$ , where R = methyl, butyl, phenyl, and L = N-methyl-m-nitrobenzohydroxamic acid [10]. Ligand acting as a bidentate and adopting octahedral geometry around tin center was suggested for the prepared complexes as shown in **Figure 1.4**.

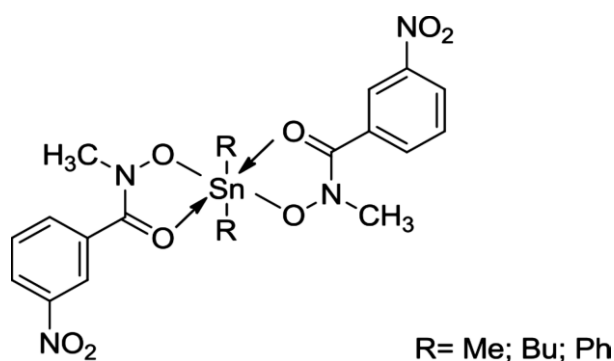


**Figure 1.4:** Structure of diorganotin(IV)-N-methyl-m-nitrobenzohydroxamic acid Complex.

It may be determined that the tin atom attached to the ligand through oxygen leading to the development of chelate of the five-member ring [10]. Also, new diorganotin(IV) carboxylates complexes like  $\text{Me}_2\text{SnL}_2$ ,  $\text{Bu}_2\text{SnL}_2$ , and  $\text{Me}_2\text{SnL}_2$  of the ligand H benzamidoleucine (L) were reported by Graisa *et al.* The ligand was synthesized by reaction of benzenecarbonyl chloride with leucine in an alkaline medium. The proposed geometry for these complexes was octahedral. Graisa *et al.* reported novel diorganotin(IV) carboxylates complexes like  $\text{Me}_2\text{SnL}_2$ ,  $\text{Bu}_2\text{SnL}_2$ , and  $\text{Ph}_2\text{SnL}_2$ , and of the ligand N-tolyl m-nitrobenzohydroxamic acid. Ligand was prepared as a result of the condensation reaction of N-tolyl hydroxylamine with 3-nitrobenzoyl chloride in the presence of sodium hydrogen carbonate ( $\text{NaHCO}_3$ ) as catalyst. These compounds were also analyzed by FT-IR, elemental analysis, Ultraviolet-visible, conductance measurements, and NMR ( $^1\text{H}$ ,  $^{13}\text{C}$ , and  $^{119}\text{Sn}$ ) spectroscopy. The octahedral geometry with bidentate mode of binding was suggested for the ligand around the complex by means of spectral analysis as shown in **Figure 1.5** [11].

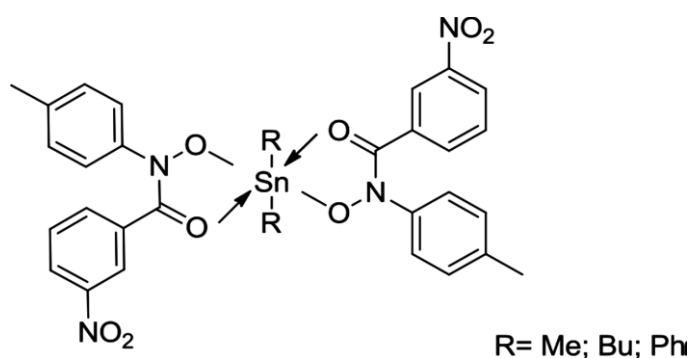


**Figure 1.5:** Structure of diorganotin(IV)- N-tolyl m-nitrobenzohydroxamic acid Complex.

Another series of diorganotin(IV) carboxylates complexes of the type  $\text{Me}_2\text{SnL}_2$ ,  $\text{Bu}_2\text{SnL}_2$ , and  $\text{Ph}_2\text{SnL}_2$  of the ligand benzamidoacetic acid (L). The ligand was synthesized by the reaction of benzenecarbonyl chloride with glycine in an alkaline

medium. It may be determined that the tin atom attached to the ligand through oxygen leading to the development of chelate of the four-member ring. Octahedral geometry was suggested for the synthesized complexes as shown in **Figure 1.6** [11].

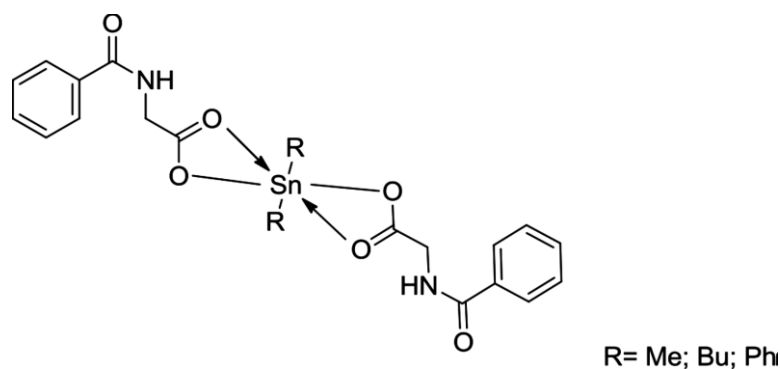


**Figure 1.6:** Structure of diorganotin(IV)- benzamidoacetic acid complex.

The ligand 2-[(phenylcarbonyl)amino] propanoic acid (HL) was prepared by the reaction of benzenecarbonyl chloride with alanine in an alkaline medium and a new series of diorganotin(IV) amide based carboxylates were prepared [12]. The carboxylate group of the ligand coordinated to the Sn atom leading to the assembly of chelate of the four-member ring. The suggested geometry for the prepared complexes was octahedral as shown in **Figure 1.7**.

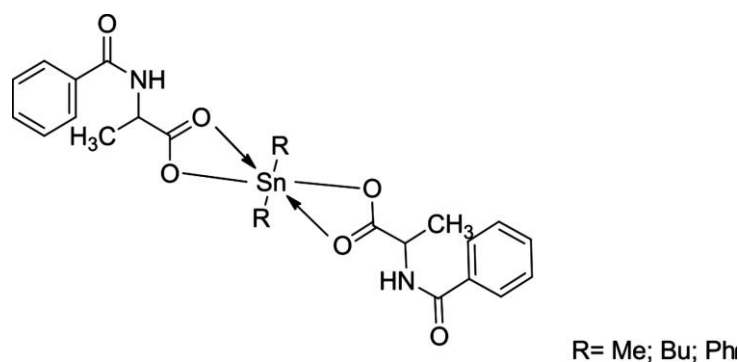


**Figure 1.7:** Structure of diorganotin(IV)- 2-[(phenylcarbonyl)amino]propanoic acid complex.

Yousif *et al.* synthesized and characterized the diorganotin(IV) carboxylates complexes with 2-thioacetic-5-phenyl-1,3,4-oxadiazole and studied their antifungal activity [7]. The suggested geometry for the fabricated complex was octahedral as shown in **Figure 1.8**.

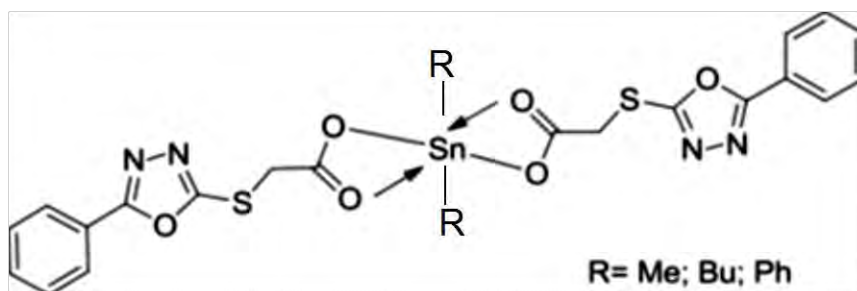


**Figure 1.8:** Structure of diorganotin(IV)- 2-thioacetic-5-phenyl-1,3,4-oxadiazole complex.

Graisa *et al.* have also disclosed bidentate and tetrahedral geometry for the synthesized complexes from the N-methyl-m-methoxybenzohydroxamic acid-based ligand and different di-organotin(IV) oxide metal to give the proposed Sn metal complexes which is shown in **Figure 1.9** [13].

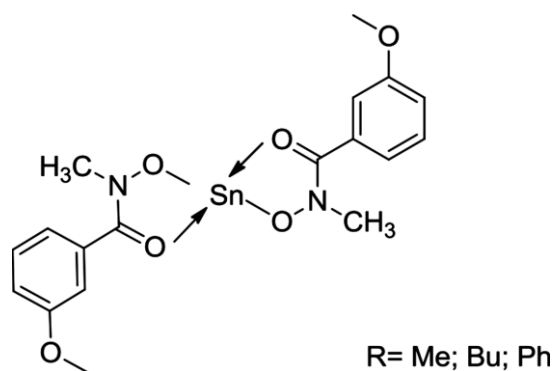


**Figure 1.9:** Structure of diorganotin(IV)- N-methyl-m-methoxybenzohydroxamic acid complex.

Najeeb *et al.* reported a novel structural class of octahedral organotin(IV) carboxylates of the ligand benzamidocysteine. The ligand was prepared in basic media by the reaction between benzoyl chloride and cysteine and a new series of diorganotin(IV) amide-based carboxylates were prepared to have octahedral geometry. Significant biological activity has been shown by these complexes against different fungal strains in dimethyl formamide by the already reported method [14]. Diorganotin(IV)-benzamidocysteine complex is shown in **Figure 1.10**.

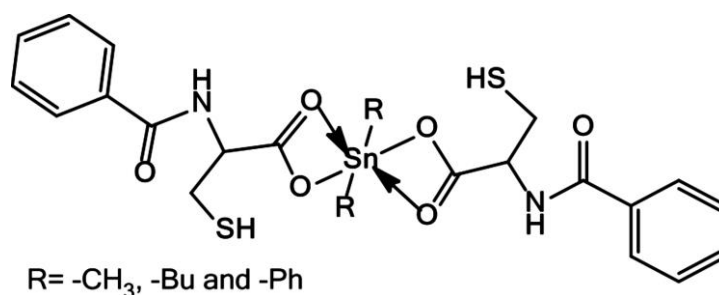
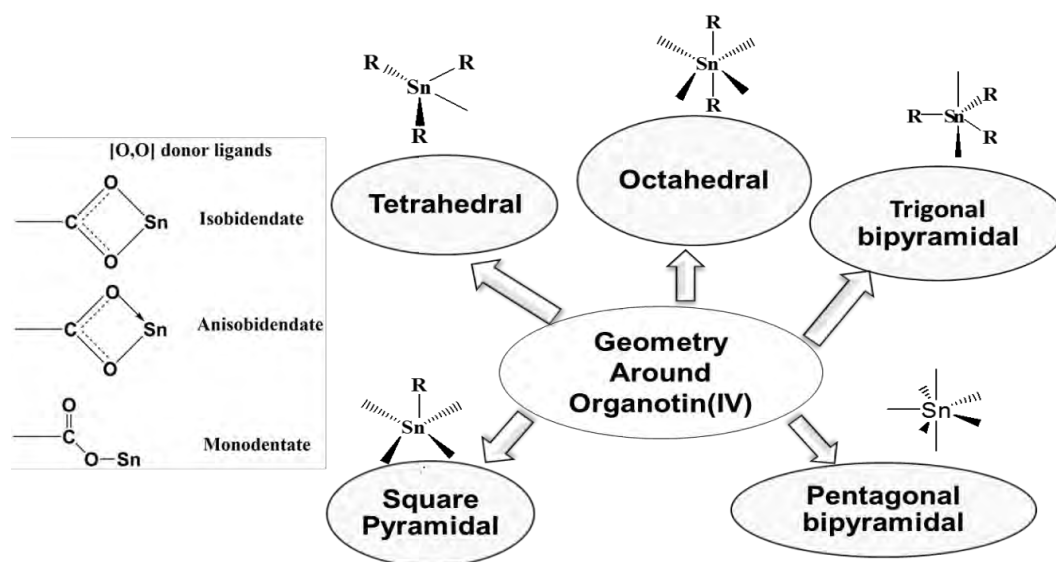


**Figure 1.10:** Structure of diorganotin(IV)- benzamidocysteine complex.

### 1.3. Structural diversity of organotin(IV) carboxylate complexes

Organotin(IV) carboxylates have shown numerous structural geometric variations. Due to the availability of vacant d orbital, the Sn atom exhibited various coordination modes, for example, four coordinated tetrahedral, five coordinated trigonal bipyramidal and square pyramid, six coordinated octahedral, and seven coordinated pentagonal bipyramidal. The triorganotin(IV) complexes have revealed 5 and 6 geometries commonly, while for diorganotin(IV) complexes 4, 5 and 6 coordination geometries are known [15, 16]. In recent years the growing attention in the organotin(IV) carboxylates of newly synthesized benzoic acid, gain a lot of interest due to the diversity in their structural geometry. Depending upon the coordination number and molecular geometry organotin(IV) carboxylates showed a fascinating range of structural diversity. The

carboxylate moieties are directly attached to the central atom either as (a) monodentate fashion, (b) bridging bidentate fashion, (c) bidentate symmetric; isobidentate, or (d) bidentate unsymmetric; anisobidentate [17, 18] and having extensive therapeutic actions [19]. As info on the structural diversity organotin(IV) based carboxylates lingers, other novels and important applications have been discovered which are mainly related to medicinal applications. The chemistry of organotin(IV) carboxylates based complexes have growing attention that mainly directed to the protracted studies on their interactions with important bio-macromolecules like carbohydrates [20-22], nuclei byproducts [23, 24], different amino acids [25, 26] and varieties of dipeptides [27-29]. The objective of the present work; to review different classes of organotin(IV) amide-based carboxylates to explain the different approaches of the carboxylate ligand of coordination/association, which was checked by crystallographic techniques. Here we will focus to elaborate the structural diversity of organotin(IV) carboxylates under the category of oxygen-donor ligands.



4

**Figure 1.11:** Different structural geometries of organotin(IV) complexes.

## 1.4. Oxygen donor ligands

The organotin(IV) content coordinates to oxygen donor ligands in a monodentate way or bidentate way in a changed stoichiometric ratio which is responsible for the structural diversity. In this section, we will explain different coordinated complexes like four, five, and six coordinated complexes.

### 1.4.1. Complexes of four coordination geometry

Oxygen-based donor ligand coordinates mainly around the tin atom in a monodentate fashion, as testified by the literature the geometry around tin metal is tetrahedral [30-33]. One of the structures of the tetrahedral class is given in **Figure 1.12**, which displays that the tetrahedral geometry around the tin atom is prominent of the ligand E-3-(3-fluorophenyl)-2-(4-chlorophenyl)-2-propionate after coordination by phenyl groups atoms like 3 ipso-carbon atoms and O1 atom [Sn1-O1 = 2.0557(14) Å]. The key change from the perfect geometry of tetrahedral is originated in the O1-Sn1-C1 angle of 96.54(7)°. The comparatively nearby attachment amid Sn1 and O2 [Sn1...O2 = 2.8309(5) Å] doesn't disturb the angle between O1-Sn1-C7 and O1-Sn1-C13 considerably, which are in the range between 108.91(7)° and 110.10(7)°, correspondingly. However, it is quite notable that the angle (119.06(8)°) of C7-Sn1-C13 is the subsequent main falsification from the perfect geometry. The approach of monodentate coordination of E-3-(3-fluorophenyl)-2-(4-chlorophenyl)-2-propionate is imitated in the disparate O1-C19 and O2-C19 bond distances of 1.313(2) and 1.229(2) Å, correspondingly, through the lengthier parting being connected with the more solid Sn1-O1 attachment [30, 33]. **Figure 1.13** showed the example of this type of complex, which indicated that the geometry is distorted tetrahedral [32].



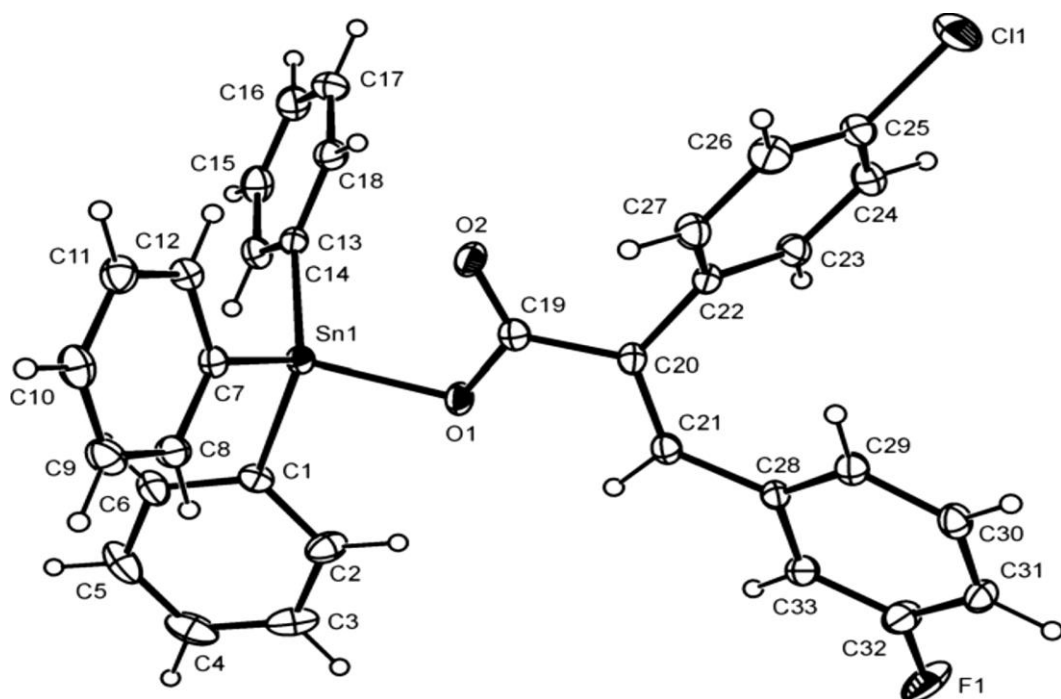


**Figure 1.12:** Structure of triphenyltin(IV) [3-(3-fluoro-phenyl)-2-(4-chlorophenyl)-2-propenoate.

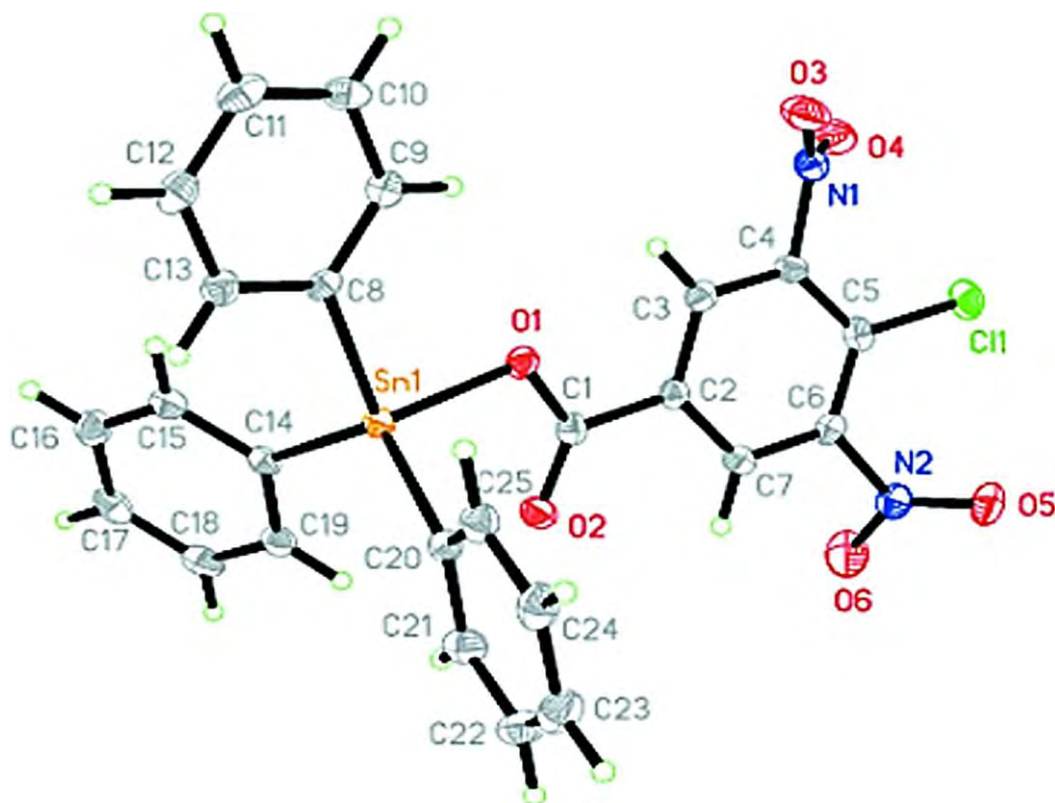


**Figure 1.13:** Structure of triphenyltin(IV)-(4-chloro-3,5-dinitrobenzoate).

#### 1.4.2. Complexes of five coordination geometry

Already reported triorganotin(IV) based complexes are the ones having distorted trigonal bipyramidal geometry and polymeric structure as well [33-36]. **Figure 1.14** displayed the example of this type of complex, which indicated that the geometry is partial trigonal bi-pyramidal. In actuals, the three attached CH<sub>3</sub>- groups to Sn having equal distance and lied at the equatorial positions [Sn-C = 2.119(6) Å]. The atomic Sn, which is more strongly bonded to the atom O1 lied to 0.065(2) Å is mainly out of the equatorial plane molded by the carbon atoms of three CH<sub>3</sub>- groups. The angles present in these complexes like O-Sn-O, C-Sn-C, and O-Sn-C is around lined [171.21(9)°, 119.24(15)°-120.62(15)° and 84.47(12)-97.24(12)°], respectively [23]. Previous research [37-40] has revealed that the coordination geometry of triorganotin(IV) complexes do not change with oxygen donor ligands having coordination of different alkyl groups which displayed the distorted trigonal bipyramidal structure with polymeric structure. **Figure 1.15, 1.16** and **1.17** showed the example of this type of complexes [37, 38]. The complex with tributyltin(IV) moiety which showed the tetrameric arrangement has displayed in **Figure. 1.18** [41]. The assembly arrangements a sequestered cyclotetrameric sixteen membered ring which is positioned around the crystallographic center of inversion hence that the two self-determining Bu<sub>3</sub>SnL units encompass the asymmetric unit. This accretion leads the carboxylates ligands to bidentate bridging, though making lop-sided bond spaces of nearly 2.24 and 2.62 Å. The exact Sn atom which coordination geometry is centered on the trans-R<sub>3</sub>SnO<sub>2</sub> trigonal bipyramid with the already specified discrepancy in the bond of Sn-O in which distances are not with-standing. For the Sn1 atom the axial angle is about to 171.19(10)° which is further significantly distorted from the Sn2 atom ideal angle of 177.62(11)°. Researchers already reported three R<sub>3</sub>Sn(O<sub>2</sub>CR') structures in the literature [42, 43] that

assume tetrameric style. The explanation of these cyclotetrameric complexes, to be supposed as intermediate between two extremes like monomeric and polymeric as defined above, vestiges indefinable. In disparity to tributyltin(IV) [44, 45] and polymer and dimer of triphenyltin(IV) [46] analogues, tribenzyltin(IV) compounds [47] unveil the similar monomeric  $\text{trans-R}_3\text{SnO}_2$  structural motifs. The tin atom has equatorial benzyl groups and the axial sites occupied with oxygen atom from the carboxylate ligands and oxygen atom from the water ligand which showed as slightly distorted trigonal bipyramidal geometry.

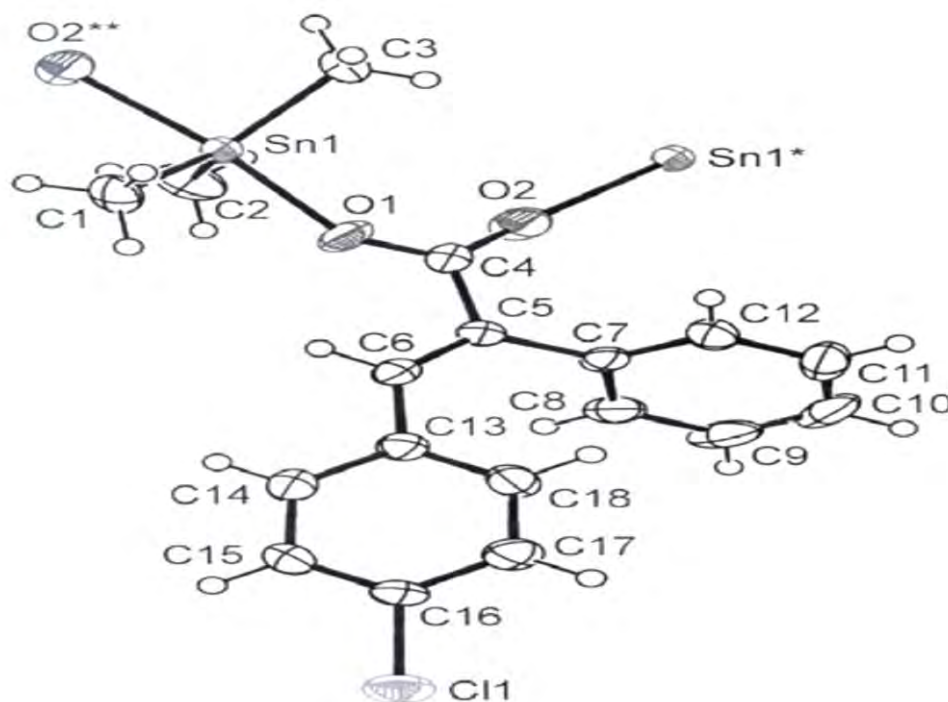


**Figure 1.14:** Structure of *catena*-poly[[tri-methyltin]- $\mu$ -2-phenyl-3-(4-chlorophenyl)propenoatoO:O].

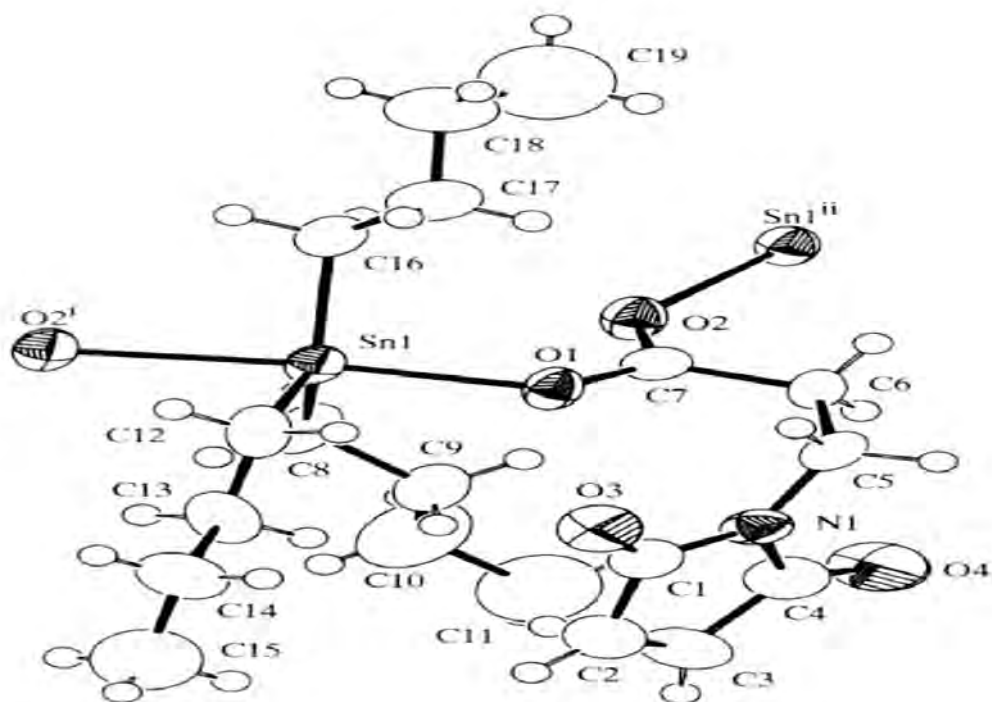


**Figure 1.15:** Structure of tri-*n*-butyl(N-maleoyl- $\beta$ -alaninato)tin.

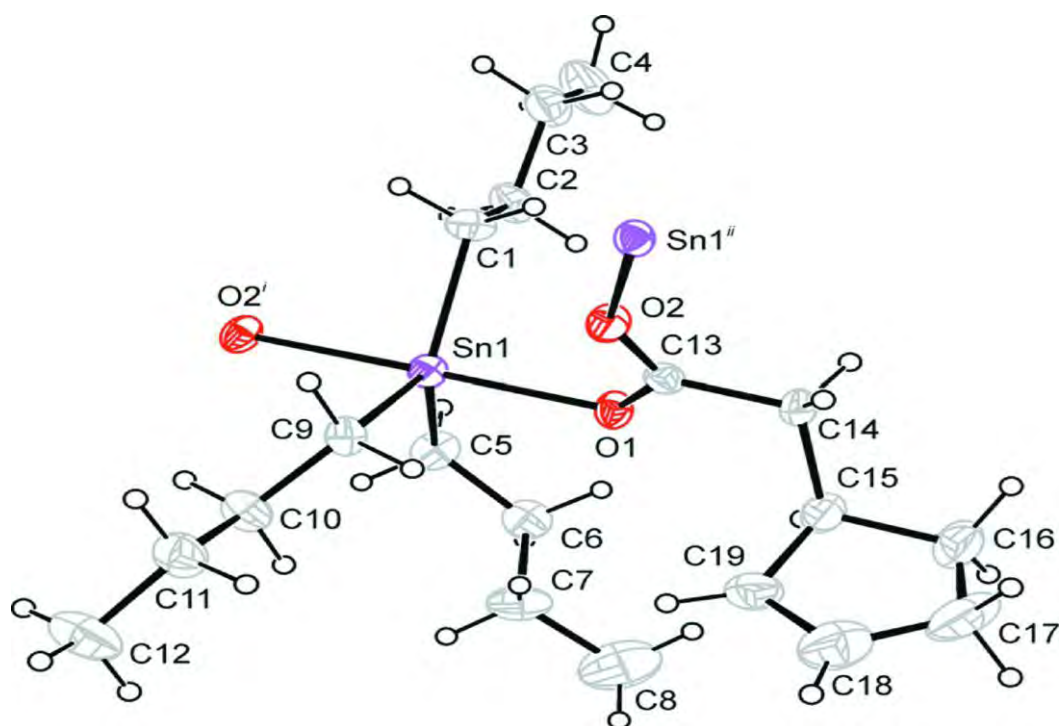


**Figure 1.16:** structure of *catena*-poly[[tri-*n*-butyltin(IV)]- $\mu$ -cyclopent-2enylacetato-O:O'].

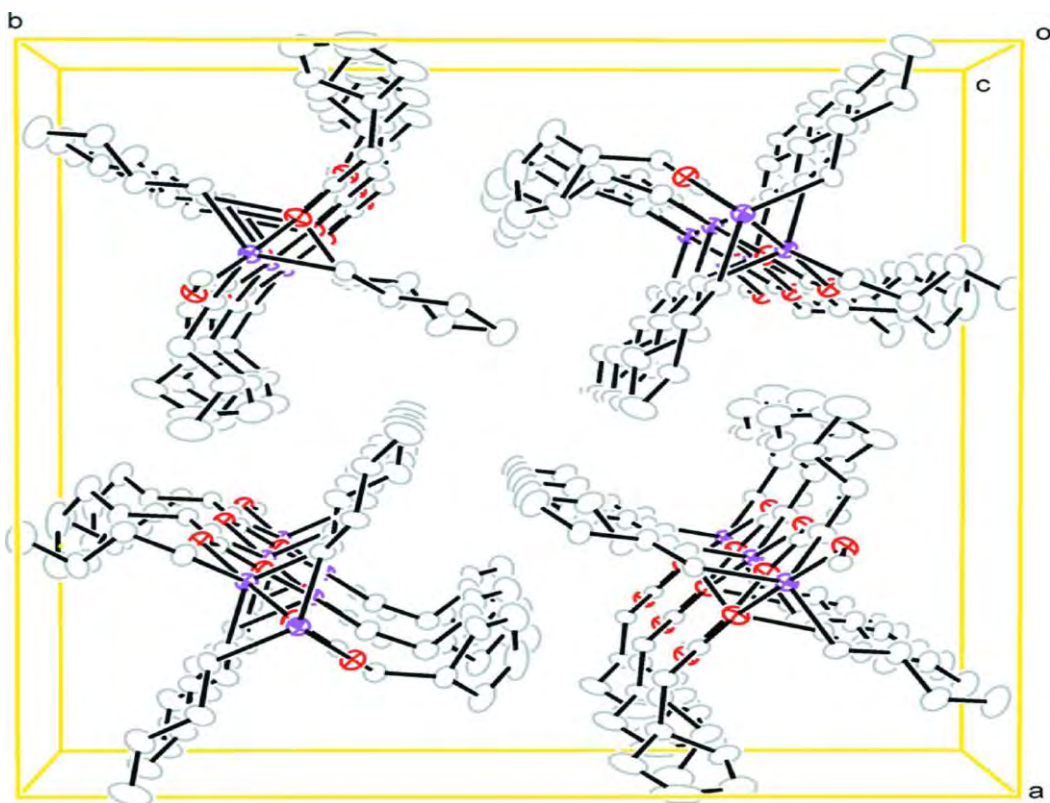


**Figure 1.17:** Structure of *catena*-poly[[tri-*n*-butyltin(IV)]-μ-cyclopent-2-enylacetato-O:O'].

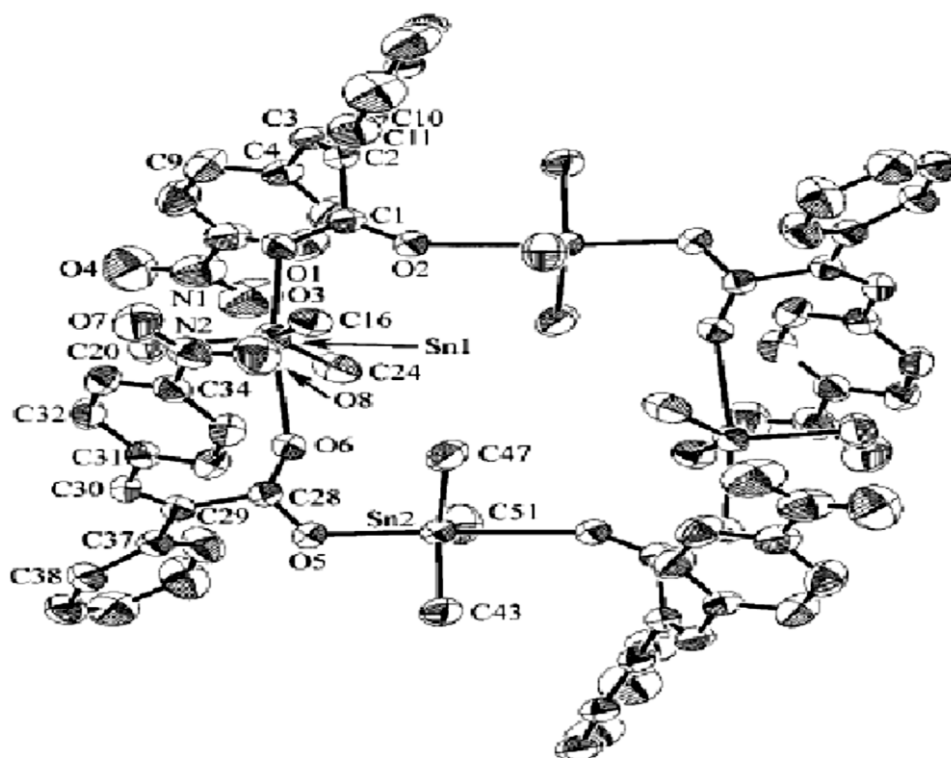


**Figure 1.18:** Structure of tetrameric *catena*-poly[[tri-*n*-butyltin(IV)]- $\mu$ -cyclopent-2-enylacetato-O:O`].

### 1.4.3. Complexes of six coordination geometry

The distorted octahedral geometry marks by irregular attachment of the carboxylates ligands attached to Sn metal in these complexes. One of the demonstrative structures of these complexes is given in **Figure 1.19** [48]. In this complex, the tin metal atoms are attached to binary *n*-butyl groups and binary 2,3-bis(4-chlorophenyl) propenoate ligands which gave a discrete monomeric structure. The highly distorted octahedral geometry around the tin atom can be better pronounced as a skew-trapezoidal planar structure that has two extra-axial ligands. The tin atom deceits 0.190(2) Å out of the plane molded by inequitably attached oxygen atoms of the carboxylate ligands, whereas both the *n*-butyl groups lie above and below this plane. The average tin and carbon (Sn-C) distance of 2.116(13) Å and carbon Sn carbon (C-Sn-C) angle of 139.17(18)° is

practical. The asymmetrically coordinated carboxylate ligands with tin atoms having (Sn-O) covalent bonds [average = 2.097(6) Å] that are much shorter than coordinate covalent bonds [mean = 2.601(12) Å]. The carboxylate groups having oxygen donor ligands coordinate with tin atom revealed distorted octahedral geometry. One of the examples of dimethyltin(IV) moiety is presented in the **Figure. 1.20** [49].

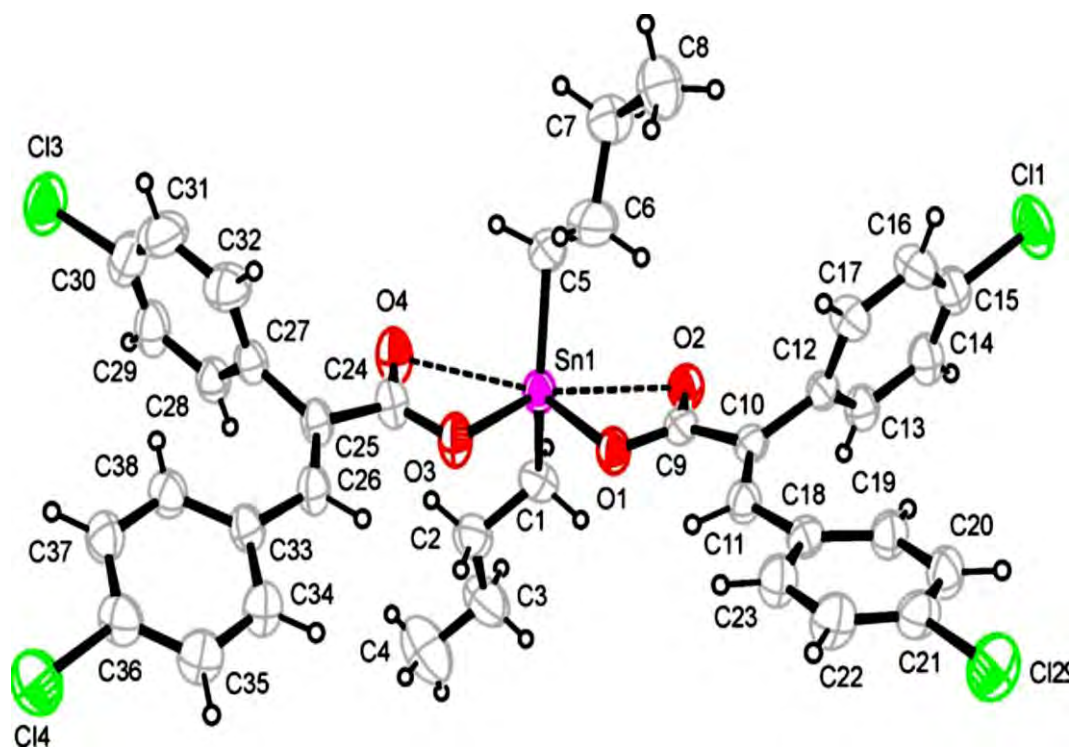


**Figure 1.19:** Structure of di-*n*-butyltin(IV) bis-[2,3-bis(4-chlorophenyl)propenoato-O,O'].

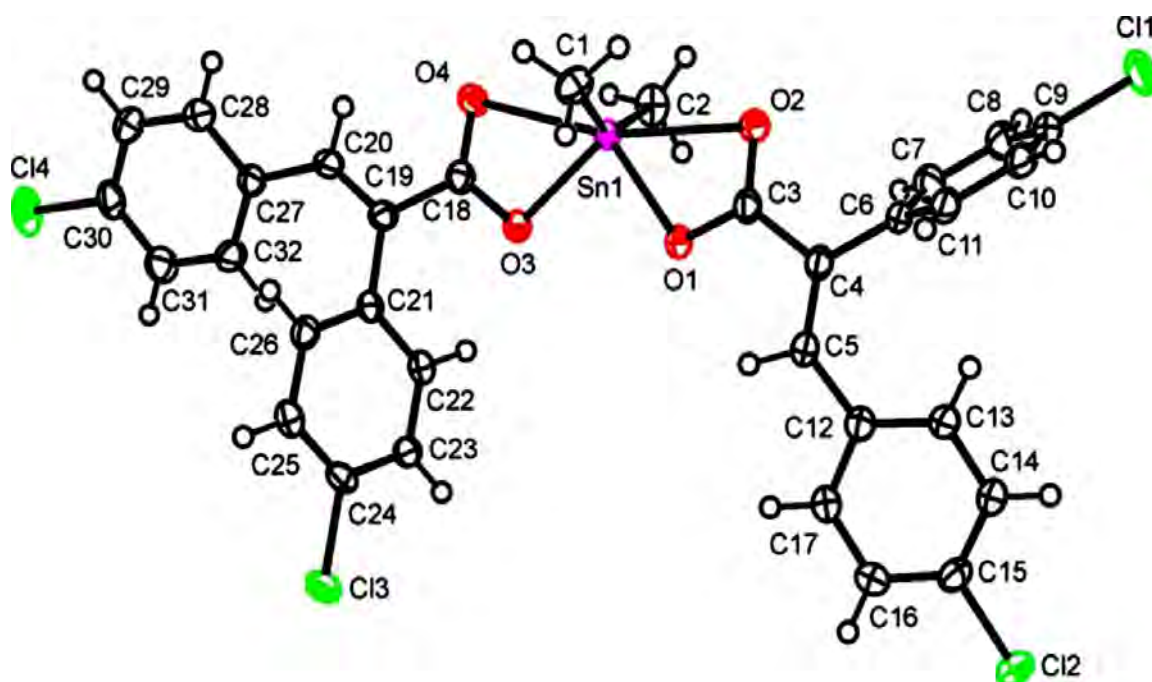


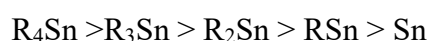
**Figure 1.20:** Structure of dimethyltin(IV) bis[2,3-bis(4-chlorophenyl)propenoato-O,O'].

### 1.5. Biological Activity

The tin-based compounds are slightly or non-toxic towards bacteria, fungi, insects, and mammals, while tin(IV) based complexes, having an organic part attached revealed different biological actions. The lengthier the alkyl series, the less is the toxicity [50, 51]. The specific array for different alkyl groups (methyl, propyl, butyl, etc) differs according to the test organism. The structural chemistry of organotin(IV) based complexes defined the biotic properties of these complexes. Those triorganotin(IV) complexes are more toxic compounds that have three Sn-C bonds [7, 52, 53] while the aromatic groups' complexes are less poisonous than aliphatic group complexes [54, 55]. The ligand X can increase or decrease the biological activity, for example, if it is with chelation to tin atom. As a result, it will decrease the activity but if it is biologically supportive or active in the passage of the complex to the active site, then it increases



the activity [56]. Complexes having O-Sn-O linkages have revealed the best activities than the complexes that have Sn atom coordinated to sulfur atom [57, 58]. For tri-n-alkyltin(IV) acetates, the trimethyltin(IV) complexes are utmost active against mammals and pests while the ethyl, propyl, and butyl complexes are more active against the bacteria and fungi. Biological activity of trialkyltin(IV) complexes groups decreases in the following order:



R is the general term used for different types organic ligands (carboxylates, Schiff bases, dithiocarbamate, xanthate, hydrazone etc) attached to the Sn metal. But the anionic X groups have a marked influence on the activity of tin(IV) compounds [59, 60]. The complexes utmost implemented on large scale is tributyltin(IV) chloride, dibutyltin(IV) dichloride, tributyltin(IV) oxide, and dibutyltin(IV)oxide as in **Figure 1.21** because these complexes amid the less poisonous alkyltin(IV) derivatives in creatures [61].

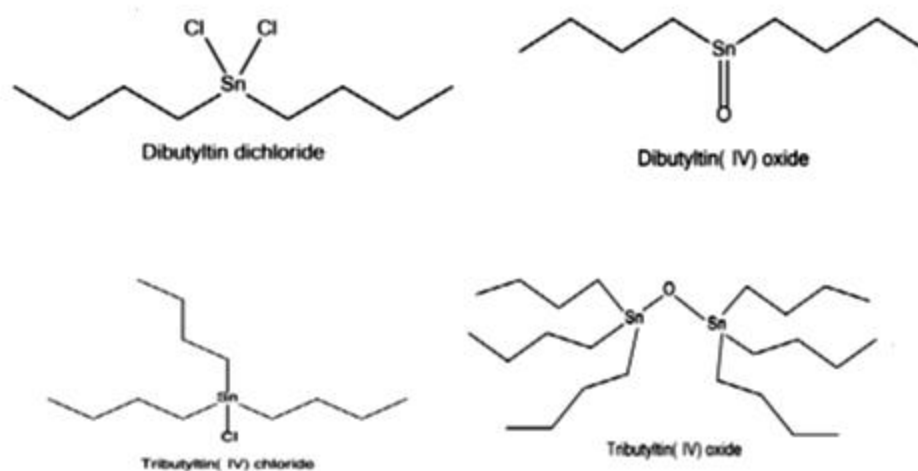


**Figure 1.21:** Some of the biologically active Organotin compounds.

### 1.5.1. Biological properties of organotin(IV) carboxylates

Di- and triorganotin(IV) complexes have established extra consideration for their biological properties than any other metal complexes having organic groups attached. The inorganic tin compounds hardly have any biological activity whereas organotin compounds exhibit high biocidal activity, probably due to their lipid solubility, which facilitates better transport to the reaction sites than the corresponding inorganic tin compounds. The systematic studies of biological activities of organotin(IV) were initiated in 1950 [62]. Van der Kerk and Luijten [63] in 1954 published that many organotin derivatives having the general formula of  $R_3SnX$  are powerful fungicides. Within any  $R_3SnX$  series, the activity is markedly dependent upon the nature of the organic group but relatively independent of the anionic radical [64-66].

The biological action of organotin(IV) complexes against bacterial strains and cancer cell lines depend on their geometry and types of ligands coordinated to tin atom. It is generally thought that the coordinated methanol molecule assisted the carriage of active triphenyltin(IV) to the active cell or active sites (receptor sites) which improved its biological activity [67].

The trialkyltin(IV) compound which has a total number of carbon atoms from 9-12 exhibited high antifungal activity [68]. Complexes of trialkyltin(IV) have been implemented in silicone curing [69], development of antifouling agents, polyurethane, and polyvinylchloride stabilization [70-74]. Organotin(IV) carboxylate complexes have momentous properties as anticancer drugs, antibacterial and antifungal agents [75].

The anticancer, antifungal and antibacterial properties of organotin(IV) based carboxylate complexes are linked to the nature and number of organic moieties linked to the Sn metal [76]. It is a well-documented fact that triorganotin(IV) based complexes

are being extra effective than their bi-analogs owing to more lipophilic character enabling them to cross the lipid layer of the cell membrane of microbes with more ease [77]. As the exploration of the diversity of the structure of organotin(IV) continues, some novel applications with better significance are being exposed which are related to medicinal uses [78]. Some of the triorganotin(IV) carboxylates showed high antitumor activities against various cancer cell lines like breast, colon, lungs, liver, and sarcoma cancer cells, etc. Remarkable activities by some of these compounds are shown competing with cis-platin [79-82].

### **1.5.2. Cancer**

Cancer, recognized by uncontrolled cell growth, is a reason for millions of deaths worldwide [83]. It is the leading cause of death after heart disease. In the USA every 4<sup>th</sup> mortality is due to cancer [84]. In the year 2005, cancer surpassed heart diseases in the USA. Chemotherapy is one of the strategies used to cure cancer.

Cisplatin was the primary inorganic cancer chemotherapeutic mediator, which remains a main and basic cure for different types of cancers [82, 83]. The clinical efficacy of cisplatin and associated drugs has been inadequate due to their substantial adverse side effects and rise resistance. So this is necessary to discover novel inorganic mediators to implement in cancer treatment with better efficiency with reduced noxious side effects. The best way is to discover new inorganic material by in-vitro screening, tracked by choosing the most active anticancer complexes, which is still the finest method of recognizing latent drug applicants. Platinum metallodrugs and non-platinum metallo-drugs have been developed as a pronounced covenant of attention in this regard. Among the non-platinum metal complexes, specific importance has been fixated on triorganotin(IV) complexes. Figure 1.22 showed cancer and its treatment methodologies. This triorganotin (IV) complexes interacts with cancerous cells either

through electrostatic or intercalation which is shown in the figures below 1.23 and 1.24 [84].

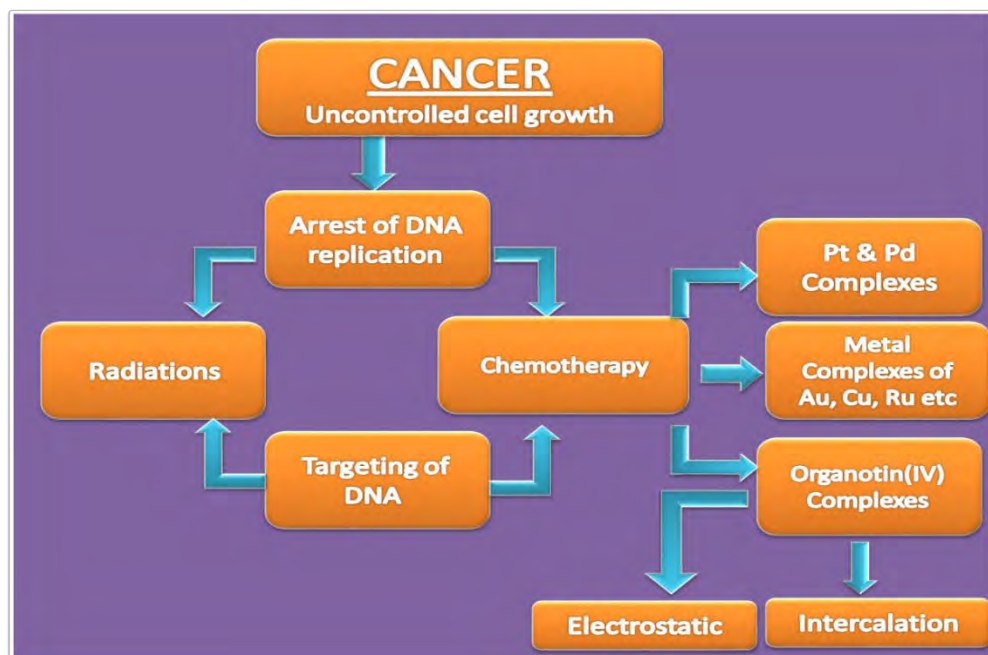


**Figure 1.22:** Cancer and its treatment methodology by chemotherapy and radiations.

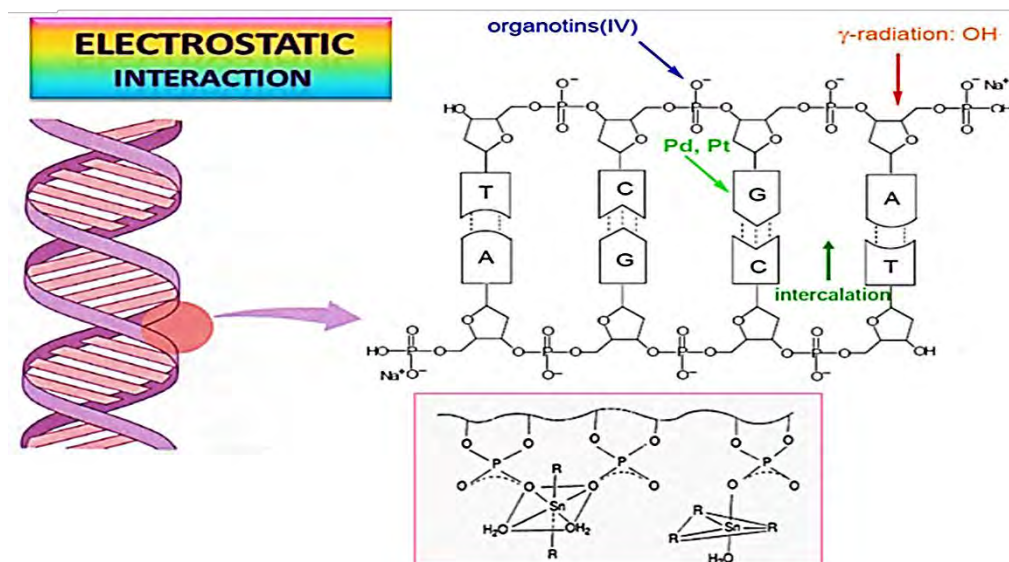


**Figure 1.23:** Electrostatic interactions of metal complexes with cancerous cells DNA and gamma radiations [85].

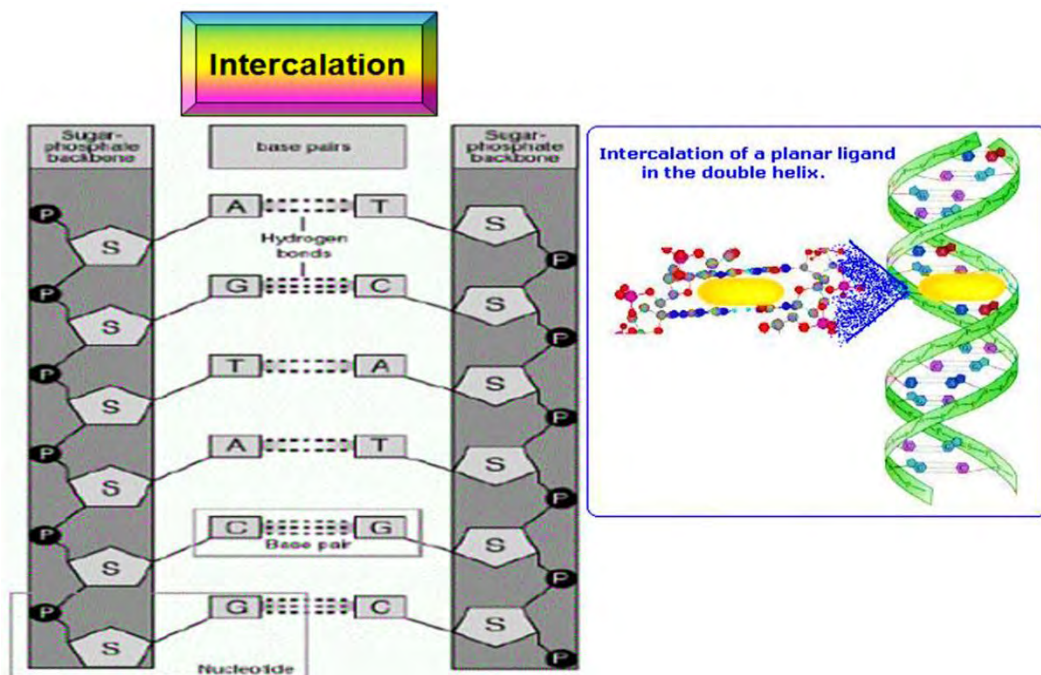


**Figure 1.24:** Intercalation interactions of metal complexes with cancerous DNA [85].

## What is breast cancer?

Normal Breast Cells

versus

Abnormal Breast Cells (Cancer)



### Normal Breast Cells

Look pretty much the same  
(the dark purple nucleus—the cell's brain—is in the same place within each cell)  
And are well organized



### Abnormal Breast Cells (Cancer)

Look different from each other  
(The dark purple nucleus—the cell's brain—is in the middle on some but on the side in others)  
The cells are disorganized and heaped up in a mass

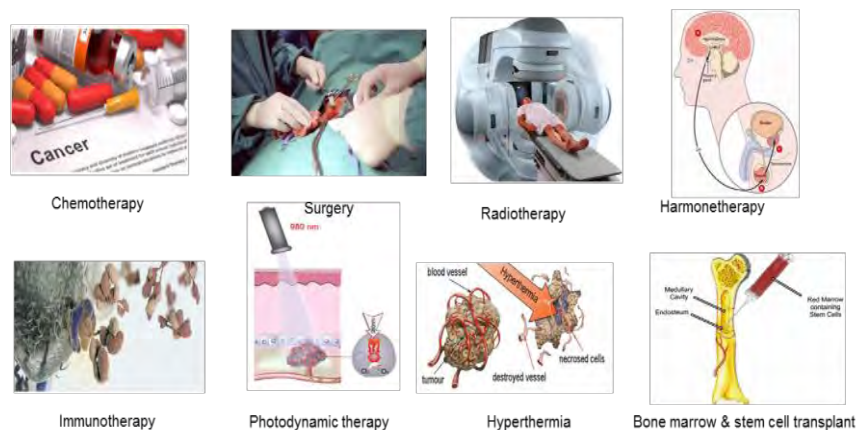


**Figure 1.25:** Breast Cancer and different types of cancer treatment [86, 87].

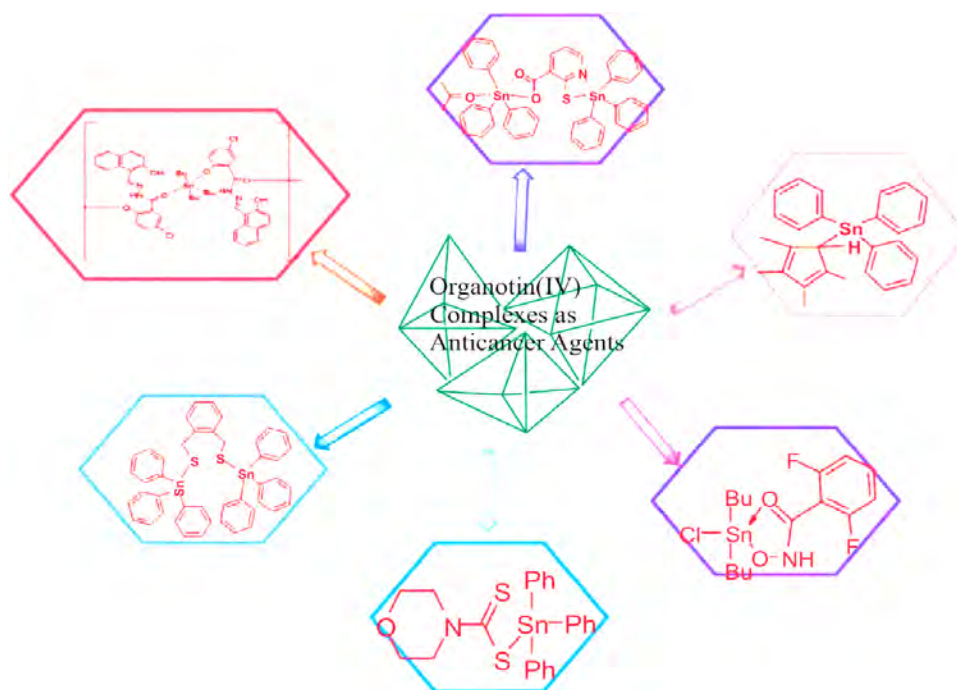


**Figure 1.26:** Organotin(IV) complexes in trial stages as an anticancer agent [88].

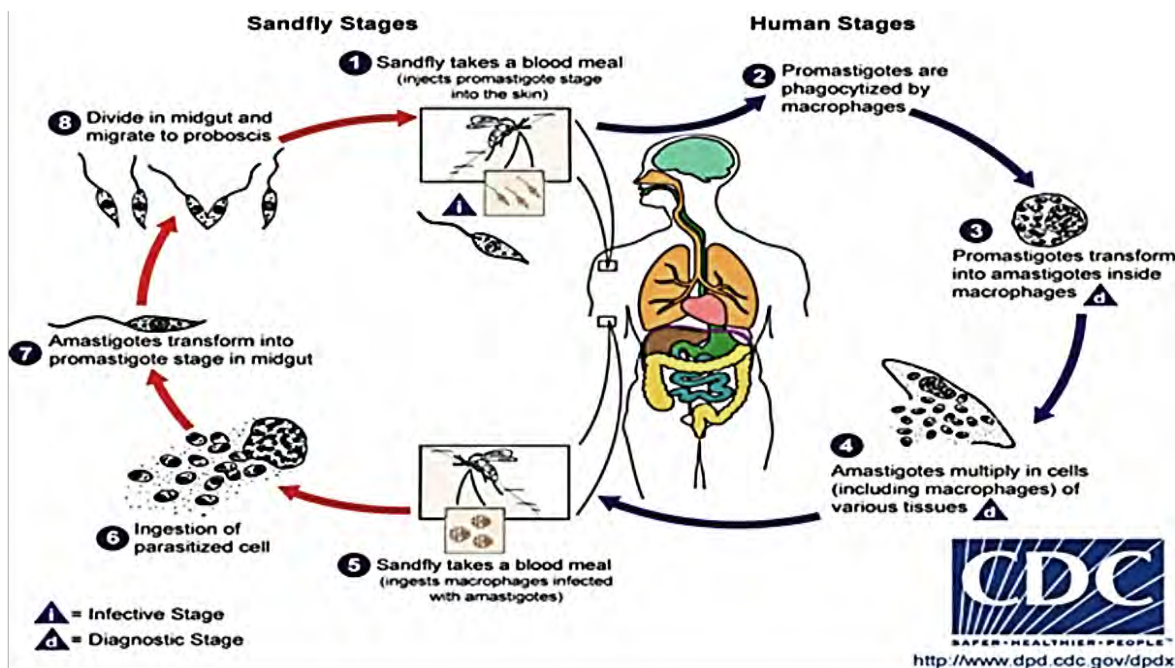
Chemotherapy with cytotoxic anticancer agents remains the backbone of treatment targeted at precise cellular mechanisms in menacing diseases. Gradually it is being used prior on in a patient's handling as an assistant to either operation or radiotherapy. The current era has seen the introduction of "targeted agents" into clinical usage with growing achievement. One of the groups of compounds are alkylating agents that work by the addition of an alkyl group to the guanine base of the deoxyribonucleic acid molecule, which stops the linking of the double helix of DNA. This causes rupturing of the DNA strands, disturbing the capability of the cancer cell to grow. Finally, the cancer cell dies. There are five traditional classes of alkylating agents, for example, nitrogen mustard (cyclophosphamide, chlorambucil), nitrosoureas (carmustine, streptozocin), alkyl sulfonates (busulfan), etc. Antitumor antibiotics are a different family of anticancer agents and they act principally by intercalation with deoxyribonucleic acid, instigating a block in the synthesis of deoxyribonucleic acid (DNA) and ribonucleic acid (RNA), or through other altered, further complex, and at a certain level yet ill-defined, mechanisms (especially anthracyclines, paromomycin, and bleomycin). Antimetabolites are anticancer drugs that stop the synthesis of deoxyribonucleic acid (DNA) by interfering with the enzymes or their reactions. They disturb the synthesis of deoxyribonucleic acid by acting as a substitute to the real metabolites that would be used in normal digestion. Examples of these types of drugs are methotrexate, fluoropyrimidines (e.g. 5FU, capecitabine), cytocinerabinose (e.g. cytarabine), etc. Antimicrotubule agents are the drugs that block cell growth by stopping cell division (mitosis). Antimicrotubule mediators interfere with microtubules which are cellular structures that assist the movement of chromosomes during cell division and in this way block the growth of cancer cells. The main examples are taxanes (docetaxel and paclitaxel), Vinca alkaloids (vincristine, vinorelbine, and vinblastine). Platinum

compounds mainly cisplatin, carboplatin, and oxaliplatin, etc, are used in the treatment of cancer [89-91].

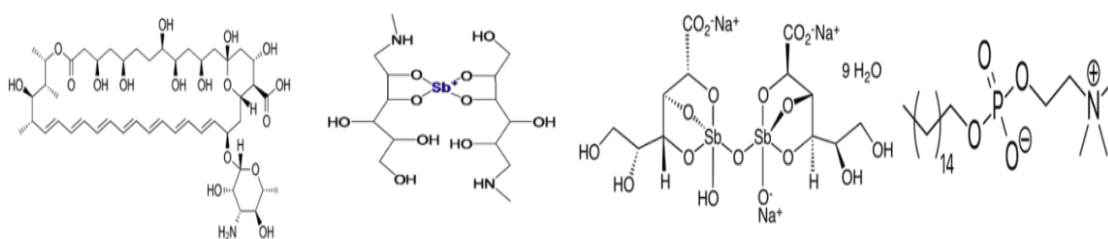
### **1.5.3. Leishmaniasis**

Leishmaniasis is a parasitic disease transmitted by the bite of sand flies. It is found in 88 countries of 5 continents (Asia, Africa, North America, South America, and Europe). Almost 350 million peoples are at risk of leishmaniasis. There are three types of this disease. The cutaneous form presents with skin ulcers, while the mucocutaneous form presents with ulcers of the skin, mouth, and nose, and the visceral form starts with skin ulcers and then later presents with fever, low red blood cells, and enlarged spleen and liver. Organotin(IV) carboxylates have also shown antileishmanial activity [92]. According to WHO, Leishmaniasis affects twelve million people that are the inhabitant of hot climatic areas. Appropriate treatment is vital during the growth of this sandy-fly mediated parasite disease otherwise patients may not be able to survive [93]. Scientists have developed several antileishmanial agents (e.g., Miltefosine, Amphotericin B, Glucantime, and Pentamidine), that were not effective due to fluctuating degrees of effectiveness and toxicity [94, 95]. The use of antimony salt displayed the worst condition [96]. Because of this, there is a dire need to develop a new chemotherapeutic agent to treat leishmaniasis. Amide-based organotin(IV) carboxylates may be one of the better alternate drugs against leishmaniasis. Antibiotic resistance is another leading problem because of various types of bacterial strains. In this context, metal-based drugs like organotin(IV) may play important role in eliminating drug resistance issues. Figure 1.28 showed the life cycle of leishmania parasite and different types of drugs used to treat this disease.





### Life cycle of Leishmania Parasite



**Liposomal Amphotericin B Meglumine antimoniate Sodium stibogluconate Miltefosine**

**Figure 1.27:** Cause and different types of drugs for Leishmania [97].

#### 1.5.4. Computational Studies

Geometry optimization of the complex structures was performed by density functional method in the Gaussian software package [98, 99]. The immobile points of the potential energy faces were located using the hybrid exchange density functional with Becke's three-parameter hybrid exchange functional (B3LYP) employing the LANL2DZ basis set [99, 100]. Computational studies serve herein as a supportive tool to the experimental data; the structural parameters of bond lengths and bond angles were

computed for comparison with the experimental values. The frontier orbital band gap energy ( $E_g$ ) and additional universal reactivity factors such as electronegativity, chemical hardness, and chemical potential were calculated through the Koopman's theorem from the highest energy molecular orbital (HOMO) and next highest energy orbital (LUMO) at the same level of theory [101]. The Mulliken atomic charge analysis was carried out to form a picture of charge distribution in the organotin carboxylates. Additionally, molecular electrostatic potential (MEP) faces have been studied to examine the electron-deficient and rich areas in the complexes.

Because of the above, we synthesized amide-based organotin(IV) carboxylates and characterized their physical and biological activities including anticancer, antileishmanial, antimicrobial, antioxidant activities, and computational details. These Complexes were also screened to evaluate their noncancerous, cytotoxic, and hemolytic activities. In the current manuscript, we present some notable and novel data regarding amide-based organotin(IV) carboxylates and their activities.

## **Chapter 2**

### **Materials and Methods/ Experimental**

## 2. Introduction

This chapter included the experimental procedures used to synthesize the ligands and organotin(IV) amide-based carboxylate complexes. This will also describe the physical methods used to characterize these compounds. The details of the synthetic methods are given here in detail to enable the reproduction of these compounds in the future. The chemicals used in the development of the synthetic procedures used in the synthesis of the ligands and complexes will be incorporated in the discussion. This was because these syntheses were a culmination of a series of experiments performed in which many parameters were altered.

### 2.1. Materials, Instrumentations and Techniques

Chemicals  $(\text{CH}_3)_3\text{SnCl}$ ,  $(\text{C}_4\text{H}_9)_3\text{SnCl}$ ,  $(\text{C}_6\text{H}_5)_3\text{SnCl}$ , 3,5-bis(trifluoromethyl)aniline, p-anisidine, 4-fluorobenzylamine, p-toluidine, 4-amino butanoic acid, maleic anhydride, succinic anhydride, phthalic anhydride, and sodium hydroxide were bought from Sigma Aldrich. The solvents were procured from Sigma Aldrich and were dried out according to the literature described in the previous paper [102]. The Melt-Temp (US) electrothermal melting apparatus was used to measure the melting points of ligands and synthesized complexes. Thermo Nicolet Impact series 10, instrument was used to record the FT-IR spectra from 4000 to 400  $\text{cm}^{-1}$  range. The elemental analysis data was collected on CE-440 Elemental Analyzer (Exeter Analytical, INc.).

$^1\text{H}$ NMR and  $^{13}\text{C}$ NMR (125 MHz) were measured using Bruker (600MHz) Avance III HD, INOVA 400MHz, INOVA 500MHz using DMSO,  $\text{CDCl}_3$ , and Methanol as internal referencing ( $^1\text{H}$ -DMSO- $d_6$ =2.5ppm and  $^{13}\text{C}$ -DMSO- $d_6$ =39.5ppm), ( $^1\text{H}$ - $\text{CDCl}_3$ =7.26 ppm and  $^{13}\text{C}$ - $\text{CDCl}_3$ =77.2ppm) and ( $^1\text{H}$ - $\text{CD}_3\text{OD}$ =4.87 and  $^{13}\text{C}$ - $\text{CD}_3\text{OD}$ =49.1). For  $^{119}\text{Sn}$  the measurement was recorded on Bruker (600MHz) Avance

III HD at a frequency of 223.81 Hz. Chemical shift ( $\delta$ ) values are specified in the ppm range and the values of coupling constants ( $J$ ) are given in the Hz. In the proton NMR ( $^1\text{H}$  NMR) the multiplicities of the signals are identified with the chemical shifts; (s=singlet, d=doublet, t=triplet, q=quartet, q=quintet, m=multiplet, dd=doublet of doublet) [103]. Bruker Apex II Cu source CCD diffractometer was used to collect the X-ray crystallographic data of complexes at 100(2) K. All the non-hydrogen atoms were refined anisotropically and hydrogen atoms bonded to carbon atoms were inserted at calculated positions using a riding model. Hydrogen atoms bonded to nitrogen and oxygen were calculated from different maps and their coordinates refined. ShelXT was used to solve the structure and ShelXL2014 to refine the structures [104].

## 2.2. Synthesis of Ligands

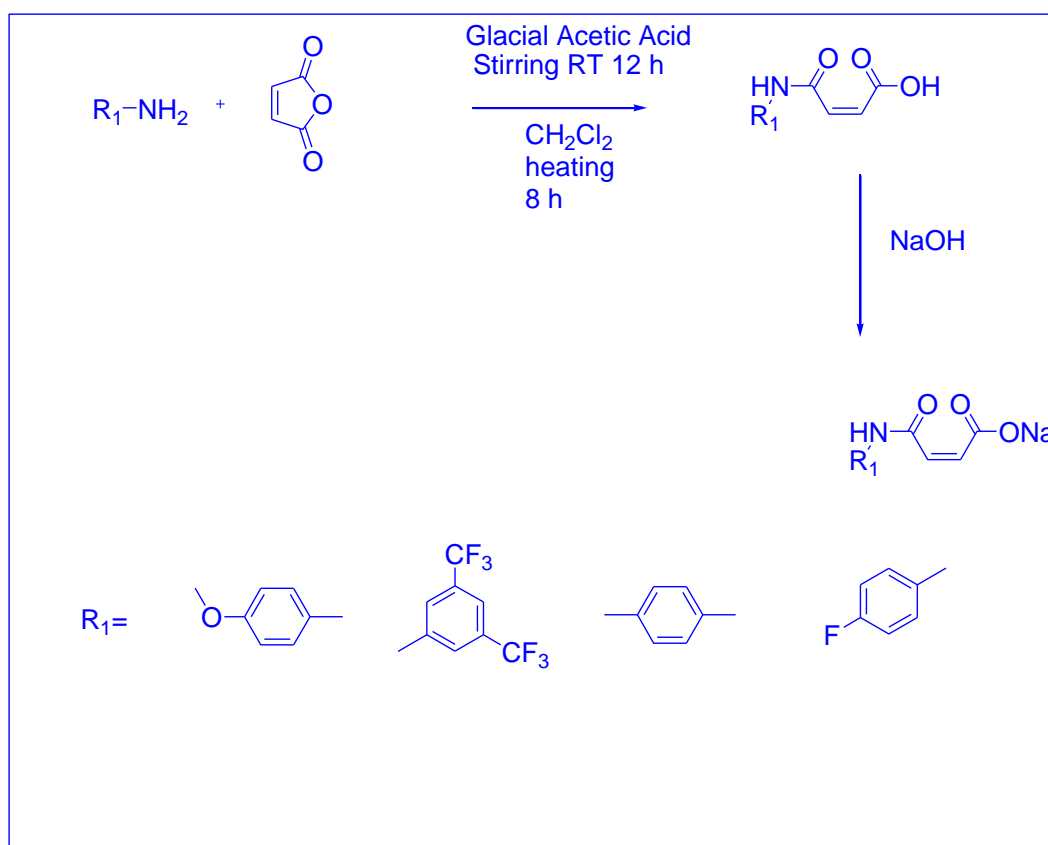
### 2.2.1. General procedures for the synthesis of ligands (scheme 1) **IL(1-4)**

For the synthesis of ligands (1-4) stoichiometric amounts of maleic anhydride and substituted amines (p-anisidine and p-toluidine) were dissolved separately in glacial acetic acid and similarly maleic anhydride and substituted amines (3,5-bis(trifluoromethyl)aniline on gentle heating and 4-fluorobenzylamine) were separately dissolved in dichloroethane. The anhydride solution was transferred to two necked round bottom flask (250 mL). The substituted amine solution was then added dropwise to maleic anhydride solution and the precipitates appeared. Some of the ligands were yellow and others were of white colors. The reaction mixture was stirred for 12 hours to complete the reaction. The precipitate was then filtered off, carefully washed with cold deionized water (to get rid of the unreacted maleic anhydride and maleic acid), and dilute (10%) hydrochloric acid (to get rid of the unreacted substituted aniline) and then dried in the open air. White or yellow powder crystals of **IL**<sup>1</sup>, **IL**<sup>2</sup>, **IL**<sup>3</sup>, and **IL**<sup>4</sup> were

developed at room temperature by gentle evaporation of acetone or ethanol solution [105].

### 2.2.2. Synthetic procedure for the salt of ligand **IL**(1-4)

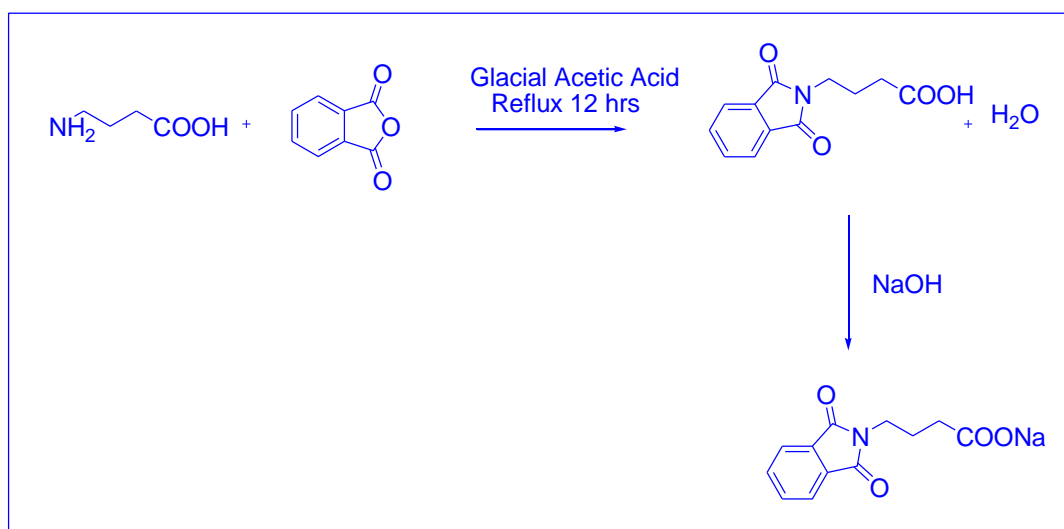
Synthesis of sodium salt of ligands: sodium 4-(p-toluidino)-4-oxobut-2-enoate, sodium 4-(1,3-dioxoisindolin-2-yl)butanoate, sodium (Z)-4-(p-toluidino)-4-oxobut-2-enoate and sodium (Z)-4-(4-fluorophenylamino)-4-oxobut-2-enoate: Sodium hydroxide dissolved in water is added to ligands(**IL**<sup>1</sup>, **IL**<sup>2</sup>, **IL**<sup>3</sup>, and **IL**<sup>4</sup>) solution suspended in DI water. The stirring is done for half an hour at room temperature until a clear solution appeared. The solution is then vaporized on rotary vapor to collect sodium salt of the ligands [106] (**Scheme 1**).



**Scheme 1:** Schematic representation of synthesis of ligands **IL**<sup>1</sup>-**IL**<sup>4</sup> and their sodium salts.

### 2.2.3. Synthetic procedure for the synthesis of ligands (Scheme 2) IL(5)

Stoichiometric amounts of glacial acetic acid were used for the dissolution of phthalic anhydride. The prepared solution was stored in two neck round bottom flask (250 ml). Glacial acetic acid was used for the dissolution of 4-amino butanoic and then added the solution dropwise to the already prepared anhydride solution. The precursor mixture was carried under reflux for six hours. After standing overnight the white precipitate appeared. The precipitate was the gathered through filtration, washed systematically using distilled water, and dilute HCl (to eradicate the unwanted maleic anhydride and maleic acid and unwanted aniline) and at last dried in air. Crystals like a white needle of (IL<sup>5</sup>) were grown in methanol solution by gentle evaporation method at 25 °C. The synthesis of salts of ligands is carried out in the same way as described in Scheme 1 [103] (Scheme 2).

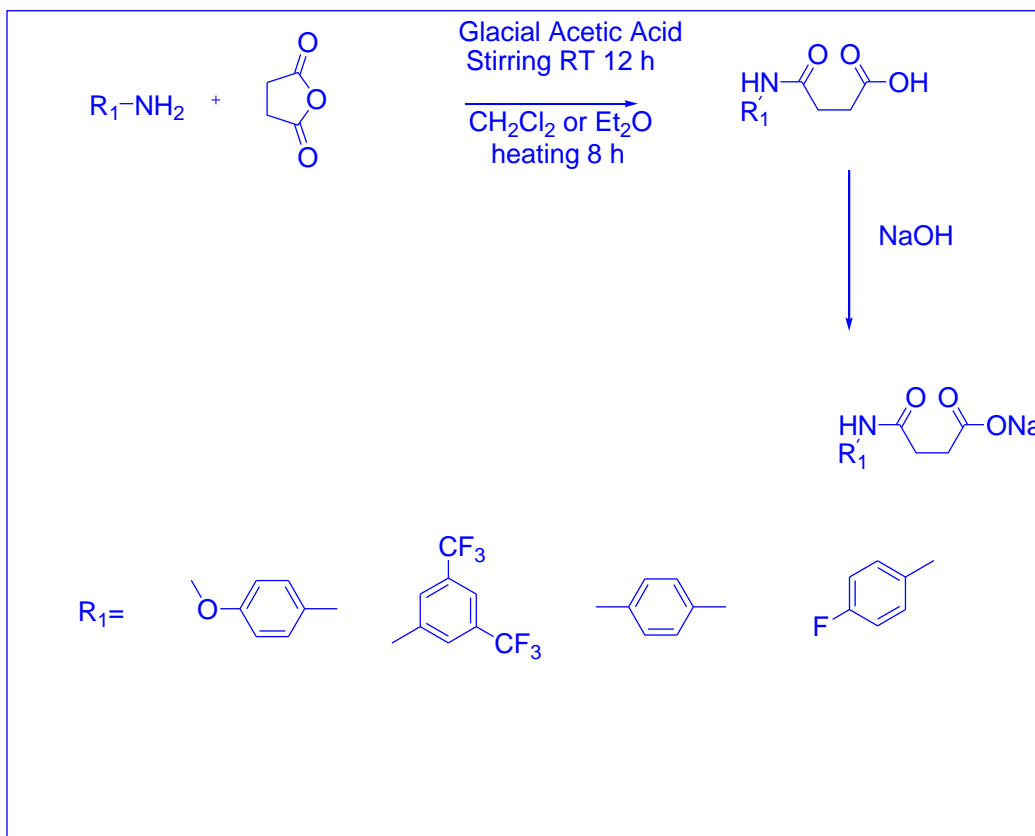


Scheme 2: Synthesis of ligand IL<sup>5</sup> and sodium salt of the ligand.

#### 2.2.4. Synthetic procedure for the synthesis of ligands (Scheme 3) IL(6-8)

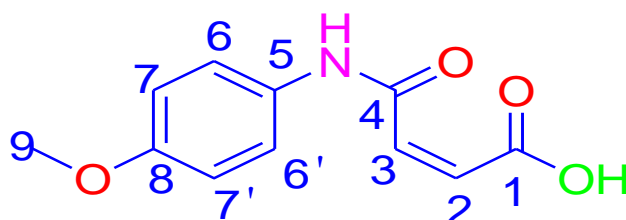
Stoichiometric amounts of succinic anhydride and substituted amines (p-anisidine and p-toluidine) having 1:1 ratio were dissolved separately in glacial acetic acid and similarly, maleic anhydride and substituted amines (3,5-bis(trifluoromethyl)aniline on gentle heating and 4-fluorobenzylamine) were separately dissolved in dichloroethane and diethyl ether. The succinic anhydride solution was transferred to two neck round bottom flask (250ml). The substituted amines solution was then added dropwise to the anhydride solution. The reaction mixture was stirred for 12 hours or under gentle heating for 8 hours. After standing overnight the precipitate appeared. The precipitate was gathered through filtration, washed systematically used with distilled water and HCl (to eradicate the unwanted maleic anhydride and maleic acid and unwanted aniline), and then at last dried in air. Crystals like a white needle of ligands were synthesized and grown in methanol-acetone solution by gentle evaporation method at 25 °C. The synthesis of salts of ligands is carried out in the same way as described in scheme 1 (Scheme 3).





Scheme 3: Synthesis of ligands **IL<sup>6</sup>-IL<sup>9</sup>** and their sodium salts.

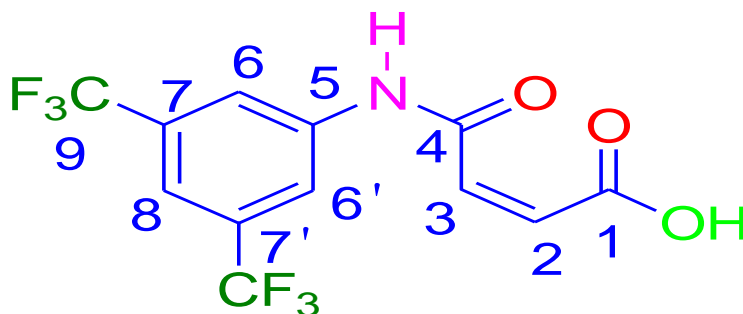
### 1. Z-4-(4-methoxyphenylamino)-4-oxobut-2-enoic acid (**IL<sup>1</sup>**)



**C<sub>11</sub>H<sub>11</sub>NO<sub>4</sub>**: Yield: 1.6 g, 89%; M.P. 199-200 °C; Mol. Wt: 221.07 g/mol. FT-IR (4000 to 400 cm<sup>-1</sup>): 3284 ν (O-H); 3124 ν (N-H); 1695 ν (amide carbonyl HN-C=O); 1537 ν (COO)<sub>asym</sub>; 1278 ν (COO)<sub>sym</sub>; 259 Δν. <sup>1</sup>H NMR (500 MHz; DMSO-d<sub>6</sub>): δ (ppm) 6.29 (d, H<sub>2</sub>,1H, <sup>3</sup>J(<sup>1</sup>H, <sup>1</sup>H)=12.14; 6.46 (d,H<sub>3</sub>,1H, <sup>3</sup>J(<sup>1</sup>H, <sup>1</sup>H)=12.16 ; 7.49 (d,H<sub>6</sub>,6, 2H, <sup>3</sup>J(<sup>1</sup>H,<sup>1</sup>H) =9.08; 6.89 (d,H<sub>7</sub>,7, 2H, <sup>3</sup>J(<sup>1</sup>H,<sup>1</sup>H)= 9.11; 3.75 (s, H<sub>9</sub>,3H) ; 10.40 (s,1H,NH); 13.5 (s,1H,COOH). <sup>13</sup> C NMR (125.8 MHz; DMSO-d<sub>6</sub>): δ (ppm) 168.3 (C1); 132.6

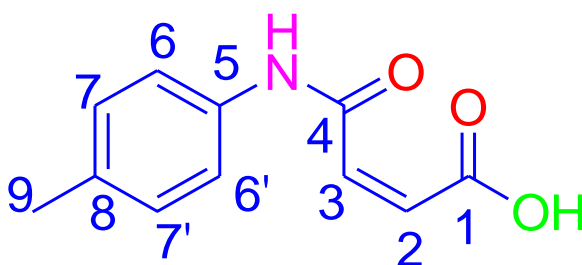
(C2); 131.9 (C3); 163.2 (C4); 131.7 (C5); 121.6 (C6); 114.4 (C7); 156.3 (C8) ; 55.6 (C9).

**2. (Z)-4-(3,5-bis(trifluoromethyl)phenylamino)-4-oxobut-2-enoic acid (IL<sup>2</sup>):**



**C<sub>12</sub>H<sub>7</sub>F<sub>6</sub>NO<sub>3</sub>**: Yield: 1.31 g, 85%; M.P.153 °C: Mol. Wt: 327.18 g/mol: FT-IR (4000 to 400 cm<sup>-1</sup>): 3286 v (O-H); 3102 v (N-H); 1711 v (amide carbonyl HN-C=O); 1569 v (COO)<sub>asym</sub>; 1278 v (COO)<sub>sym</sub>; 291 Δv. <sup>1</sup>H NMR (400 MHz; CD<sub>3</sub>OD): δ (ppm) 6.38 (d,H2, 1H, <sup>3</sup>J(<sup>1</sup>H, <sup>1</sup>H)=11.88; 6.50 ( d,H3,1H, <sup>3</sup>J(<sup>1</sup>H, <sup>1</sup>H)=11.90; 8.32 (s,H6,6, 2H) ; 7.84 (s,H8,1H) ; 10.89 (s,1H,NH) ; 12.90 (s,1H,COOH). <sup>13</sup>CNMR (125 MHz; CD<sub>3</sub>OD): δ (ppm) 172.4 (C1); 130.5 (C2); 140.5 (C3); 166.7 (C4); 132.5 (C5); 119.7 (C6) ; 131.9 (C7); 118.7 (C8); 124.5 (C9). <sup>19</sup>F NMR (375 MHz; CDCl<sub>3</sub>): δ (ppm) -57.

**3. (Z)-4-(p-toluidino)-4-oxobut-2-enoic acid (IL<sup>3</sup>):**

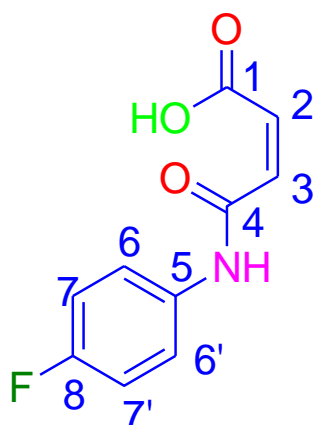


**C<sub>11</sub>H<sub>11</sub>NO<sub>3</sub>**:

Yield: 1.4 g, 82%; M.P. 180-181<sup>0</sup>C: Mol. Wt: 205.21 g/mol. FT-IR (4000 to 400 cm<sup>-1</sup>): 3284 v (O-H); 3211 v (N-H); 1695 v (HN-C=O); 1505 v (COO)<sub>asym</sub>; 1325 v

(COO)<sub>sym</sub>: 180 Δv. <sup>1</sup>H NMR (500 MHz; DMSO-d<sub>6</sub>): δ (ppm) 6.30 (d, H<sub>2</sub>,1H, <sup>3</sup>J(<sup>1</sup>H,<sup>1</sup>H)=12.04 Hz; 6.46 (d,H<sub>3</sub>,1H, <sup>3</sup>J(<sup>1</sup>H,<sup>1</sup>H)=12.07 Hz ; 7.50 (d,H<sub>6</sub>,6, 2H, <sup>3</sup>J(<sup>1</sup>H,<sup>1</sup>H)=8.42 Hz ; 6.78 (d,H<sub>7</sub>,7, 2H, <sup>3</sup>J(<sup>1</sup>H,<sup>1</sup>H)=8.46 Hz ; 2.24 (s, H<sub>9</sub>,3H) ; 10.36 (s,1H,NH) ; 13.26 (s,1H,COOH). <sup>13</sup>CNMR (125 MHz; DMSO-d<sub>6</sub>) δ: 172.1 (C1); 135.9 (C2); 141.1 (C3); 168.2 (C4); 136.7 (C5); 124.8 (C6); 134.4 (C7); 138.2 (C8); 25.7 (C9).

**4. (Z)-4-(4-fluorophenylamino)-4-oxobut-2-enoic acid (IL<sup>4</sup>):**

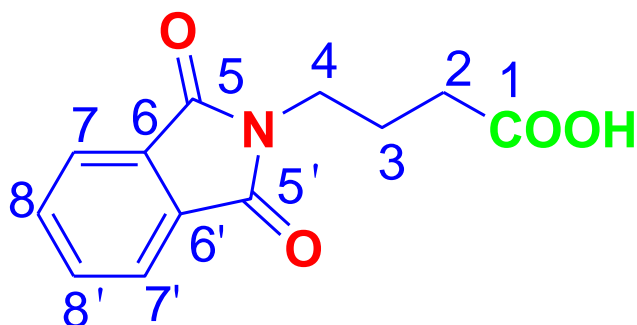


**C<sub>10</sub>H<sub>8</sub>FNO<sub>3</sub>:**

Yield: 1.54 g, 90%; M.P. 213<sup>0</sup>C: Mol. Wt: 209.05 g/mol. FT-IR (4000 to 400 cm<sup>-1</sup>): 3294 ν (O-H); 3222 ν (N-H); 1698 ν (HN-C=O); 1485 ν (COO)<sub>asym</sub>; 1225 ν (COO)<sub>sym</sub>: 260 Δv. <sup>1</sup>H NMR (500 MHz, CDCl<sub>3</sub>): δ (ppm) 6.34 (d, H<sub>2</sub>,1H, <sup>3</sup>J(<sup>1</sup>H,<sup>1</sup>H)=12.08 Hz; 6.45 (d,H<sub>3</sub>,1H, <sup>3</sup>J(<sup>1</sup>H,<sup>1</sup>H)=12.08 Hz ; 7.62 (dd,H<sub>6</sub>,6, 2H, <sup>4</sup>J and <sup>3</sup>J(<sup>1</sup>H,<sup>19</sup>F: <sup>1</sup>H,<sup>1</sup>H) = 5.03 Hz, 9.16 Hz; 7.16 (t,H<sub>7</sub>,7, 2H, <sup>3</sup>J(<sup>1</sup>H,<sup>19</sup>F; <sup>1</sup>H,<sup>1</sup>H)= 8.94 Hz,8.94 Hz; 10.41 (s,1H,NH) ; 13.23 (s,1H,COOH). <sup>13</sup>CNMR (CDCl<sub>3</sub>, 125 Hz) δ (ppm): 172 (C1); 135.4 (C2); 140.2 (C3); 168.3 (C4); 136.9 (C5); 126.5 (C6); 120.7 (C7) ; 162.5 (C8).

<sup>19</sup>F NMR (CDCl<sub>3</sub>, 375 MHz): δ (ppm) -114

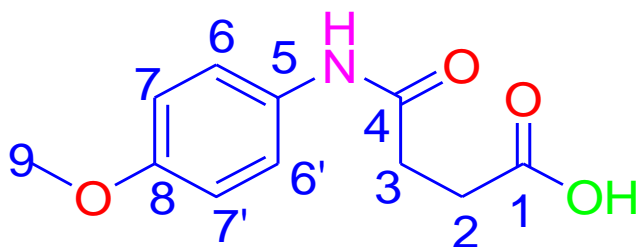
**5. 4-(1,3-dioxoisindolin-2-yl)butanoic acid (IL<sup>5</sup>):**



**C<sub>12</sub>H<sub>11</sub>NO<sub>4</sub>:**

Yield: 2.1 g, 82%; M.P. 116-118<sup>0</sup>C: Mol. Wt: 235.06 g/mol. FT-IR (4000 to 400 cm<sup>-1</sup>): 3270 v (O-H); 1765 v (HN-C=O); 1699 v (COO)<sub>asym</sub>; 1394 v (COO)<sub>sym</sub>; 305 Δv. <sup>1</sup>H NMR (400 MHz: DMSO-d<sub>6</sub>): δ (ppm) 2.04 (t,H<sub>2</sub>,2H) <sup>3</sup>J (<sup>1</sup>H, <sup>1</sup>H)=7.34 Hz ; 1.66-1.60 (qn,H<sub>3</sub>,2H) <sup>3</sup>J (<sup>1</sup>H, <sup>1</sup>H)=7.10 Hz; 3.39 (t,H<sub>4</sub>,2H, <sup>3</sup>J (<sup>1</sup>H,<sup>1</sup>H) =19.7 Hz; 7.46-7.40 (m,H<sub>7</sub>,7 & H<sub>8</sub>,8, 4H); 10.45 (s,1H,COOH). <sup>13</sup>C NMR (DMSO-d<sub>6</sub>,125.8 MHz): δ (ppm) 175.3 (C1); 32.4 (C2); 23.7 (C3); 37.3 (C4); 168.4 (C5); 132.1 (C6); 123.4 (C7); 134.7 (C8).

**6. 4-(4-methoxyphenylamino)-4-oxobutanoic acid (IL<sup>6</sup>):**

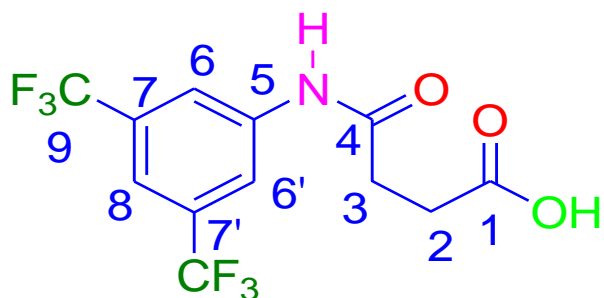


**C<sub>11</sub>H<sub>13</sub>NO<sub>4</sub>:**

Yield: 78% (1.6 g): M.P. 166-168 °C: Mol. Wt: 223.23 g/mol. FT-IR (4000 to 400 cm<sup>-1</sup>): 3284 v (O-H); 3124 v (N-H); 1695 v (HN-C=O); 1537 v (COO)<sub>asym</sub>; 1278 v(COO)<sub>sym</sub>; 259 Δv. <sup>1</sup>H NMR (400 MHz, DMSO-d<sub>6</sub>): δ (ppm) 2.45 ( t,H<sub>2</sub>,2H, <sup>3</sup>J (<sup>1</sup>H,

$^1\text{H}$ )=6.14; 2.32 (t, H3,2H,  $^3J(^1\text{H}, ^1\text{H})=6.14$ ; 7.44 (d,H6,6, 2H,  $^3J(^1\text{H}, ^1\text{H})= 9.04$ ; 6.82 (d,H7,7, 2H,  $^3J(^1\text{H}, ^1\text{H}) =9.05$ ; 3.6 (s, H9,3H) ; 9.76 (s,1H,NH); 12.10 (s,1H,COOH).  
 $^{13}\text{C}$  NMR (DMSO- $d_6$ , 125.8 MHz):  $\delta$  (ppm) 174.4 (C1); 32.8 (C2); 30.6 (C3); 170.2 (C4); 132.9 (C5); 121.8 (C6); 114.2 (C7); 156.4 (C8); 55.5 (C9).

**7. 4-(3,5-bis(trifluoromethyl)phenylamino)-4-oxobutanoic acid (IL<sup>7</sup>):**

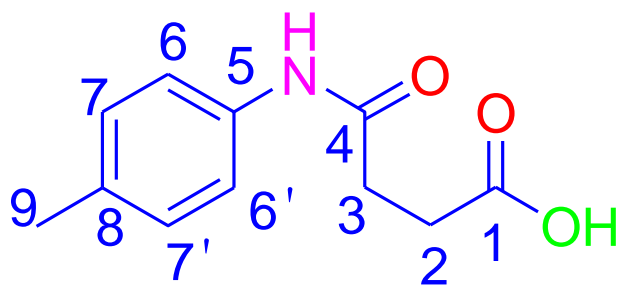


**C<sub>12</sub>H<sub>9</sub>F<sub>6</sub>NO<sub>3</sub>:**

Yield: 1.31 g, 85%; M.P.153 °C: Mol. Wt: 329.2 g/mol: FT-IR (4000 to 400  $\text{cm}^{-1}$ ): 3286  $\nu$  (O-H); 3102  $\nu$  (N-H); 1711  $\nu$  (HN-C=O); 1569  $\nu$  (COO)<sub>asym</sub>; 1278  $\nu$  (COO)<sub>sym</sub>: 291  $\Delta\nu$ .  $^1\text{H}$  NMR (400 MHz; DMSO- $d_6$ ):  $\delta$  (ppm) 2.67 ( t,H2,2H,  $^3J(^1\text{H}, ^1\text{H})=6.29$  ; 2.52 (t, H3,2H,  $^3J(^1\text{H}, ^1\text{H})= 5.98$ ; 8.16 (s,H6,6,2H) ; 7.67 (s,H8,1H) ; 10.62 (s,1H,NH) ; 12.16 (s,1H,COOH).  $^{13}\text{C}$  NMR (125 MHz; DMSO- $d_6$ ):  $\delta$  (ppm) 174.2 (C1); 32.8 (C2); 30.3 (C3); 172 (C4) ; 141.5 (C5); 119.9 (C6);131.5 (C7); 117.1 (C8); 124.8 (C9).

$^{19}\text{F}$  NMR (375 MHz; DMSO- $d_6$ ):  $\delta$  (ppm) -62.

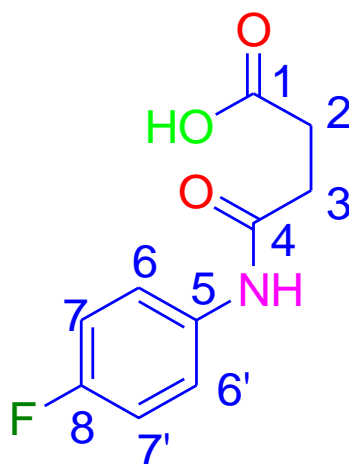
#### 8. 4-(p-toluidino)-4-oxobutanoic acid (IL<sup>8</sup>):



#### C<sub>11</sub>H<sub>13</sub>NO<sub>3</sub>:

Yield: 1.72 g, 95%; M.P. 176-179 °C; Mol. Wt: 207.23 g/mol. FT-IR (4000 to 400 cm<sup>-1</sup>): 3284 v (O-H); 3211 v (N-H); 1695 v (HN-C=O); 1505 v (COO)<sub>asym</sub>; 1325 v (COO)<sub>sym</sub>; 180 Δv. <sup>1</sup>H NMR (500 MHz; DMSO-d<sub>6</sub>): δ (ppm) 2.59 (t, H<sub>2</sub>, 2H, <sup>3</sup>J(<sup>1</sup>H, <sup>1</sup>H)=6.27; 2.47 (t, H<sub>3</sub>, 2H, <sup>3</sup>J(<sup>1</sup>H, <sup>1</sup>H)=5.98; 7.41 (d, H<sub>6</sub>, 6, 2H, <sup>3</sup>J(<sup>1</sup>H, <sup>1</sup>H)=8.37 Hz; 7.04 (d, H<sub>7</sub>, 7, 2H, <sup>3</sup>J(<sup>1</sup>H, <sup>1</sup>H)=8.34 Hz; 2.20 (s, H<sub>9</sub>, 3H); 9.8 (s, 1H, NH); 12.1 (s, 1H, COOH). <sup>13</sup>C NMR (125 MHz, DMSO-d<sub>6</sub>): δ (ppm) 174.4 (C1); 32.5 (C2); 30.3 (C3); 170.3 (C4); 137.3 (C5); 119.4 (C6); 129.5 (C7); 132.1 (C8); 21 (C9).

#### 9. 4-(4-fluorophenylamino)-4-oxobutanoic acid (IL<sup>9</sup>):



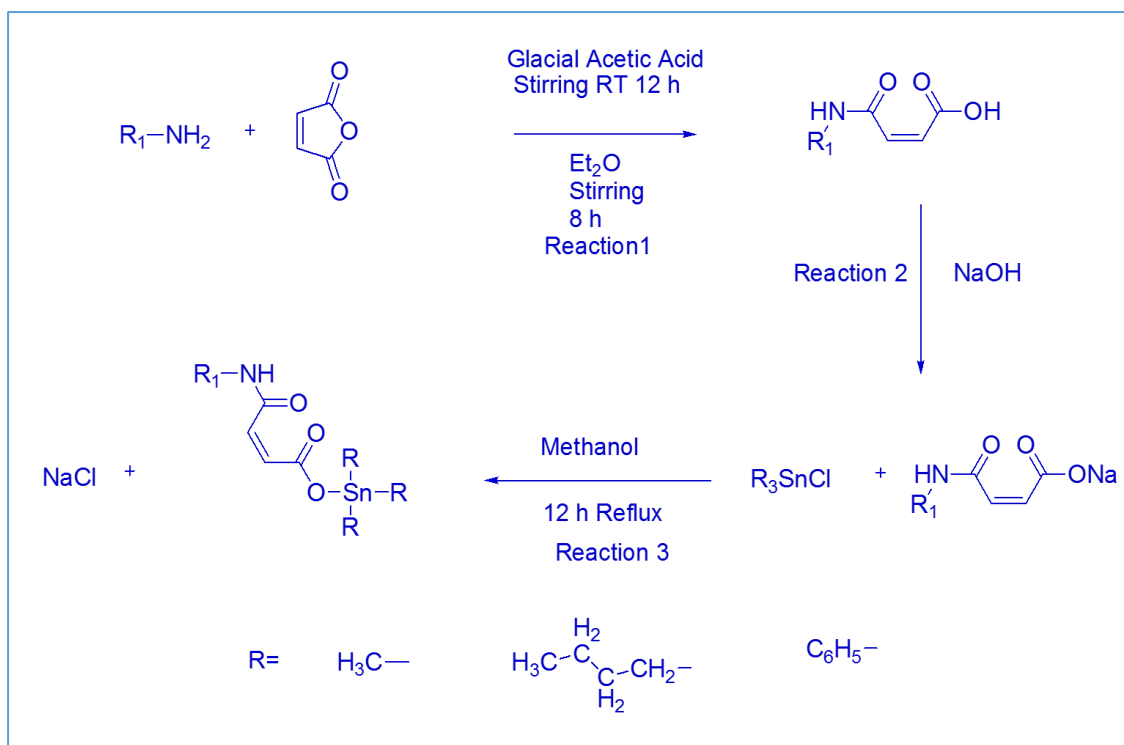
**C<sub>10</sub>H<sub>10</sub>FNO<sub>3</sub>:**

Yield: 1.54 g, 90%; M.P. 213<sup>0</sup>C; Mol. Wt: 211.11 g/mol. FT-IR (4000 to 400 cm<sup>-1</sup>): 3294 v (O-H); 3222 v (N-H); 1698 v (HN-C=O); 1485 v (COO)<sub>asym</sub>; 1225 v (COO)<sub>sym</sub>; 260 Δv. <sup>1</sup>H NMR (500 MHz; DMSO-d<sub>6</sub>): δ (ppm) 2.56 (t, H<sub>2</sub>, 2H, <sup>3</sup>J(<sup>1</sup>H, <sup>1</sup>H)=6.29; 2.52 (t, H<sub>3</sub>, 2H, <sup>3</sup>J(<sup>1</sup>H, <sup>1</sup>H)= 5.98; 7.56 (dd, H<sub>6</sub>, 6, 2H, <sup>3</sup>J(<sup>1</sup>H, <sup>19</sup>F; <sup>1</sup>H, <sup>1</sup>H)=5.02 Hz, 9.21 Hz ; 7.09 (t, H<sub>7</sub>, 7, 2H, <sup>3</sup>J(<sup>1</sup>H, <sup>1</sup>H; <sup>1</sup>H, <sup>19</sup>F) =8.95 Hz, 8.95 Hz ; 10.04 (s, 1H, NH) ; 12.19 (s, 1H, COOH). <sup>13</sup>C NMR (125 MHz; DMSO-d<sub>6</sub>): δ (ppm) 175.2 (C1); 32.4 (C2); 30.2 (C3); 171.4 (C4); 136.1 (C5); 121 (C6); 115.6 (C7); 159.1 (C8).

<sup>19</sup>F NMR (375 MHz; CDCl<sub>3</sub>): δ (ppm) -115.

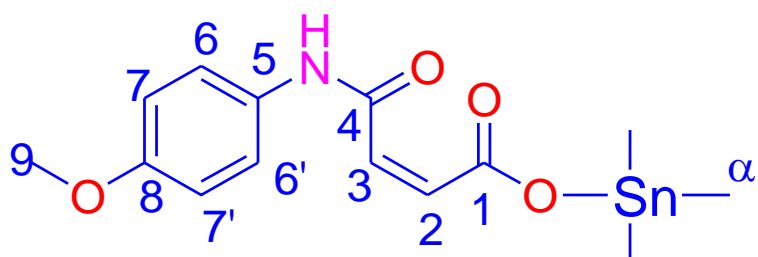
### **2.2.5 General procedure for the Synthesis of triorganotin(IV) amide-based carboxylates complexes**

Triorganotin(IV) based carboxylates were synthesized by refluxing equimolar amount of R<sub>3</sub>SnCl (R=Phenyl, methyl, and butyl) and sodium salt of the ligands in dry methanol for 12 hours. The solution was left for one night at room temperature. The sodium salt was precipitated out and removed by filtration and the solution was evaporated by rotary vapor to get our desired products. The solid was then dissolved in acetone and acetonitrile and the remaining sodium chloride was allowed to precipitate out and removed. The powdered product was obtained by slow evaporation. The products were then purified by recrystallization from chloroform, acetone, or a mixture of n-hexane and chloroform or acetone[107-109].



Scheme 4: Synthesis procedure for the synthesis of organotin(IV) amide-based carboxylates.

### 1. (Z)-trimethylstannyl 4-(4-methoxyphenylamino)-4-oxobut-2-enoate



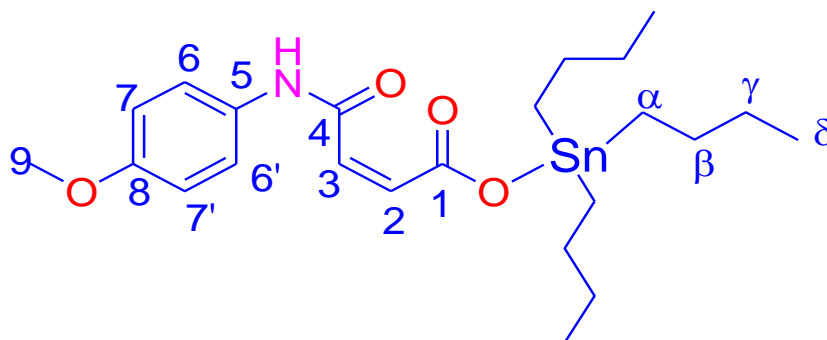
Yield: 0.62 g, 78%; M.P. 158°C: Mol. Wt: 385.07 g/mol: Elemental analytical cal. for  $C_{14}H_{19}NO_4Sn$ : C: 43.70 (43.79); H: 5.10 (4.99); N: 3.72 (3.65). FT-IR (4000 to 400  $cm^{-1}$ ): 3468  $\nu$  (N-H); 1711  $\nu$  (HN-C=O); 1547  $\nu$  (COO)<sub>asym</sub>; 1308  $\nu$  (COO)<sub>sym</sub>; 239  $\Delta\nu$ ; 530  $\nu$  (Sn-C); 460  $\nu$  (Sn-O).  $^1H$  NMR ( $CD_3OD-d_6$ , 300 MHz)  $\delta$  (ppm): 6.23 (d, H2, 1H,  $^3J(^1H, ^1H)=13.45$ ); 6.29 (d, H3, 1H,  $^3J(^1H, ^1H)=13.44$ ); 6.72 (d, H6, 6, 2H,  $^3J(^1H, ^1H)$ )



=12.59 ; 6.29 (d,H7,7, 2H,  $^3J(^1\text{H},^1\text{H})=13.44$ ; 3.80 (s, H9,3H) ; 11.6 (s,1H,NH); 0.67 (s,H $\alpha$ ,3H)  $^2J[^{119}\text{Sn}-^1\text{H}\alpha]=57\text{Hz}$ ),  $^{13}\text{C}$ NMR (CD<sub>3</sub>OD-d<sub>6</sub>, 125.8 MHz)  $\delta$  (ppm): 171.4 (C1); 131.9 (C2); 138.7 (C3); 162.1 (C4); 122.1 (C5); 113.7 (C6); 131.4 (C7); 156.4 (C8); 55.5 (C9); -2.07 (C $\alpha$ )  $^1J[^{119}\text{Sn}-^{13}\text{C}\alpha]=446\text{ Hz}$ ..

$^{119}\text{Sn}$  NMR (CD<sub>3</sub>OD, 225 MHz)  $\delta$  (ppm) = -46.

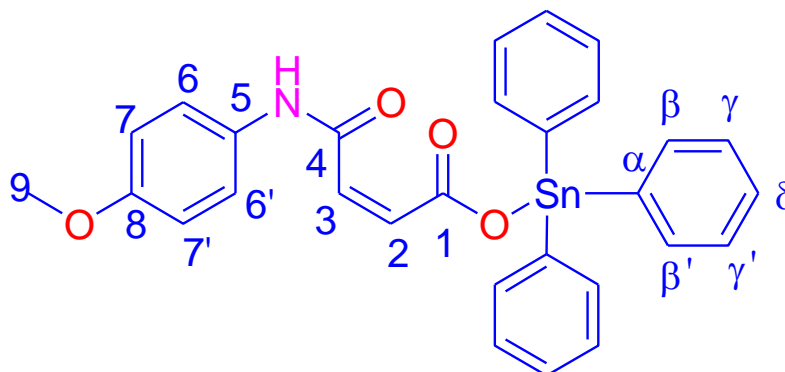
## 2. (Z)-tributylstannyl 4-(4-methoxyphenylamino)-4-oxobut-2-enoate



Yield: 0.82 g, 78%; M.P. 90°C: Mol.Wt: 511.17 g/mol: Elemental analytical cal. for C<sub>23</sub>H<sub>37</sub>NO<sub>4</sub>Sn: C: 54.2 (54.14); H: 7.26 (7.31); N: 2.78 (2.75). FT-IR (4000 to 400 cm<sup>-1</sup>): 3327 v (N-H); 1693 v (HN-C=O); 1570 v (COO)<sub>asym</sub>; 1289 v (COO)<sub>sym</sub>; 281  $\Delta$ v; 523 v (Sn-C); 470 v (Sn-O).  $^1\text{H}$ NMR (CDCl<sub>3</sub>, 400 MHz)  $\delta$  (ppm): 6.42 (d,H2,1H,  $^3J(^1\text{H},^1\text{H})$ ); 6.46; 6.86 (d,H3,1H)  $^3J(^1\text{H},^1\text{H})=6.46$ ; 7.52 (s,H6,6,2H) ,  $^3J(^1\text{H},^1\text{H})=7.80$ ; 6.89 (s,H7,7,2H) ,  $^3J(^1\text{H},^1\text{H})=7.80$ ; 3.73 (s,H9,3H); 12.9 (s,NH,H4); 1.30 (t, H $\alpha$ ,2H,)  $^3J(^1\text{H},^1\text{H})$ ; 7.3,  $^2J[^{119}\text{Sn}-^1\text{H}\alpha]=59\text{Hz}$ ; 1.36-1.30 (m, H $\beta$ ,2H); 1.64-1.60 (m, H $\gamma$ ,2H); 0.89 (t,H $\delta$ ,3H)  $^3J(^1\text{H},^1\text{H})=7.33$ .  $^{13}\text{C}$ NMR (CDCl<sub>3</sub>, 125.8 MHz)  $\delta$  (ppm): 172.1 (C1); 131.6 (C2); 138 (C3); 162 (C4) ; 127.9 (C5) ; 121.3 (C6); 114 (C7); 156 (C8); 55.4 (C9); 17 (C $\alpha$ )  $^1J[^{119}\text{Sn}-^{13}\text{C}\alpha]=365\text{ Hz}$ ; 25 (C $\beta$ )  $^2J[^{119}\text{Sn}-^{13}\text{C}\beta]=75\text{ Hz}$ ; 27.7 (C $\gamma$ )  $^3J[^{119}\text{Sn}-^{13}\text{C}\gamma]=24\text{ Hz}$ ; 13.5 (C $\delta$ ).

$^{119}\text{Sn}$  NMR (CDCl<sub>3</sub>, 225 MHz)  $\delta$  (ppm) = 136.

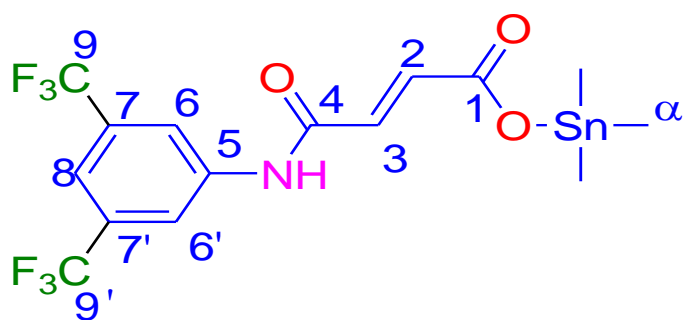
### 3. (Z)-Triphenylstannyl 4-(4-methoxyphenylamino)-4-oxobut-2-enoate



Yield: 0.93 g, 81%; M.P. 102°C: Mol. Wt: 570.22 g/mol: Elemental analytical cal. for  $C_{29}H_{25}NO_4Sn$ : C: 60.92(61.01); H: 4.54 (4.42); N: 2.54 (2.46): FT-IR (4000 to 400  $cm^{-1}$ ): 3124 v (N-H); 1727 v (HN-C=O); 1562 v (COO)asym; 1303 v (COO)sym; 259  $\Delta$ v; 510 v (Sn-C); 447 v (Sn-O).  $^1H$ NMR (DMSO- $d_6$ , 500 MHz)  $\delta$  (ppm): 5.94 (d,H2,1H,  $^3J(^1H,^1H)=13.34$  Hz); 6.14 (d,H3,1H,  $^3J(^1H,^1H)=13.4$  Hz); 7.52 (d,H6,6, 2H,  $^3J(^1H,^1H)=8.82$  Hz); 7.10 (d, H7,7,2H,  $^3J(^1H,^1H)=8.82$  Hz); 7.46-7.56 (m,10H, aromatic); 7.84-7.92 (m,5H,aromatic); 3.78 (s, H9,3H); 10.32 (s,1H,NH).  $^{13}C$ NMR (DMSO- $d_6$ , 125 MHz)  $\delta$  (ppm): 170.1 (C1); 133.4 (C2); 139.70 (C3); 167.3 (C4); 132.4 (C5); 122.7 (C6); 119.5 (C7); 156.6 (C8); 55.4 (C9); 138.4 (C $\alpha$ )  $^1J(^{119}Sn-^{13}C\alpha)=542$  Hz]; 134.4 (C $\beta,\beta'$ )  $^2J(^{119}Sn-^{13}C\beta,\beta')=47$  Hz; 127.2 (C $\gamma,\gamma'$ )  $^3J(^{119}Sn-^{13}C\gamma,\gamma')=56$  Hz; 129.8 (C $\delta$ ).

$^{119}Sn$  NMR (DMSO- $d_6$ , 225 MHz)  $\delta$  (ppm) = 152.

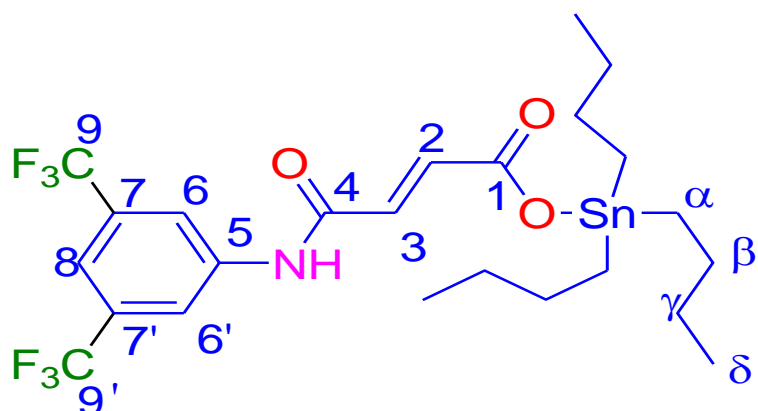
#### 4. Trimethylstannyl 4-(3,5-bis(trifluoromethyl)phenylamino)-4-oxobut-2-enoate



Yield: 0.72 g, 80%; M.P. 123°C; Mol. Wt: 491 g/mol; Elemental analytical cal. for  $C_{15}H_{15}F_6NO_3Sn$ : C: 36.89 (36.77); H: 3.2 (3.09); N: 2.74(2.86); FT-IR (4000 to 400  $cm^{-1}$ ): 3117  $\nu$  (N-H); 1675  $\nu$  (HN-C=O); 1575  $\nu$  (COO)asym; 1275  $\nu$  (COO)sym; 300  $\Delta\nu$ ; 546  $\nu$  (Sn-C); 452  $\nu$  (Sn-O).  $^1H$ NMR ( $CDCl_3$ , 400 MHz)  $\delta$  (ppm): 6.26 (d, H2, 1H,  $^3J$  (1H, 1H)); 13.47; 6.34 (d, H3, 1H,  $^3J$  (1H, 1H)=13.47; 7.57 (s, H6, 6, 2H); 8.1 (s, H8, 1H); 12.5 (s, 1H, NH); 0.67 (s, H $\alpha$ , 3H)  $^2J$  [ $^{119}Sn$ - $^1H\alpha$ ]=58 Hz).  $^{13}C$ NMR ( $CDCl_3$ , 125 MHz)  $\delta$  (ppm): 172.8 (C1); 130.4 (C2); 139.5 (C3); 162.9 (C4); 136.7 (C5); 119.8 (C6); 117.2 (C7); 132.2 (C8); 128.4 (C9); -1.7 (C $\alpha$ )  $^1J$  [ $^{119}Sn$ - $^{13}C\alpha$ ] = 392 Hz.

$^{119}Sn$  NMR ( $CDCl_3$ , 225 MHz)  $\delta$  (ppm) = 151.  $^{19}F$  NMR ( $CDCl_3$ , 375 MHz)  $\delta$  (ppm) = -63

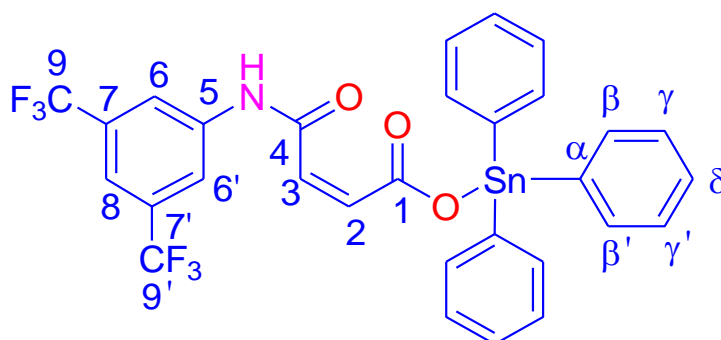
#### 5. Tributylstannyl 4-(3,5-bis(trifluoromethyl)phenylamino)-4-oxobut-2-enoate



Yield: 0.81 g, 71%; M.P. 104°C: Mol.Wt: 617.1 g/mol: Elemental analytical cal. for  $C_{24}H_{33}F_6NO_3Sn$ : C: 46.92 (46.78); H: 5.32 (5.4); N: 2.38 (2.27): FT-IR (4000 to 400  $cm^{-1}$ ): 3120  $\nu$  (N-H); 1683  $\nu$  (HN-C=O); 1576  $\nu$  (COO)<sub>asym</sub>; 1274  $\nu$  (COO)<sub>sym</sub>; 302  $\Delta\nu$ ; 525  $\nu$  (Sn-C); 452  $\nu$  (Sn-O).  $^1H$ NMR ( $CDCl_3$ , 500 MHz)  $\delta$  (ppm): 6.29 (d,H<sub>2</sub>,1H,  $^3J$  (1H,1H); 13.46; 6.36 (d,H<sub>3</sub>,1H,  $^3J$  (1H,1H)=13.46; 7.58 (s,H<sub>6</sub>,6,2H); 8.08 (s,H<sub>8</sub>, 1H); 12.5 (s,1H,NH); 1.30 (t,H $\alpha$ ,2H,  $^3J$  ( $^1H$ , $^1H$ )=7.4,  $^2J$ [ $^{119}Sn$ - $^1H$ ]=56Hz); 1.36-1.32 (m,H $\beta$ ,2H); 1.66-1.60 (m,H $\gamma$ ,2H); 0.91(t,H $\delta$ ,3H)  $^3J$  ( $^1H$ , $^1H$ )=7.33.  $^{13}C$ NMR ( $CDCl_3$  125 MHz)  $\delta$  (ppm): 171.5 (C<sub>1</sub>); 129.8 (C<sub>2</sub>); 138.9 (C<sub>3</sub>); 162.5 (C<sub>4</sub>); 136.1 (C<sub>5</sub>); 119.7 (C<sub>6</sub>); 117.1 (C<sub>7</sub>); 132.03 (C<sub>8</sub>); 124.4 (C<sub>9</sub>); 17.3 (C $\alpha$ )  $^1J$  [ $^{119}Sn$ - $^{13}C\alpha$ ] = 416 Hz; 26.9 (C $\beta$ )  $^2J$  [ $^{119}Sn$ - $^{13}C\beta$ ] = 68 Hz; ; 27.6 (C $\gamma$ )  $^3J$  [ $^{119}Sn$ - $^{13}C\delta$ ] =24 Hz; 13.3 (C $\delta$ ).

$^{119}Sn$  NMR ( $CDCl_3$ , 225 MHz)  $\delta$  (ppm) = 137.  $^{19}F$  NMR ( $CDCl_3$ , 375 MHz)  $\delta$  (ppm) = -63

## 6. Triphenylstannyl 4-(3,5-bis(trifluoromethyl)phenylamino-4-oxobut-2-enoate

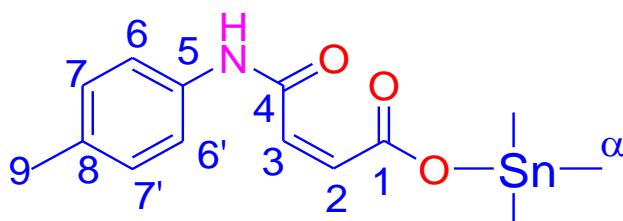


Yield: 0.81 g, 81%; M.P. 112°C: Mol.Wt: 679.06 g/mol: Elemental analytical cal. for  $C_{30}H_{23}F_6NO_3Sn$ : C: 53.79 (53.43); H: 3.34 (3.42); N: 2.14(2.07): FT-IR (4000 to 400  $cm^{-1}$ ): 3310  $\nu$  (N-H); 1670  $\nu$  (HN-C=O); 1552  $\nu$  (COO)<sub>asym</sub>; 1272  $\nu$  (COO)<sub>sym</sub>; 280  $\Delta\nu$ ; 532  $\nu$  (Sn-C); 443  $\nu$  (Sn-O).  $^1H$ NMR ( $CDCl_3$ , 500 MHz)  $\delta$  (ppm): 6.26 (d,H<sub>2</sub>,1H,  $^3J$  (1H,1H)=13.4; 6.34 (d,H<sub>3</sub>,1H,  $^3J$  (1H,1H); 13.4; 7.52 (s,H<sub>6</sub>,6,2H); 8.02 (s,H<sub>8</sub>,1H); 7.45-7.55 (m, 10H,Ph-H);7.60-7.70 (m,5H,Ph-H); 12.5 (s,1H,NH).  $^{13}C$ NMR ( $CDCl_3$

125 MHz)  $\delta$  (ppm): 170.9 (C1); 130.4 (C2); 139.6 (C3); 162.9 (C4); 136.7 (C5); 119.8 (C-6); 117.2 (C7); 132.2 (C8); 128.4 (C9); 139.4 (C $\alpha$ )  $^1J[^{119}\text{Sn}-^{13}\text{C}\alpha]=546$  Hz]; 135 (C $\beta,\beta$ )  $^2J[^{119}\text{Sn}-^{13}\text{C}\beta]=49$  Hz; 128.2 (C $\gamma,\gamma$ )  $^3J[^{119}\text{Sn}-^{13}\text{C}\gamma]=58$  Hz; 130.8 (C $\delta$ ).

$^{119}\text{Sn}$  NMR (CDCL<sub>3</sub>, 225 MHz)  $\delta$  (ppm) = 151.  $^{19}\text{F}$  NMR (CDCL<sub>3</sub>, 375 MHz)  $\delta$  (ppm) = -63

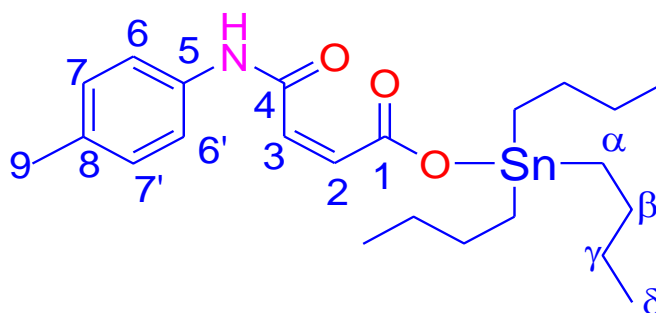
**7. (Z)-trimethylstannyl 4-(p-toluidino)-4-oxobut-enoate:**



Yield: 1.48 g, 74%; M.P. 135-140°C: Mol.Wt: 369.04 g/mol: Anal cal. for C<sub>14</sub>H<sub>19</sub>NO<sub>3</sub>Sn: C: 45.92(45.69); H: 5.07 (5.20); N: 3.96 (3.81): FT-IR (4000 to 400 cm<sup>-1</sup>): 3468 v (N-H); 1711 v (HN-C=O); 1547 v (COO)asym; 1308 v (COO)sym; 239  $\Delta$ v; 530 v (Sn-C); 460 v (Sn-O).  $^1\text{H}$ NMR (DMSO-d<sub>6</sub>, 300 MHz)  $\delta$  (ppm): 5.97 (d, H2,1H,  $^3J(^1\text{H}, ^1\text{H})=12.7$  Hz; 6.13 (d, H3,1H,  $^3J(^1\text{H}, ^1\text{H})=12.7$  Hz; 7.50 (d, H6,6, 2H,  $^3J(^1\text{H}, ^1\text{H})=8.27$  Hz; 7.10 (d, H7,7, 2H,  $^3J(^1\text{H}, ^1\text{H})=8.27$  Hz; 3.32 (s, H9,3H); 0.37 (s, H $\alpha$ ,3H)  $^2J[^{119}\text{Sn}-^1\text{H}\alpha]=59$ Hz).  $^{13}\text{C}$ NMR (DMSO-d<sub>6</sub>, 125 MHz)  $\delta$  (ppm): 174.7 (C1); 134.9 (C2); 141.9 (C3); 168.5 (C4); 137.1 (C5); 124.2 (C6); 134.3 (C7); 139.7 (C8); 25.6 (C9); 5.7 (C $\alpha$ )  $^2J[^{119}\text{Sn}-^{13}\text{C}\alpha]=417$  Hz.

$^{119}\text{Sn}$  NMR (DMSO-d<sub>6</sub>, 225 MHz)  $\delta$  (ppm) = -15.

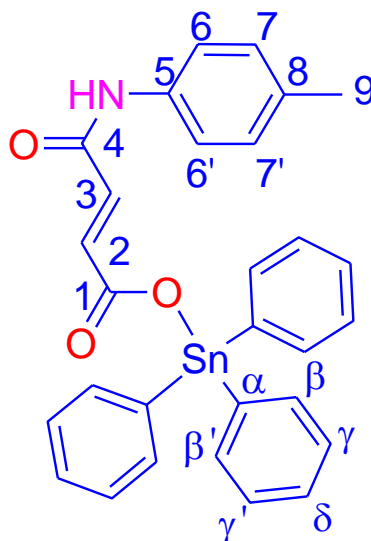
**8. (Z)Tributylstannyl 4-(*p*-toluidino)-4-oxobut-2-enoate:**



Yield: 0.48 g, 69%; M.P. 118°C: Mol.Wt: 494.25 g/mol: Elemental analytical cal. for  $C_{23}H_{37}NO_3Sn$ : C: 55.76 (55.89); H: 7.26 (7.55); N: 2.63 (2.83): FT-IR (4000 to 400  $cm^{-1}$ ): 3243  $\nu$  (N-H); 1711  $\nu$  (HN-C=O); 1559  $\nu$  (COO)<sub>asym</sub>; 1312  $\nu$  (COO)<sub>sym</sub>; 247  $\Delta\nu$ ; 522  $\nu$  (Sn-C); 434  $\nu$  (Sn-O).  $^1H$ NMR (DMSO- $d_6$ )  $\delta$ : 5.96 (d, H<sub>2</sub>,1H,  $^3J(^1H, ^1H)=12.93$ ); 6.14 (d, H<sub>3</sub>,1H,  $^3J(^1H, ^1H)=12.73$ ); 7.50 (d, H<sub>6</sub>,6, 2H,  $^3J(^1H, ^1H)=8.33$ ); 7.10 (d, H<sub>7</sub>,7, 2H,  $^3J(^1H, ^1H)=7.85$ ); 2.28 (s, H<sub>9</sub>,3H); 1.04 (t, H $\alpha$ , 2H,  $^3J[^1H, ^1H]=10.67$  & 18.34; 1.32-1.38 (m, H $\beta$ ,2H); 1.22-1.28 (m, H $\gamma$ ,2H); 0.87 (t, H $\delta$ ,3H,  $^3J[^1H, ^1H]$ ; 7.2 Hz).  $^{13}C$ NMR (DMSO- $d_6$ , 125 MHz)  $\delta$ 174.5 (C1); 135.8 (C2); 142 (C3); 168.4 (C4); 137.1 (C5); 124.1 (C6); 134.2 (C7); 139.5 (C8); 25.6 (C9); 23.7 (C $\alpha$ )  $^1J[^{119}Sn-^{13}C\alpha] = 426$  Hz; 32.9 (C $\beta$ )  $^2J[^{119}Sn-^{13}C\beta] = 72$  Hz; 31.85 (C $\gamma$ )  $^3J[^{119}Sn-^{13}C\delta] = 26$  Hz; 18.78(C $\delta$ ).

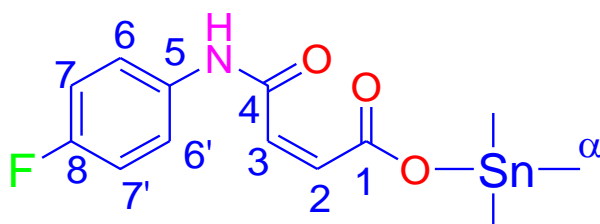
$^{119}Sn$  NMR (CDCl<sub>3</sub>, 225 MHz)  $\delta$  (ppm) = -29.91.

**9. (Z)-triphenylstannyl 4-(*p*-toluidino)-4-oxobut-2-enoate:**



Yield: 1.4 g, 84%; M.P. 165°C: Mol.Wt: 555.22 g/mol: Elemental analytical cal. for  $C_{29}H_{25}NO_3Sn$ : C: 62.97(62.85); H: 4.72 (4.55); N: 2.44 (2.53): FT-IR (4000 to 400  $cm^{-1}$ ): 3124  $\nu$  (N-H); 1727  $\nu$  (HN-C=O); 1562  $\nu$  (COO)<sub>asym</sub>; 1303  $\nu$  (COO)<sub>sym</sub>; 259  $\Delta\nu$ ; 510  $\nu$  (Sn-C); 447  $\nu$  (Sn-O).  $^1H$ NMR (DMSO- $d_6$ , 500 MHz)  $\delta$  (ppm): 6.02 (d, H<sub>2</sub>, 1H,  $^3J(^1H, ^1H)=14.01$  Hz); 6.22 (d, H<sub>3</sub>, 1H,  $^3J(^1H, ^1H)=13.8$  Hz); 7.52 (d, H<sub>6</sub>, 6, 2H,  $^3J(^1H, ^1H)=8.9$  Hz); 7.07 (d, H<sub>7</sub>, 7, 2H,  $^3J(^1H, ^1H)=8.9$  Hz); 2.28 (s, H<sub>9</sub>, 3H); 7.36-7.46 (m, 10H, aromatic); 7.76-7.82 (m, 5H, aromatic); 10.38 (s, 1H, NH).  $^{13}C$ NMR (DMSO- $d_6$ , 125 MHz)  $\delta$  (ppm): 171.5 (C<sub>1</sub>); 133.4 (C<sub>2</sub>); 139.7 (C<sub>3</sub>); 164.3 (C<sub>4</sub>); 134.4 (C<sub>5</sub>); 119.8 (C<sub>6</sub>); 130.6 (C<sub>7</sub>); 135.8 (C<sub>8</sub>); 19.6 (C<sub>9</sub>); 139.7 (C $\alpha$ )  $^1J(^{119}Sn-^{13}C\alpha)=552$  Hz]; 136 (C $\beta$ ,  $\beta'$ )  $^2J(^{119}Sn-^{13}C\beta, \beta')=45$  Hz; 128.2 (C $\gamma$ ,  $\gamma'$ )  $^3J(^{119}Sn-^{13}C\gamma, \gamma')=58$  Hz; 128.8 (C $\delta$ ).  $^{119}Sn$  NMR (DMSO- $d_6$ , 225 MHz)  $\delta$  (ppm) = -167.

**10. (Z)-trimethylstannyl 4-(4-fluorophenylamino)-4-oxobut-2-enoate:**

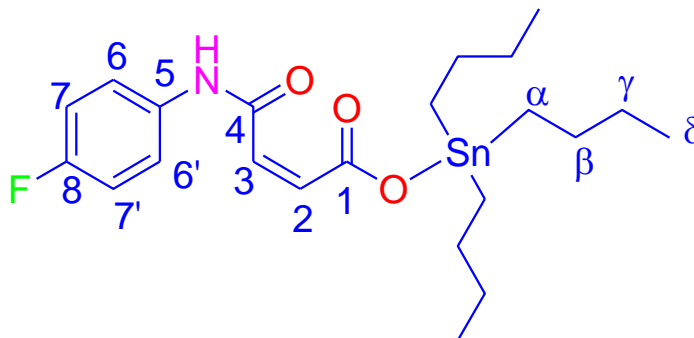


Yield: 0.47 g, 81%; M.P. 154°C; Mol.Wt: 371.98 g/mol; Elemental analytical cal. for  $C_{13}H_{16}FNO_3Sn$ : C: 42.12(41.98); H: 4.26 (4.34); N: 3.92 (3.77); FT-IR (4000-400  $cm^{-1}$ ): 3294  $\nu$  (N-H); 1738  $\nu$  (HN-C=O); 1575  $\nu$  (COO)asym; 1306  $\nu$  (COO)sym; 269  $\Delta\nu$ ; 513  $\nu$  (Sn-C); 441  $\nu$  (Sn-O).  $^1H$ NMR  $CDCl_3$ , 500 MHz)  $\delta$  (ppm): 6.28 (d, H2,1H,  $^3J$  ( $^1H$ ,  $^1H$ )=13.02 Hz; 6.40 (d,H3,1H,  $^3J$  ( $^1H$ ,  $^1H$ )=13.02 Hz; 7.61 (dd,H6,6,2H,  $^3J$  ( $^1H$ , $^{19}F$ ;  $^1H$ , $^1H$ )=4.82 Hz, 8.83 Hz; 7.04 (t,H7,7, 2H,  $^3J$  ( $^1H$ , $^1H$ ;  $^1H$ , $^{19}F$ ) =9.8 Hz,7.72 Hz; 11.21 (s,1H,NH); 0.67 (t,H $\alpha$ ,3H),  $^2J$ [ $^{119}Sn$ - $^1H\alpha$ ]=57 Hz.  $^{13}C$ NMR ( $CDCl_3$ , 125 MHz)  $\delta$  (ppm): 170.1 (C1); 130 (C2); 134.4 (C3); 164.1 (C4); 136.1 (C5); 121.1 (C6); 115.8 (C7); 157.1 (C8); 0.9 (C $\alpha$ )  $^1J$ [ $^{119}Sn$ - $^{13}C\alpha$ ] =382 Hz.

$^{19}F$  NMR ( $CDCl_3$ , 375 MHz)  $\delta$  (ppm) = -63 Hz, -118.3.

$^{119}Sn$  NMR:  $CDCl_3$ , 225 MHz)  $\delta$  (ppm) = -11.2.

**11. (Z)-tributylstannyl 4-(4-fluorophenylamino)-4-oxobut-2-enoate**



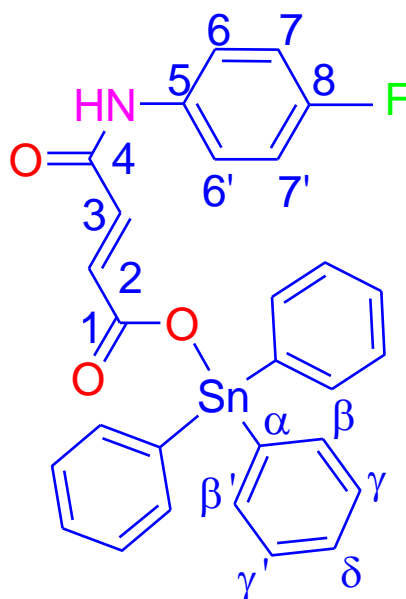


Yield: 0.82 g, 73%; M.P. 76 °C; Mol. Mass: 499.15 g/mol; Elemental analytical cal. for C<sub>22</sub>H<sub>34</sub>FNO<sub>3</sub>Sn: C: 54.72(54.03); H: 6.72 (6.88); N: 2.97 (2.81); FT-IR (4000 to 400 cm<sup>-1</sup>): 3294 v (N-H); 1738 v (HN-C=O); 1575 v (COO)asym; 1306 v (COO)sym; 269 Δv; 513 v (Sn-C); 441 v (Sn-O). <sup>1</sup>HNMR (CDCl<sub>3</sub>, 500 MHz) δ (ppm): 6.40 (d, H<sub>2</sub>,1H, <sup>3</sup>J(<sup>1</sup>H, <sup>1</sup>H)=13.06 Hz; 6.48 (d, H<sub>3</sub>,1H, <sup>3</sup>J(<sup>1</sup>H, <sup>1</sup>H)=13.06 Hz; 7.59 (dd, H<sub>6,6'</sub>, 2H, <sup>3</sup>J(<sup>1</sup>H, <sup>19</sup>F; <sup>1</sup>H, <sup>1</sup>H)=4.89 Hz, 9.13 Hz; 6.91 (dd, H<sub>7,7'</sub>, 2H, <sup>3</sup>J(<sup>1</sup>H, <sup>1</sup>H; <sup>1</sup>H, <sup>19</sup>F) =9.8 Hz, 7.72 Hz; 11.41 (s, 1H, NH); 1.30 (t, H<sub>α</sub>, 2H, <sup>3</sup>J(<sup>1</sup>H, <sup>1</sup>H)=12.4 Hz; 1.38-1.32 (m, H<sub>γ</sub>, 2H); 1.66-1.60 (m, H<sub>β</sub>, 2H); 0.98 (t, H<sub>δ</sub>, 3H) <sup>3</sup>J(<sup>1</sup>H, <sup>1</sup>H)=7.31 Hz; <sup>13</sup>CNMR (CDCl<sub>3</sub>, 125 MHz) δ (ppm): 173 (C1); 128.6 (C2); 137.7 (C3); 162.1 (C4); 134.4 (C5); 122.4 (C6); 115.4 (C7); 160.1 (C8); 17.05 (C<sub>α</sub>) <sup>1</sup>J [<sup>119</sup> Sn-<sup>13</sup>C<sub>α</sub>]=356 Hz; 27.0 (C<sub>β</sub>) <sup>2</sup>J [<sup>119</sup> Sn-<sup>13</sup>C<sub>β</sub>]= 67 Hz; 27.7 (C<sub>γ</sub>) <sup>3</sup>J [<sup>119</sup> Sn-<sup>13</sup>C<sub>γ</sub>]= 23 Hz; 13.3(C<sub>δ</sub>).

<sup>19</sup>F NMR (CDCl<sub>3</sub>, 375 MHz) δ (ppm) = -118.

<sup>119</sup> Sn NMR (CDCl<sub>3</sub>, 225 MHz) δ (ppm) = 132.

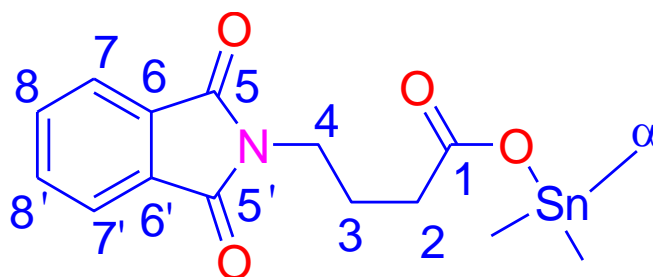
## 12. (Z)-triphenylstannyl 4-(4-fluorophenylamino)-4-oxobut-2-enoate



Yield: 0.96 g, 77%; M.P. 139°C: Mol.Wt: 559.06 g/mol: Anal cal. for C<sub>28</sub>H<sub>22</sub>FNO<sub>3</sub>Sn: C: 60.35(60.25); H: 4.52 (3.97); N: 2.61 (2.52): FT-IR (4000 to 400 cm<sup>-1</sup>): 3136 v (N-H); 1709 v (HN-C=O); 1575 v (COO)<sub>asym</sub>; 1300 v (COO)<sub>sym</sub>; 275 Δv; 515 v (Sn-C); 448 v (Sn-O). <sup>1</sup>HNMR (CDCl<sub>3</sub>, 500 MHz) δ (ppm): 6.69 (d, H<sub>2</sub>,1H, <sup>3</sup>J(<sup>1</sup>H, <sup>1</sup>H)=12.06 Hz; 6.87 (d, H<sub>3</sub>,1H, <sup>3</sup>J(<sup>1</sup>H, <sup>1</sup>H)=12.06 Hz; 7.32 (dd, H<sub>6</sub>,6, 2H, <sup>3</sup>J(<sup>1</sup>H, <sup>19</sup>F; <sup>1</sup>H, <sup>1</sup>H)=7.45 Hz, 12.22 Hz ; 7.17 (t, H<sub>7</sub>,7, 2H, <sup>3</sup>J(<sup>1</sup>H, <sup>1</sup>H; <sup>1</sup>H, <sup>19</sup>F) =8.51 Hz,8.51 Hz; 7.52-7.46 (m, 10H, Ph-H); 7.72-7.66 (m, 5H, Ph-H); 11.1 (s, 1H, NH). <sup>13</sup>CNMR (CDCl<sub>3</sub>, 125.8 MHz) δ (ppm): 173.3 (C1); 130.7 (C2); 138.6 (C3); 162.1 (C4); 132.4 (C5); 123.4 (C6) ; 115.7 (C7)); 166.1 (C8); 138.2 (Cα) <sup>1</sup>J[<sup>119</sup> Sn-<sup>13</sup>Cα]=630 Hz; 136.4 (Cβ,β) <sup>2</sup>J[<sup>119</sup> Sn-<sup>13</sup>Cβ,β]=48 Hz; 129.1 (Cγ,γ) <sup>3</sup>J[<sup>119</sup> Sn-<sup>13</sup>Cγ,γ]= 63 Hz; 130.1 (Cδ).

<sup>119</sup> Sn NMR (CDCl<sub>3</sub>, 225 MHz) δ (ppm) = 122.

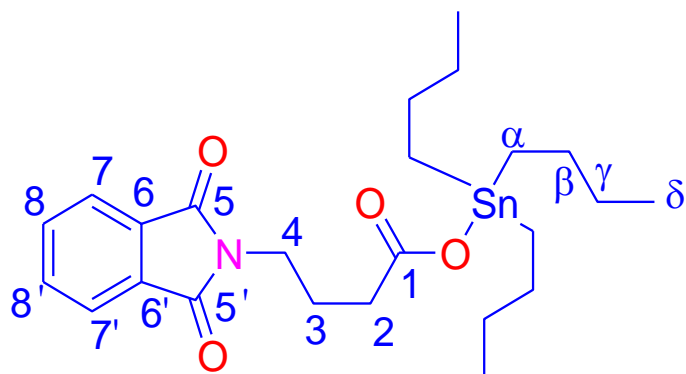
### 13. Trimethylstannyl 4-(1,3-dioxoisindolin-2-yl)butanoate:



Yield: 0.64 g, 60%; M.P. 164 °C: Mol.Wt: 397.03 g/mol: Anal cal. for C<sub>15</sub>H<sub>19</sub>NO<sub>4</sub>Sn: C: 45.49(45.72); H: 4.84 (5.22); N: 3.54 (3.76): FT-IR (4000 to 400 cm<sup>-1</sup>): 3456 v (N-H); 1707 v (HN-C=O); 1549 v (COO)<sub>asym</sub>; 1320 v (COO)<sub>sym</sub>; 229 Δv; 548 v (Sn-C); 499 v (Sn-O). <sup>1</sup>HNMR (CDCl<sub>3</sub>, 400 MHz) δ (ppm): 2.34 (t, H<sub>2</sub>,2H, <sup>3</sup>J(<sup>1</sup>H, <sup>1</sup>H)=7.39 Hz,7.39 Hz; 1.98-1.92 (m, H<sub>3</sub>,2H); 3.73 (t, H<sub>4</sub>,2H, <sup>3</sup>J(<sup>1</sup>H, <sup>1</sup>H)=6.88 Hz,6.88 Hz); 7.89-7.81 (m, H<sub>7</sub>,7, 2H); 7.74-7.69 (m, H<sub>8</sub>,8, 2H); 0.51 (s, Hα,9H) <sup>2</sup>J[<sup>119</sup>Sn-<sup>1</sup>Hα]=57 Hz. <sup>13</sup>CNMR (CDCl<sub>3</sub>, 125 MHz) δ (ppm): 178 (C1); 31.9 (C2); 24.6 (C3); 37.4 (C4); 168.3 (C5); 132.1 (C6); 123.2 (C7); 133.8 (C8); 2.5 (Cα) <sup>1</sup>J[<sup>119</sup>Sn-<sup>13</sup>Cα]=389 Hz.

$^{119}\text{Sn}$  NMR ( $\text{CDCl}_3$ , 225 MHz)  $\delta$  (ppm) = 134.4.

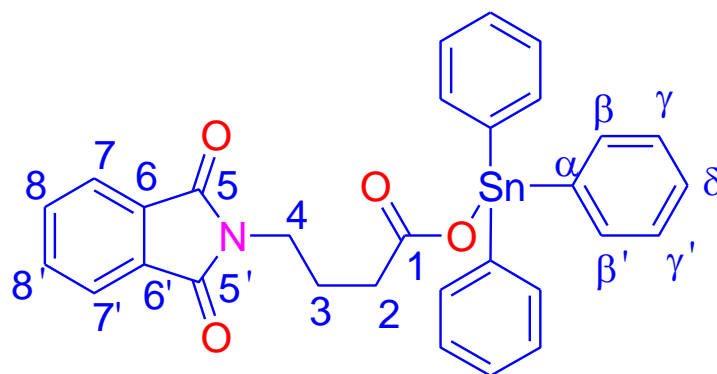
#### 14. Tributylstannyl 4-(1,3-dioxoisindolin-2-yl)butanoate:



Yield: 0.81 g, 84%; M.P. 69 °C; Mol.Wt: 522.26 g/mol; Elemental analytical cal. for  $\text{C}_{24}\text{H}_{37}\text{NO}_4\text{Sn}$ : C: 55.49(55.19); H: 7.32 (7.14); N: 2.52 (2.68); FT-IR (4000 to 400  $\text{cm}^{-1}$ ): 3338  $\nu$  (N-H); 1737  $\nu$  (HN-C=O); 1571  $\nu$  (COO)asym; 1301  $\nu$  (COO)sym; 270  $\Delta\nu$ ; 544  $\nu$  (Sn-C); 465  $\nu$  (Sn-O).  $^1\text{H}$ NMR ( $\text{CDCl}_3$ , 500 MHz)  $\delta$  (ppm): 2.33 (t, H<sub>2</sub>, 2H,  $^3J(^1\text{H}, ^1\text{H})=7.56$  Hz, 7.56 Hz); 1.97-1.92 (m, H<sub>3</sub>, 2H); 3.72 (t, H<sub>4</sub>, 2H,  $^3J(^1\text{H}, ^1\text{H})=6.97$  Hz, 6.97 Hz); 7.84-7.82 (m, H<sub>7</sub>, 7, 2H); 7.72-7.68 (m, H<sub>8</sub>, 8, 2H); 1.24 (t, H <sub>$\alpha$</sub> , 2H,  $^3J(^1\text{H}, ^1\text{H})=12.3$  Hz); 1.58-1.52 (m, H <sub>$\beta$</sub> , 2H); 1.31-1.27 (m, H <sub>$\gamma$</sub> , 2H); 0.88 (s, H <sub>$\delta$</sub> , 3H)  $^3J(^1\text{H}, ^1\text{H})=7.31$ .  $^{13}\text{C}$ NMR ( $\text{CDCl}_3$ , 125 MHz)  $\delta$  (ppm): 178 (C<sub>1</sub>); 32.2 (C<sub>2</sub>); 24.8 (C<sub>3</sub>); 37.5 (C<sub>4</sub>); 168.3 (C<sub>5</sub>); 132.1 (C<sub>6</sub>); 123.2 (C<sub>7</sub>); 133.8 (C<sub>8</sub>); 13.6 (C <sub>$\alpha$</sub> )  $^1J[^{119}\text{Sn}-^{13}\text{C}_\alpha]=396$  Hz; 26.97 (C <sub>$\beta$</sub> )  $^2J[^{119}\text{Sn}-^{13}\text{C}_\beta]=48$  Hz; 27.80 (C <sub>$\gamma$</sub> )  $^3J[^{119}\text{Sn}-^{13}\text{C}_\gamma]=21$  Hz; 8.70 (C <sub>$\delta$</sub> ).

$^{119}\text{Sn}$  NMR ( $\text{CDCl}_3$ , 225 MHz)  $\delta$  (ppm) = 109.7.

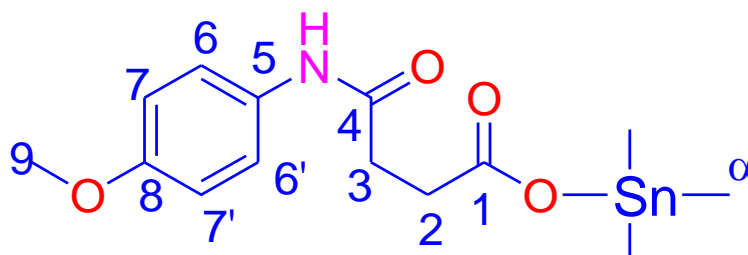
### 15. I-C-32. Triphenylstannyl 4-(1,3-dioxoisindolin-2-yl)butanoate:



Yield: 0.81 g, 83%; M.P.79 °C: Mol.Wt: 583.08 g/mol: Elemental analytical cal. for  $C_{30}H_{25}NO_4Sn$ : C: 61.78 (61.89); H: 4.27 (4.33); N: 2.48 (2.41). FT-IR (4000 to 400  $cm^{-1}$ ): 3231 v (N-H); 1715 v (HN-C=O); 1578 v (COO)asym; 1312 v (COO)sym: 266  $\Delta v$ ; 532 v (Sn-C); 442 v (Sn-O).  $^1H$ NMR ( $CDCl_3$ , 500 MHz)  $\delta$ (ppm): 2.30 (t,H2,2H,  $^3J(^1H,^1H)=7.50$  Hz, 7.50 Hz); 1.88-1.84 (m,H3,2H); 3.62 (t,H4,2H,  $^3J(^1H,^1H)=6.84$  Hz,6.84 Hz); 7.87-7.84 (m,H7,7, 2H) ; 7.74-7.70 (m,H8,8,2H); 7.46-7.42 (m, 10H,Ph-H);7.64-7.60 (m,5H,Ph-H).  $^{13}C$ NMR ( $CDCl_3$ , 125 MHz)  $\delta$  (ppm): 175.4 (C1); 33.2 (C2); 24.8 (C3); 34.6 (C4); 169.2 (C5); 133.1 (C6); 124.2 (C7); 134.2 (C8); 139.2 (C $\alpha$ )  $^1J[^{119}Sn-^{13}C\alpha]=640$  Hz; 137.1 (C $\beta,\beta$ )  $^2J[^{119}Sn-^{13}C\beta,\beta]=52$  Hz; 129.2 (C $\gamma,\gamma$ )  $^3J[^{119}Sn-^{13}C\gamma,\gamma]=65$  Hz; 132.2 (C $\delta$ ).

$^{119}Sn$  NMR ( $CDCl_3$ , 225 MHz)  $\delta$  (ppm) = 121.4.

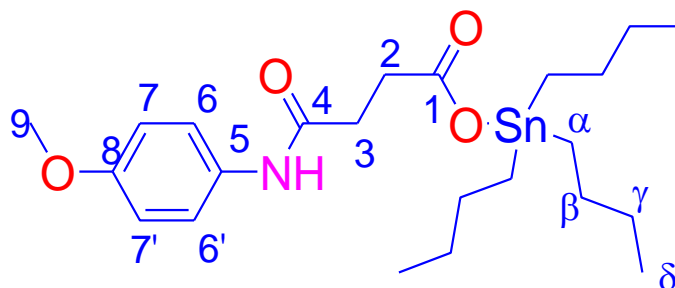
### 16. Trimethylstannyl 4-(4-methoxyphenylamino)-4-oxobutanoate:



Yield: 0.72 g, 85%; M.P. 132 °C; Mol.Wt: 386.03 g/mol; Elemental analytical cal. for  $C_{14}H_{21}NO_4Sn$ : C: 43.72 (43.56); H: 5.26 (5.48); N: 3.57 (3.63). FT-IR (4000 to 400  $cm^{-1}$ ): 3173  $\nu$  (N-H); 1715  $\nu$  (HN-C=O); 1552  $\nu$  (COO)<sub>asym</sub>; 1316  $\nu$  (COO)<sub>sym</sub>; 246  $\Delta\nu$ ; 536  $\nu$  (Sn-C); 428  $\nu$  (Sn-O).  $^1H$ NMR ( $CDCl_3$ , 600 MHz)  $\delta$  (ppm): 2.30 (t, H<sub>2</sub>, 2H)  $^3J(^1H, ^1H)=6.34$  Hz;; 2.34 (t, H<sub>3</sub>, 2H)  $^3J(^1H, ^1H)=6.34$  7.52 (d, H<sub>6</sub>, 6, 2H,  $^3J(^1H, ^1H)=9.13$ ; 6.84 (d, H<sub>7</sub>, 7, 2H,  $^3J(^1H, ^1H)=9.13$ ; 3.75 (s, H<sub>9</sub>, 3H); 8.8 (s, 1H, NH); 0.42 (s, H $\alpha$ , 3H)  $^2J[^{119}Sn-^1H\alpha]=57$  Hz.  $^{13}C$ NMR ( $CDCl_3$ , 125 MHz)  $\delta$  (ppm); 171.5 (C1); 30.9 (C2); 34.7 (C3); 164.2 (C4); 133.9 (C5); 121.2 (C6); 113.9 (C7); 156.2 (C8); 56.4 (C9); 4.3 (C $\alpha$ )  $^1J[^{119}Sn-^{13}C\alpha]=416$  Hz.

$^{119}Sn$  NMR ( $CDCl_3$ , 225 MHz)  $\delta$  (ppm) = 132.4.

#### 17. Tributylstannyl 4-(4-methoxyphenylamino)-4-oxobutanoate:

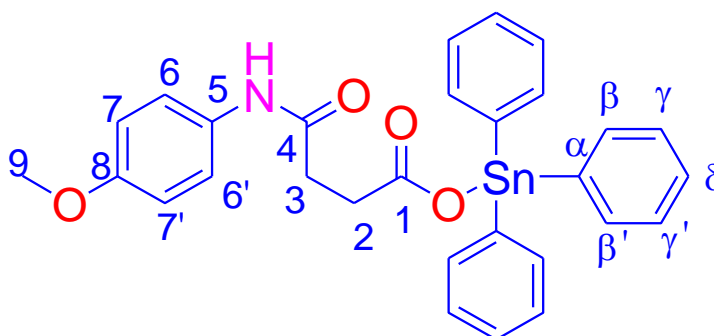


Yield: 0.82 g, 78%; M.P. 126 °C; Mol.Wt: 513.19 g/mol; Elemental analytical cal. for  $C_{23}H_{39}NO_4Sn$ : C: 54.21 (53.93); H: 7.58 (7.67); N: 2.82 (2.73). FT-IR (4000 to 400  $cm^{-1}$ ): 3329  $\nu$  (N-H); 1739  $\nu$  (HN-C=O); 1561  $\nu$  (COO)<sub>asym</sub>; 1302  $\nu$  (COO)<sub>sym</sub>; 259  $\Delta\nu$ ; 509  $\nu$  (Sn-C); 455  $\nu$  (Sn-O).  $^1H$ NMR ( $CDCl_3$ , 500 MHz)  $\delta$  (ppm): 2.29 (d, H<sub>2</sub>, 1H,  $^3J(^1H, ^1H)=13.8$  Hz; 2.40 (d, H<sub>3</sub>, 1H,  $^3J(^1H, ^1H)=13.8$  Hz; 7.48 (s, H<sub>6</sub>, 6, 2H),  $^3J(^1H, ^1H)=7.74$ ; 6.82 (s, H<sub>7</sub>, 7, 2H),  $^3J(^1H, ^1H)=7.74$ ; 3.69 (s, H<sub>9</sub>, 3H); 9.97 (s, 1H, NH); 1.03 (t, H $\alpha$ , 2H,  $^3J(^1H, ^1H)=7.74$ ,  $^2J[^{119}Sn-^1H\alpha]=56$  Hz; 1.60-1.56 (m, H $\beta$ , 2H); 1.20-1.24 (m, H $\gamma$ , 2H); 0.83 (t, H $\delta$ , 3H)  $^3J(^1H, ^1H)=7.33$ .  $^{13}C$ NMR ( $CDCl_3$ , 125 MHz)  $\delta$  (ppm): 175.1

(C1); 32.6 (C2); 31.9 (C3); 173.3 (C4); 134.4 (C5); 122.2 (C6); 116.1 (C7); 157.1 (C8); 54.9 (C9); 21.7 (C $\alpha$ )  $^1J[^{119}\text{Sn}-^{13}\text{C}\alpha]=348$  Hz; 25.4  $^2J(\text{C}\beta)$  [ $^{119}\text{Sn}-^{13}\text{C}\beta$ ]= 72 Hz; 27.9  $^3J(\text{C}\gamma)$  [ $^{119}\text{Sn}-^{13}\text{C}\gamma$ ]= 26 Hz; 14.18 (C $\delta$ );.

$^{119}\text{Sn}$  NMR (CDCL<sub>3</sub>, 225 MHz)  $\delta$  (ppm) = 109.

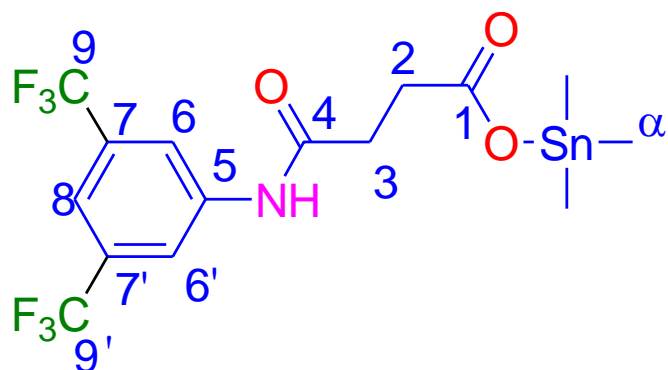
### 18. Triphenylstannyl 4-(4-methoxyphenylamino)-4-oxobutanoate:



Yield: 0.93 g, 81%; M.P. 82°C: Mol.Wt: 571.94 g/mol: Elemental analytical cal. for C<sub>29</sub>H<sub>27</sub>NO<sub>4</sub>Sn: C: 60.73 (60.87); H: 4.58 (4.76); N: 2.62 (2.45): FT-IR (4000 to 400 cm<sup>-1</sup>): 3329 v (N-H); 1735 v (HN-C=O); 1561 v (COO)<sub>asym</sub>; 1302 v (COO)<sub>sym</sub>; 259  $\Delta$ v; 523 v (Sn-C); 446 v (Sn-O).  $^1\text{H}$ NMR (DMSO-d<sub>6</sub>, 300 MHz)  $\delta$  (ppm): 2.34 (t, H<sub>2</sub>, 2H,  $^3J(^1\text{H}, ^1\text{H})=6.38$  Hz; 2.36 (t, H<sub>3</sub>, 2H,  $^3J(^1\text{H}, ^1\text{H})=6.38$ ; 6.88 (d, H<sub>6</sub>, 6, 2H,  $^3J(^1\text{H}, ^1\text{H})=8.84$  Hz; 6.84 (d, H<sub>7</sub>, 7, 2H,  $^3J(^1\text{H}, ^1\text{H})=8.84$  Hz; 7.36-7.32 (m, 9H, aromatic); 7.46-7.40 (m, 3H, aromatic); 7.86-7.82 (m, 3H, aromatic); 3.71 (s, H<sub>9</sub>, 3H); 9.75 (s, 1H, NH).  $^{13}\text{C}$ NMR (DMSO-d<sub>6</sub>, 125 MHz)  $\delta$  (ppm): 175.8 (C1); 32.9 (C2); 29.8 (C3); 172.2 (C4); 129.8 (C5); 122.2 (C6); 116.2 (C7); 156.1 (C8); 56.3 (C9); 137.1 (C $\alpha$ )  $^1J[^{119}\text{Sn}-^{13}\text{C}\alpha]=552$  Hz]; 133.2  $^2J(\text{C}\beta, \beta)$  [ $^{119}\text{Sn}-^{13}\text{C}\beta$ ]= 49 Hz; 127.8  $^3J(\text{C}\gamma, \gamma)$  [ $^{119}\text{Sn}-^{13}\text{C}\gamma$ ]= 59 Hz; 129.9 (C $\delta$ ).

$^{119}\text{Sn}$  NMR (DMSO-d<sub>6</sub>, 225 MHz)  $\delta$  (ppm) = 78

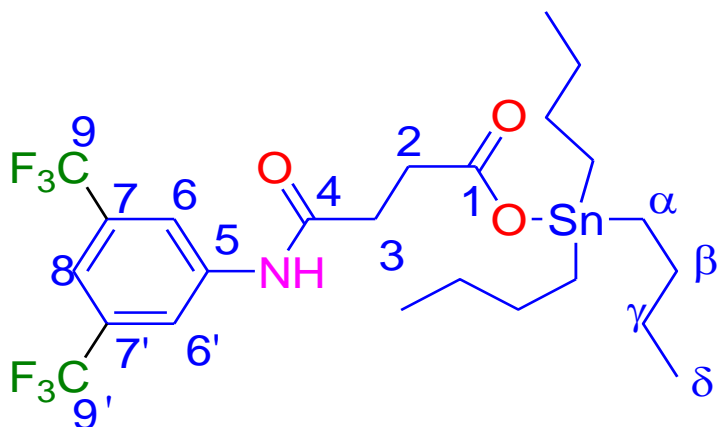
### 19. Trimethylstannyl 4-(3,5-bis(trifluoromethyl)phenylamino)-4-oxobutanoate:



Yield: 0.72 g, 80%; M.P. 123°C; Mol.Wt: 493.01 g/mol; Anal cal. for C<sub>15</sub>H<sub>17</sub>F<sub>6</sub>NO<sub>3</sub>Sn: C, 36.78 (36.62); H, 3.39 (3.48); N, 2.781(2.85). FT-IR (4000-400 cm<sup>-1</sup>): 3134 v (N-H); 1655 v (HN-C=O); 1590 v (COO)<sub>asym</sub>; 1206 v (COO)<sub>sym</sub>; 284 Δv; 556 v (Sn-C); 432 v (Sn-O). <sup>1</sup>HNMR (CDCl<sub>3</sub>, 300 MHz) δ (ppm): 2.40 (t, H<sub>2</sub>, 2H, <sup>3</sup>J (1H, 1H)=6.42; 2.54 (t, H<sub>3</sub>, 2H, <sup>3</sup>J (1H, 1H); 6.42; 7.92 (s, H<sub>6</sub>, 6, 2H); 7.39 (s, H<sub>8</sub>, 1H); 12.1 (s, 1H, NH); 0.76 (s, H<sub>α</sub>, 3H) <sup>2</sup>J [<sup>119</sup>Sn-<sup>1</sup>Hα]=59 Hz. <sup>13</sup>CNMR (CDCl<sub>3</sub>, 125 MHz) δ (ppm): 176.2 (C1); 33.4 (C2); 30.4 (C3); 169.7 (C4); 139.3 (C5); 121.5 (C6); 131.6 (C7); 119.2 (C8); 127.4 (C9); -3.7 (Cα) <sup>1</sup>J [<sup>119</sup>Sn-<sup>13</sup>Cα] = 392 Hz.

<sup>119</sup>Sn NMR (CDCl<sub>3</sub>, 225 MHz) δ (ppm) = 116. <sup>19</sup>F NMR (CDCl<sub>3</sub>, 375 MHz) δ (ppm) = -64

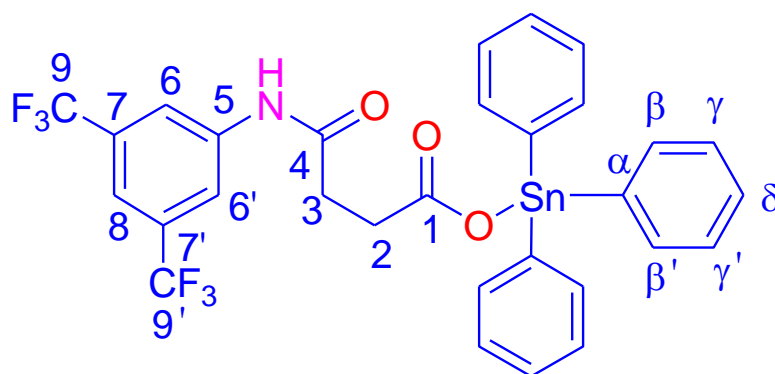
### 20. Tributylstannyl 4-(3,5-bis(trifluoromethyl)phenylamino)-4-oxobutanoate:



Yield: 0.81 g, 71%; M.P. 104°C: Mol.Wt: 617.1 g/mol: Anal cal. for C<sub>24</sub>H<sub>33</sub>F<sub>6</sub>NO<sub>3</sub>Sn: C: 46.92 (46.78); H: 5.32 (5.4); N: 2.38 (2.27): FT-IR (4000 to 400 cm<sup>-1</sup>): 3120 v (N-H); 1683 v (HN-C=O); 1576 v (COO)<sub>asym</sub>; 1274 v (COO)<sub>sym</sub>; 302 Δv; 525 v (Sn-C); 451 v (Sn-O). <sup>1</sup>HNMR (CDCl<sub>3</sub>, 300 MHz) δ (ppm): 2.34 (t,H<sub>2</sub>,1H,<sup>3</sup>J(<sup>1</sup>H,<sup>1</sup>H)=6.52; 2.48 (t,H<sub>2</sub>,1H, <sup>3</sup>J(<sup>1</sup>H,<sup>1</sup>H); 6.52; 8.02 (s,H<sub>6</sub>,6, 2H); 7.52 (s,H<sub>8</sub>,1H); 11.9 (s,1H,NH); 1.06 (t, H<sub>α</sub>,2H,); <sup>3</sup>J[<sup>1</sup>H-<sup>1</sup>H]=7.72; 1.66-1.60 (m, H<sub>β</sub>, 2H); 1.36-1.30 (m,H<sub>γ</sub>,2H); 0.82 (t,H<sub>δ</sub>,3H) <sup>3</sup>J(<sup>1</sup>H,<sup>1</sup>H)=7.28. <sup>13</sup>CNMR (CDCl<sub>3</sub>, 125 MHz) δ (ppm): 172.9 (C1); 30.8 (C2); 34.2 (C3); 164.4 (C4); 138.2 (C5) ; 121.7 (C6); 131.8 (C7); 117.3 (C8); 125.6 (C9); 19.8 (C<sub>α</sub>) <sup>1</sup>J[<sup>119</sup>Sn-<sup>13</sup>C<sub>α</sub>] = 436 Hz; 26.2 (C<sub>β</sub>) <sup>2</sup>J[<sup>119</sup> Sn-<sup>13</sup>C<sub>β</sub>] = 66 Hz; 27.8 (C<sub>γ</sub>) <sup>3</sup>J[<sup>119</sup> Sn-<sup>13</sup>C<sub>δ</sub>] =25 Hz; 14.6 (C<sub>δ</sub>).

<sup>119</sup>Sn NMR (CDCl<sub>3</sub>, 225 MHz) δ (ppm) = 124. <sup>19</sup>F NMR (CDCl<sub>3</sub>, 375 MHz) δ (ppm) = -63.

## 21.Triphenylstannyl 4-(3,5-bis(trifluoromethyl)phenylamino-4-oxobutanoate:



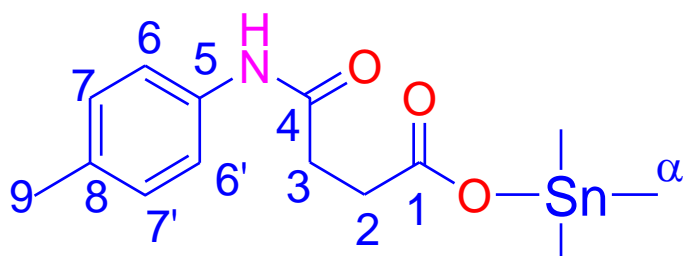
Yield: 0.72 g, 80%; M.P. 123°C: Mol.Wt: 679.06 g/mol: Anal cal. for C<sub>30</sub>H<sub>23</sub>F<sub>6</sub>NO<sub>3</sub>Sn: C, 53.32 (53.13); H, 3.38 (3.42); N, 2.14 (2.07): FT-IR (4000 to 400 cm<sup>-1</sup>): 3310 v (N-H); 1670 v (HN-C=O); 1552 v (COO)<sub>asym</sub>; 1272 v (COO)<sub>sym</sub>; 280 Δv; 532 v (Sn-C); 443 v (Sn-O). <sup>1</sup>HNMR (CDCl<sub>3</sub>, 300 MHz) δ (ppm): 2.36 (t,H<sub>2</sub>,1H,<sup>3</sup>J(<sup>1</sup>H,<sup>1</sup>H)=6.44; 2.46 (d,H<sub>3</sub>,1H, <sup>3</sup>J(<sup>1</sup>H,<sup>1</sup>H)=6.44; 8.2 (s,H<sub>6</sub>,6, 2H); 7.52 (s,H<sub>8</sub>,1H); 7.84-7.76 (m,6H,



aromatic); 7.36-7.30 (m,9H,aromatic); 10.7 (s,1H,NH).  $^{13}\text{C}$ NMR ( $\text{CDCl}_3$ , 125 MHz)  $\delta$  (ppm): 175.4 (C1); 32.2 (C2); 33.5 (C3); 172.9 (C4); 136.8 (C5); 121.9 (C6); 131.7 (C7); 118.9 (C8); 125.5 (C9); 141.8 (C $\alpha$ )  $^1J[^{119}\text{Sn}-^{13}\text{C}\alpha]=420$  Hz]; 136.8 (C $\beta,\beta$ )  $^2J[^{119}\text{Sn}-^{13}\text{C}\beta,\beta]=76.2$  Hz; 128.8 (C $\gamma,\gamma$ )  $^3J[^{119}\text{Sn}-^{13}\text{C}\gamma,\gamma]=59$  Hz; 128.1 (C $\delta$ ).

$^{119}\text{Sn}$  NMR ( $\text{CDCl}_3$ , 225 MHz)  $\delta$  (ppm) = 161.  $^{19}\text{F}$  NMR ( $\text{CDCl}_3$ , 375 MHz)  $\delta$  (ppm) = -62

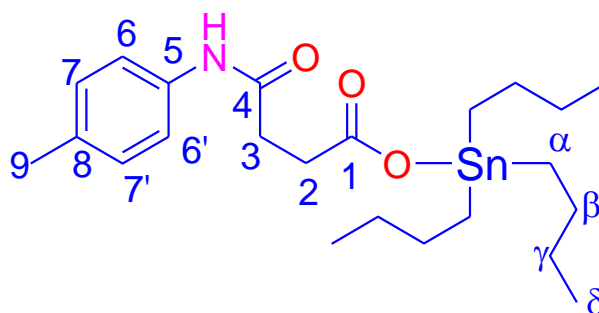
## 22. Trimethylstannyl 4-(*p*-toluidino)-4-oxobutanoate



Yield: 0.48g, 78.6%; M.P. 90-95 °C: Mol.Mass: 370.03 g/mol: Elemental analytical cal. for  $\text{C}_{14}\text{H}_{21}\text{NO}_3\text{Sn}$ : C: 55.49(55.19); H: 7.32 (7.14); N: 2.52 (2.68): FT-IR (4000 to 400  $\text{cm}^{-1}$ ): 3273  $\nu$  (N-H); 1731  $\nu$  (HN-C=O); 1567  $\nu$  (COO)asym; 1306  $\nu$  (COO)sym: 261  $\Delta\nu$ ; 548  $\nu$  (Sn-C); 442  $\nu$  (Sn-O).  $^1\text{H}$ NMR ( $\text{CDCl}_3$ , 500 MHz)  $\delta$  (ppm): 2.58 (t,H2,2H)  $^3J(^1\text{H},^1\text{H})=7.23$ ; 2.68 (t,H3,2H)  $^3J(^1\text{H},^1\text{H})=7.23$ ; 7.34 (d,H6,6, 2H,  $^3J=8.26$ ; 7.06 (d,H7,7, 2H,  $^3J=8.262$ ; 2.7(s,H9,3H); 8.5 (s,1H,NH). 0.55 (s, H $\alpha$ ,3H) 0.76 (s,H $\alpha$ ,3H)  $^2J[^{119}\text{Sn}-^1\text{H}\alpha]=58$  Hz.  $^{13}\text{C}$ NMR ( $\text{CDCl}_3$ , 125 MHz)  $\delta$  (ppm): 177.7 (C1); 33.1 (C2); 31.7 (C3); 171.6 (C4); 135.5 (C5); 119.4 (C6); 129.1 (C7); 133.1 (C8); 20.6 (C9); -2.00 (C $\alpha$ )  $^1J[^{119}\text{Sn}-^{13}\text{C}\alpha]=455$  Hz].

$^{119}\text{Sn}$  NMR ( $\text{CDCl}_3$ , 225 MHz)  $\delta$  (ppm) = 126.8

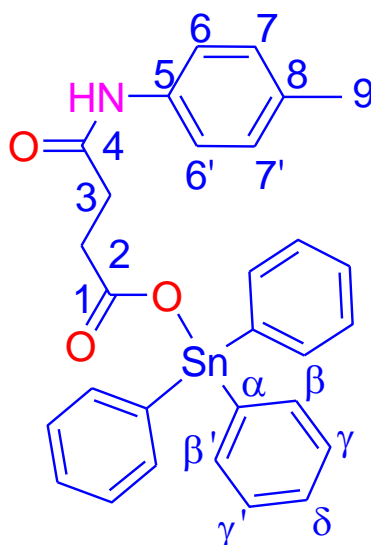
### 23. Tributylstannyl 4-(*p*-toluidino)-4-oxobutanoate:



Yield: 0.38 g, 77%; M.P. 112°C; Mol.Wt: 496.27 g/mol; Elemental analytical cal. for  $C_{23}H_{39}NO_3Sn$ : C: 55.46 (55.66); H: 7.66 (7.92); N: 2.74 (2.82); FT-IR (4000 to 400  $cm^{-1}$ ): 3281  $\nu$  (N-H); 1732  $\nu$  (HN-C=O); 1586  $\nu$  (COO)<sub>asym</sub>; 1332  $\nu$  (COO)<sub>sym</sub>; 254  $\Delta\nu$ ; 526  $\nu$  (Sn-C); 438  $\nu$  (Sn-O).  $^1H$ NMR ( $CDCl_3$ , 500 MHz)  $\delta$  (ppm): 2.62 (t, H<sub>2</sub>, 2H,  $^3J$  ( $^1H, ^1H$ ) = 6.4 Hz; 2.70 (t, H<sub>3</sub>, 2H,  $^3J$  ( $^1H, ^1H$ ) = 6.4; 7.40 (d, H<sub>6,6'</sub>, 2H,  $^3J$  ( $^1H, ^1H$ ) = 8.35; ; 7.10 (d, H<sub>7,7'</sub>, 2H,  $^3J$  ( $^1H, ^1H$ ) = 8.20 ; 2.26 (s, H<sub>9</sub>, 3H); 8.6 (s, 1H, NH); 1.27 (t, H $\alpha$ , 2H,  $^3J$  ( $^1H, ^1H$ ) = 10.67 & 18.34; 1.69-1.55 (m, H $\beta$ , 2H); 1.36-1.30 (m, H $\gamma$ , 2H); 0.96 (t, H $\delta$ , 3H,  $^3J$  ( $^1H, ^1H$ ) = 7.33 Hz;  $^{13}C$ NMR  $CDCl_3$ , 125 MHz)  $\delta$  (ppm): 172.6 (C1); 30.9 (C2); 33.5 (C3); 166.7 (C4); 135.2 (C5); 119.1 (C6); 128.3 (C7); 133.3 (C8); 20.8 (C9); 17.1 (C $\alpha$ )  $^1J$  [ $^{119}Sn-^{13}C\alpha$ ] = 426 Hz; 26.9 (C $\beta$ )  $^2J$  [ $^{119}Sn-^{13}C\beta$ ] = 66 Hz; 27.8 (C $\gamma$ )  $^3J$  [ $^{119}Sn-^{13}C\delta$ ] = 23 Hz; 13.6 (C $\delta$ ).

$^{119}Sn$  NMR ( $CDCl_3$ , 225 MHz)  $\delta$  (ppm) = 155.8

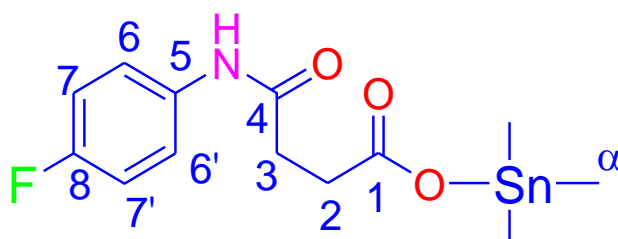
## 24. Triphenylstannyl 4-(*p*-toluidino)-4-oxobutanoate:



Yield: 0.93 g, 81%; M.P. 127°C: Mol.Mass: 556.24 g/mol: Elemental analytical cal. for  $C_{29}H_{27}NO_3Sn$ : C: 60.69(60.62); H: 4.98 (4.89); N: 2.46 (2.52). FT-IR (4000 to 400  $cm^{-1}$ ): 3350  $\nu$  (N-H); 1737  $\nu$  (HN-C=O); 1556  $\nu$  (COO)asym; 1315  $\nu$  (COO)sym; 241  $\Delta\nu$ ; 505  $\nu$  (Sn-C); 449  $\nu$  (Sn-O).  $^1H$ NMR (DMSO- $d_6$ , 300 MHz)  $\delta$  (ppm): 2.35 (t, H3, 2H,  $^3J$  ( $^1H, ^1H$ ) = 6.38 Hz); 2.48 (t, H2, 2H,  $^3J$  ( $^1H, ^1H$ ) = 6.38; 7.06 (d, H6, 6, 2H,  $^3J$  ( $^1H, ^1H$ ) = 8.28 Hz); 7.2 (d, H7, 7, 2H,  $^3J$  ( $^1H, ^1H$ ) = 8.28 Hz; 7.40-7.34 (m, 9H, aromatic); 7.46-7.40 (m, 3H, aromatic); 7.89-7.85 (m, 3H, aromatic); 2.5 (s, H9, 3H); 10.1 (s, 1H, NH).  $^{13}C$ NMR (DMSO- $d_6$ , 125 MHz)  $\delta$  (ppm): 176.1 (C1); 33.1 (C2); 33.8 (C3); 171.5 (C4); 147.3 (C5); 119.4 (C6); 127.3 (C7); 128.8 (C8); 20.9 (C9); 137.3 (C $\alpha$ ) [ $^1J$  ( $^{119}Sn-^{13}C\alpha$ ) = 462 Hz]; 136.65 (C $\beta, \beta'$ ) [ $^2J$  ( $^{119}Sn-^{13}C\beta$ ) = 64 Hz]; 127.84 (C $\gamma, \gamma'$ ) [ $^3J$  ( $^{119}Sn-^{13}C\gamma$ ) = 26 Hz]; 129.4 (C $\delta$ ).

$^{119}Sn$  NMR (DMSO- $d_6$ , 225 MHz)  $\delta$  (ppm) = 132.4

## 25. Trimethylstannyl 4-(4-fluorophenylamino)-4-oxobutanoate

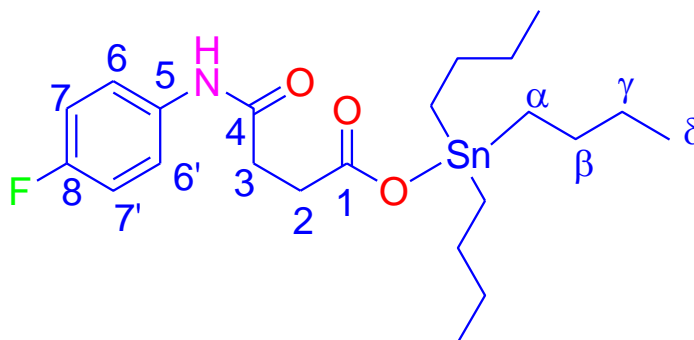


Yield: 0.47 g, 78%; M.P. 146 °C: Mol.Mass: 374 g/mol: Elemental analytical cal. for  $C_{13}H_{18}FNO_3Sn$ : C: 42.67(41.75); H: 4.62 (4.85); N: 3.88 (3.75): FT-IR (4000 to 400  $cm^{-1}$ ): 3319  $\nu$  (N-H); 1739  $\nu$  (HN-C=O); 1580  $\nu$  (COO)<sub>asym</sub>; 1296  $\nu$  (COO)<sub>sym</sub>; 284  $\Delta\nu$ ; 551  $\nu$  (Sn-C); 433  $\nu$  (Sn-O).  $^1H$ NMR (DMSO- $d_6$ , 300 MHz)  $\delta$  (ppm): 2.26 (d, H2,1H,  $^3J(^1H, ^1H)=6.48$  Hz); 2.41 (d, H3,1H,  $^3J(^1H, ^1H)=6.48$  Hz); 7.6 (dd, H6,6, 2H,  $^3J(^1H, ^{19}F; ^1H, ^1H)=5.03$  Hz, 9.06 Hz); 7.1 (dd, H7,7, 2H,  $^3J(^1H, ^1H; ^1H, ^{19}F)=9.74$  Hz, 7.68 Hz); 10.1 (s, 1H, NH); 0.40 (t, H $\alpha$ , 3H)  $^2J[^{119}Sn-^1H\alpha]=71$  Hz.  $^{13}C$ NMR (DMSO- $d_6$ , 125 MHz)  $\delta$  (ppm): 2.70 (C $\alpha$ )  $^1J[^{119}Sn-^{13}C\alpha]=382$ ; 175.9 (C1); 33.4 (C2); 32.3 (C3); 171.5 (C4); 136.4 (C5); 121.5 (C6); 115.5 (C7); 158.1 (C8).

$^{19}F$  NMR (DMSO- $d_6$ , 375 MHz)  $\delta$  (ppm) = -63 Hz, -117.3 Hz.

$^{119}Sn$  NMR (DMSO- $d_6$ , 225 MHz)  $\delta$  (ppm) = 56.2.

## 26. Tributylstannyl 4-(4-fluorophenylamino)-4-oxobutanoate:

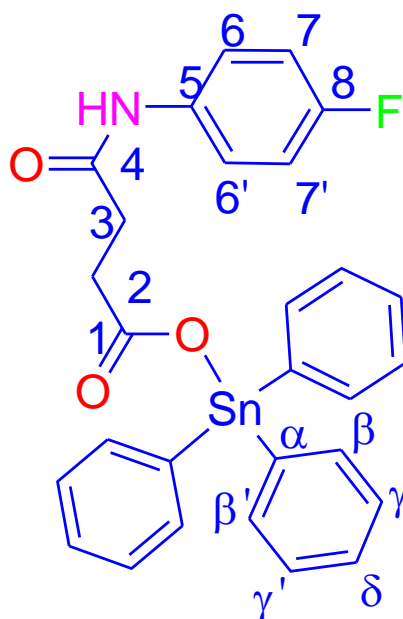


Yield: 0.82 g, 76%; M.P. 76 °C: Mol.Wt: 501.17 g/mol: Elemental analytical cal. for  $C_{22}H_{36}FNO_3Sn$ : C: 52.76(52.82); H: 7.32 (7.25); N: 2.89 (2.80). FT-IR (4000 to 400  $cm^{-1}$ ): 3297  $\nu$  (N-H); 1726  $\nu$  (HN-C=O); 1550  $\nu$  (COO)<sub>asym</sub>; 1275  $\nu$  (COO)<sub>sym</sub>; 285  $\Delta\nu$ ; 498  $\nu$  (Sn-C); 429  $\nu$  (Sn-O).  $^1H$ NMR (DMSO- $d_6$ , 300 MHz)  $\delta$  (ppm): 2.28 (t, H<sub>2</sub>,1H,  $^3J(^1H, ^1H)=6.7$  Hz; 2.42 (t, H<sub>2</sub>,1H,  $^3J(^1H, ^1H)=6.7$  Hz; 7.60 (dd, H<sub>6,6</sub>, 2H,  $^3J(^1H, ^{19}F; ^1H, ^1H)=5.09$  Hz, 9.06 Hz; 7.08 (dd, H<sub>7,7</sub>, 2H,  $^3J(^1H, ^1H; ^1H, ^{19}F)=9.7$  Hz, 7.64 Hz; 10.11 (s, 1H, NH); 1.02 (t, H <sub>$\alpha$</sub> , 6H,  $^3J(^1H, ^1H)=12.4$  Hz; ; 1.26-1.22 (m, H <sub>$\gamma$</sub> , 2H); 1.60-1.55 (m, H <sub>$\beta$</sub> , 2H); 0.82 (t, H <sub>$\delta$</sub> , 3H)  $^3J(^1H, ^1H)=7.33$  Hz.  $^{13}C$ NMR (DMSO- $d_6$ , 125 MHz)  $\delta$  (ppm): 175.9 (C1); 32.4 (C2); 33.6 (C3); 171.5 (C4); 136.5 (C5); 115.6 (C6); 120.9 (C7); 159.6 (C8). 20.6 (C $\alpha$ )  $^1J[^{119}Sn-^{13}C\alpha]=376$  Hz; 27.2 (C $\beta$ )  $^2J[^{119}Sn-^{13}C\beta]=69$  Hz; 28.5 (C $\gamma$ )  $^3J[^{119}Sn-^{13}C\gamma]=26$  Hz; 14.2 (C $\delta$ ).

$^{19}F$  NMR (DMSO- $d_6$ , 375 MHz)  $\delta$  (ppm) = -114.

$^{119}Sn$  NMR (DMSO- $d_6$ , 225 MHz)  $\delta$  (ppm) = 126

## 27. Triphenylstannyl 4-(4-fluorophenylamino)-4-oxobutanoate:



Yield: 0.82 g, 77%; M.P. 139°C; Mol.Wt: 561.08 g/mol; Anal cal. for C<sub>28</sub>H<sub>24</sub>FNO<sub>3</sub>Sn:  
C: 60.11 (60.03); H: 4.46 (4.32); N: 2.41 (2.50); FT-IR (4000 to 400 cm<sup>-1</sup>): 3319 v (N-  
H); 1739 v (HN-C=O); 1580 v (COO)<sub>asym</sub>; 1296 v (COO)<sub>sym</sub>; 284 Δv; 551 v (Sn-C);  
433 v (Sn-O). <sup>1</sup>HNMR (DMSO-d<sub>6</sub>, 300 MHz) δ (ppm): 2.36 (t, H<sub>2</sub>,1H, <sup>3</sup>J(<sup>1</sup>H, <sup>1</sup>H)=6.7  
Hz; 2.46 (t, H<sub>3</sub>,1H, <sup>3</sup>J(<sup>1</sup>H, <sup>1</sup>H)=6.7 Hz; ; 7.60 (dd, H<sub>6,6</sub>, 2H, <sup>3</sup>J(<sup>1</sup>H, <sup>19</sup>F; <sup>1</sup>H, <sup>1</sup>H)=5.07  
Hz, 9.1 Hz; 7.08 (dd, H<sub>7,7</sub>, 2H, <sup>3</sup>J(<sup>1</sup>H, <sup>1</sup>H; <sup>1</sup>H, <sup>19</sup>F) =9.68 Hz, 7.66 Hz; 7.42-7.36 (m,  
10H, Ph-H); 7.95-7.88 (m, 5H, Ph-H); 10.03 (s, 1H, NH). <sup>13</sup>CNMR (DMSO-d<sub>6</sub>, 125 MHz)  
δ (ppm): 171.3 (C<sub>1</sub>); 28.92 (C<sub>2</sub>); 33.2 (C<sub>3</sub>); 159.7 (C<sub>4</sub>); 146.1 (C<sub>5</sub>); 115.7 (C<sub>6</sub>); 120.9  
(C<sub>7</sub>); 156.54 (C<sub>8</sub>); 137.2 (C<sub>α</sub>) <sup>1</sup>J[<sup>119</sup> Sn-<sup>13</sup>C<sub>α</sub>]=630 Hz; 136.2 (C<sub>β,β</sub>) <sup>2</sup>J[<sup>119</sup> Sn-<sup>13</sup>C<sub>β</sub>]=  
48 Hz; 127.6 (C<sub>γ,γ</sub>) <sup>3</sup>J[<sup>119</sup> Sn-<sup>13</sup>C<sub>γ</sub>]= 63 Hz; 128.5 (C<sub>δ</sub>).

<sup>19</sup>F NMR (DMSO-d<sub>6</sub>, 375 MHz) δ (ppm) = -113.

<sup>119</sup> Sn NMR (DMSO-d<sub>6</sub>, 225 MHz) δ (ppm) = 108

## **2.3. Biological studies**

### **2.3.1. Anticancer and Noncancerous Cell Activity**

Breast cancer cell lines (MCF-7) and human endometrial stromal cells (hESCs) were used for cytotoxic analysis. MCF-7 was grown in EMEM with 1% penicillin/streptomycin, 10% FBS and 0.01 mg/ml insulin. hESCs were grown in DMEM/Ham's F12 with 10 % FBS and 1% penicillin/streptomycin. Both the cells were maintained in a humidified incubator with 5% CO<sub>2</sub>. For cytotoxic analysis, 4 X 10<sup>4</sup> cells were seeded per well in a 96 well plate and allowed to reach 80% confluence. The salts were dissolved in DMSO, added to the cells (final concentrations of 1000, 500, 250, 125, 62.5, 31.25 & 15.63 μM), and incubated for 48 h. The cell survival was determined by MTT assay according to the manufacturer's instruction (Vybrant™ MTT Cell Proliferation Assay Kit, Thermofisher).

### **2.3.2. Antileishmanial activity**

*L. tropica* promastigote forms (1 x 10<sup>4</sup> cells/well) were planted in 96-well microtiter plates in RPMI-1640 (Gibco®) supplemented with 10% FBS (Gibco®) and 1% antibiotics and endorsed to cultivate either in the existence of different concentrations (1000, 500 and 250 μg/mL) of test compounds or in the absence (negative control) of the test compound for 72 hrs at 25°C. After the incubation period was completed, the viability of the promastigote form was assessed by MTT (3-(4,5- dimethylthiazol-2yl)-2,5-diphenyltetrazolium bromide) colorimetric method. For this, 100μl of the MTT dye was added to all wells and the plates were placed for 3 hours at 37°C. In last, 40μl of the DMSO as solubilization solution was added into each well and the readings were recorded using an ELISA plate reader (Biotek Elx800) at 570 nm. The experiment was

performed in triplicates while counting of leishmania promastigote was done using Neubauer chamber [110].

### **2.3.3. Hemolysis Assay**

Hemolysis assay was accomplished for the reason to pattern the cytotoxicity of the compounds on the human blood erythrocytes. For this study 8 mL of the blood sample was taken from an unnamed human contributor with prior consent and as per ethical guidelines provided by the ...ethics committee...., of the Department of Biotechnology Abdul Wali Khan University Mardan and transfer immediately into K<sub>2</sub>-EDTA tubes to stop clotting. Blood dilution was done at pH 7.04 using 1:3 ratios with autoclaved Phosphate Saline Buffer (PSB). For Erythrocytes collection centrifugation was used at 1500 rpm for 10 minutes. The remaining supernatant was cast-off and wash the pellet using PBS thrice and collected through centrifugation after each cycle with the above-mentioned condition. The pellets were transferred into a conical flask of 50 mL and PBS was added thrice to the real volume of the already used blood. The screening compounds (Ligands and their organotin(IV) complexes) were added into Eppendorf tubes already containing 1 mL of blood erythrocytes to make three different concentrations i.e. 25 ppm, 50 ppm, and 100 ppm. Triton X-100 (0.5%) was implemented as a positive control as it has almost 100% hemolysis ratio while as negative control DMSO was used. The Eppendorf tube that containing the targeted compounds and blood erythrocytes were placed for one hour at 37°C. After incubation, The erythrocyte suspensions were collected through a centrifuge at 1000 ×g for ten minutes and the cell lysis (hemoglobin release) was determined spectrophotometrically at 576 nm on a spectrophotometer (Agilent-DAD, 8453, Agilent Tech., Germany) [111, 112]. The results were determined by evaluating the percentage of hemolysis compared to the negative and positive controls. Using the following formula.



Haemolysis (%) = [(O.D. 576 nm in the sample solution – O.D. 576 nm in DMSO)/ (O.D. 576 nm in 0.5% Triton X-100 – O.D. 576 nm in DMSO)] x 100

#### **2.3.4. Antibacterial activity**

The liability of ligands and complexes were tested against three different bacterial strains given in the previous method [113]. Here three types of different strains of Gram-negative bacteria (*B. bronchiseptica*, *S. typhimurium* and *E. aerogenes*) were used for tests. These strains were first cultivated in nutrient bisque media and placed for twenty-four hours at 37°C temperature. Sterilized pure water was implemented to regulate the turbidity value to 10<sup>4</sup> CFU/mL via relating with McFarland 0.5 BaSO<sub>4</sub> turbidity value (standard). The 100 microlitres of rested inoculum were then dabbed on Petri plates holding twenty-milliliter nutrient agar. Investigated samples using five microlitres of twenty milligrams per milliliter dimethylsulfoxide; 100 micrograms per disc were imbued on 6 mm of disinfected filter paper discs and positioned on planted nutrient agar dish. Cefixime-USP at a concentration of 20 micrograms per disc and dimethylsulfoxide soaked discs were involved as positive and negative controls, correspondingly. Later on, after twenty-four hours of incubation, pure regions of growing inhibition were analyzed.

#### **2.3.5. Antifungal activity**

Antifungal screening of these complexes was assessed next previously described typical protocol [114]. The fungal strains (*A. fumigatus*, *F. soloni* and *N.niger*) bought from fungal culture group of Pakistan) were cultivated on SDA. Aforementioned in the sensitivity determination, the spores were gathered in Tween 20 (0.02%) solution and adjusted turbidity according to McFarland 0.5 turbidity standard. An amount of 100 µL of each gathered spores was mopped on dishes comprising twenty-five milliliter of disinfected SDA. Filter paper discs overloaded thru five microlitres of the experimental

sample (20 mg/mL dimethyl sulfoxide; 100 µg/disc) as well as standard antifungal terbinafine (50 µg/disc) and dimethyl sulfoxide were positioned on sowed SDA dishes. The dishes were incubated at 28°C for 24 to 48 hours. Afterwards, a Vernier caliper was used to measure the pure regions of inhibition around the discs.

### **2.3.6. Brine shrimp lethality assay**

Brine Shrimp Lethality was done in a ninety-six (96) well dish against *Artemia salina* a brine shrimp larvae as earlier discussed thru minor variation. *Artemia salina* ova (Oceanic star. the USA) were nurtured for twenty-four to forty-eight hours in light at thirty-two degree centigrade in replicated marine water (thirty-eight gram per liter added with six milligrams per liter desiccated yeast) in a particularly planned two-compartment elastic dish. 10 developed phototropic nauplii were reaped by the assistance of Pasteur tube and shifted to for each well-plate. Equivalent V of each extract having less than one percent dimethylsulfoxide in marine water at ultimate concentrations of 500 and 200µg/mL was shifted to the subsequent wells comprising marine water and brine shrimp larvae. The ultimate V in for each of the wells was retained with 300 microlitres. Control wells of positive and negative including series of concentrations using doxorubicin and DMSO of 1%, correspondingly. When twenty-four hours of incubation is completed, the % of deaths was determined and live shrimps were calculated. Table curve 2D v5.01 software was used to calculate the median lethal concentration (LC<sub>50</sub>) [114].

### **2.3.7. Antioxidant Activities**

#### **2.3.7.1. Total antioxidant capacity (TAC)**

The total antioxidant capacity was estimated by a technique used in the literature (Naz et al., 2017) with minor modification. Take hundred microlitre amount from a standard solution of each extract (four mg/mL using dimethylsulfoxide) was mixed with nine

hundred microliter amount of components solutions including sulfuric acid (0.6 Molar), ammonium molybdate (4 mmol.) and sodium phosphate (28 mmol.). The final reaction blends were placed at 95°C for ninety min, then cooled at room temperature and a microplate reader was used to measure the absorbance at 695 nm. DMSO was used as a control. Ascorbic acid was used as a positive control for the calibration curve. The subsequent TAC has been stated as microgram ascorbic acid was equal to per milligram dry weight ( $\mu\text{g AAE/mg DW}$ ) [115, 116].

#### **2.3.7.2. Total reducing power assay**

Reduction potential was examined as already mentioned in the literature (Tabassum et al., 2017). Simply, 100  $\mu\text{L}$  amount of each used sample (extract in DMSO used 4 mg/mL) was mixed with 200  $\mu\text{L}$  amount of phosphate buffer (0.2 M at pH6.6) and 250  $\mu\text{L}$  amount of 1% w/v potassium ferricyanide. The resulting solution mixture was placed for 20 min at 50 °C. In the next step, the reaction was protonated with 200  $\mu\text{L}$  amount of 10% w/v trichloroacetic acid. The subsequent mixtures were collected through a centrifuge at speed of 3000 rpm for at least 10 min and 150  $\mu\text{L}$  of the supernatant layer was mixed with 50  $\mu\text{L}$  amount of 0.1% w/v ferric chloride solution and optical density was analyzed at a wavelength of 630 nm. Ascorbic acid was continued as positive control and results were stated as  $\mu\text{g}$  ascorbic acid which is equal to per mg dry weight ( $\mu\text{g AAE/mg DW}$ ) [115, 116].

#### **2.3.7.3. DPPH free radical scavenging assay**

To determination the free radical scavenging action, 2,2-diphenyl-1-picryl hydroxyl reagent was employed (Tabassum *et al.* 2017) with minor modification. Briefly, ten  $\mu\text{L}$  of extract (four mg/mL) was poured in 190  $\mu\text{L}$  of DPPH solution using methanol as solvent (0.004% w/v)). The reactant media was kept in dark nearly for one hr. A microplate reader was used to analyze the optical density at a wavelength of 515 nm.

As a positive standard, Ascorbic acid was used and DMSO was used as a negative standard. Initially, test samples were screened using 200  $\mu\text{g/mL}$  of concentration, and those samples displaying better activity of quenching ( $\geq 50\%$ ) were tested at a minor concentration (200, 66.6, 22.2, 7.41  $\mu\text{g/mL}$ ) to find  $\text{IC}_{50}$  values. Following formula was used to calculate the percent inhibition value:

$$\text{Test sample \% inhibition} = \text{Scavenging activity (\%)} = (1 - \text{Abs}_s / \text{Abs}_c) \times 100$$

Where  $\text{Abs}_s$  stands for the absorbance of DPPH solution and  $\text{Abs}_c$  designates the absorbance of the negative control. The table curve software 2D Ver 4 was used to calculate the  $\text{IC}_{50}$  values [115, 116].

### 2.3.8. Computational Details

In this work, first-principles non-spin polarized calculations were performed to investigate the electronic properties of triorganotin(IV) carboxylates using DFT [117, 118]. The fully-relaxed crystal structures, formation energy, band structures, total density-of-states (TDOS), and partial density of states (PDOS), have been investigated within the framework of the Quantum Espresso code and ultrasoft pseudopotentials [119]. We used generalized gradient approximation (GGA), for the exchange-correlation energy functional, developed by Perdew-Burke and Ernzerhof (PBE) [120]. The kinetic-energy cutoff of 50 Ry and charge-density cutoff of 200 Ry, were used for Kohn-Sham states wave functions, which were expanded in the plane-wave (PW) basis sets. The Brillouin-zone (BZ) was sampled according to the Monkhorst-Pack grid using  $3 \times 5 \times 1$  ( $3 \times 3 \times 1$ ) mesh for the organotin(IV) carboxylates compound geometry optimization and a denser mesh,  $4 \times 6 \times 2$  ( $5 \times 5 \times 1$ ) for the electronic structure calculations [121]. For self-consistent field calculations, the convergence criteria of total energy were set to  $10^{-4}$  Ry, and all the internal coordinates were allowed to fully

relaxed until the forces (Hellmann-Feynman) were get smaller than  $10^{-3}$  Ry/Bohr. It is observed by previous studies that GGA calculations underestimate the band-gap for insulators and semiconductors [122], because it does not include van-der Waals interactions (vdW). So to account for the long-rang vdW interactions and weak inter-molecular interactions the DFT+D2 (empirical dispersion corrected DFT) method proposed by Grimme was used [122]. The formation energy  $E_f$ (eV) was calculated by taking the difference between the total energy of the system and the chemical potentials of its constituents to divide by the total number of atoms. For example, for organotin(IV) carboxylates compound, mathematically it is defined as

$$E_f = \{E_{tot}[IC11] - 76\mu_H - 16\mu_O - 56\mu_C - 4\mu_{Sn} - 4\mu_N\}/156$$

The chemical potential of each constituent was calculated by considering the isolated atomic phase. Finally, we calculated vacuum potential, HOMO, LUMO, and work function of organotin(IV)carboxylates to find their possible applications in electronic devices.

## **Chapter 3**

### **Results and Discussion**

### 3. Spectroscopic Characterization

#### 3.1 Infrared Spectroscopy

The FT-IR spectra of ligands and metal complexes were recorded in the mid-infrared region in the range of 4000-400  $\text{cm}^{-1}$ . The IR major bands of the compounds were identified on the foundation of identical compounds. The significant IR absorption bands of the ligands and their corresponding metal complexes and their assignments are displayed in the experimental part.

The preliminary materials for the preparation of ligands are different types of anhydrides and substituted amines respectively. The appearance of a broad peak (around 3100-2500  $\text{cm}^{-1}$ ) for OH and a relatively sharp peak for NH in the range of 3102  $\text{cm}^{-1}$  to and 3400  $\text{cm}^{-1}$  indicates the synthesis of ligands. For organotin(IV) carboxylates, the related absorption frequencies of prime significance are  $\nu(\text{COO}^-)$ ,  $\nu(\text{Sn-O})$ , and  $\nu(\text{Sn-C})$  [123-125]. The absence of a broad peak pertinent to OH and a new peak for Sn-O (430-480  $\text{cm}^{-1}$ ) has appeared which indicates coordination of carboxylate ligand to organotin moiety. The difference in  $\text{COO}^-$  asymmetric and symmetric stretch ( $\Delta\nu = \nu(\text{COO}^-_{\text{asym}}) - (\text{COO}^-_{\text{sym}})$ ) gives valuable information about the approach of coordination of the carboxylate ligands to the tin center.  $\Delta\nu$  value falls in the range 302-239  $\text{cm}^{-1}$  demonstrating monodentate attachment of carboxylate with Sn atom. The presence of Sn-C peak (580-520  $\text{cm}^{-1}$ ) signifies that the alkyl groups remain intact with Sn during synthesis [126, 127].

The ligands IR spectra in the region of 1600-1000  $\text{cm}^{-1}$  are similar to their corresponding metal complexes due to similar organic functional group present in both ligand and their corresponding metal complexes.

The IR spectra of the metal complexes, in comparison with the free ligands spectra, showed significant differences that can be correlated with the formation of metal-based

complexes. The free ligands IR spectra showed broad and weak absorption bands at 3400-3600  $\text{cm}^{-1}$  which attributable to  $\nu(\text{N-H})$ , hence this shows that the ligands remain in the carbonyl amine when present in solid-state. Spectral bands of IR are mostly used for the determination of various ways of coordination of the ligands are  $\nu(\text{C=O})$ ,  $\nu(\text{N-C})$ , and  $\nu(\text{C=C})$  vibrations. A comparison of ligands IR spectra with their corresponding metal-based complexes indicates that the  $\nu(\text{N-H})$  bands of the free ligands observed at 3400-3200 $\text{cm}^{-1}$  for ligands are present in the spectra of the complexes supporting no deprotonation of the ligands  $\nu(\text{N-H})$  proton during coordination. The breathing motion of carboxylates is shifted to a higher frequency upon complexation and is consistent with the mono-coordinate mode of coordination [128].

In addition, the same ligands for investigation against selected bacteria and fungi argues that the shift of the  $\nu(\text{C-N})$  bands of the free ligands to lower wavenumbers and the shift of  $\nu(\text{C=C})$  bands to higher wavenumbers in the IR spectra of the complexes support coordination of the ligands to the metal atom via the carboxylate oxygen atom. However, the latter is not surprising since the  $\nu(\text{C-N})$  band is expected to couple with other bands and its shifting will depend on how much it is in combination with these bands, and as such it is not a reliable indicator of the coordination mode. Ligand **II**<sup>4</sup> and **II**<sup>9</sup> show  $\nu(\text{C-F})$  modes at 800  $\text{cm}^{-1}$  and 825  $\text{cm}^{-1}$  respectively [129, 130].

Consequently, the  $\nu(\text{C-N})$  modes are observed at about 1100  $\text{cm}^{-1}$  and 1150  $\text{cm}^{-1}$  in metal complexes and their corresponding ligands confirming that complexation these peak in both the ligands and metal complexes. Based on the above spectral signals, it's become confirmed that the fabricated free ligands are monodentate, coordinating via carboxylate moieties [129].



### 3.2. $^1\text{H}$ , $^{13}\text{C}$ , $^{119}\text{Sn}$ , and $^{19}\text{F}$ NMR studies

$^1\text{H}$ ,  $^{13}\text{C}$ ,  $^{119}\text{Sn}$ , and  $^{19}\text{F}$  NMR spectra for the synthesized complexes were carried out in DMSO- $d_6$  solvent and the data is given in the experimental part.

#### 3.2.1. $^1\text{H}$ NMR studies

In complexes, the absence of acidic OH peak (10-13 ppm) has confirmed the coordination of carboxylate anion to organotin(IV) moieties. The methyl proton in trimethyltin(IV) derivatives gave a sharp singlet with  $^2J_{[^{119}\text{Sn}, ^1\text{H}]}$  with coupling values of 57 Hz, 56 Hz, and 58 Hz, etc, thus confirming tetrahedral geometry around Sn in solution state. In tributyltin(IV) complexes,  $\beta$  and  $\gamma$  protons of the tributyl(IV) were observed as multiplets, Sn attached  $\text{CH}_2$  as a triplet having ranged from (1.60-1.66 ppm) and gave coupling constant values {1.62 ppm and  $^2J_{^1\text{H}, ^1\text{H}} = 8.0$  Hz and 1.64 ppm and  $^2J_{^1\text{H}, ^1\text{H}} = 8.0$  Hz} etc. depending on the ppm values in the proton NMR spectrum and terminal  $\text{CH}_3$  as an upfield triplet {0.98-94 ppm} which indicated the coupling constant value is for {0.96 ppm is  $^2J_{^1\text{H}, ^1\text{H}} = 7.3$  Hz and for 0.91 ppm is  $^2J_{^1\text{H}, ^1\text{H}} = 7.3$  Hz} etc., [131] which are given in the experimental section. There is no significant downfield shift of NH is observed and it also confirms the NH proton. All the aromatic protons are found in their respective regions. The calculated  $\theta$  for complexes using Lockhart equations confirmed that the complexes exhibit tetrahedral geometry in solution [132]. Some of the representative proton NMR spectra of ligands and complexes are given in the Figures below from 3.1-3.5.

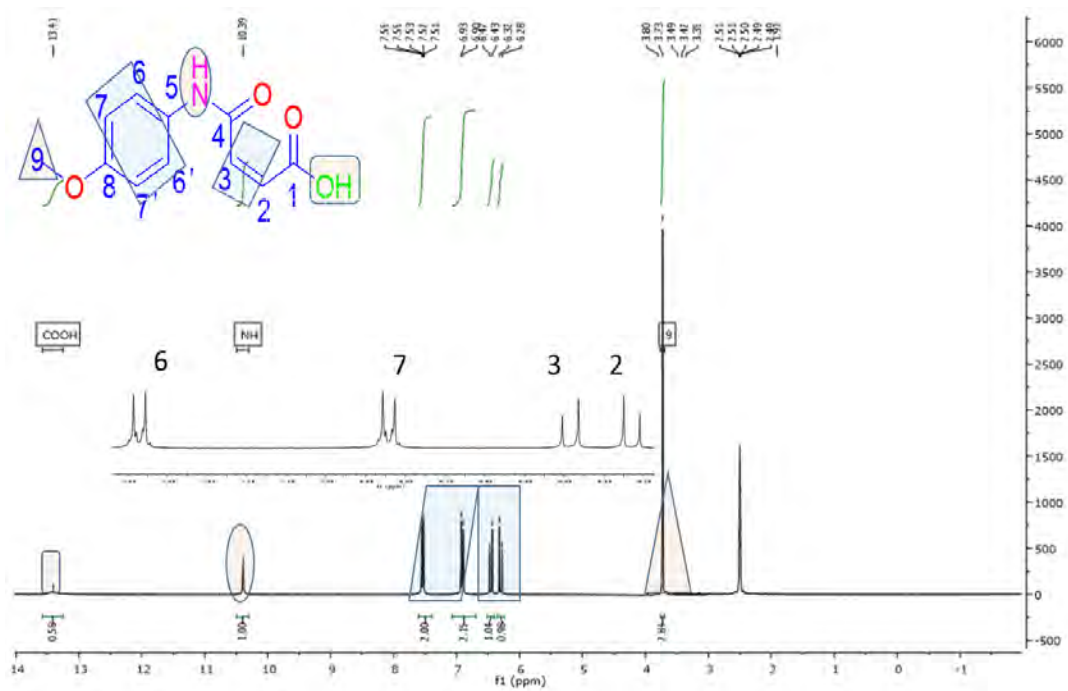


Figure 3.1: Representative  $^1\text{H}$  NMR spectrum of Ligand IL<sup>1</sup>.

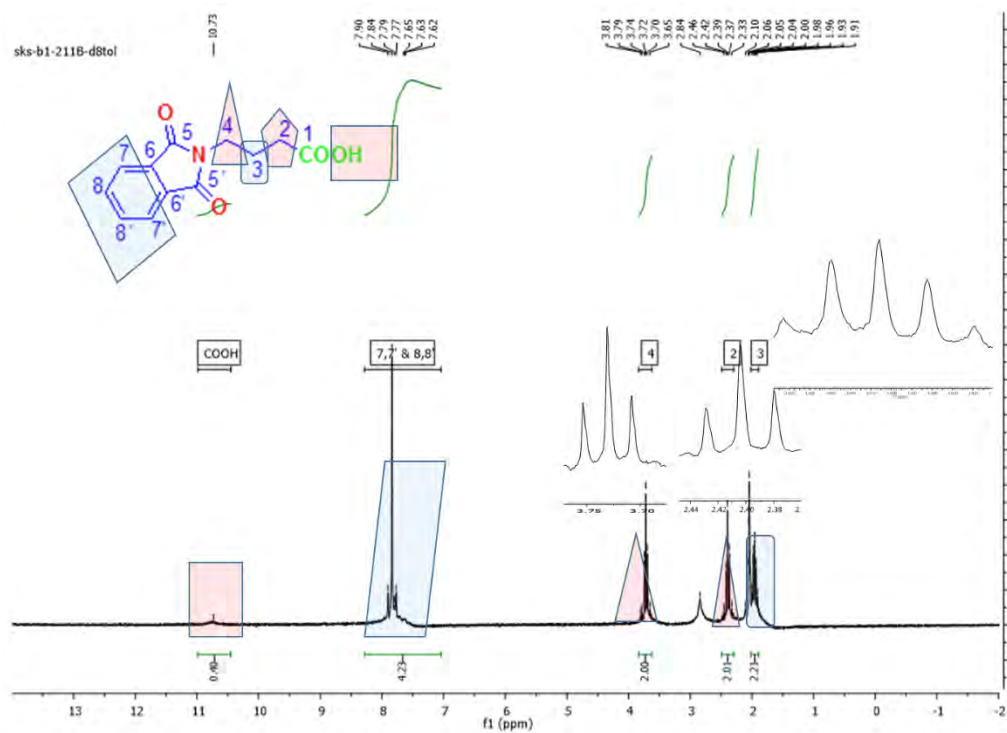


Figure 3.2: Representative  $^1\text{H}$  NMR spectrum of Ligand IL<sup>5</sup>.

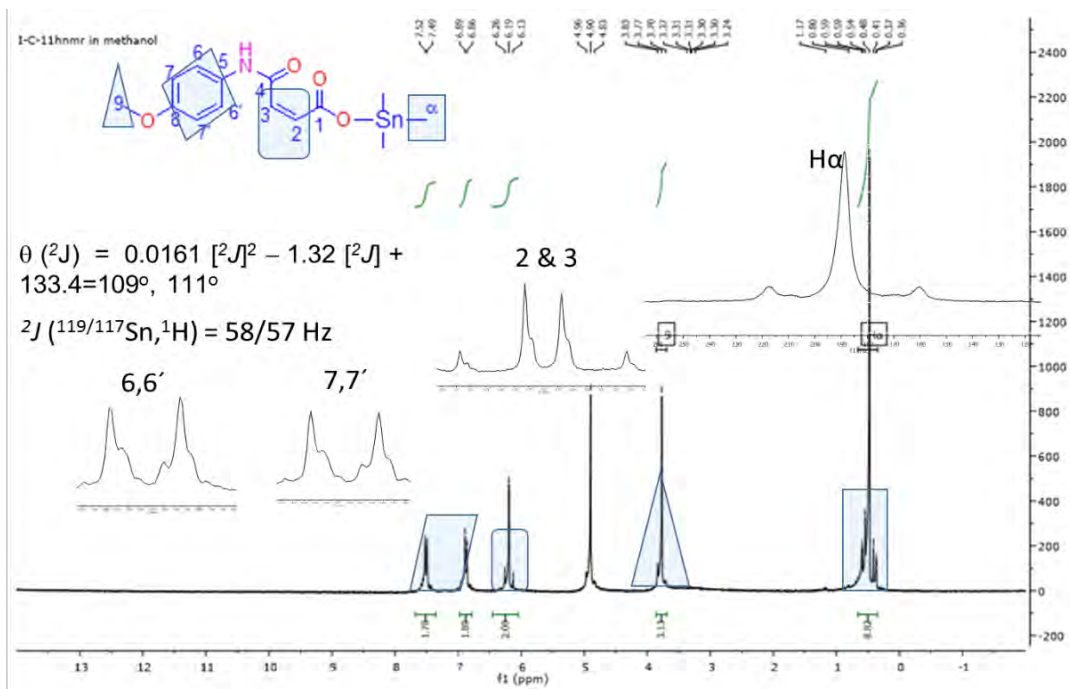


Figure 3.3: Representative  $^1\text{H}$  NMR spectrum of Complex 1.

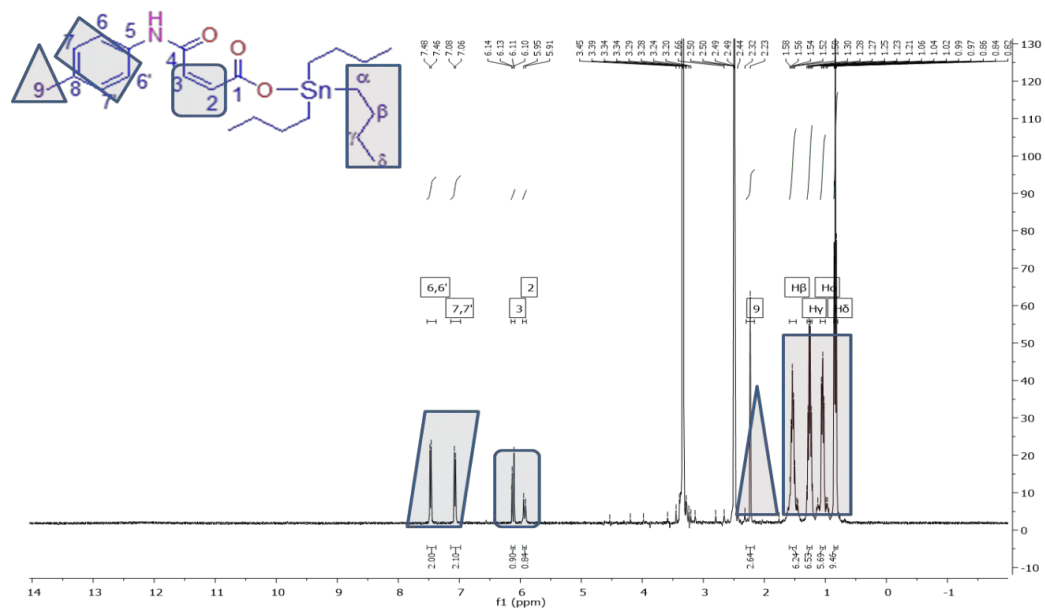
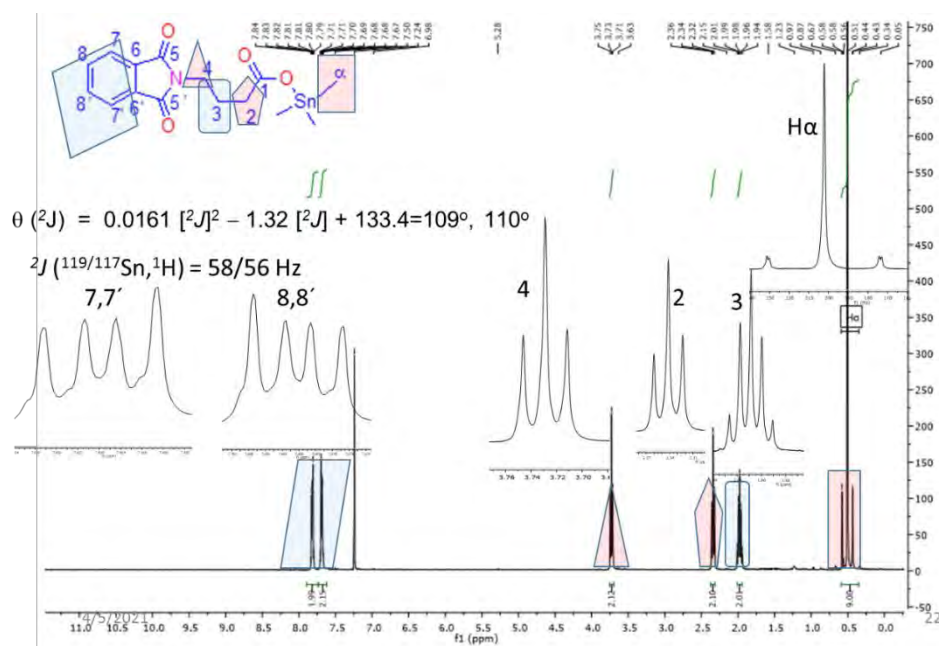


Figure 3.4: Representative  $^1\text{H}$  NMR spectrum of Complex 8.



**Figure 3.5:** Representative  ${}^1\text{H}$  NMR spectrum of Complex 13.

### 3.2.2. ${}^{13}\text{C}$ NMR spectroscopic studies

${}^{13}\text{C}$  NMR spectra of the organotin(IV) derivatives were recorded to elucidate the structure. The carboxylic carbon shifted downfield, because of diminution of the electron density at carboxylic carbon upon complexation than the free ligand, thus confirming coordination of oxygen with Sn [133]. While, the signal for aryl,  $-\text{C}-\text{N}$ , and alkyl groups connected to tin atom seemed in their expected regions. By using Lockhart's equation and adding a value of  ${}^1J [{}^{119}\text{Sn}, {}^{13}\text{C}]$  in it, the theta value can be calculated. The bond angle of  $\text{C}-\text{Sn}-\text{C}$  can be measured for methyltin(IV) and butyltin(IV), and phenyl(IV) based derivatives as displayed in the result and discussion spectral part. The result of some of complexes exhibit  ${}^1J [{}^{119}\text{Sn}, {}^{13}\text{C}]$ , 402/385 Hz (112 $^\circ$ , 110.5 $^\circ$ ) (**1**), 365 Hz (108.7 $^\circ$ ) (**2**), 392 Hz (111.14 $^\circ$ ) (**4**) and 416 Hz (113.2 $^\circ$ ) (**5**) etc., respectively, which represent tetra-coordinated tin(IV) atom in solution [134, 135]. The representative spectra of the carbon-13 NMR are given below in Figures 3.6-3.10.

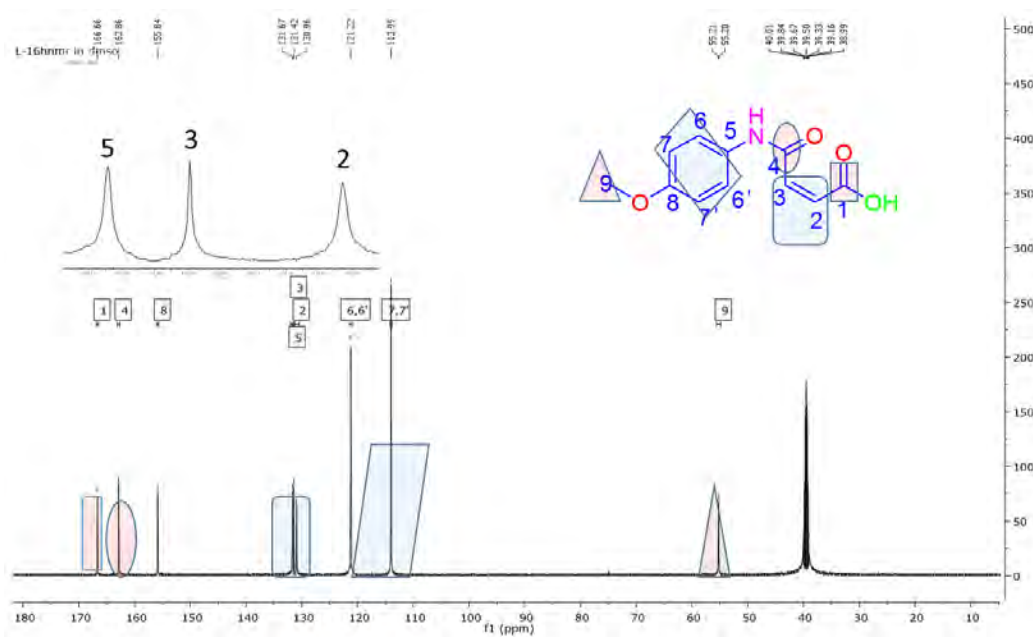


Figure 3.6: Representative  $^{13}\text{C}$  NMR spectrum of Ligand IL<sup>1</sup>.

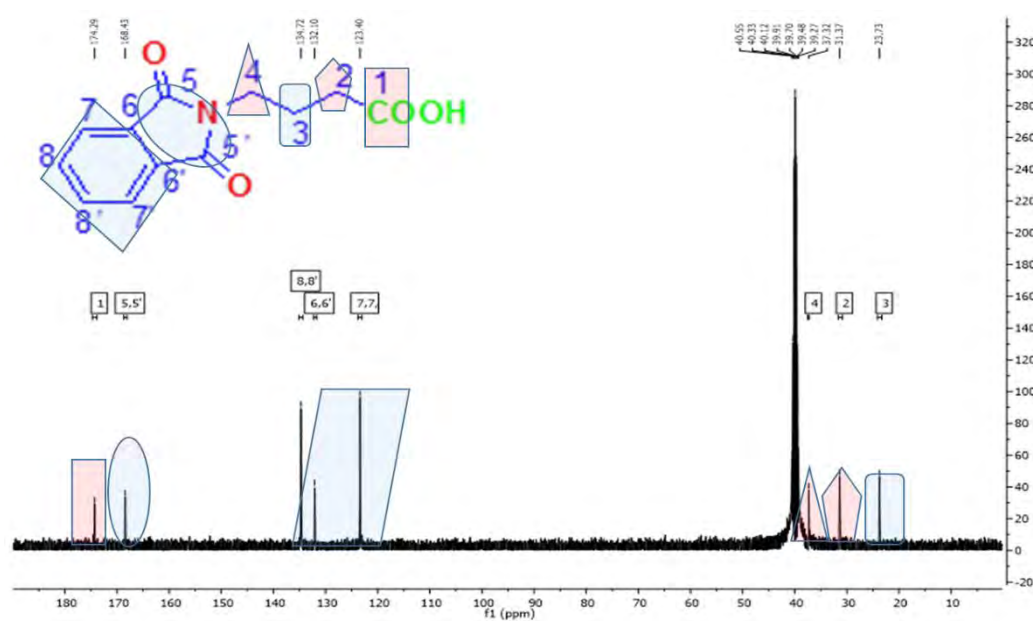


Figure 3.7: Representative  $^{13}\text{C}$  NMR spectrum of Ligand IL<sup>5</sup>.

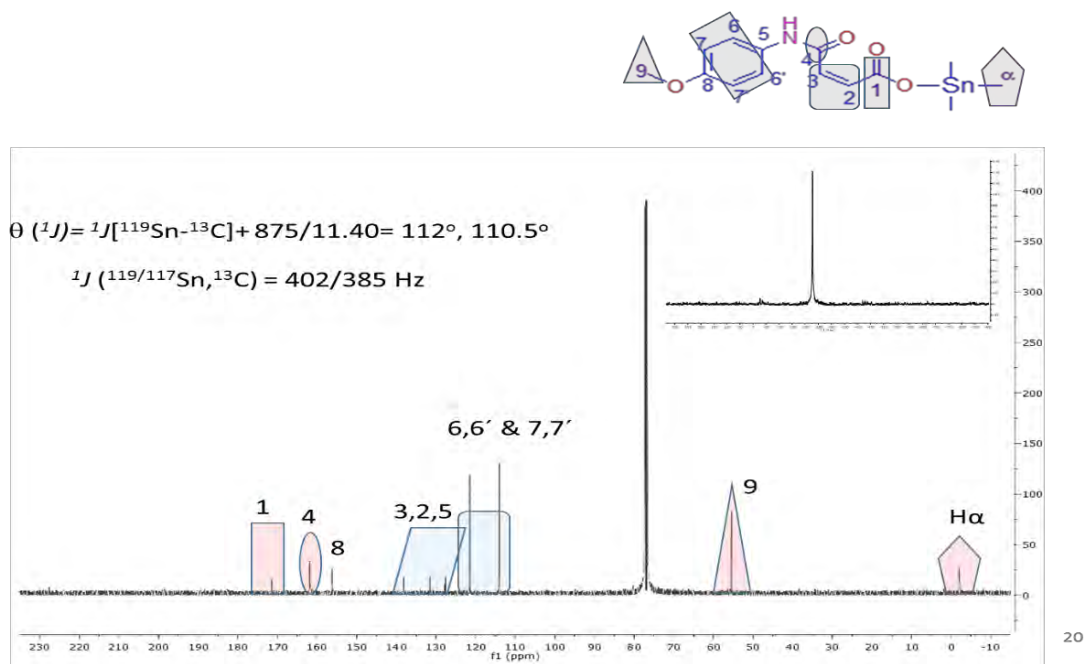


Figure 3.8: Representative  $^{13}\text{C}$  NMR spectrum of Complex 1.

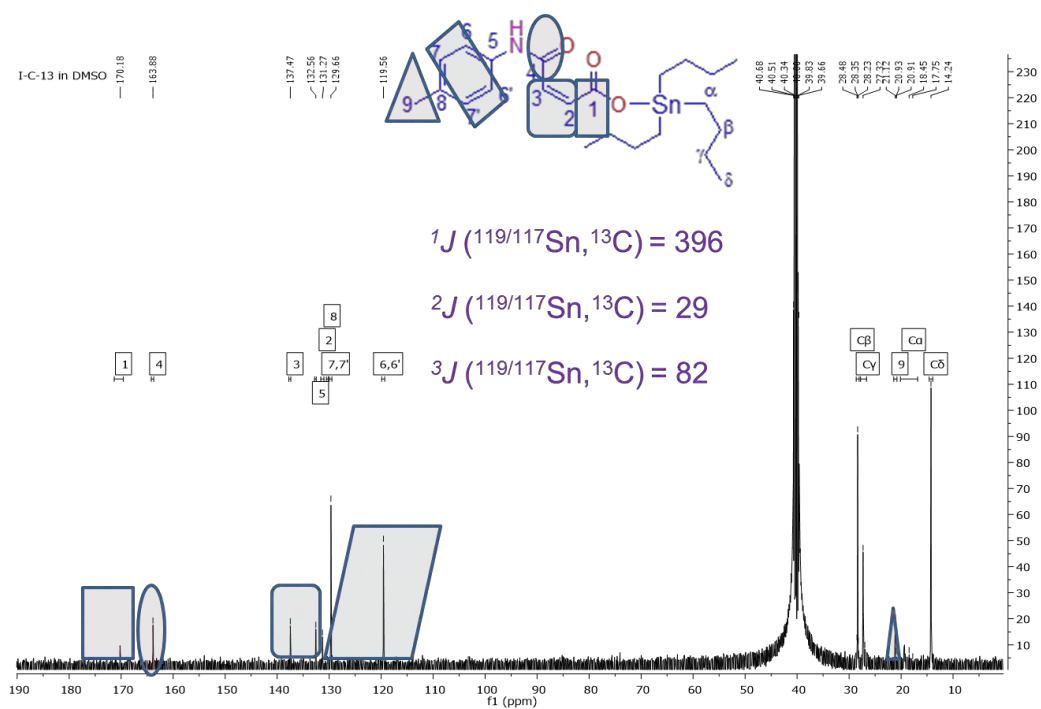
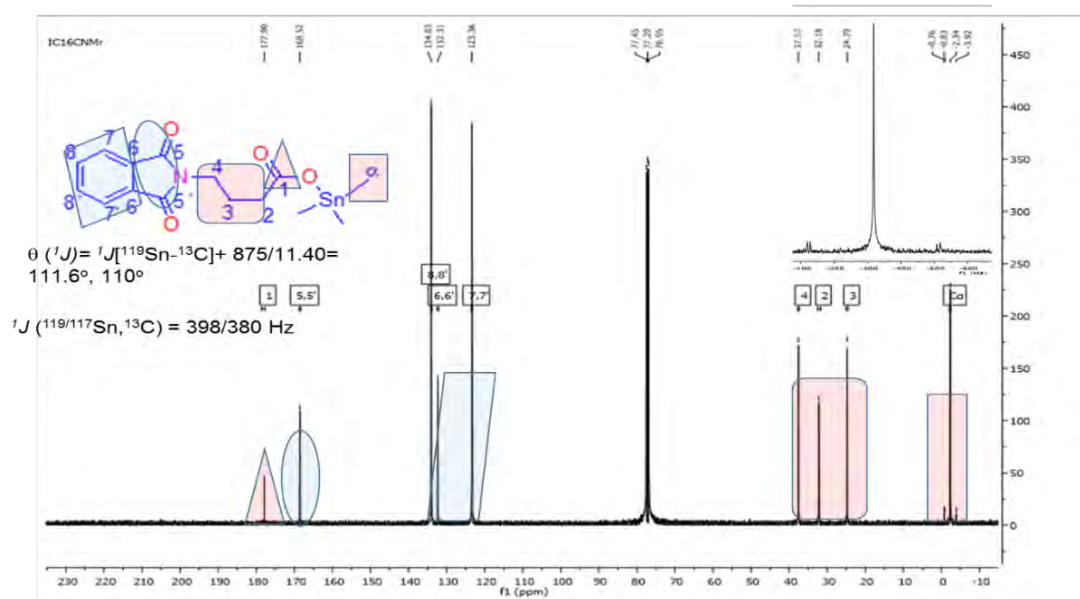


Figure 3.9: Representative  $^{13}\text{C}$  NMR spectrum of Complex 8.



**Figure 3.10:** Representative  $^{13}\text{C}$  NMR spectrum of Complex 13.

### 3.2.3. $^{119}\text{Sn}$ NMR studies

The presence of  $^{119}\text{Sn}$  NMR peak at -16 (**1**), 136 (**8**), 151 (**3**), and 134 (**13**) ppm authenticated tetra coordination of tin. The electron-withdrawing and donating groups of ligands and the substituent and its electronegativity effect at the tin atom seem responsible for variation in  $^{119}\text{Sn}$  NMR value [136-139]. All other complexes also indicated similar peaks observed in the four coordinated ranges in solution states. The representative spectra of  $^{119}\text{Sn}$  NMR are given below in Figures 3.11-3.13.

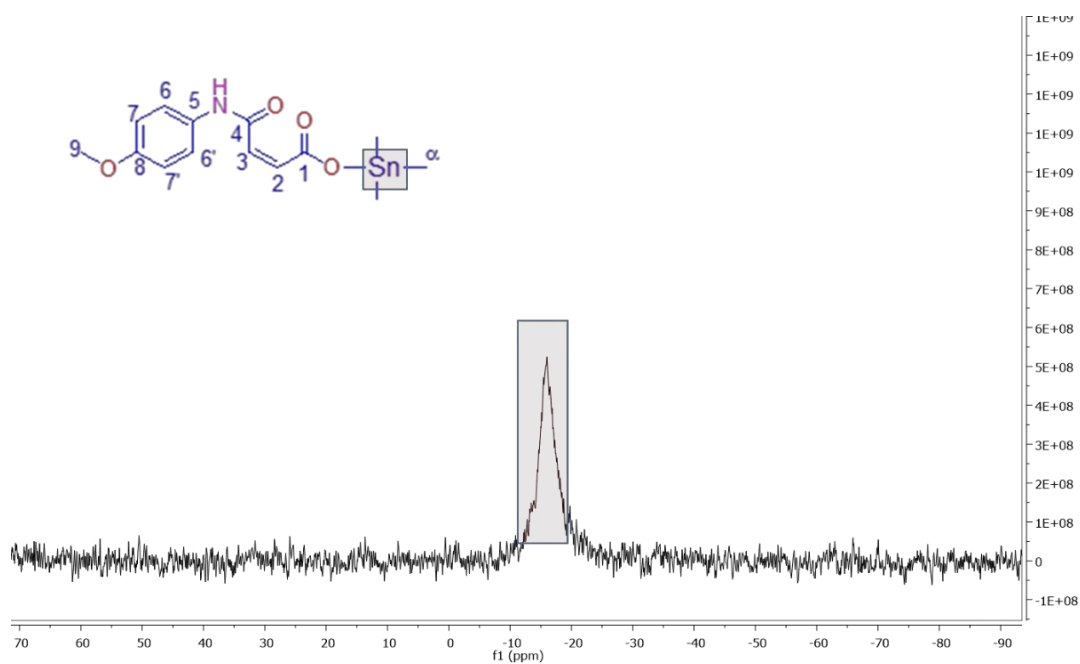


**Figure 3.11:** Representative  $^{119}\text{Sn}$  NMR spectrum of Complex 1.

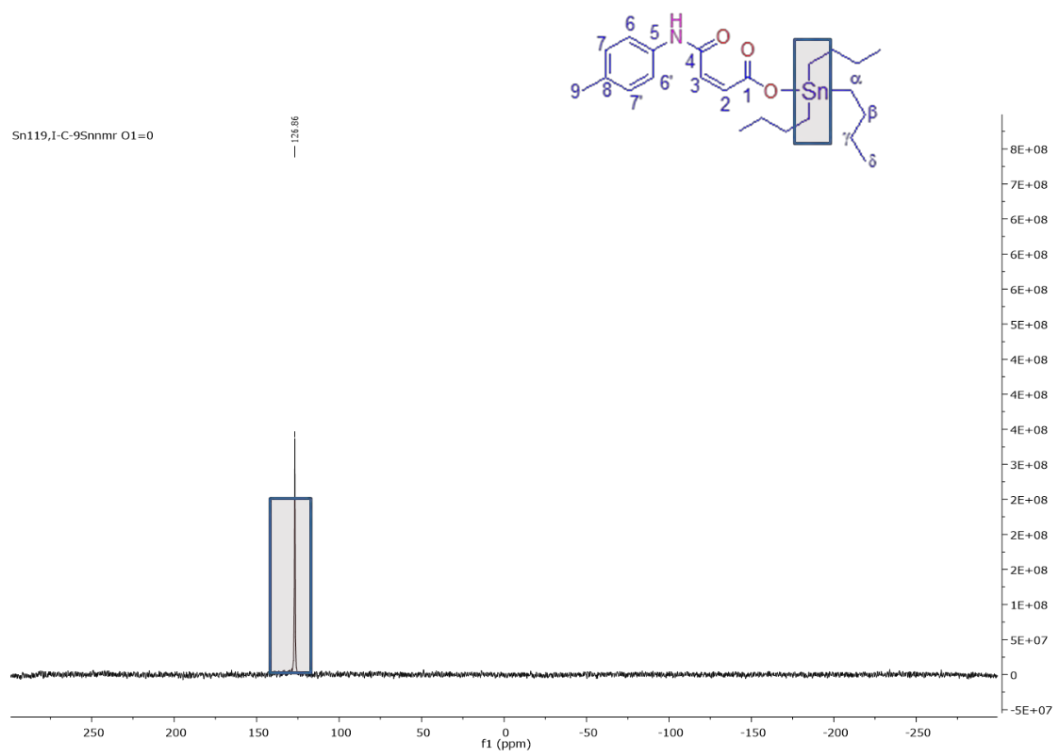


**Figure 3.12:** Representative  $^{119}\text{Sn}$  NMR spectrum of Complex 8.



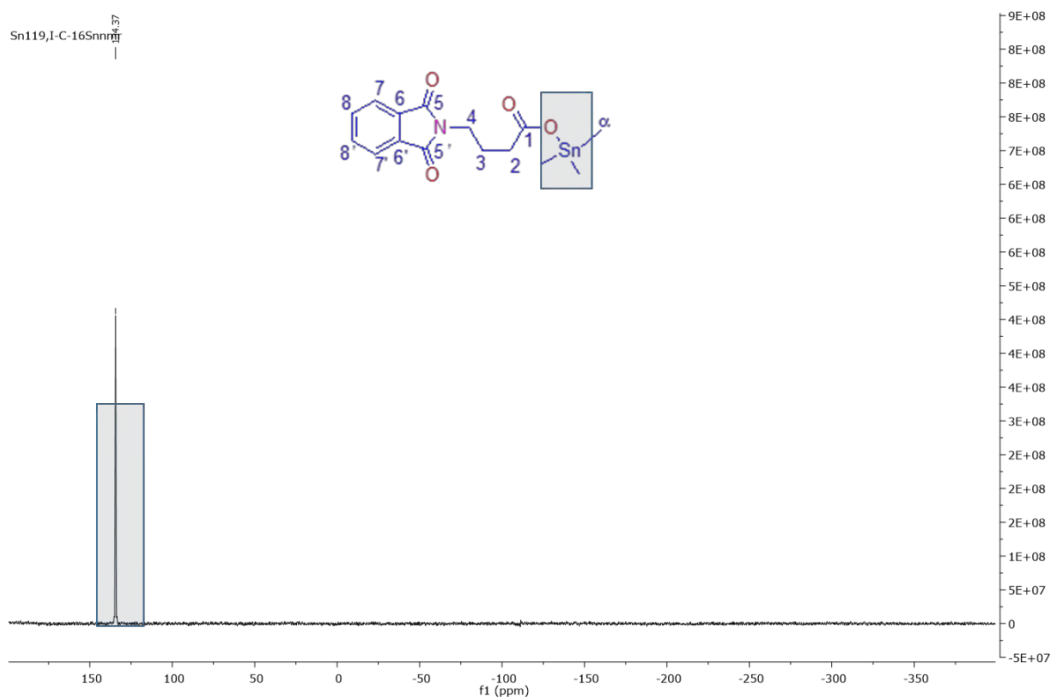


**Figure. 3.13:** Representative  $^{119}\text{Sn}$  NMR spectrum of Complex 13.

### 3.2.4. $^{19}\text{F}$ NMR studies

The fluoro bonded  $^{13}\text{C}$  gave a specific pattern of  $^{13}\text{C}$  chemical shift values. In **II**<sup>2</sup> the fluorine signal of  $\text{CF}_3$  appeared at -57 ppm, which was shifted upfield (-63 ppm) in complexes **4** and **5**. This upfield shift may be because of the back donation of electron density from the metal center to the ligand which increases electron density on fluorine atom upon complexation of the corresponding ligand with electropositive tin atom [140]. The representative spectra of  $^{19}\text{F}$  NMR are given below in Figures **3.14** and **3.15**.

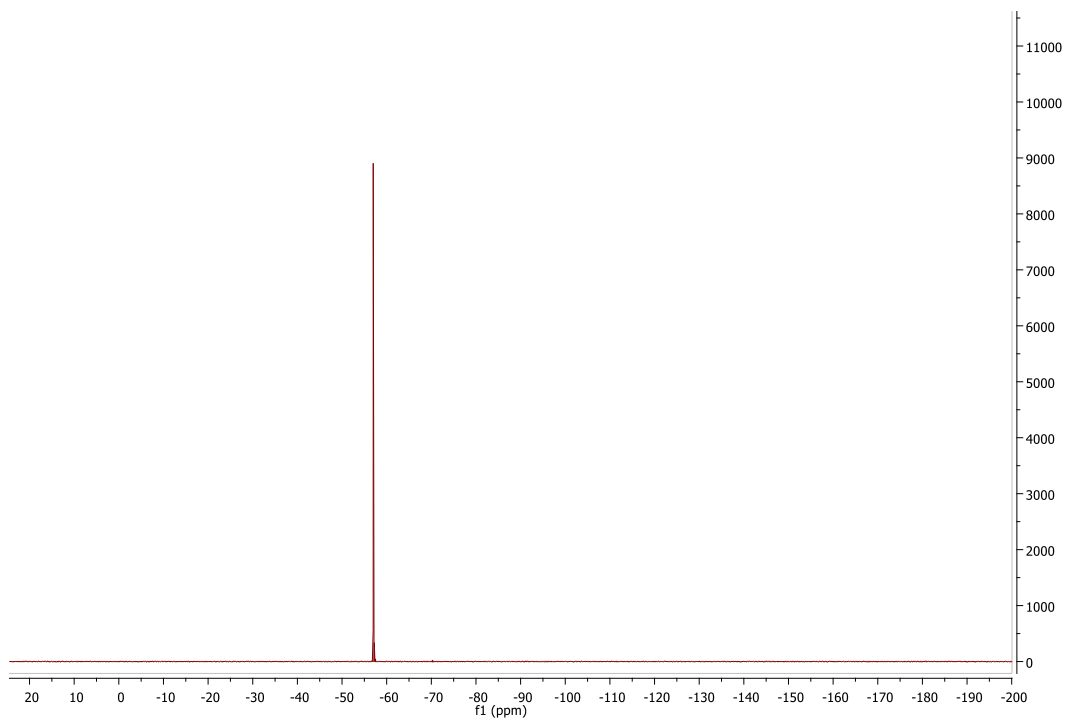


**Figure. 3.14:** Representative  $^{19}\text{F}$  NMR spectrum of ligand IL<sup>2</sup>.

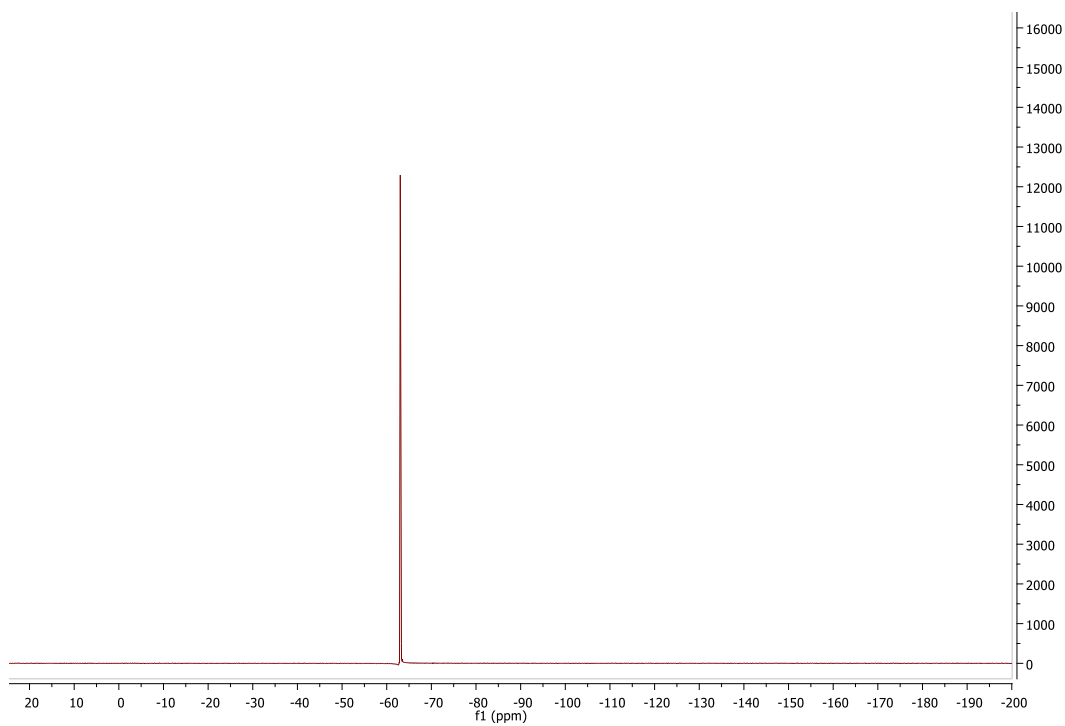


**Figure. 3.15:** Representative  $^{19}\text{F}$  NMR spectrum of complex 4.

### 3.3 Biological Activities

#### 3.3.1. Anticancer potential and cytotoxic activities of organotin(IV) amide-based carboxylate derivatives

These synthesized ligands and organotin(IV) amide-based carboxylate complexes were selected for in vitro cytotoxic studies against various cell lines such as breast cancer cell lines (MCF-7) and human endometrial stromal cells (hESCs) by the MTT [Tetrazolium [3-(4,5-dimethylthiazol-2-yl)-2,5-diphenyltetrazolium bromide] method. Cisplatin which is known as the most effective anticancer drug was used as a standard. MCF-7 was grown in EMEM with 1% penicillin/streptomycin, 10% FBS and 0.01 mg/ml insulin. hESCs were grown in DMEM/Ham's F12 with 10 % FBS and 1% penicillin/streptomycin. Both the cells were preserved in a moistened incubator with 5% CO<sub>2</sub>. For cytotoxic analysis, 4 X 10<sup>4</sup> cells were seeded per well in a 96 well plate and permitted to reach 80% confluence. The salts were dissolved in DMSO, added to the cells (final concentrations of 1000, 500, 250, 125, 62.5, 31.25 & 15.63 μM), and incubated for 48 h. The cell survival was determined by MTT analysis according to the manufacturer's instruction (Vybrant™ MTT Cell Proliferation Assay Kit, Thermofisher).

This growth inhibition study of the ligands and organotin(IV) amide-based carboxylates compounds suggested that the target biomolecule could be DNA but others also like cisplatin. For the determination of the cytotoxic effect of compounds on cancer and normal cell line, the cells were treated with ligands (**IL**<sup>1</sup>, **IL**<sup>2</sup>) and complexes **1-6** at various concentrations and determined the cytotoxicity by MTT assay and compared the results which expressed as a concentration required to inhibit the cancer cells growth by 50% (IC<sub>50</sub>) along with % viability of cells. The IC<sub>50</sub> values of the compounds are represented in Figure **3.16**. Compounds **2** and **4** have shown strong growth inhibition

properties with  $IC_{50} < 15.6$  against both cancer and normal cell line. However, **5** can be a good anticancer compound for further evaluation as it is twenty times more active against anticancer cells as compared to normal cells. The toxicity of compound **1** is almost comparable for both cancerous and non-cancerous cells which showed that it is not a good anticancer agent. Similarly, the compound **3** and **6** also showed very strong anticancer activities against the anticancer cells (Breast cancer cells) as compared to noncancerous cells (HESCs). The ligands **IL<sup>1</sup>** and **IL<sup>2</sup>** are almost inactive. The higher activity of complexes **4**, **5** and **6** to arrest the DNA replication may be due to the presence of fluoro group as well as oxygenated moieties, which form strong hydrogen bonds with nucleotide of DNA.

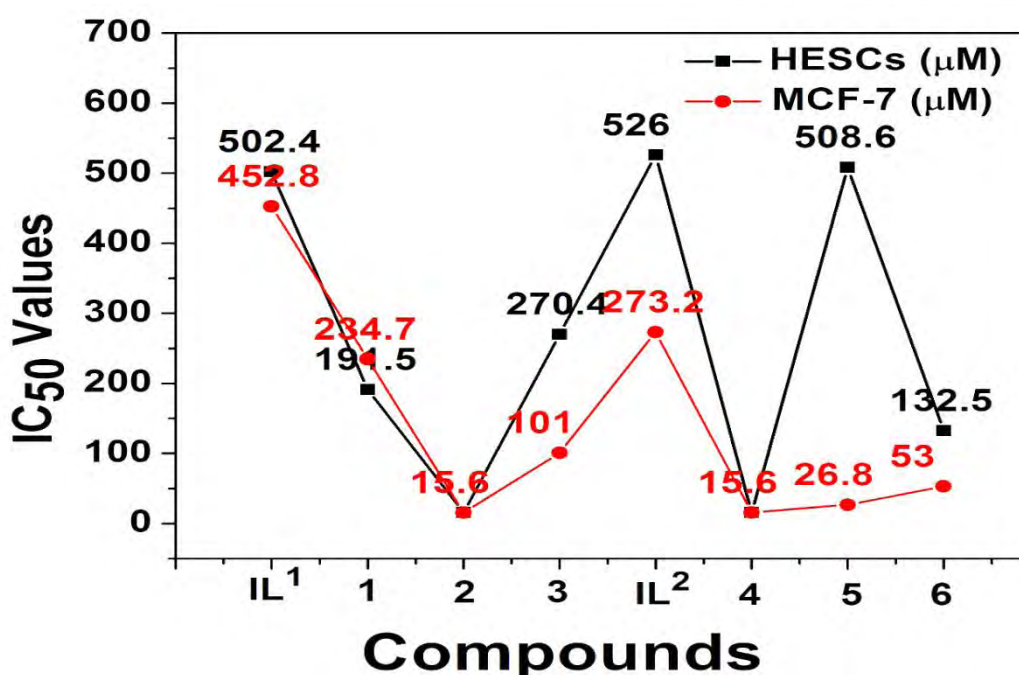


**Figure 3.16:**  $IC_{50}$  ( $\mu\text{M}$ ) values of synthesized Ligands and complexes against breast cancer cell line (MCF-7) and human endometrial stromal cells (hESCs).

For the determination of the cytotoxic significance of another series of compounds on cancer and normal cell line, we treated the noncancerous cell line and cancerous cell line with compounds **IL<sup>3</sup>**, **IL<sup>4</sup>**, **7**, **8**, **9**, **10**, **11**, and **12** at various concentrations and determined the cytotoxicity by MTT assay and compared the results. The  $IC_{50}$  values

of the compounds are given in figure 3.17. The ligand **IL**<sup>3</sup> has IC<sub>50</sub> value for MCF-7 cells is less than as compared hESCs while ligand **IL**<sup>4</sup> showed lower IC<sub>50</sub> value for MCF-7 cells as compared hESCs cells which IC<sub>50</sub> value is 3 times high which showed that **IL**<sup>4</sup> is a good candidate as compared to **IL**<sup>3</sup> as an anticancer agent. In the case of compound 7, the IC<sub>50</sub> for MCF7 is almost comparable with the hESCs which showed that this compound is not suitable as an anticancer agent. The compounds 8, 9, and 10 have lower IC<sub>50</sub> value for MCF-7 cells as compared to hESCs cells and the compounds are highly cytotoxic even at the lowest concentration we have tested. Compounds 11 and 12 disclosed essentially good activity which 6 times more active against MCF-7 as compared to hESCs. Compounds 12 can be a good candidate as an anticancer agent. Further experiments are needed to ascertain and characterize the anticancer activity of these complexes.

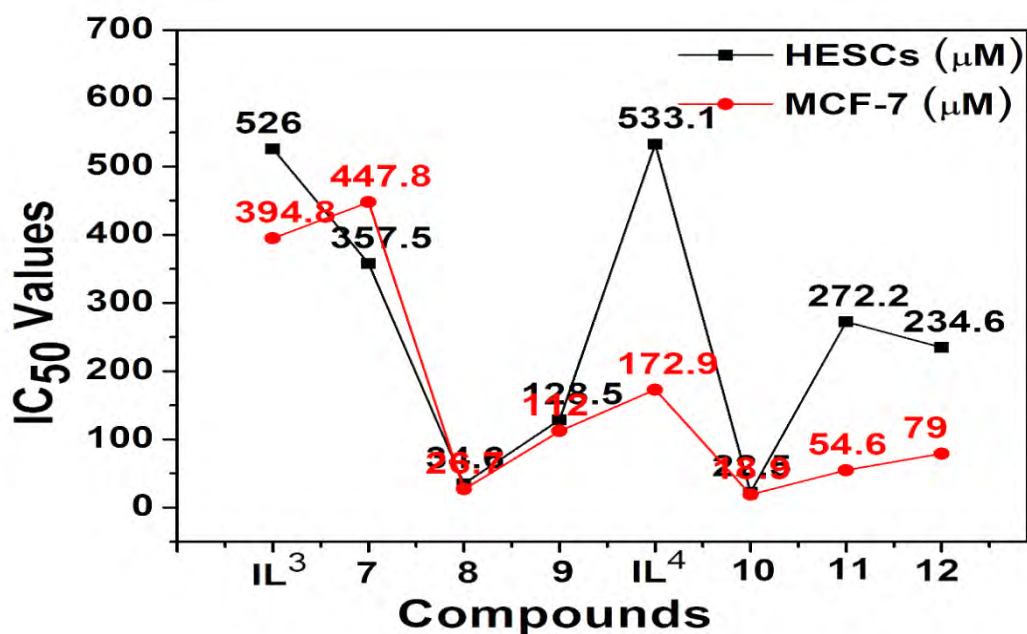


**Figure 3.17:** IC<sub>50</sub> (μM) values of synthesized ligands and complexes against breast cancer cell line (MCF-7) and human endometrial stromal cells (hESCs).

Similarly, one of the series of Ligand **IL<sup>5</sup>** and their three complexes **13**, **14**, and **15** were screened for the in vitro anticancer against MCF-7 and noncancerous against hESCs cell line. The inhibitory concentration (IC<sub>50</sub>) values have been assayed for Ligand **IL<sup>5</sup>** and complexes **13**, **14**, and **15**. The collected values of IC<sub>50</sub> are given in Figure **3.18** below. The ligand **IL<sup>5</sup>** has a very high IC<sub>50</sub> value for the cancerous and noncancerous cells, which showed that it is not a good anticancer agent. Complex **13** is almost two times more active against the cancer cells as compared to normal cell lines. Complexes **14** and **15** having the best anticancer agents as compared with the standard drugs Cisplatin but further stages of screening are needed to there in vitro and in vivo to assess their potential as good anticancer agents.

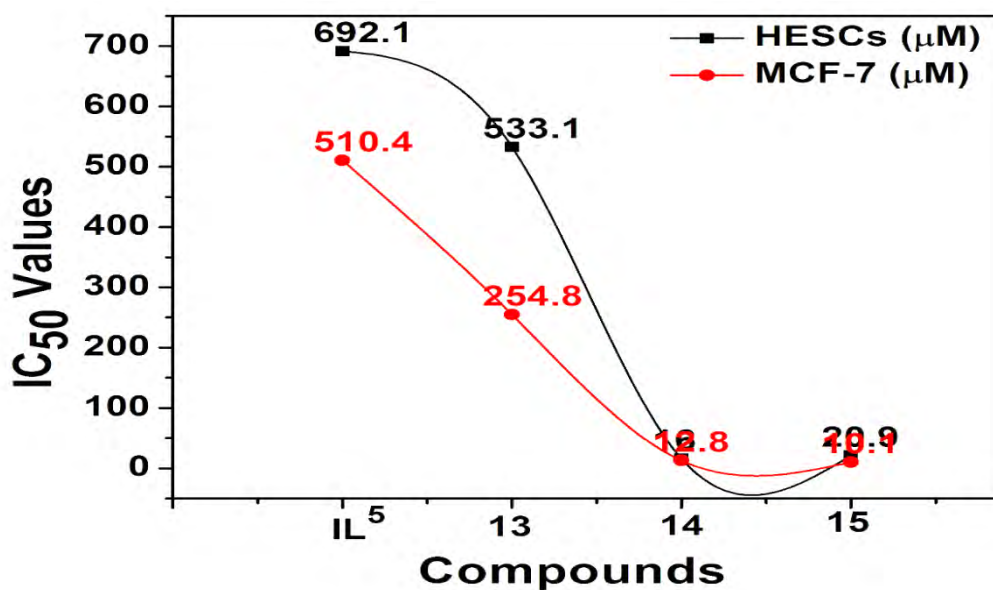


**Figure. 3.18:** IC<sub>50</sub> (μM) values of synthesized ligand and complexes against breast cancer cell line (MCF-7) and human endometrial stromal cells (hESCs).

### 3.3.2. Antileishmanial potency of the synthesized ligands and complexes

The promastigote forms of *L. tropica* ( $1 \times 10^4$  cells/well) were seeded in 96-well microtiter plates in RPMI-1640 (Gibco<sup>®</sup>) supplemented with 10% FBS (Gibco<sup>®</sup>) and 1% antibiotics and allowed to grow either in the presence of various concentrations (1000, 500 and 250  $\mu\text{g/mL}$ ) of test compounds (**IL**<sup>1</sup>, **IL**<sup>2</sup>, **IL**<sup>3</sup>, **IL**<sup>4</sup>, **IL**<sup>5</sup> and their complexes from **1** to **15**) or in the absence (negative control) of the test compound for 72 hours at 25°C. After the incubation period was completed, the viability of the promastigote form was assessed by MTT (3-(4,5-dimethylthiazol-2-yl)-2,5-diphenyltetrazolium bromide) colorimetric method. For this, 100 $\mu\text{l}$  of the MTT dye was added to each well and the plates were incubated for 3 hours at 37°C. In last, 40 $\mu\text{l}$  of the DMSO as solubilization solution was added into each well and the readings were recorded using an ELISA plate reader (Biotek Elx800) at 570 nm. The experiment was performed in triplicates while counting of leishmania promastigote was done using Neubauer chamber [141].

For the anti-leishmanial assay, the prepared ligands and their corresponding complexes were solubilized used DMSO. The percent inhibition and IC<sub>50</sub> values are given in the Figures below. All compounds showed good results except **IL**<sup>1</sup> in terms of percentage inhibition. Interestingly, **IL**<sup>2</sup> showed high percentage inhibition at higher concentrations but its potency lowers at low concentrations. It is important to point out that compound **5** showed high anti-leishmanial activity at all three concentrations in terms of percentage inhibition but have not a good IC<sub>50</sub> value. The observed anti-leishmanial activity order is **6** > **3** > **2** > **4** > **1** > **5** which is shown below Figures **3.19** and **3.20**. Similarly, all of the compounds showed good results except **IL**<sup>3</sup> and **IL**<sup>4</sup> in terms of percentage inhibition. Interestingly **7**, **8**, and **9** showed high percentage inhibition at higher concentrations but its potency highly decreases on low

concentrations. Figures 3.21 and 3.22 given below showed the name of the compounds along with their percent inhibition and IC<sub>50</sub> values at different concentrations. It is important to point out that compound 12 showed high anti-leishmanial activity at all three concentrations in terms of percentage inhibition but having a good IC<sub>50</sub> value as well. In comparison, the anti-leishmanial activity of compounds 12, 9, and 7 was excellent followed by 11, 8, and 10. Ligands IL<sup>3</sup> and IL<sup>4</sup> are the least active compounds.

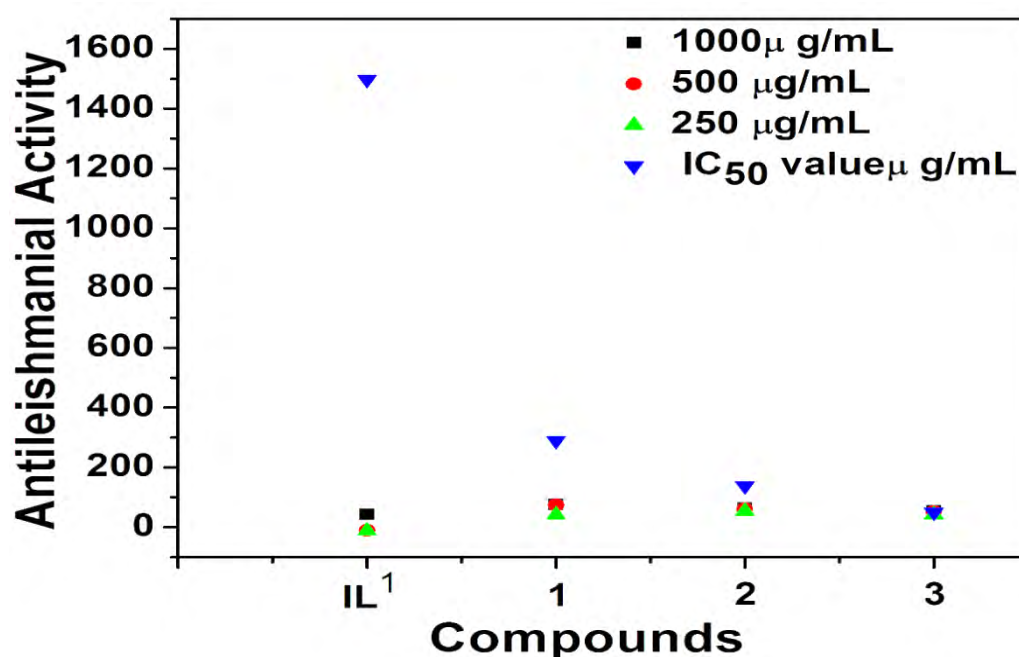


Figure 3.19: Antileishmanial activities of ligand (IL<sup>1</sup>) and complexes (1-3).



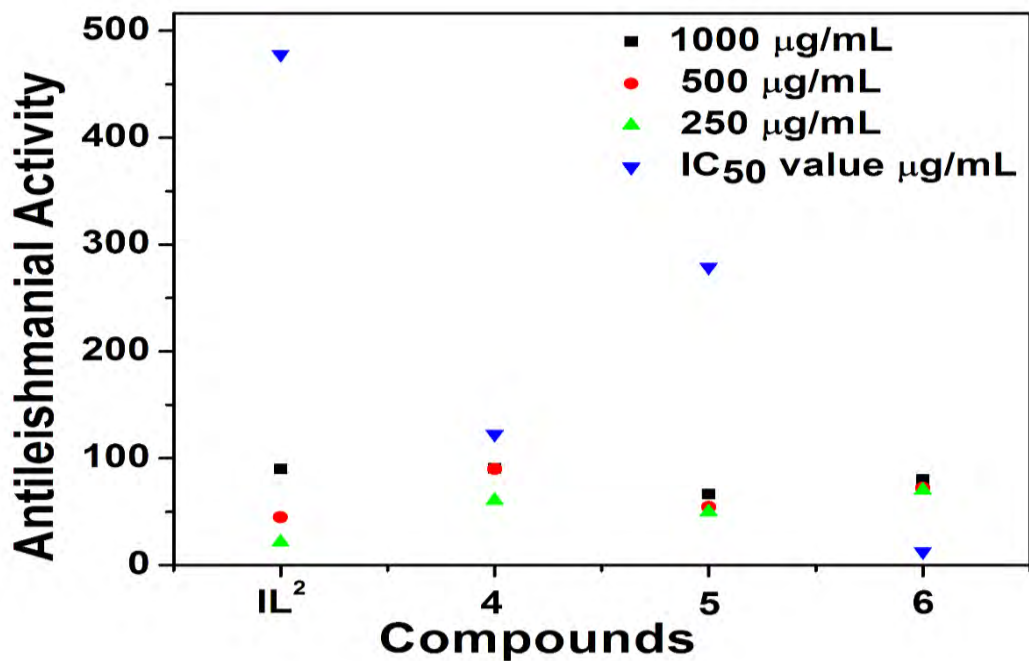


Figure 3.20: Antileishmanial activities of ligand ( $IL^2$ ) and complexes (4-6).

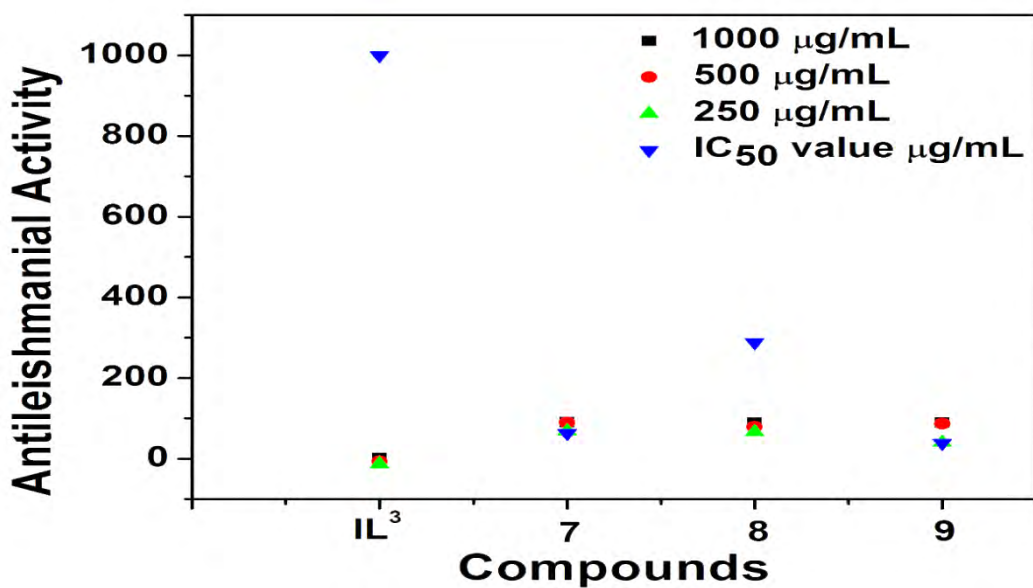
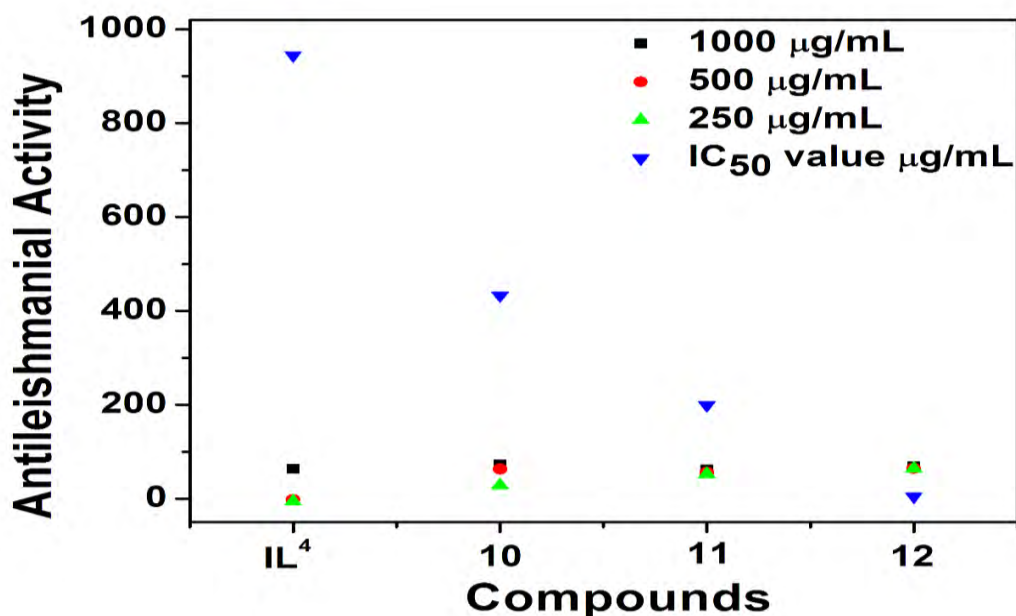


Figure 3.21: Antileishmanial activities of ligand ( $IL^3$ ) and complexes (7-9).



**Figure 3.22:** Antileishmanial activities of ligand ( $\text{IL}^4$ ) and complexes (10-12).

MTT analysis was also implemented on the synthesized ligands and their complexes to study in-vitro antileishmanial activity against  $\text{IL}^5$  major leishmanial promastigote forms. A significant reduction was observed by applying the fabricated compounds in sustainable promastigotes as displayed in Figure 3.23. Different concentrations of compounds were used to study the antileishmanial activity and shown strong activity in all cases. In all the above experiments, the standard was amphotericin B. Figure 3.23, displayed  $\text{IC}_{50}$  values which confirm that the compound **15** was the most potent against major leishmanial promastigote forms and discovered an  $\text{IC}_{50}$  value of  $4.31 \mu\text{g/mL}$  which is concomitant with to  $\text{IC}_{50}$  value of amphotericin B, which has  $0.49 \mu\text{g/mL}$ . Compounds **13** also showed moderate potency against leishmania, while the Ligand  $\text{IL}^5$  and compound **14** exhibited poor antileishmanial activity against major leishmanial promastigote forms. This activity may be due to intervention with the normal mitochondrial function of a parasite. The present study thus confirmed the possible use of these complexes as a foundation of pristine representatives for the curing of leishmaniasis.

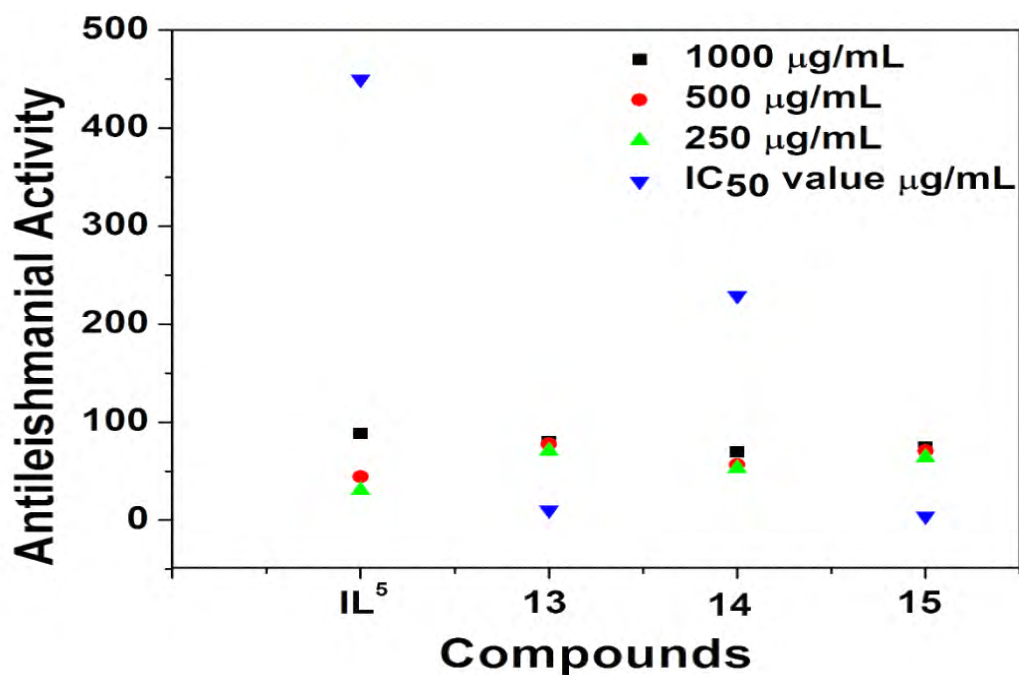


Figure 3.23: Antileishmanial activities of ligand (IL<sup>5</sup>) and complexes (13-15).

### 3.3.3. Hemolysis Assay

Hemolysis assay was done to evaluate compounds cytotoxicity on human blood erythrocytes. The synthesized compounds were checked for their cytotoxic activity and were likened with Triton X-100 (0.5%). The results showed that IL<sup>2</sup> was found to be the least toxic in term of percent hemolysis, followed by 1, 4, 3, and IL<sup>1</sup>, 6 while 5 and 2 were observed to be highly toxic as compared to Triton X-100 with a high percent hemolysis ratio in the figures 3.24 and 3.25 A similar pattern is observed in all other compounds given in figures 3.26, 3.27, 3.28.

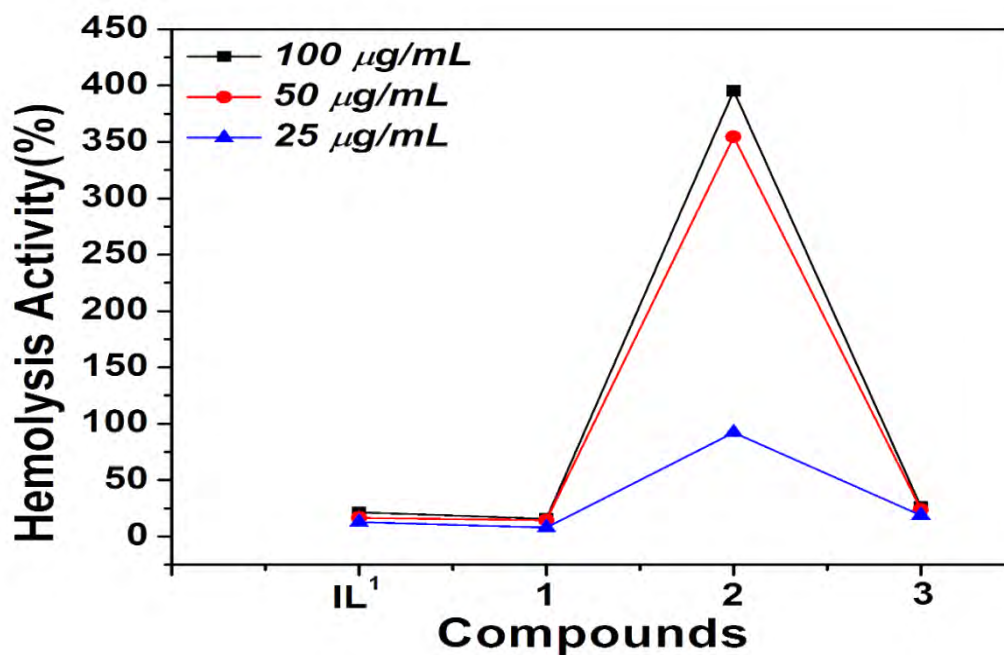


Figure 3.24: Hemolytic assay activities of ligand (IL<sup>1</sup>) and complexes (1-3).

Table 3.1: Percent hemolysis and IC<sub>50</sub> values of ligand IL<sup>1</sup> and complexes (1-3).

Name	25 (µg/ml)	50 (µg/ml)	100 (µg/ml)	IC <sub>50</sub> values (µg/ml)
IL <sup>1</sup>	13.34 ± 0.012	16.64 ± 0.04	21.46 ± 0.115	>1000
1	8.22 ± 0.918	14.34 ± 0.019	15.64 ± 0.045	379.46
2	96.36 ± 0.035	354.45 ± 0.041	395.36 ± 0.046	0.80
3	13.34 ± 0.033	13.54 ± 0.290	15.44 ± 0.661	>1000

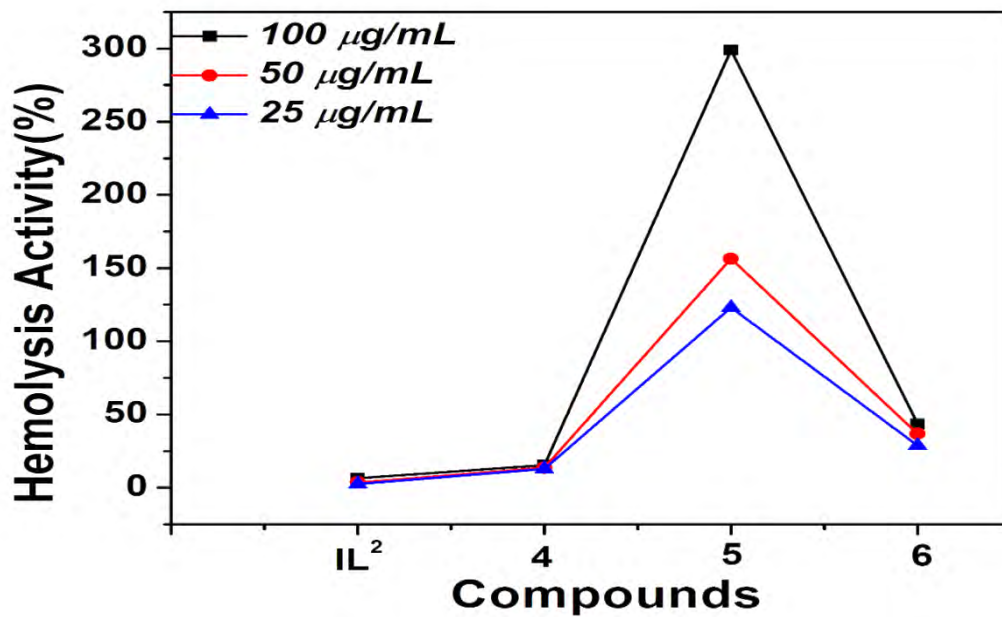


Figure 3.25: Hemolytic assay activities of ligand ( $IL^2$ ) and complexes (4-6).

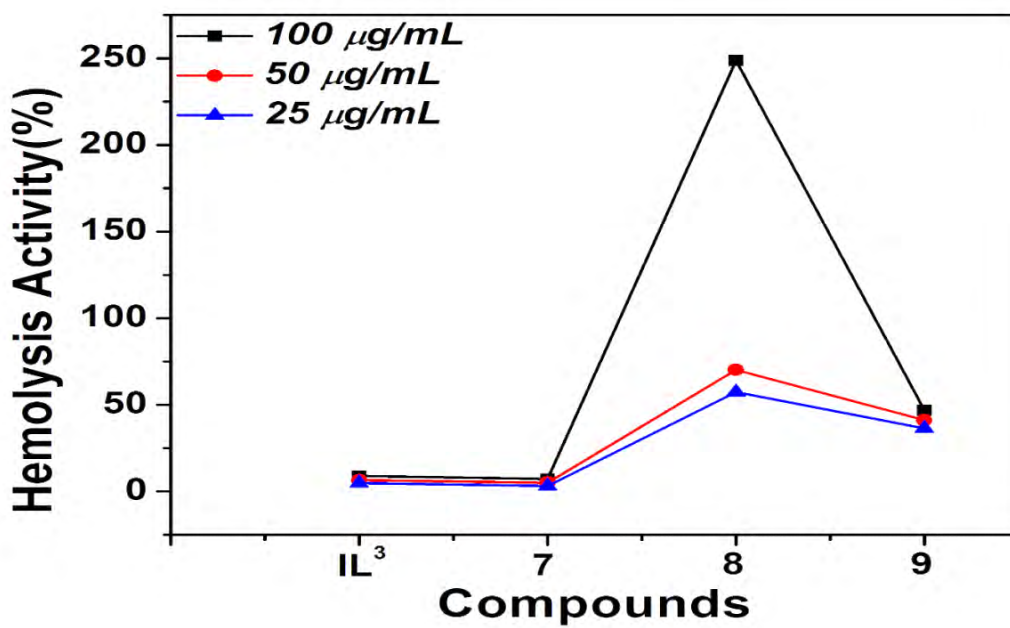


Figure 3.26: Hemolytic assay activities of ligand ( $IL^3$ ) and complexes (7-9).

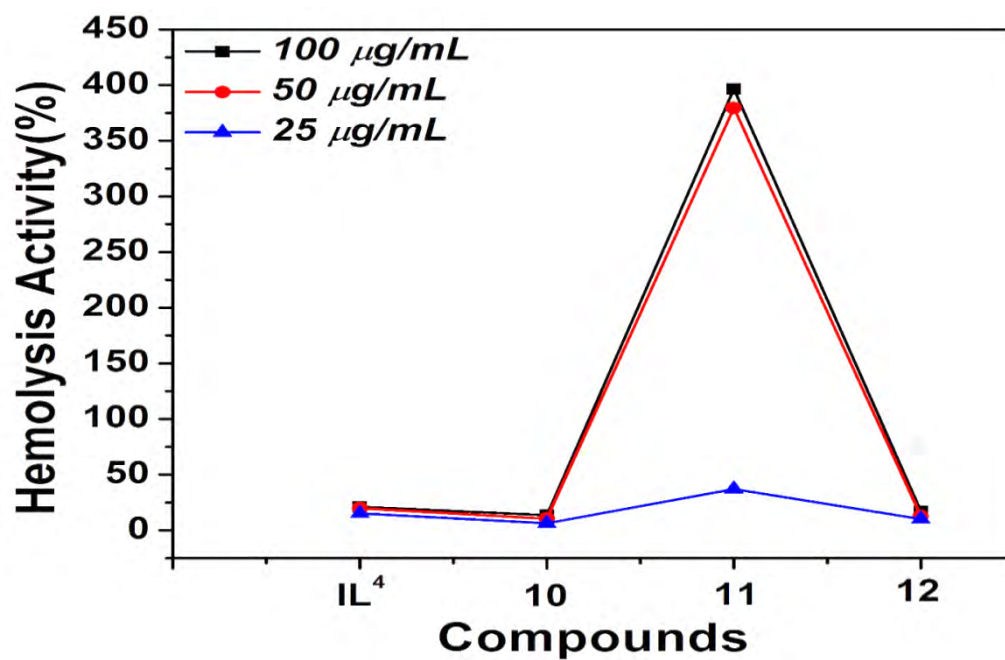


Figure 3.27: Hemolytic assay activities of ligand ( $IL^4$ ) and complexes (10-12).

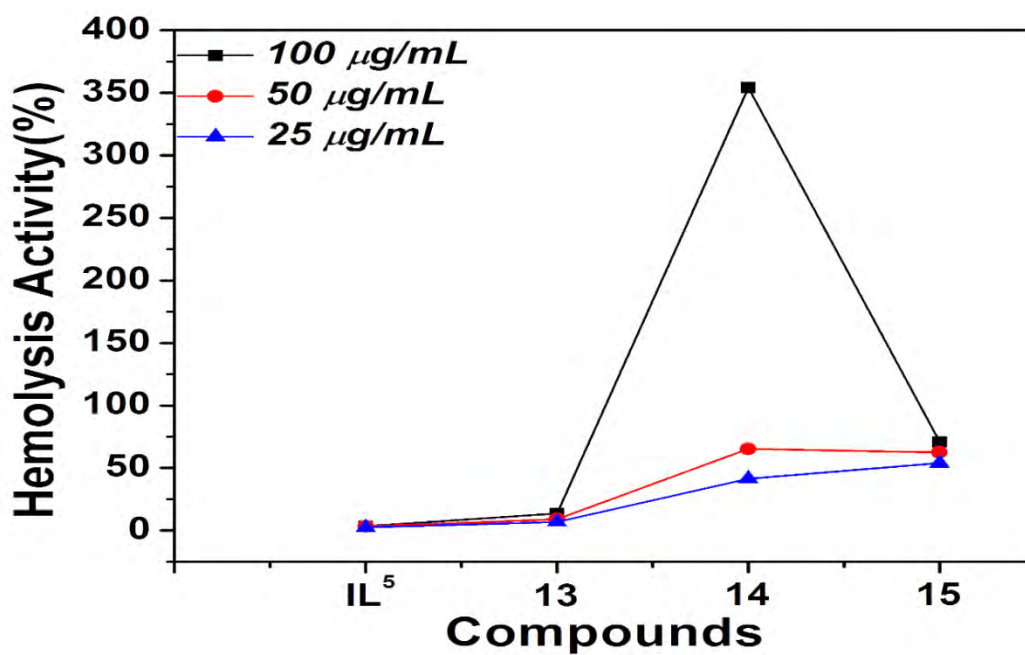


Figure 3.28: Hemolytic assay activities of ligand ( $IL^5$ ) and complexes (13-15).

### 3.3.4. Antibacterial activities of the synthesized ligands and their complexes

The ligands ( $IL^1$  and  $IL^2$ ) and their complexes (1-6) were screened against three types of the strain of Gram-negative bacteria (*B. bronchiseptica*, *S. typhimurium* and *E. aerogenes*) according to the formerly described procedure [142] and the statistics are represented in Figure 3.29. A criterion for the activity is based on the zone of inhibition. All the compounds except complex 4, showed activity against all strains. A mixed behavior of activity is observed among the ligands and their complexes and order differ from one strain to another strain. The data revealed that triorganotin(IV) based compounds are more effective than their corresponding ligands, an observation in consonance with earlier reports [143]. Furthermore, ligand  $IL^1$  and its organotin compounds were found more active than the ligand  $IL^2$  and its organotin compounds. Compound 1 was found active against all the three strains, however, 2 showed better activity than 1 against *B. Bronchiseptica*. Higher activity of 5 than 6 can be attributed to the more lipophilic nature of the tributyltin than triphenyltin. Meanwhile, complex 3 showed the best activity against strain *S. Typhimurium* and medium activity against strain *B. bronchiseptica* and strain *E. aerogenes* [144].

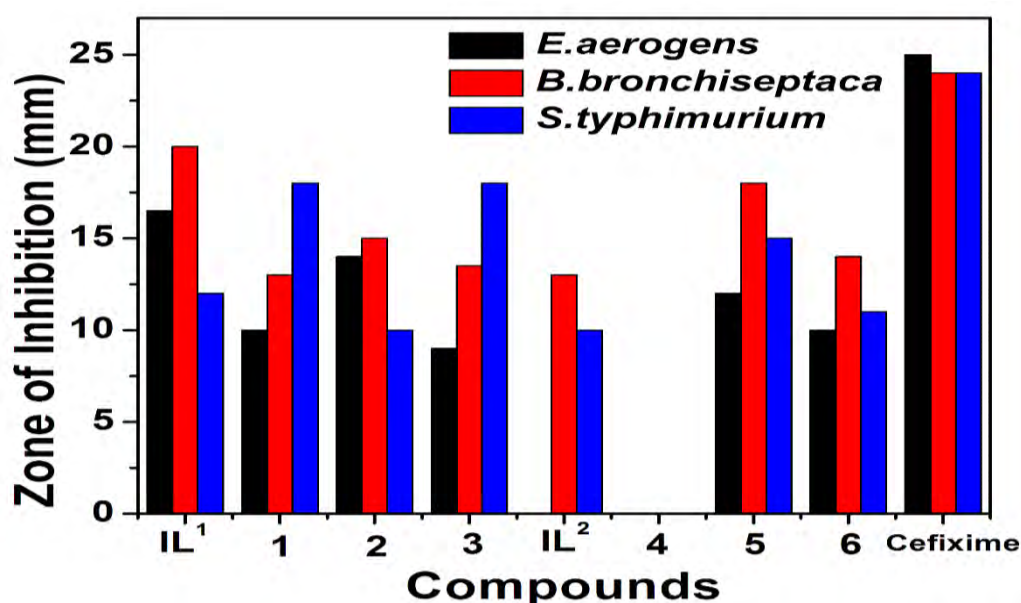
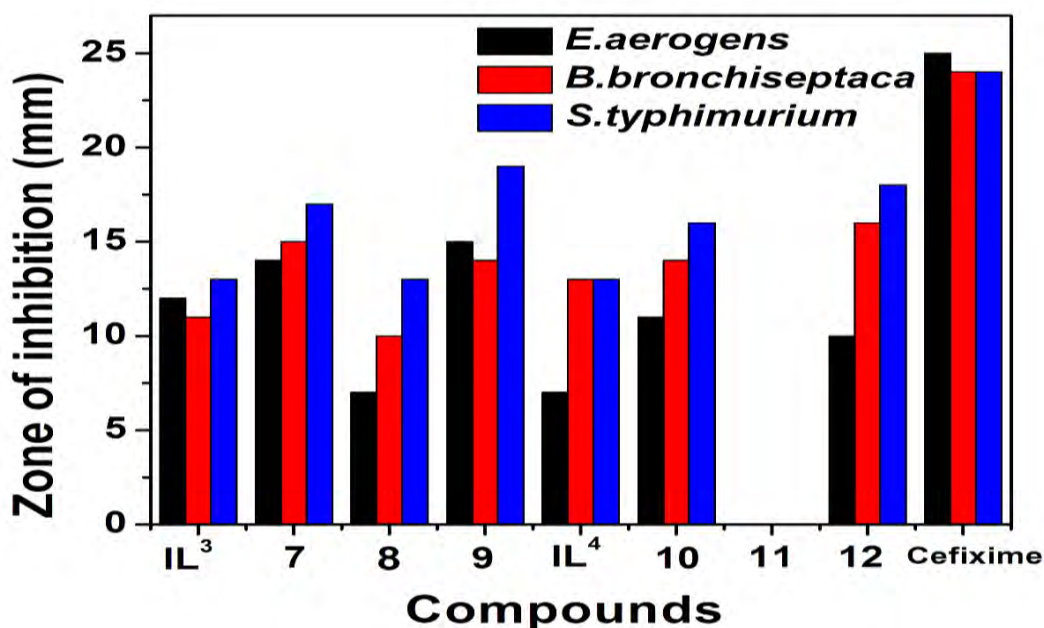


Figure 3.29: Antibacterial activity data of ligand ( $IL^1$  and  $IL^2$  and complexes (1-6).

Antibacterial activity of another series of the synthesized Ligands (**IL**<sup>3</sup> & **IL**<sup>4</sup>) and complexes(**7-12**) were tested for their antibacterial activity against three types of the strain of Gram-negative bacteria (*Bordetella bronchiseptica*, *Salmonella typhimurium*, and *Enterobacter aerogenes*) according to the formerly described procedure and the data are listed in the Figure **3.30**. All the compounds showed activity against all strains except compound Complex **11**. According to the already reported data [145-47] triorganotin(IV) based complexes are more effective complexes but here a mixed behavior is experienced among the ligands and different triorganotin(IV) carboxylates. During the present study and order differs from one strain to another strain. However, ligand **IL**<sup>3</sup> more active than the ligand **IL**<sup>4</sup>, and complex **7** showed good activity against all the three strains but compound **8** showed a fair activity against all three strains and complex **9** is the most active compound against all the three strains. Complex **10** is also active against all three strains but compound-complex **11** is almost inactive against all three strains. Compound **12** can also be a good candidate as an antibacterial agent. Carboxylate groups having a good lipophilic characteristic can vintage an important improvement in antibacterial activity, allowing the easier crossing of biological barriers, which is important for biocidal activity against many microorganisms. This action can be associated with the establishment of new bonds between the tin(IV) center with the electron donor species in active biological centers [148].





**Figure 3.30:** Antibacterial activity data of ligand (IL<sup>3</sup> and IL<sup>4</sup> and complexes (7-12).

The ligands IL<sup>5</sup> and their complexes (13,14 & 15) were screened against three types of strain of Gram-negative bacteria (*Bordetella bronchiseptica*, *Salmonella typhimurium*, and *Enterobacter aerogenes*) according to the formerly described procedure [149] and the statistics are represented in Figure 3.31. A criterion for the activity is based on the zone of inhibition. All the compounds except ligand IL<sup>5</sup> showed activity against all strains. A mixed behavior of activity is observed among the ligands and their complexes and order differ from one strain to another strain. The data revealed that triorganotin(IV) based compounds are more effective than their corresponding ligands, an observation in consonance with earlier reports [150]. Furthermore, Complex 13 was found active against all the three strains, however, 14 showed better activity than 13 against *B. Bronchiseptica*. Complex 15 has also shown better antibacterial activities against all three strains [141]. A similar pattern of activities is observed among the other ligands and their complexes as well which is shown in Figures 3.32 and 3.33.

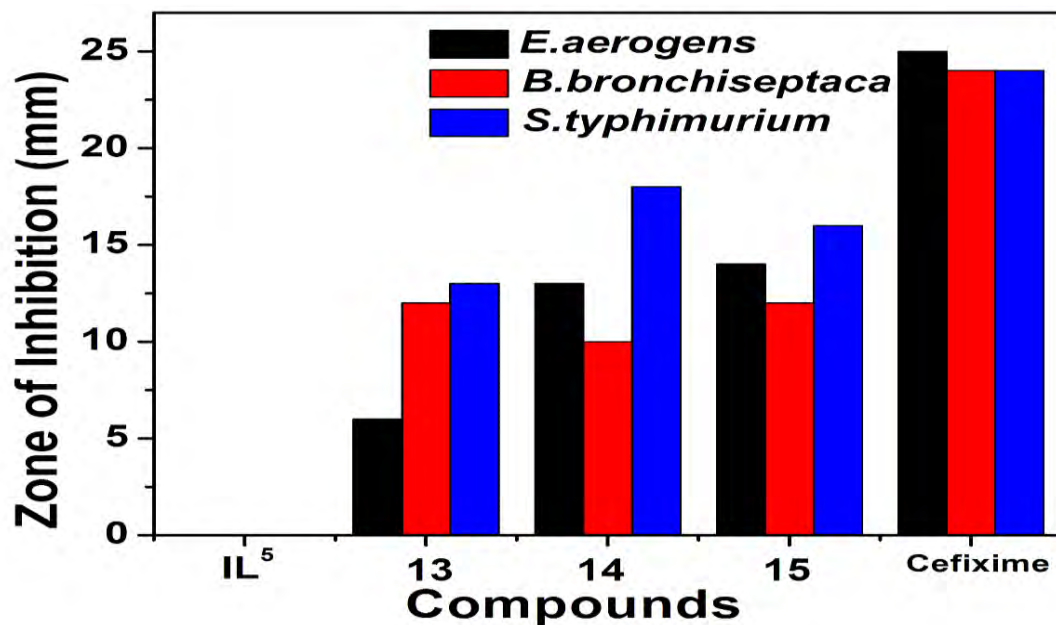


Figure 3.31: Antibacterial activity data of ligand (IL<sup>5</sup>) and complexes (13-15).

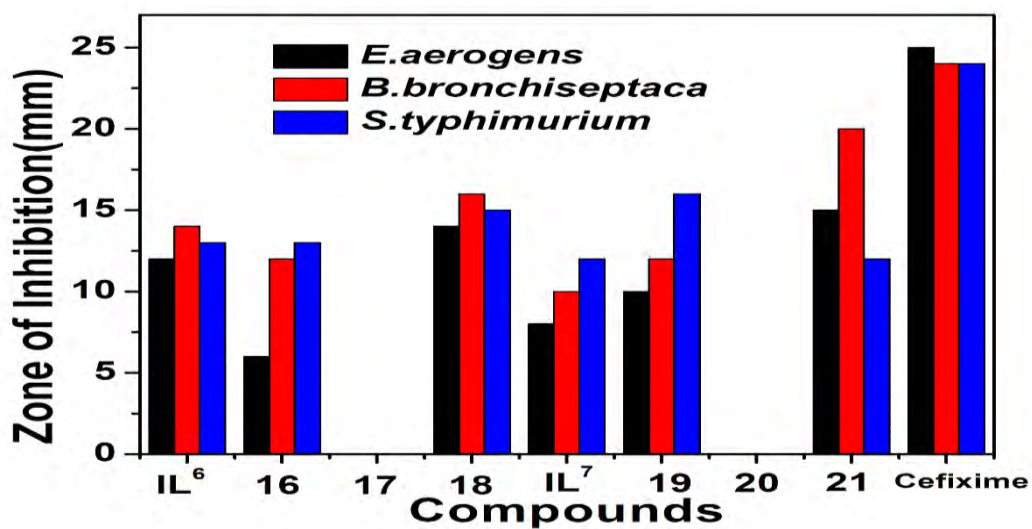


Figure 3.32: Antibacterial activity data of ligand (IL<sup>6</sup> and IL<sup>7</sup>) and complexes (16-21).

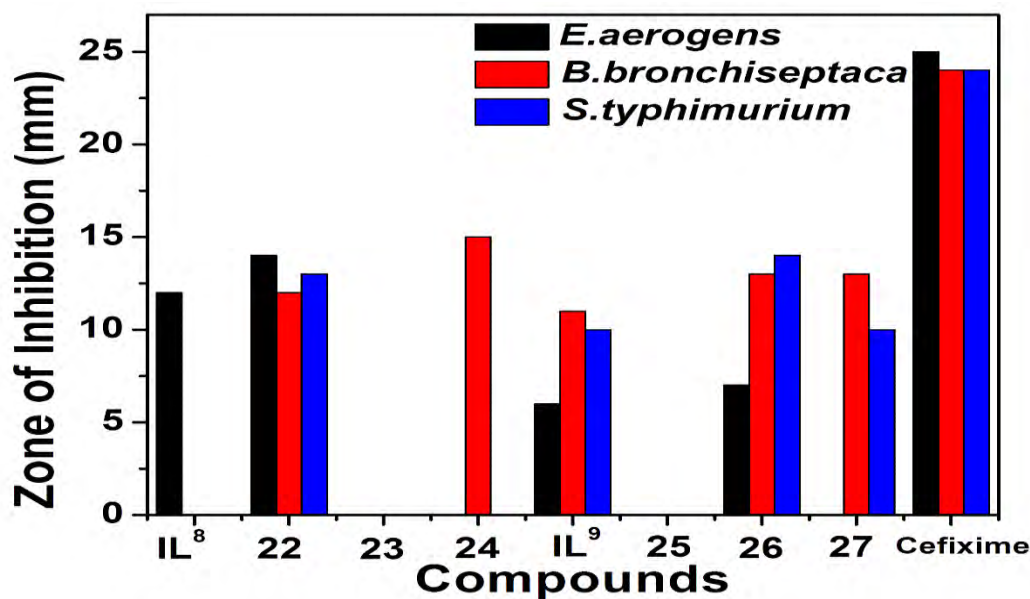
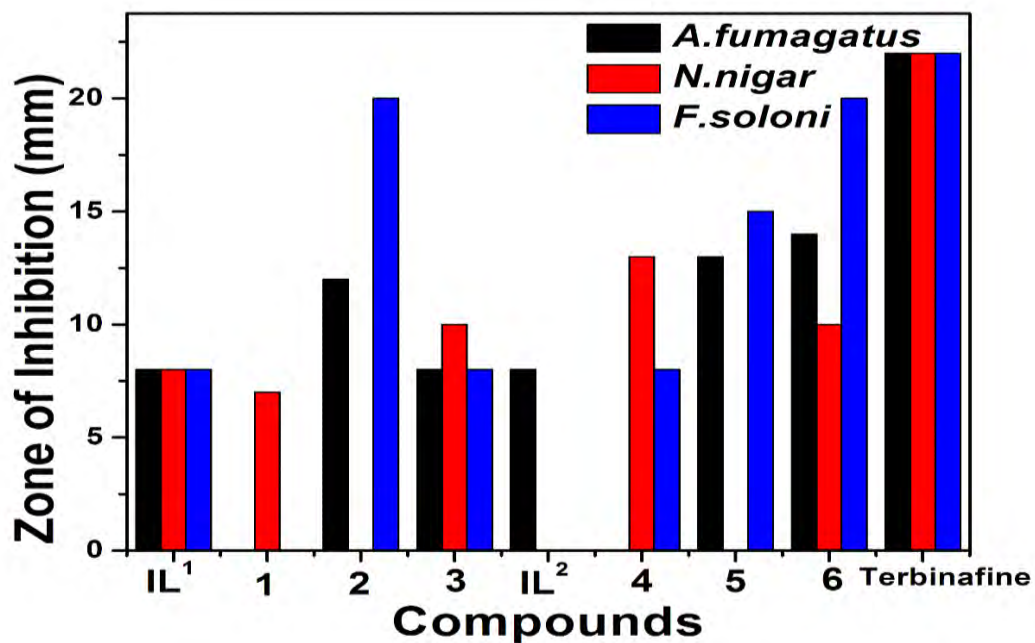


Figure 3.33: Antibacterial activity data of ligand (IL<sup>8</sup> and IL<sup>9</sup> and complexes (22-27)).

### 3.3.5. Antifungal activities of the synthesized ligands and their complexes

Extracts Antifungal activity was assessed via already designated standard protocol [151]. The antifungal activity of the synthesized ligands (IL<sup>1</sup> and IL<sup>2</sup>) and complexes (1-6) were tested against three types of the strain of fungi (*A. fumigatus*, *F. solani*, *N. niger*) which are represented in Figure 3.34. All antifungal activity of the complexes was greater than the ligands with rare exceptions. tributyltin(IV) based derivatives were experienced more effective than the trimethyltin(IV) derivatives, a behavior reasonably reliable with the previous report.



**Figure 3.34:** Antifungal activity data of ligand (IL<sup>1</sup> and IL<sup>2</sup>) and complexes (1-6).

The antifungal activity of the synthesized compounds was also tested for ligands (IL<sup>3</sup> & IL<sup>4</sup>) and their complexes (7-12) against three types of the strain of fungi (*A. fumigatus*, *F. solani*, *N.niger*), and data are listed in the Figure 3.35 below. All the complexes revealed distinctly higher antifungal efficiency than the ligands with rare exceptions. Compound **8** is almost inactive against all the strains while compound **10** showed the least activities as compared to others complexes [152].

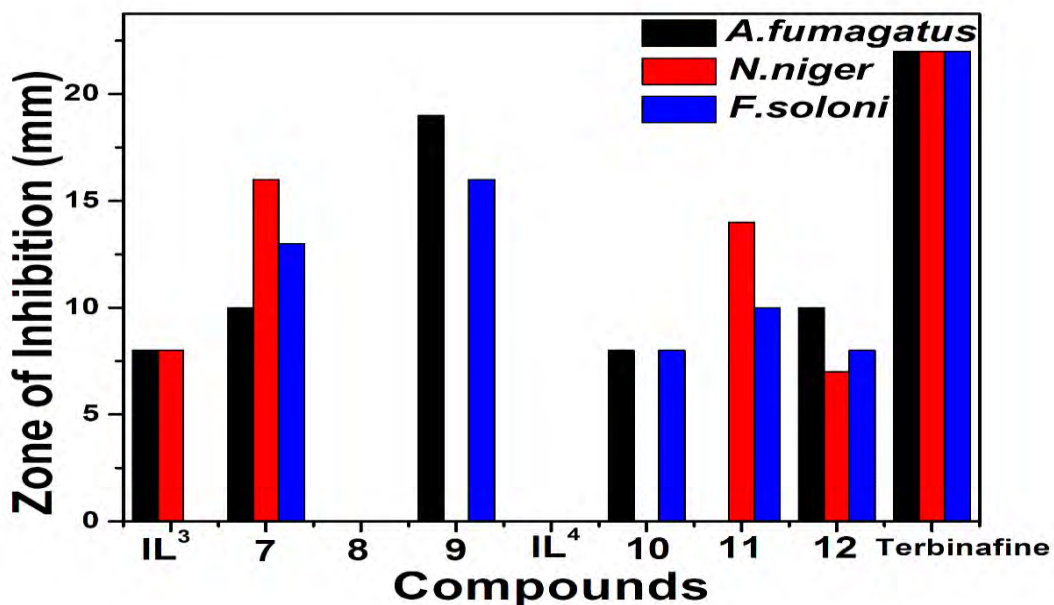


**Figure 3.35:** Antifungal activity data of ligand (IL<sup>3</sup> and IL<sup>4</sup> and complexes (7-12)).

One of the series of Ligand IL<sup>5</sup> and complexes 12-15 were screened against three different fungal strains as well. The ligand L<sup>5</sup> was inactive against the F. Soloni and showed poor activity against the other two strains. Complex 14 was almost inactive while complex 15 indicate better activities as compared to complex 12 against all the three strains which are given in Figure 3.36. Mix type of pattern is also observed in the rest of the complexes as well which is presented in Figures 3.37 and 3.38.

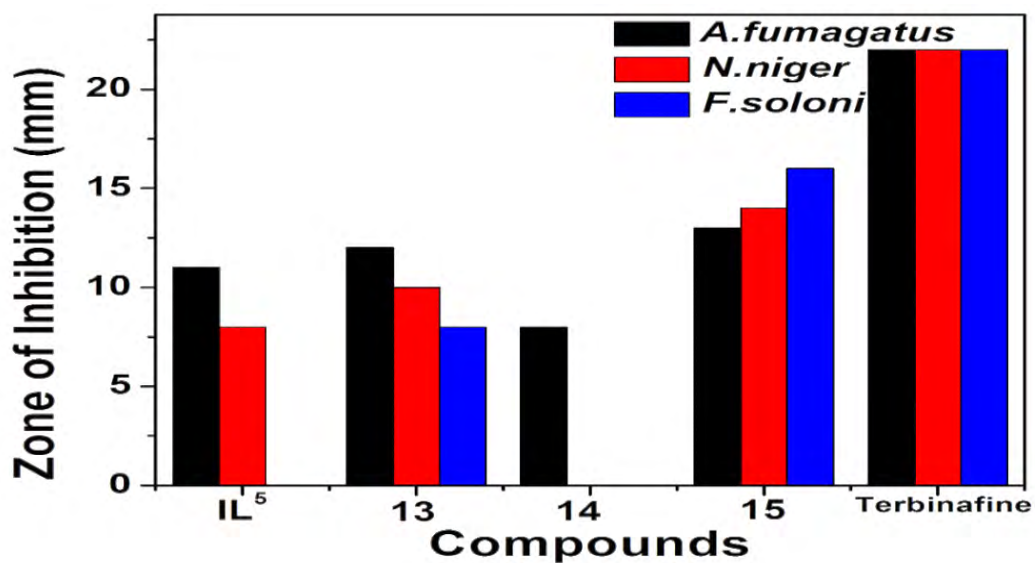


Figure 3.36: Antifungal activity data of ligand (IL<sup>5</sup>) and complexes (13-15).

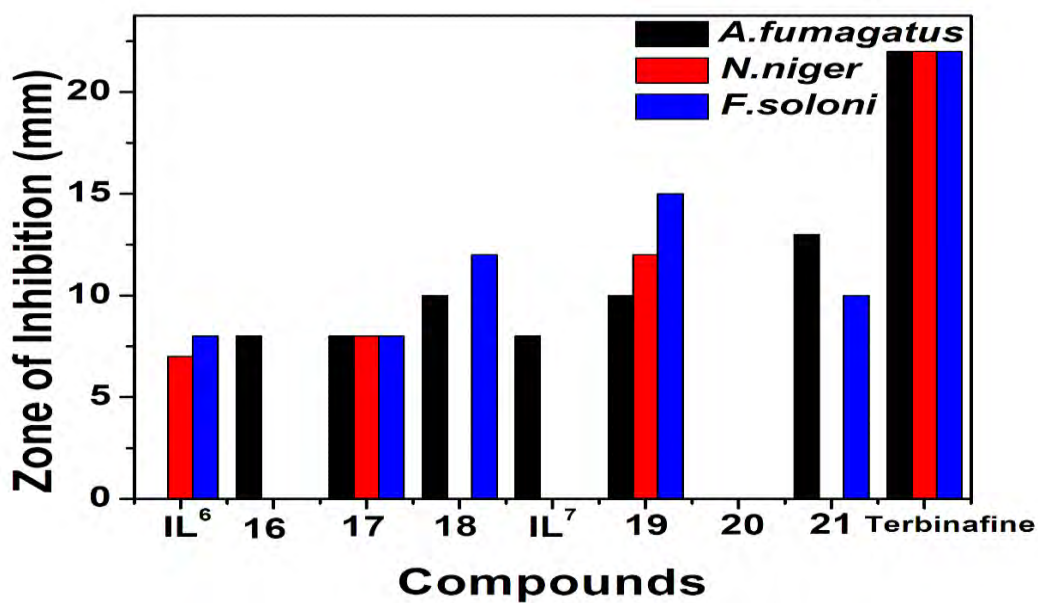
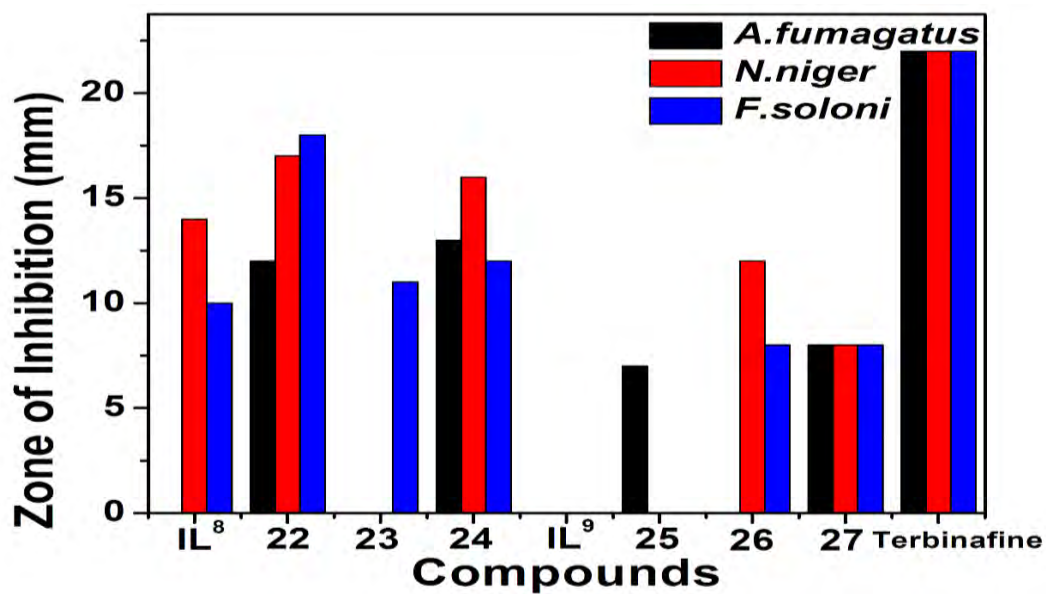


Figure 3.37: Antifungal activity data of ligand (IL<sup>6</sup> and IL<sup>7</sup>) and complexes (16-21).



**Figure 3.38:** Antifungal activity data of ligand (IL<sup>8</sup> and IL<sup>9</sup>) and complexes (22-27).

### 3.3.6. Cytotoxicity

The synthesized ligands (IL<sup>1</sup> & IL<sup>2</sup>) and complexes 1-6 were also screened for cytotoxicity using the Brine shrimp (*Artemia salina*) bioassay lethality method [141] and results are displayed in Figure 3.39. The data illustrate that all compounds are cytotoxic and the LD<sub>50</sub> values decreased in the following sequence: 1>4>6>2>5>3.

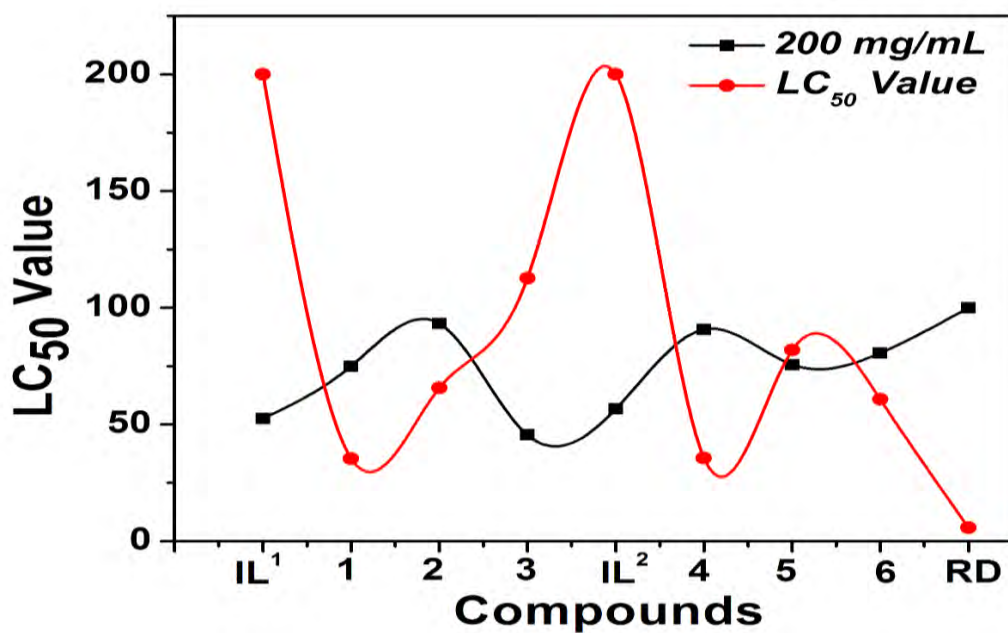


**Figure 3.39:** Cytotoxicity data of ligand (IL<sup>1</sup> and IL<sup>2</sup> and complexes (1-6).

The synthesized compounds ligands and complexes were also screened for cytotoxic data, using the Brine shrimp (*Artemia salina*) bioassay lethality method, and results were shown in figure 3.40. The data illustrate that all the compounds showed cytotoxicity. However, the LC<sub>50</sub> value for complexes 7, 8, 10, and 11 showed the best cytotoxic effect near to the standard drug, and ligands IL<sup>3</sup> and IL<sup>4</sup> have the least cytotoxic effects while complexes 9 and 12 were found to be good cytotoxic agents as well [153].



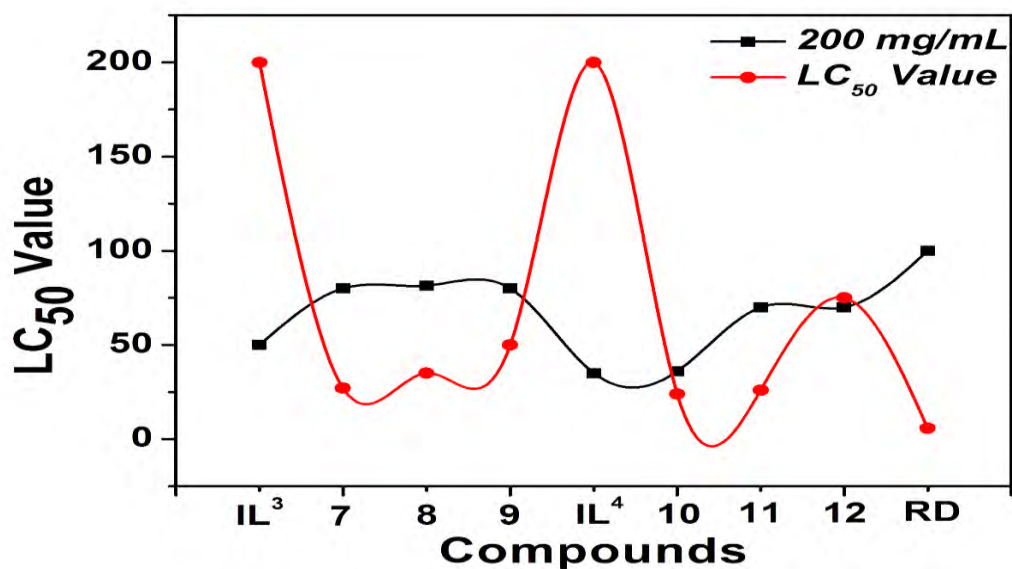


Figure 3.40: Cytotoxicity data of ligand (IL<sup>3</sup> and IL<sup>4</sup> and complexes (7-12).

Similarly, another series of the synthesized compounds ligands and complexes were also screened for cytotoxic data, using the Brine shrimp (*Artemia salina*) bioassay lethality method, and results were shown in Figure 3.41. The data illustrate that all the compounds showed cytotoxicity. However, the LC<sub>50</sub> value for compounds 13 and 15 showed the best cytotoxic effect near to the standard drug and complex 14 and ligand IL<sup>5</sup> have the least cytotoxic effects. Same arrays have been observed in Figures 3.42 and 3.43.

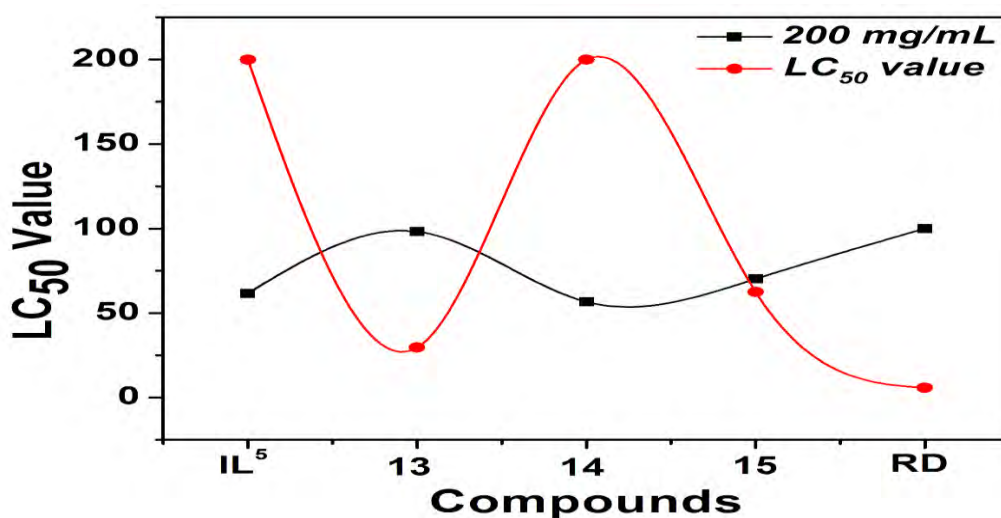


Figure 3.41: Cytotoxicity data of ligand (IL<sup>5</sup> and complexes (13-15).

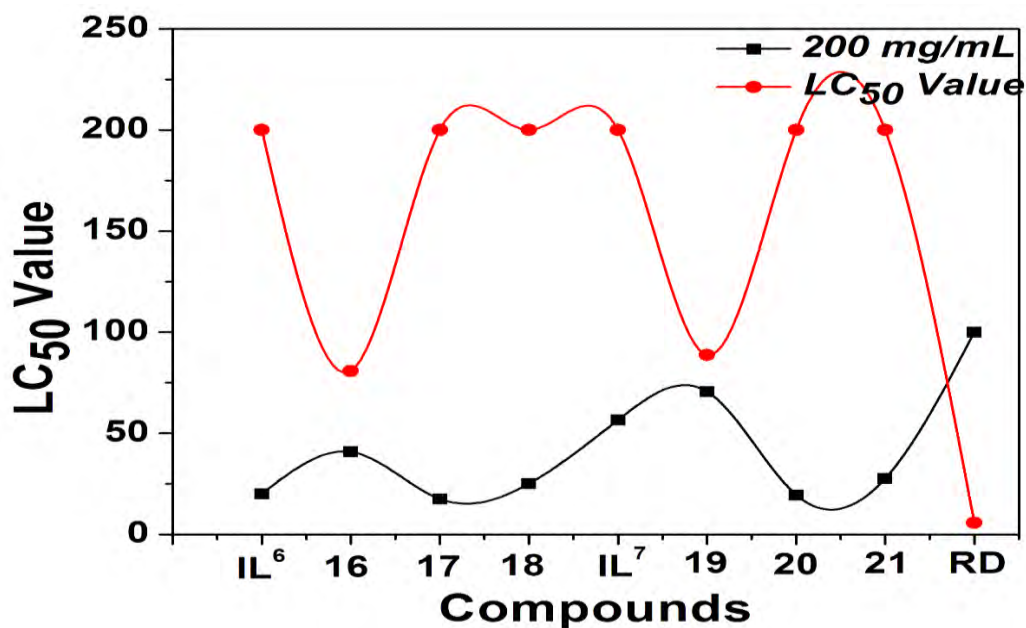


Figure 3.42: Cytotoxicity data of ligand (IL<sup>6</sup> and IL<sup>7</sup> complexes (16-21).

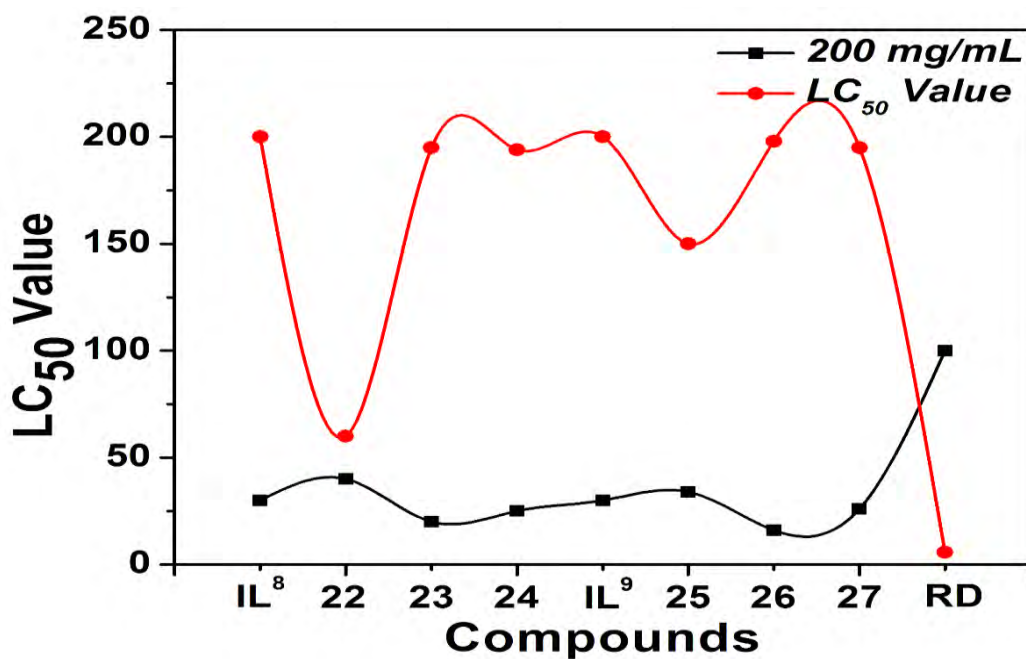


Figure 3.43: Cytotoxicity data of ligand (IL<sup>8</sup> and IL<sup>9</sup> complexes (22-27).

### 3.3.7. Antioxidant Activities

#### 3.3.7.1. Total Antioxidant Capacity

The antioxidant activities of the compounds were assessed by method described in the literature [154]. The antioxidant activities of the prepared compounds were evaluated

by the already reported method. A significant antioxidant capacity of 25.0, 22.0, 21.0, and 11.5  $\mu\text{g}$  AAE/mg extract was found in compounds **6**, **3** followed by **4**, **2**, **1**, **4**, and ligands **L<sup>1</sup>** and **L<sup>2</sup>** respectively as depicted in Figures 3.44. Similarly, all other ligands were screened for their total antioxidant capacities which showed that tributyltin(IV) carboxylates are the highest antioxidant capacities followed by triphenyltin(IV) carboxylates and trimethyltin(IV) carboxylates respectively while all the ligands having the least total antioxidant capacities which are shown in Figure 3.45, 3.46, 3.47 and 3.48.

AAE=Ascorbic acid Equivalent

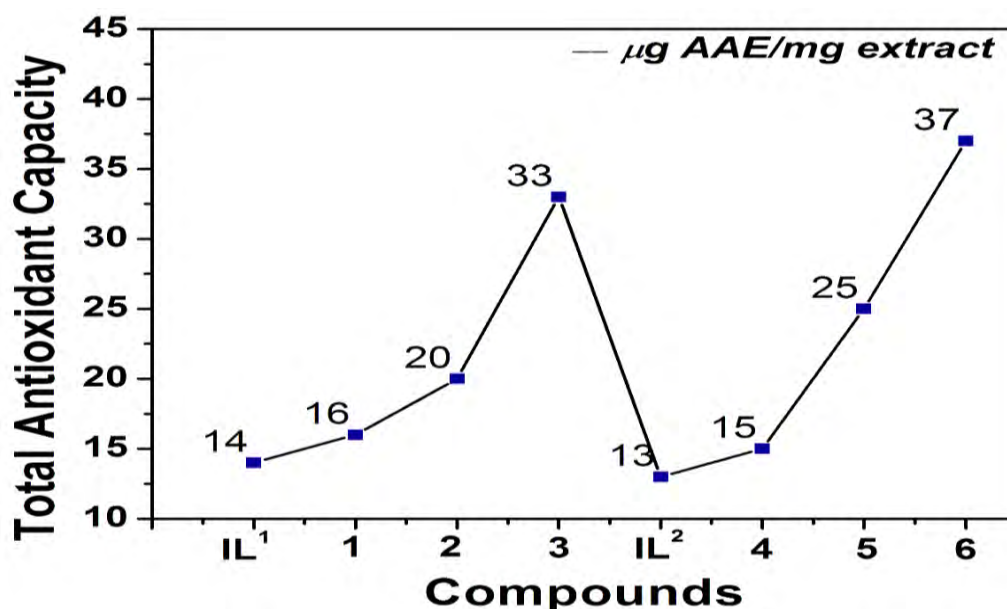


Figure 3.44: Total antioxidant capacity of the synthesized ligands (**IL<sup>1</sup>** and **IL<sup>2</sup>**) and complexes **1-6**.

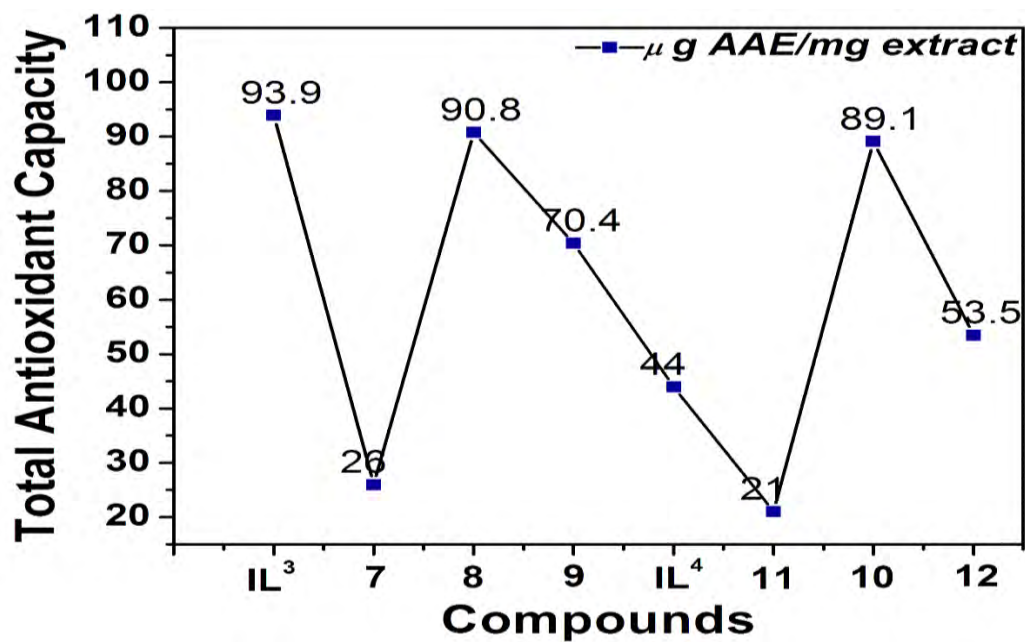


Figure 3.45: Total antioxidant capacity of the synthesized ligands (IL<sup>3</sup> and IL<sup>4</sup>) and complexes 7-12

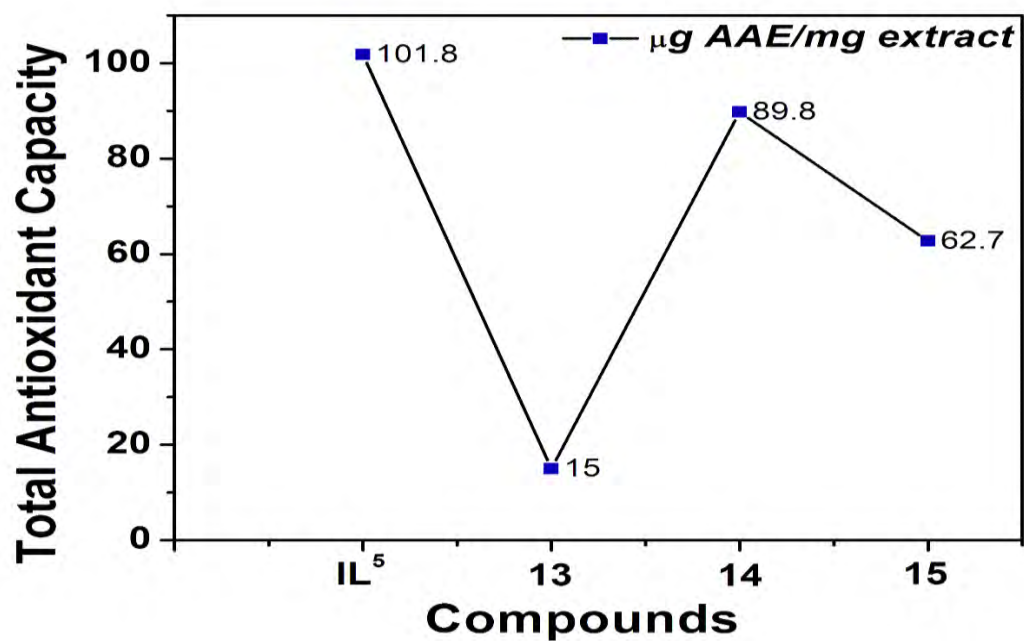


Figure 3.46: Total antioxidant capacity of the synthesized ligands (IL<sup>5</sup>) and complexes 13-15.

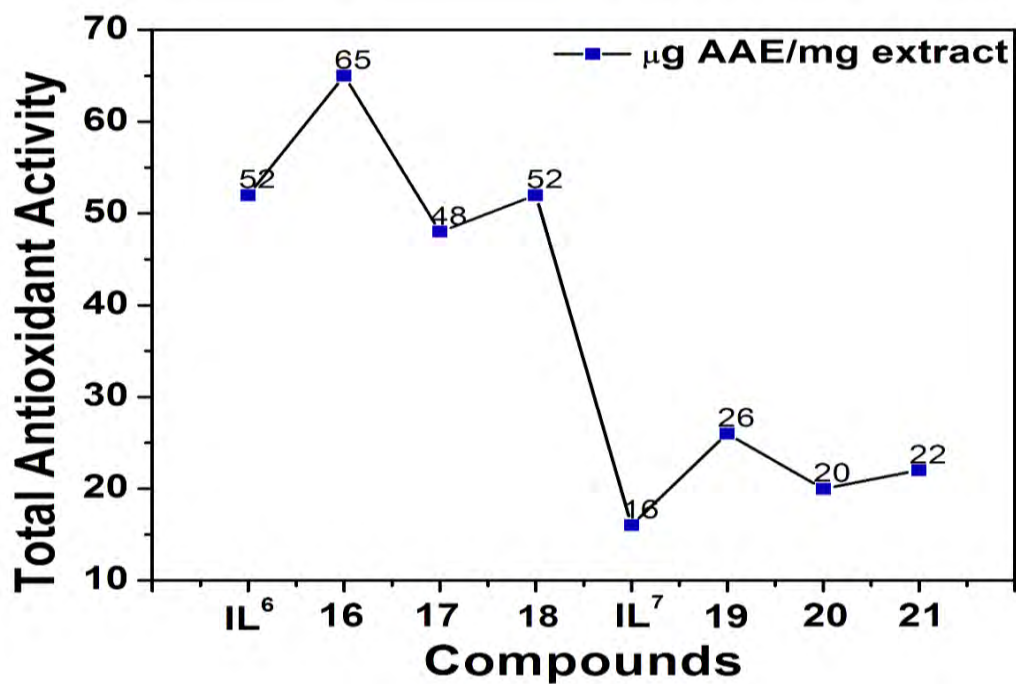


Figure 3.47: Total antioxidant capacity of the synthesized ligands (IL<sup>6</sup> and IL<sup>7</sup>) and complexes 16-21.

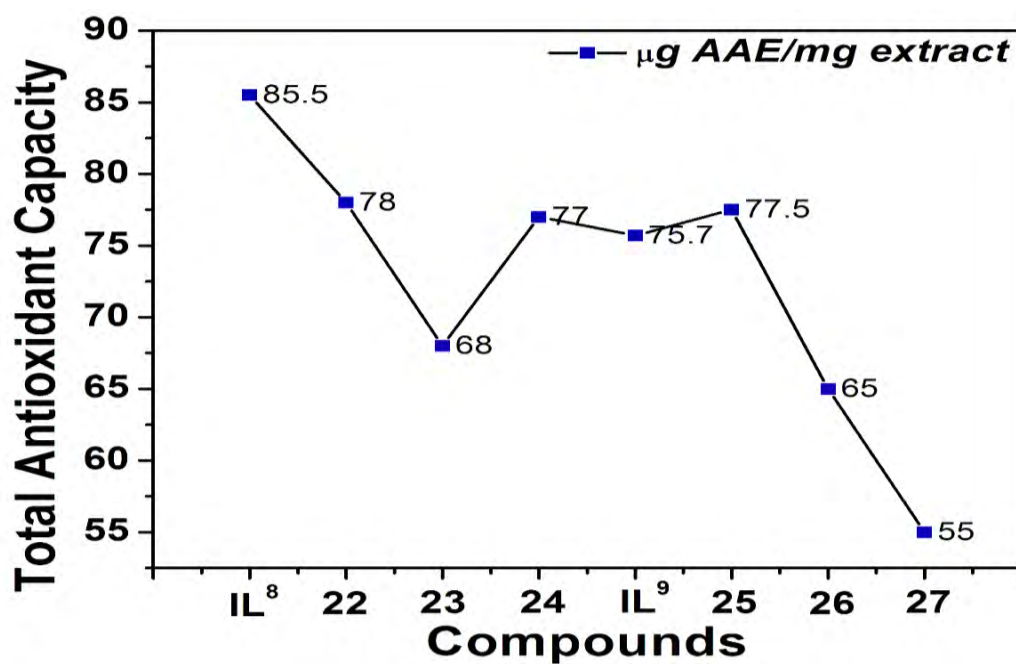
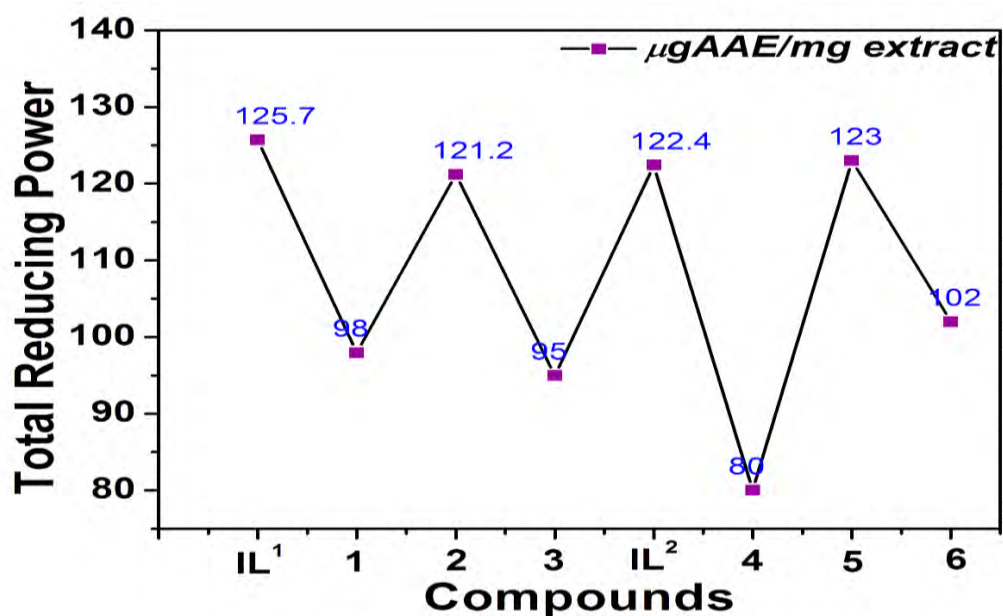


Figure 3.48: Total antioxidant capacity of the synthesized ligands (IL<sup>8</sup> and IL<sup>9</sup>) and complexes 22-27.

### 3.3.7.2. Total Reducing Power

In the TRP assay, the highest reducing power potential was observed for **IL<sup>1</sup>**, followed by **2, 3, 1** while ligand **IL<sup>2</sup>** and **5** exhibited the best activity as compared to **4** and **6** (Figure 3.49). The results are comparable to the earlier reports [150][174]. In TRP assay similarly we tested all other synthesized ligands and their compounds the highest reducing power potential (125.7  $\mu\text{g AAE}/\text{mg extract}$ ) was observed by compound tributyltin(IV) carboxylates followed by triphenyltin(IV) carboxylates, trimethyltin(IV) carboxylates, and amide based carboxylic acid ligands.



**Figure 3.49:** Total reducing power of the synthesized ligands (**IL<sup>1</sup>** and **IL<sup>2</sup>**) and complexes **1-6**.

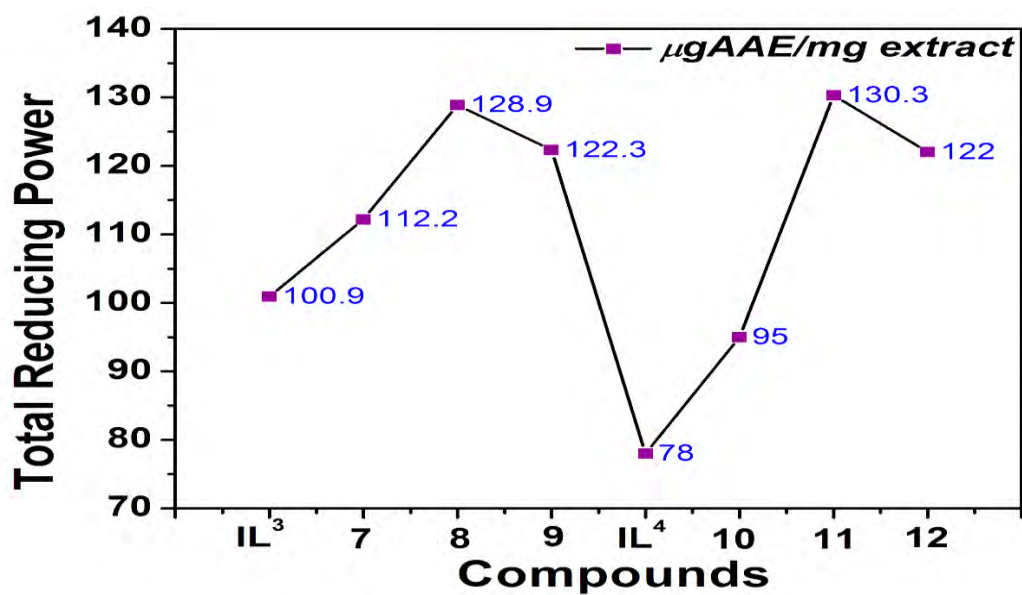


Figure 3.50: Total Reducing Power of the synthesized ligands (IL<sup>3</sup> and IL<sup>4</sup>) and complexes 7-12.

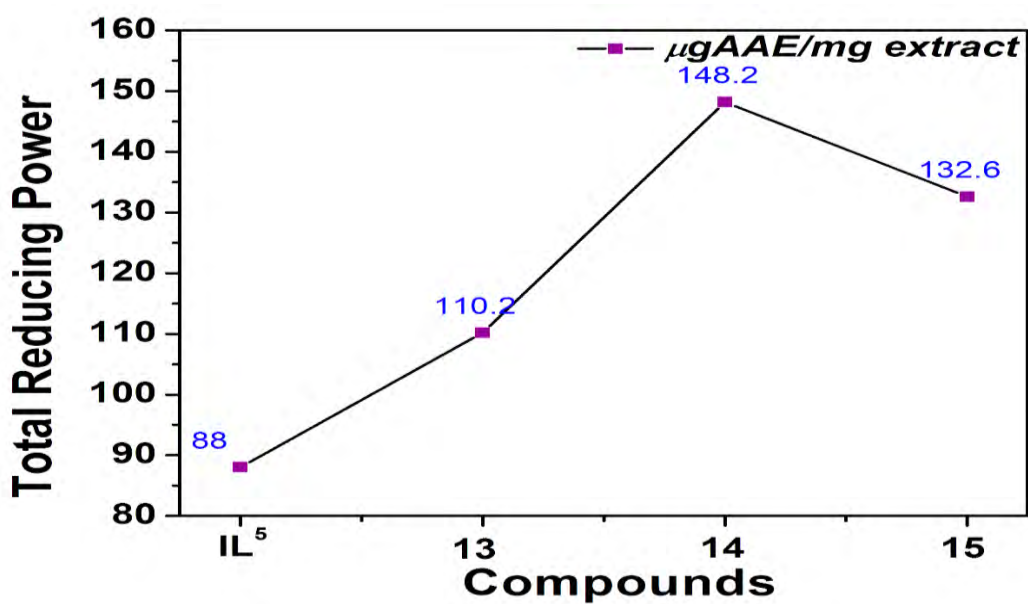


Figure 3.51: Total reducing power of the synthesized ligands (IL<sup>5</sup>) and complexes 13-15.

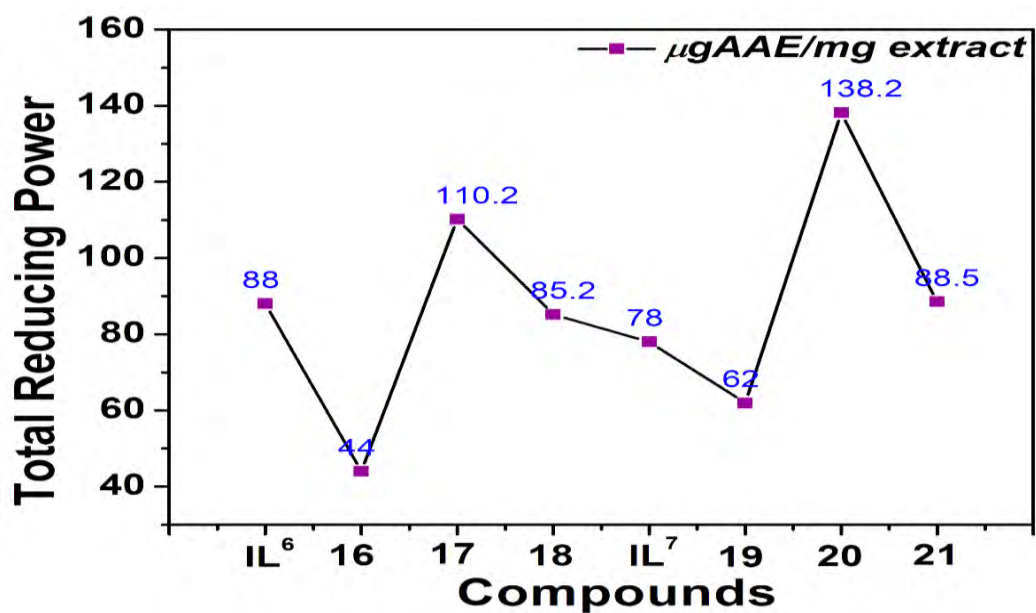


Figure 3.52: Total reducing power of the synthesized ligands (IL<sup>6</sup> and IL<sup>7</sup>) and complexes 16-21.

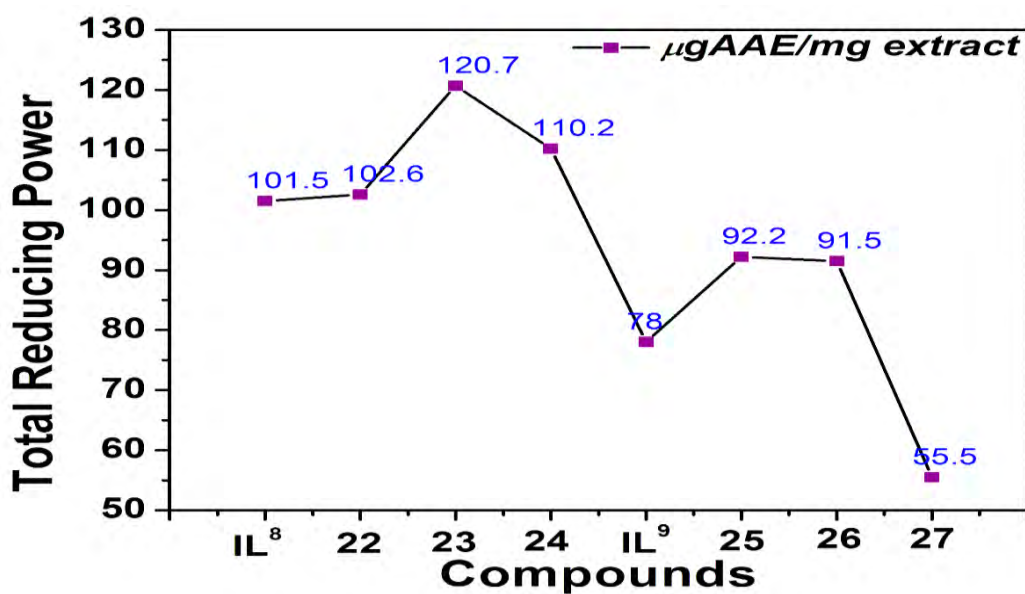
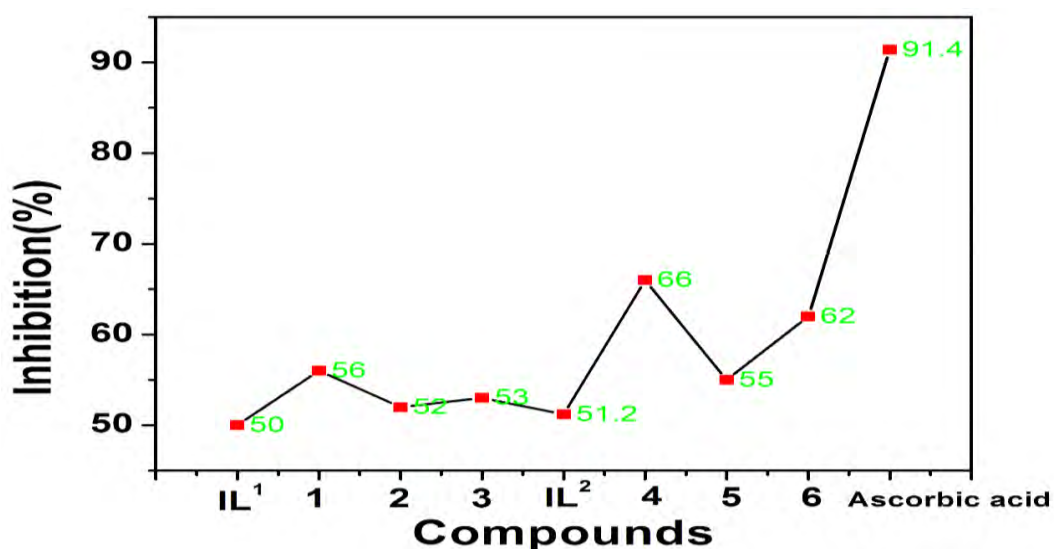


Figure 3.53: Total reducing power of the synthesized ligands (IL<sup>8</sup> and IL<sup>9</sup>) and complexes 22-27.



### 3.3.7.3. DPPH Free Radical Scavenging Assay

The free radical scavenging potential of DPPH was found by the capability of antioxidants to decolorize 2,2-diphenyl-2-picryl-hydrazyl. Among all compounds analyzed the %inhibition ranged from 55 to 91.4. The activity varies the following sequence  $4 > 6 > 1 > 5 > 3 > 2 > IL^2 > IL^1$  (Figure 3.54). The results are comparable to the earlier reports [177]. Among all the compounds analyzed the percentage inhibition ranged from 66 to 50 was observed. similarly, we screened all other synthesized ligands and their compounds the highest reducing power potential ( $125.7 \mu\text{g AAE/mg extract}$ ) was observed by compound tributyltin(IV) carboxylates followed by triphenyltin(IV) carboxylates, trimethyltin(IV) carboxylates, and amide based carboxylic acid ligands with a few exceptions.



**Figure 3.54:** Percentage scavenging of DPPH by the synthesized ligands ( $IL^1$  and  $IL^2$ ) and complexes 1-6.

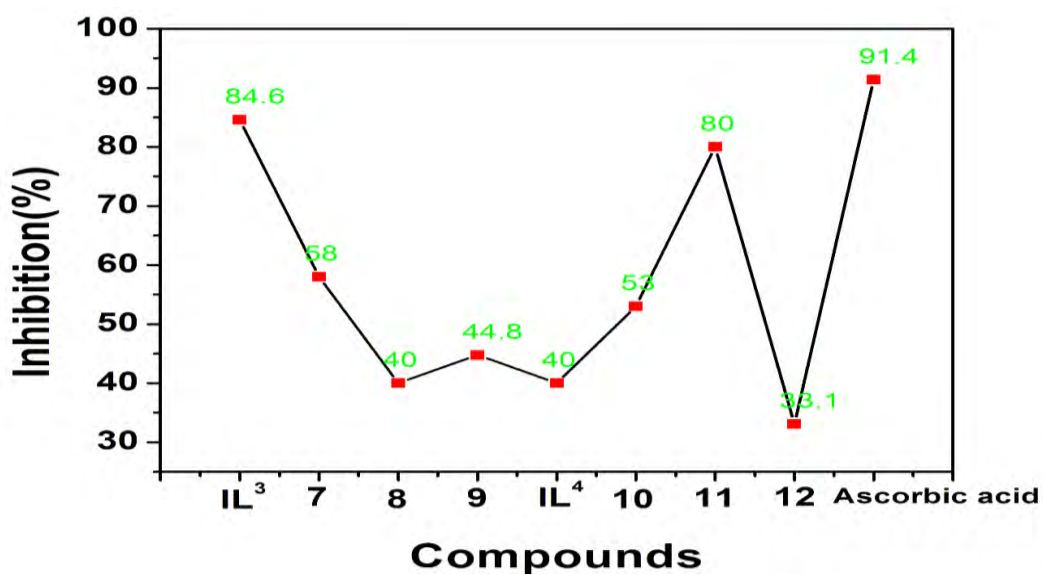


Figure 3.55: Percentage scavenging of DPPH by the synthesized ligands (IL<sup>3</sup> and IL<sup>4</sup>) and complexes 7-12.

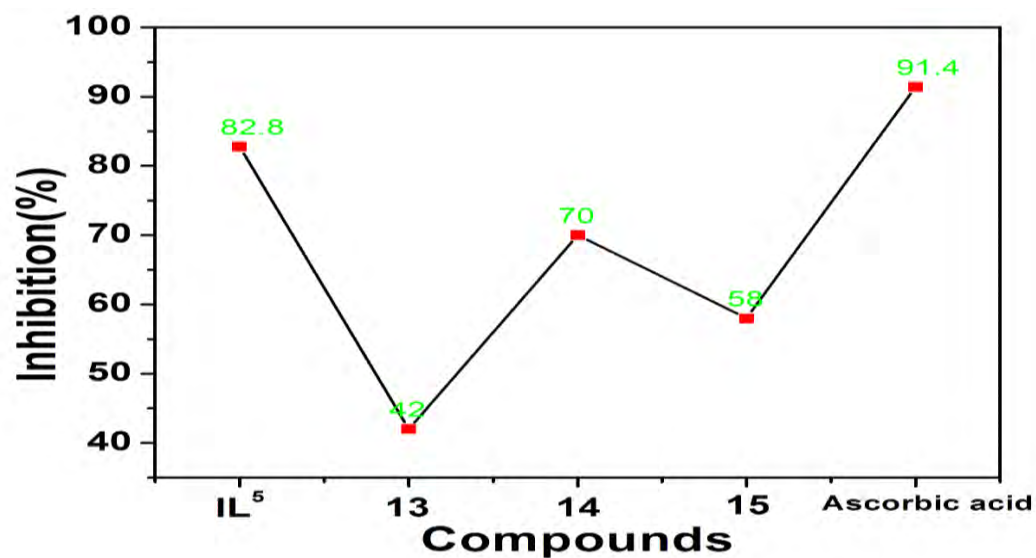


Figure 3.56: Percentage scavenging of DPPH by the synthesized ligands (IL<sup>5</sup>) and complexes 13-15.

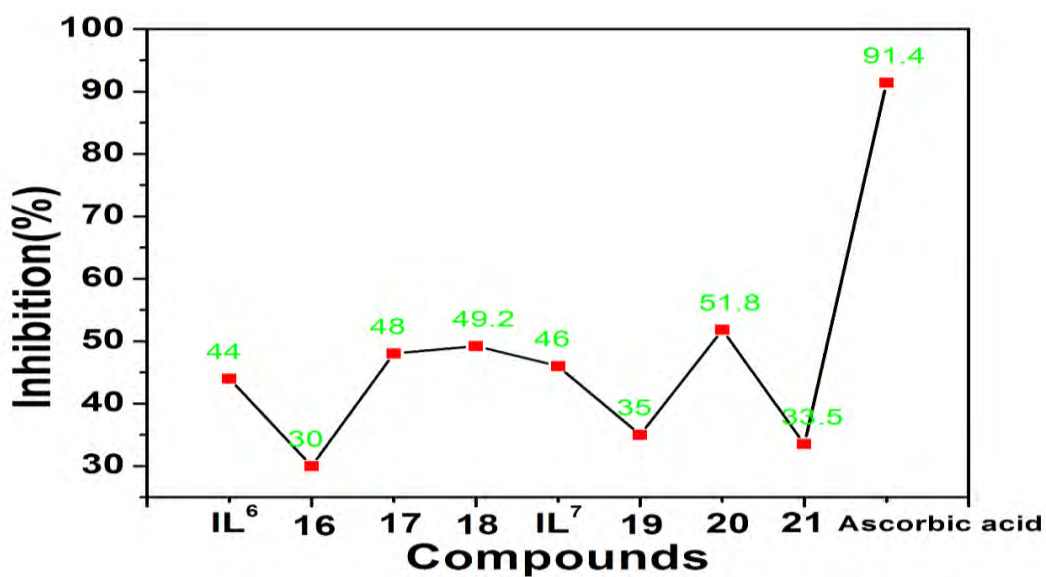


Figure 3.57: % Scavenging of DPPH by the synthesized ligands (IL<sup>6</sup> and IL<sup>7</sup>) and complexes 16-21.

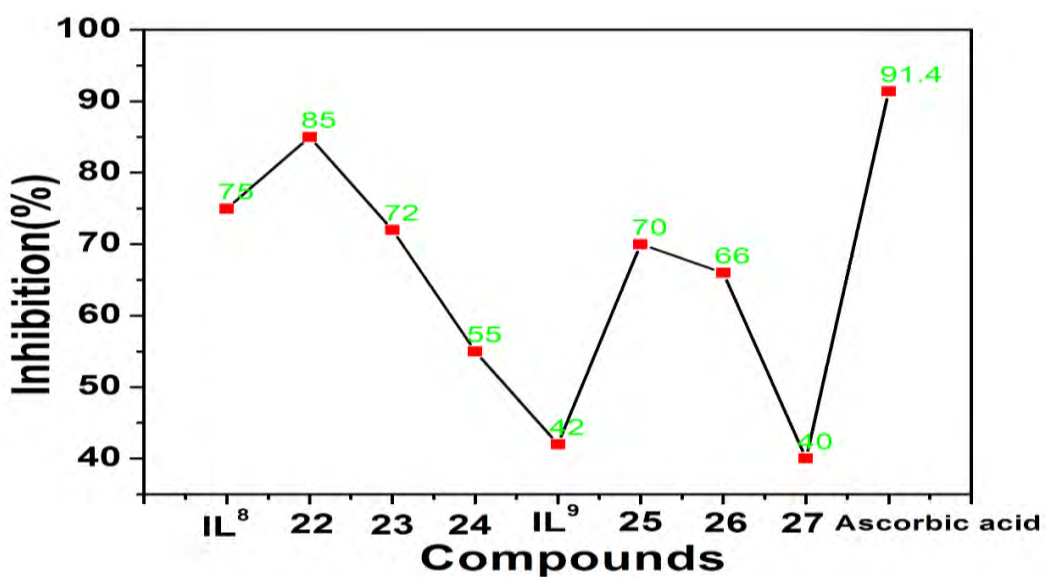
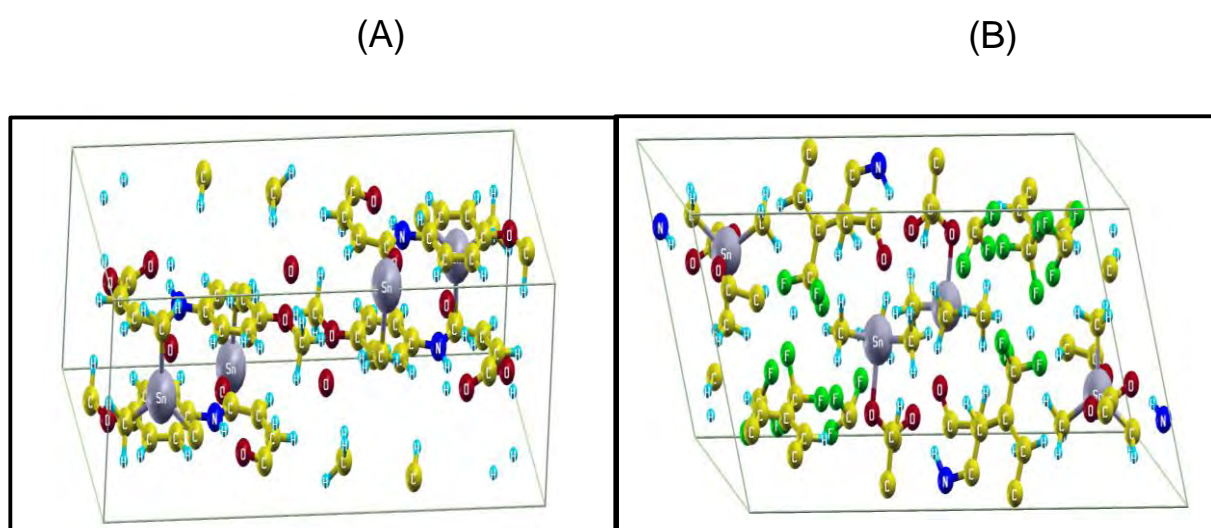


Figure 3.58: % Scavenging of DPPH by the synthesized ligands (IL<sup>8</sup> and IL<sup>9</sup>) and complexes 22-27.

### 3.5. Computational Details

For computational studies, we have selected two complexes one with electron-donating and the other with electron-withdrawing substituents attached at the aromatic rings in the synthesized complexes. First, we take the experimental lattice parameters and fully

relaxed the crystal structures of complexes **1** and **4**. Figure 3.59(A) shows the relaxed crystal structures of compound **1**, which consists of four monomers layers held together by dispersion forces. It has a monoclinic crystal structure at experimental lattice constants of  $a = 9.5 \text{ \AA}$ ,  $b = 6.9 \text{ \AA}$ ,  $c = 23.3 \text{ \AA}$ ,  $\alpha = 90.0^\circ$ ,  $\beta = 91.7^\circ$  and  $\gamma = 90.0^\circ$ . Figure 3.59(B) shows the relaxed crystal structure of compound **4** which has a distorted monoclinic crystal structure, at the experimental lattice constant  $a = 15.3 \text{ \AA}$ ,  $b = 10.9 \text{ \AA}$ ,  $c = 22.7 \text{ \AA}$ ,  $\alpha = 90.0^\circ$ ,  $\beta = 112.8^\circ$  and  $\gamma = 90.0^\circ$ , respectively.

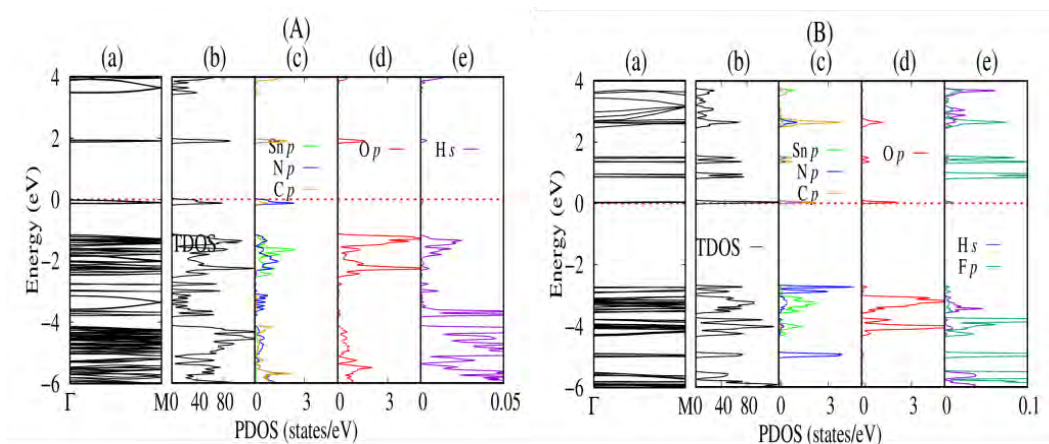


**Figure 3.59:** Side view of (A) compound **1** and (B) compound **4**. In both Figures, the yellow, blue, red, green, slate, and cyan balls represent C, N, O, F, Sn, and H atoms, respectively.

The structural parameters computed in this work using DFT, for both compounds are in close agreement with experimental data. The calculated formation energy of compounds **1** compound **4** is  $-5.4 \text{ eV}$  ( $-5.49 \text{ eV}$ ) respectively at their equilibrium lattice constant. However, the negative formation energy predicts that both compounds are thermodynamically stable. Next, the GGA band structures have been calculated with and without spin polarization and we confirmed that compounds **1** and **4** compounds

are non-magnetic semiconductors. So the non-spin polarized calculations are justified due to the absence of magnetism.

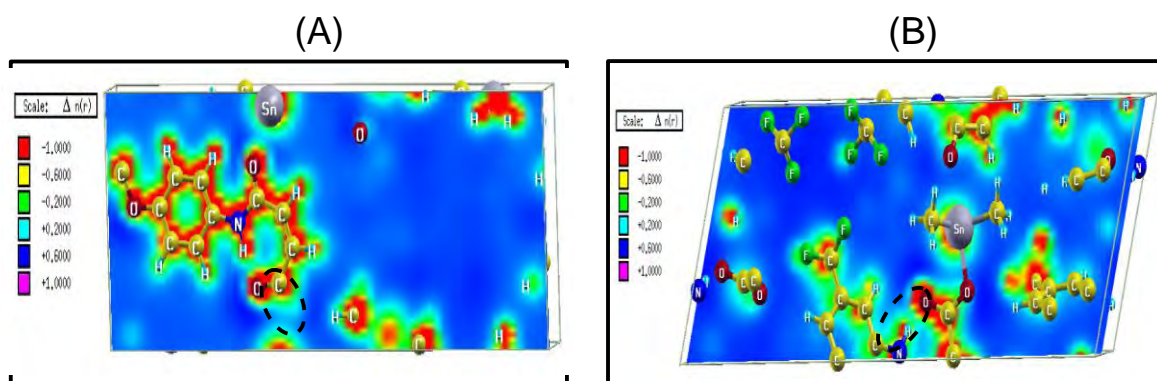
Figure 3.60 (A) (a) shows the calculated electronic band structure of compound 1 which has an uninterrupted band gap  $\Gamma$ - $\Gamma$  of 1.87 eV, which is smaller than the experimentally observed optical band-gap of 2.92 eV. This is consistent with previous results because GGA underestimates the band gap than experimental band-gap values. The valence band maximum (VBM) and conduction band minimum (CBM) located at the  $\Gamma$ -point. The Fermi level lies at the top of valence band edges which shows a **p**-type character of compound 1 (as displayed in Figure 3.60(A) (a)). Figure 3.60 (A) & (b) shows the TDOS, which confirmed the semiconducting behavior of compound 1. To further investigate the orbital character of electronic bands around the Fermi energy, we presented the PDOS as shown in Figure 3.60 (A) (c-e). The states at the Fermi energy (see Figure 3.60 (A) (c-e)) are mainly contributed by N *p*-orbital, which partially hybridized with C *p*-orbital. Further analysis of the DOS reconfirmed that compound 1 shows p-type behavior which is consistent with electronic band structure. Figure 3.61 (A) shows the charge-density of compound 1 which shows that H-O2 bonding is purely van-der Waal-like bonding as shown by the dotted ellipse. The H-O2 bond length is 1.59 Å which is larger than the bond length of the H-(O2) with nearby atoms N1(C4) is 1.06 Å (1.25 Å). Finally, the Fermi energy is 2.3263 eV and the work-function is 2.73 eV. The calculated valence band maximum (VBM) also called HOMO and conduction band minimum (CBM) called LUMO energies obtained are -3.62 eV and -1.75 eV concerning the vacuum potential of 5.06 eV as a reference level.



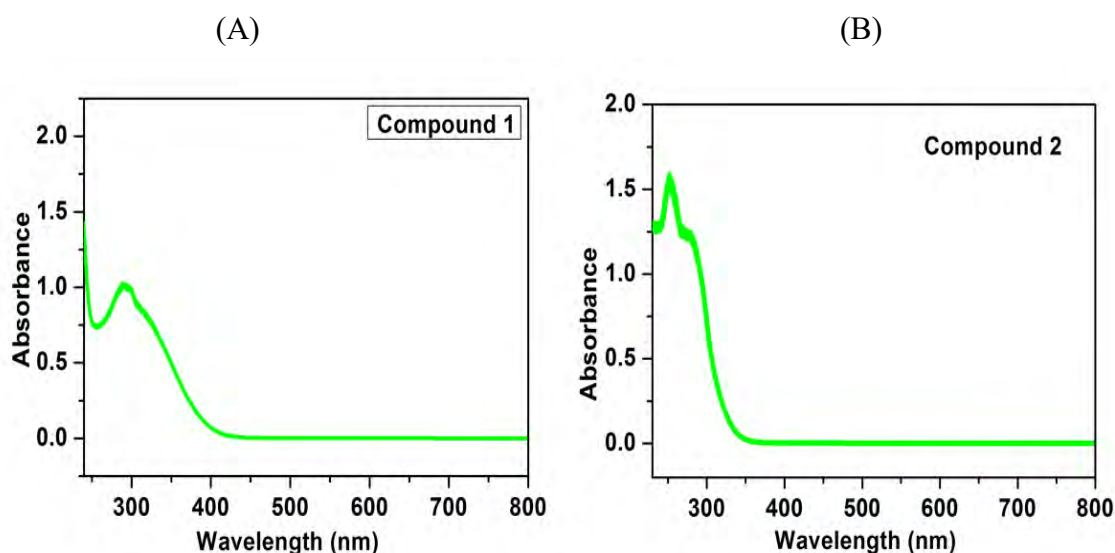
**Figure 3.60:** (A) left side for compound **1** and (B) right side for compound **4**. In both cases, (a) show GGA calculated band structures, the Fermi energy is set to zero as shown by the horizontal dashed red line. (b) The total density of states (TDOS) and (c-d) projected density of states (PDOS) of these compounds. The black line shows the TDOS, were green, blue, yellow, red, magenta lines and dark green show the PDOS of Sn, N, C, O, H and F respectively.

Figure **3.60** (B) (a) shows the band structure for compound **4**, which has a direct band gap  $\Gamma$ - $\Gamma$  of 2.73 eV semiconductors, which is smaller than the optical band gap of 3.80 eV experimentally observed in this work. The  $\text{CF}_3$  group creates isolated bands above the Fermi energy in the conduction band lies at 0.85 eV and shows **n**-type character. Because the Fermi level is shifted to the conduction band due to the presence of the  $\text{CF}_3$  group. Figure **3.60** (B) (b) shows the TDOS, which is consistent with the band structure. Figure **3.60** (B) (c-d) shows PDOS which demonstrates that the isolated band near the Fermi energy mainly comes from C  $p$ -, O,  $p$ -orbitals which partially hybridized with N  $p$ -, F  $p$ -orbitals. To show the van-der interaction between H-O<sub>2</sub>, the charge-density for compound **4** is shown in Figure **3.61**(B). We plotted the charge density in such a way that H and O<sub>2</sub> lie in the same plane. The dotted ellipse shows the van-der Walls interaction with a respective bond length of H-O<sub>2</sub> is 1.59 Å which is larger than the bond length of the H(O<sub>2</sub>) with covalently bonded atoms N1(C1) is 1.06 Å (1.26 Å).

The VBM (HOMO) and CBM (LUMO) energies obtained are -4.36 eV and -1.62 eV concerning the vacuum potential of 5.065 eV. The Fermi energy is 2.01 eV and the calculated work-function is 3.05 eV larger than compound 4.



**Figure 3.61:** Top view of the charge-density plot (A) of compound 1, i.e., for a single monomer of compound 1. (B) of compound 4. In both cases, we plot the charge density such that H and O2 lie in the same plane. In both cases, the dotted ellipse represents the van-der Waals interaction between the H-O2 bond. The yellow, white-blue, dark-blue, gray red balls, green balls represent C, H, N, Sn, O, and F atoms, respectively.



**Figure 3.62:** Optical spectra calculated for (A) compound 1, (B) for compound 4.

The experimentally observed optical spectra as a function of wavelength are presented in Figure 3.62 (A-B). It is observed that compound **4(B)** hardly adsorb light in the visible range in contrast it is observed that compound **1(A)** adsorb light in both the UV and visible range (250 nm 350 nm). We suggest that CF<sub>3</sub> presence in compound **4** modify the orbital character which results in an enhanced optical absorption spectrum in the UV range. Using DFT the structural and electronic properties of **p**-type compound **1** and **n**-type compound **4** have been investigated. The negative values of the  $E_f$  obtained suggest that both compounds are thermally stable consistent with experimental realization. The van-der Waals nature of the H-O<sub>2</sub> bonding was confirmed in both compounds using the DFT study. The electronic properties such as band gaps, Fermi energy, work-function, vacuum potential, HOMO, and LUMO were calculated. These properties are very important for constructing polymers-based electronic devices. The band gap of compound **4** was found larger than compound **1**. The CF<sub>3</sub> dye enhanced the electronic properties and also thermodynamic stability.

### 3.6. Computational Methods

Geometry optimization of the complex structures was performed by density functional method in the Gaussian software package [155]. The stationary points of the potential energy surfaces were located using the hybrid exchange density functional with Becke's three-parameter hybrid exchange functional (B3LYP) employing the LANL2DZ basis set [156, 157]. Computational studies serve herein as a supportive tool to the experimental data; the structural parameters of bond lengths and bond angles were computed for comparison with the experimental values. The frontier orbital band gap ( $E_g$ ) and other global reactivity parameters such as chemical hardness, electronegativity, and chemical potential were calculated through the Koopman's theorem [158] from the highest occupied molecular orbital (HOMO) and lowest unoccupied molecular orbital



(LUMO) at the same level of theory. The Mulliken atomic charge analysis was carried out to form a picture of charge distribution in the organotin carboxylates. Additionally, molecular electrostatic potential (MEP) surfaces have been analyzed to examine the electron-rich and deficient regions in the complexes.

### 3.6.1 Quantum Chemical Calculations

The geometry optimization of the ligands (**IL**<sup>3</sup>, **IL**<sup>4</sup>) and the synthesized compounds (**C7-C12**) was performed in the gas phase using density functional theory (DFT) at the B3LYP/LANL2DZ level. All the calculations were performed in the Gaussian software tool; the choice of the basis set is dictated by its efficacy where atoms of higher atomic numbers are concerned [159]. An effective core potential is employed in the case of LANL2 with double zeta (DZ) basis to effectively explain the structural parameters [160]. Selected bond lengths and angles along with their experimental values for the compounds **IL**<sup>3</sup>, **C7**, **C8**, and **C9** are listed in Table **3.1.** and Table **3.2.** with excellent comparability. The optimized geometrical structures of the compounds, as obtained from DFT are provided in **Appendix S1** at the end of the dissertation. All the computed C-C bond lengths are found to fall in the range of 1.40 – 1.50 Å for all the compounds, while the C-N bond distances vary in the range of 1.33 – 1.45 Å. In the case of the C-O bond lengths, the usual range of 1.25 – 1.35 Å is observed while the Sn-C bond distances do not show much variation at 2.12 - 2.14 Å. The slight differences between the theoretical and experimentally obtained values may be attributed to the presence of intermolecular interactions in the solid crystalline form.

**Table 3.2:** Selected experimental and theoretical bond lengths (Å) for compound **II**<sup>3</sup>, **C7**, **C8**, and **C10**. The theoretical bond lengths are calculated using DFT at the B3LYP/LANL2DZ level.

<b>II<sup>1</sup></b>			<b>C7</b>		
<b>Bond</b>	<b>Experimental</b>	<b>Theoretical</b>	<b>Bond</b>	<b>Experimental</b>	<b>Theoretical</b>
O1-C8	1.2522(17)	1.25174	Sn1-O1	2.1806(12)	2.0397
O3-C11	1.2250(18)	1.24010	Sn1- O3 <sup>1</sup>	2.4211(12)	-
O2-C11	1.3090(18)	1.37756	Sn1-C2	2.1323(18)	2.12708
N1-C1	1.4120(19)	1.45712	Sn1-C1	2.114(2)	2.12915
N1-C8	1.3408(18)	1.40947	Sn1-C3	2.1177(18)	2.12641
C1-C2	1.402(2)	1.40785	O2-C4	1.233(2)	1.25974
C1-C6	1.393(2)	1.40744	O1-C4	1.289(2)	1.35322
C8-C9	1.479(2)	1.50201	O3- Sn1 <sup>2</sup>	2.4211(12)	--
C9-C10	1.341(2)	1.35545	O3-C7	1.2477(19)	1.2578
C10-C11	1.495(19)	1.50418	N1-C7	1.331(2)	1.3817
C2-C3	1.380(2)	1.40537	N1-C8	1.409(2)	1.4359
<b>C8</b>			<b>C10</b>		
<b>Bond</b>	<b>Experimental</b>	<b>Theoretical</b>	<b>Bond</b>	<b>Experimental</b>	<b>Theoretical</b>
Sn1-O1	2.1797(16)	2.04193	Sn1-O1	2.1715(11)	2.02570
Sn1-O31	2.5408(17)	--	Sn1- O3 <sup>1</sup>	2.5004(11)	--
Sn1-C12	2.140(2)	2.14924	Sn1-C1	2.1237(18)	2.12867
Sn1-C16	2.145(2)	2.15128	Sn1-C3	2.1225(18)	2.12629
Sn1-C20	2.142(2)	2.14942	Sn1-C2	2.1228(19)	2.12638
O1-C1	1.288(3)	1.34792	F1-C11	1.3596(17)	1.40352
O2-C1	1.236(3)	1.26145	O1-C4	1.294(2)	1.35042
O3-Sn12	2.5408(17)	---	O2-C4	1.2368(19)	1.26058
O3-C4	1.237(3)	1.25927	O3- Sn1 <sup>2</sup>	2.5004(11)	--
N1-C4	1.339(3)	1.38162	O3-C7	1.2483(18)	1.25650
N1-C5	1.409(3)	1.43618	N1-C8	1.4086(19)	1.43426

**Table 3.3:** Selected experimental and theoretical bond angles ( $\theta$ ) for compound **IL<sup>3</sup>**, **C7**, **C8**, and **C10**. The theoretical bond angles are calculated using DFT at the B3LYP/LANL2DZ level.

<b>IL<sup>3</sup></b>			<b>C7</b>		
<b>Bond</b>	<b>Experimental</b>	<b>Theoretical</b>	<b>Bond</b>	<b>Experimental</b>	<b>Theoretical</b>
C8-N1-C1	129.18(12)	124.043	O1-Sn1-O3 <sup>1</sup>	176.22(5)	120.87
C2-C1-N1	116.37(12)	119.261	C2-Sn1-O1	89.15(6)	106.60
C6-C1-N1	124.72(13)	120.856	C2-Sn1-O3 <sup>1</sup>	90.65(6)	109.20
C6-C1-C2	118.87(13)	119.827	C1-Sn1-O1	93.28(6)	106.45
O1-C8-N1	123.19(13)	121.051	C1-Sn1-O3 <sup>1</sup>	83.50(6)	67.54
O1-C8-C9	123.64(13)	120.635	C1-Sn1-C2	118.53(8)	114.88
N1-C8-C9	113.17(11)	118.239	C1-Sn1-C3	124.17(8)	114.37
C10-C9-C8	128.79(12)	129.097	C3-Sn1-O1	100.60(6)	98.95
C9-C10-C11	131.69(13)	131.316	C3-Sn1-O3 <sup>1</sup>	82.89(6)	129.22
O3-C11-O2	121.31(13)	120.246	C3-Sn1-C2	115.50(8)	113.67
O3-C11-C10	118.23(13)	119.963	C4-O1-Sn1	113.73(10)	122.94
O2-C11-C10	120.45(13)	119.771	C7-O3-Sn1 <sup>2</sup>	150.90(11)	82.30
<b>C8</b>			<b>C10</b>		
<b>Bond</b>	<b>Experimental</b>	<b>Theoretical</b>	<b>Bond</b>	<b>Experimental</b>	<b>Theoretical</b>
O1-Sn1-O3 <sup>1</sup>	171.97(6)	115.143	O1-Sn1-O3 <sup>1</sup>	176.50(4)	121.47
C12-Sn1-O1	90.82(8)	106.71	C1-Sn-O1	89.66(6)	98.89
O1-Sn1-O3 <sup>1</sup>	81.42(8)	115.143	C1-Sn-O3 <sup>1</sup>	88.52(5)	129.08
C12-Sn1-C16	113.19(9)	115.57	C3-Sn1-O1	100.09(6)	106.51
C12-Sn1-C20	115.86(9)	117.67	C3-Sn1-O3 <sup>1</sup>	83.40(5)	129.07

C16-Sn1-O1	96.82(8)	103.51	C3-Sn1-C1	118.66(8)	113.87
C16-Sn1-O3 <sup>1</sup>	88.21(8)	113.71	C3-Sn1-C2	119.65(7)	114.94
C20-Sn1-O1	97.07(8)	96.28	C2-Sn1-O1	95.80(5)	106.12
C20-Sn1-O3 <sup>1</sup>	84.55(8)	124.47	C2-Sn1-O3 <sup>1</sup>	82.51(5)	67.71
C20-Sn1-C16	128.54(10)	113.67	C2-Sn1-C1	119.25(8)	114.49
C1-O1-Sn1	113.86(14)	121.63	C4-O1-Sn1	116.49(10)	123.59
C4-O3-Sn1 <sup>2</sup>	160.39(16)	90.14	C7-O3-Sn1 <sup>2</sup>	152.75(11)	81.53

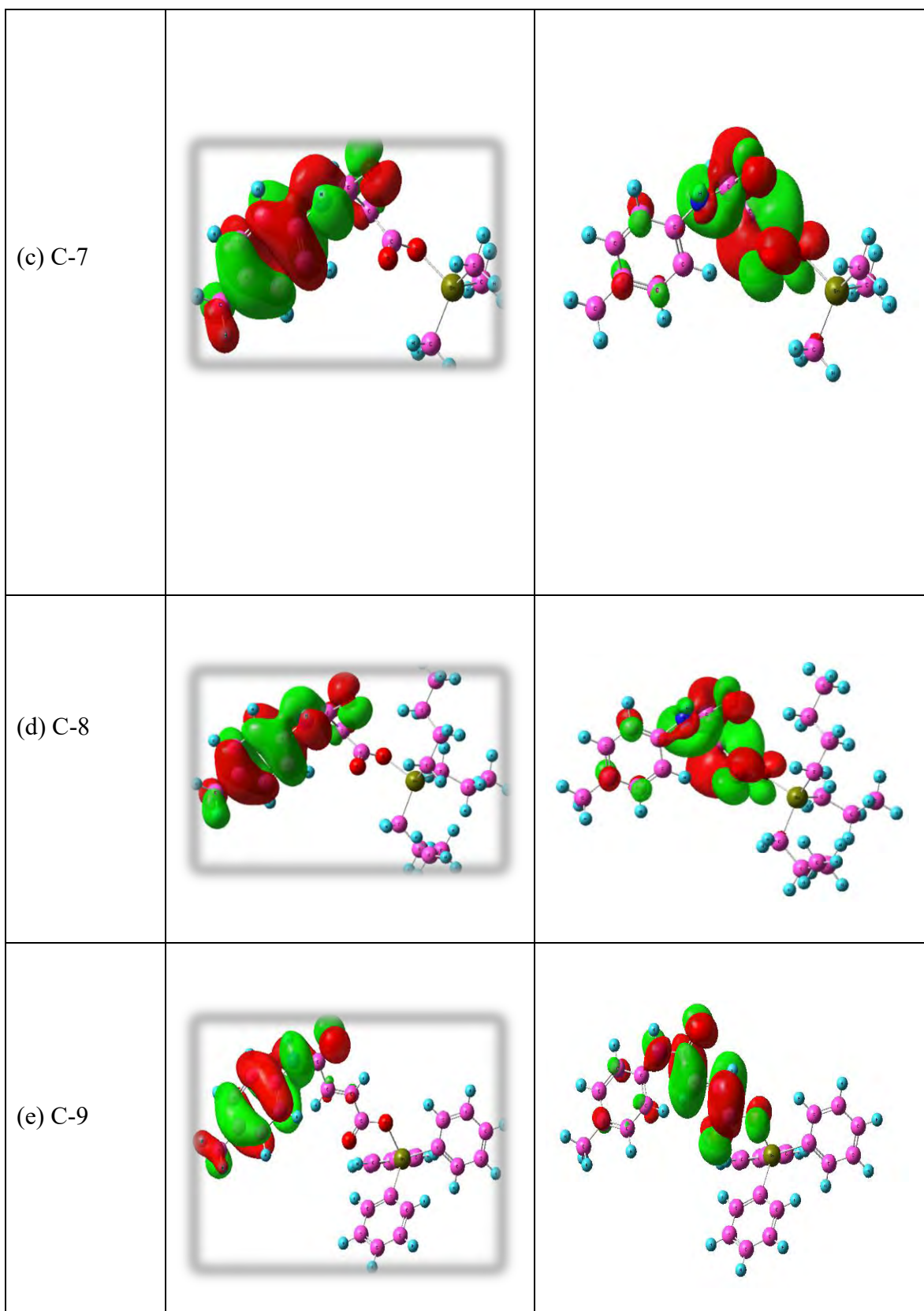
The frontier molecular orbitals of the ligands (**IL**<sup>3</sup>, **IL**<sup>4</sup>) and the compounds (**C-7**, **C-8**, **C-9**, **C-10**, **C-11**, and **C-12**) are computed at the B3LYP/LANL2DZ level of theory to understand the chemical stability and electronic properties of these molecular systems. The (outermost) highest occupied molecular orbital (HOMO) typically shows electron-donating behavior and as such, represents regions of highest electron density, while the (innermost) lowest unoccupied molecular orbital (LUMO) acts as an electron acceptor and is therefore susceptible to a nucleophilic attack [161, 162]. A schematic representation of the frontier molecular orbitals for the ligands and the compounds is provided in Table 3.3. In the studied complexes, the HOMO is primarily located on the phenyl ring and the amide functional group, while the iso-density in LUMO of the compounds is shifted toward the carboxylate moiety directly linked to the tin atom, indicating susceptibility towards nucleophilic attack.

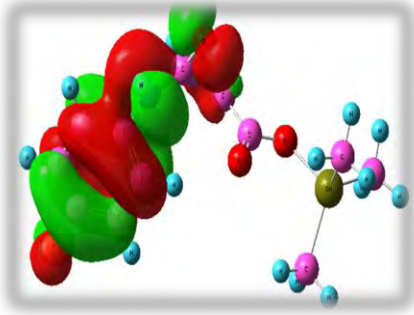
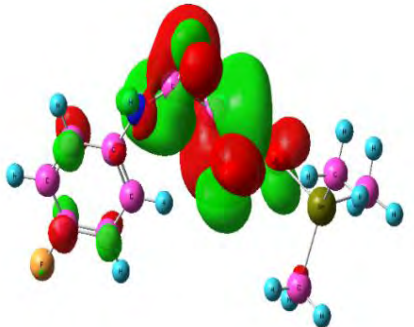
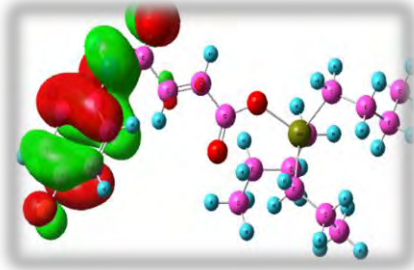
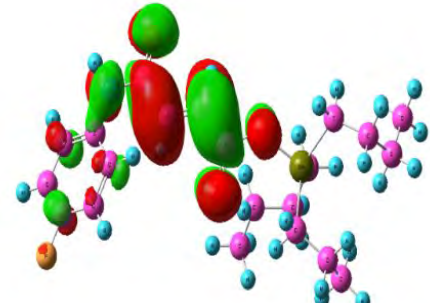
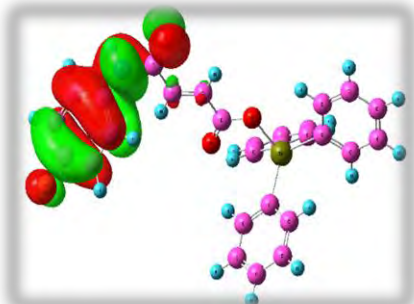
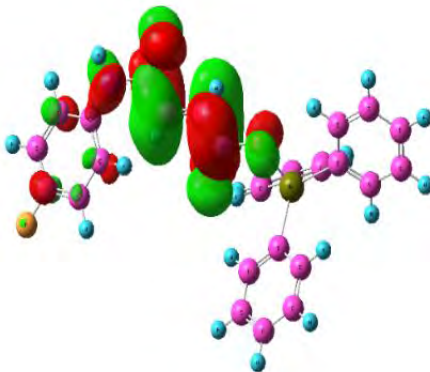
It is a determined fact that the band gap between the frontier molecular orbitals (FMOs) is related to the stability and kinetic stability of the compound under investigation [163, 164]. A smaller energy gap represents the greater ability of the complex to undergo a

chemical reaction while a higher band gap indicates its stability towards redox reactions [165] [166]. In this study, the computed HOMO-LUMO band gaps (Table 3.4.) for the compounds C-7 to C-12 are found to be 4.544, 4.625, 3.945, 4.761, 4.244, and 4.136 eV, while the values of  $E_g$  for the ligands  $IL^3$  and  $IL^4$  are 4.642 and 4.680 eV respectively. The smallest frontier orbital band gap is observed for C9, while all the other synthesized complexes show good kinetic stability. Global reactivity parameters such as electronegativity ( $\chi$ ), softness ( $\sigma$ ), hardness ( $\eta$ ) and dipole moment ( $\mu$ ) calculated from the eigen energy data (equations in Appendix at the end of chapter) [167] are listed in Table 3.4.

**Table 3.4:** Frontier molecular orbitals of ligands ( $IL^3$ ,  $IL^4$ ) and the compounds (C-7, C-8, C-9, C-10, C-11, and C-12) compounds are depicted with the following color index of atoms: Red=O, Blue=N, Green=Sn, Yellow= F, Pink=C.

Compound	HOMO	LUMO
(a) $IL^3$		
(b) $IL^4$		



(f) C-10		
(g) C-11		
(e) C-12		

**Table 3.5:** Frontier orbital energies, their band gap ( $E_g$ ), and global reactivity parameters\* of metal complexes obtained by B3LYP with a LANL2DZ basis set.

Quantum Parameters	Compounds							
	IL <sup>3</sup>	IL <sup>4</sup>	C-7	C-8	C-9	C-10	C-11	C-12
$E_{HOMO}$ (eV)	-7.156	-7.619	-6.258	-6.261	-6.340	-6.639	-6.612	-6.721
$E_{LUMO}$ (eV)	-2.666	-2.911	-1.687	-1.605	-2.394	-1.877	-2.367	-2.585
$E_g$ (eV)	4.490	4.707	4.544	4.625	3.945	4.761	4.244	4.136
$\mu$ (eV)	-4.911	-5.265	-3.972	-3.933	-4.367	-4.258	-4.489	-4.653
$I$ (eV)	7.156	7.619	6.258	6.261	6.340	6.639	6.612	6.721
$A$ (eV)	2.666	2.911	1.687	1.605	2.394	1.877	2.367	2.585
$\chi$ (eV)	4.911	5.265	3.972	3.933	4.367	4.258	4.489	4.653
$\eta$ (eV)	2.245	2.354	2.285	2.328	1.973	2.376	2.122	2.068
$s$ (eV <sup>-1</sup> )	0.445	0.424	0.437	0.429	0.506	0.420	0.471	0.483

\* Chemical potential ( $\mu$ ), ionization potential ( $I$ ), electron affinity ( $A$ ), electronegativity ( $\chi$ ), softness ( $\sigma$ ), and global hardness ( $\eta$ )

According to Pearson's acid-base concept (HSAB) and its correlation to molecular orbital theory [167], a large HOMO-LUMO gap indicates a higher value of global hardness ( $\eta$ ) in a chemical system. In the present study, the compound C-10 shows the largest  $E_g$  value at 4.761 eV and is, therefore, less polarizable, while compound C-9 with the lowest band gap (3.945 eV) is the softest molecule with a high degree of polarizability. Additionally, the acidic or basic behavior of a chemical entity can be predicted based on its absolute electronegativity ( $\chi$ ). As such, the ligand IL<sup>2</sup> with a high  $\chi$  value of 5.265 eV typically behaves as acid, while C-8 with the lowest  $\chi$  (3.933 eV) acts as an electron acceptor. The calculated results further suggest that all the compounds (except C-10) are more soft and polarizable in comparison to IL<sup>2</sup>. Soft



molecules are more reactive vis-à-vis electron transfer; while compound C-10 shows more structural stability.

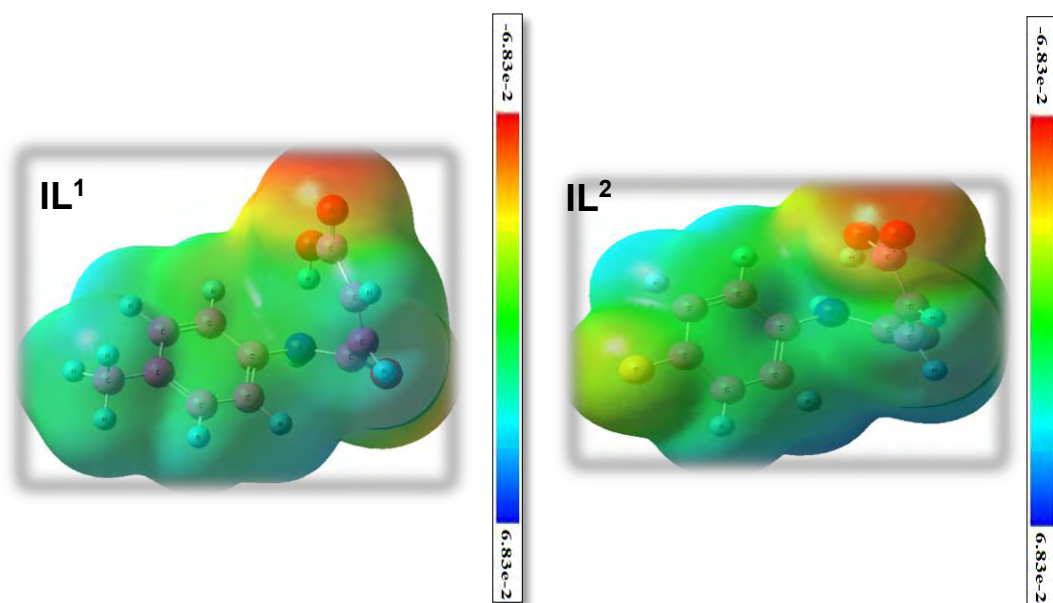
Mulliken charge analysis is a powerful descriptor of the distribution of atomic charges in a molecular system and points a way towards donor and acceptor moieties involved in the charge transfer [168]. Selected charges from the Mulliken charge distribution of the tin carboxylates calculated at the B3LYP/LANL2DZ level are listed in Table 3.5. It can be readily observed that highly electronegative hetero atoms (O and N) in the carboxylate and amide linkages have the highest negative charge densities, while the Sn atom has the largest positive atomic charge (range: 1.28-1.35) and therefore acts as an electrophilic center. Most of the carbon atoms carry a negative charge.

**Table 3.6:** Mulliken charges were obtained using DFT (B3LYP) manner with a LANL2DZ basis set. The atom internal numbering is mentioned in parenthesis within each column along with the atomic charge.

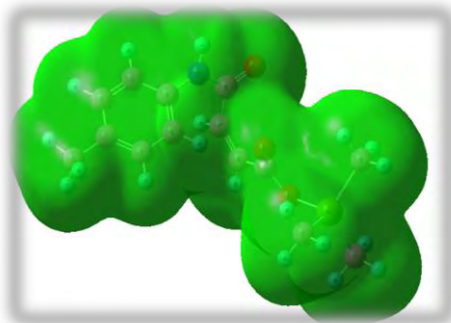
Mulliken charges	Compounds							
	IL <sup>3</sup>	IL <sup>4</sup>	C-7	C-8	C-9	C-10	C-11	C-12
q <sub>N</sub>	-0.5101 (12)	-0.5127 (11)	-0.4388 (12)	-0.4366 (12)	-0.4426 (12)	-0.4429 (11)	-0.4493 (11)	-0.4469 (11)
q <sub>o</sub>	-0.2545 (17)	-0.2485 (16)	-0.3408 (17)	-0.3392 (17)	-0.3536 (17)	-0.3453 (16)	-0.3286 (16)	-0.3506 (16)
q <sub>o</sub>	-0.4237 (18)	-0.4238 (17)	-0.6277 (18)	-0.5993 (18)	-0.6034 (18)	-0.6244 (17)	-0.6148 (17)	-0.6020 (17)
q <sub>o</sub>	-0.2295 (19)	-0.2236 (18)	-0.2786 (19)	-0.2873 (19)	-0.2967 (19)	-0.2727 (18)	-0.2946 (18)	-0.2903 (18)
q <sub>Sn</sub>	-	-	1.3590	1.2305	1.2801	1.3577	1.2377	1.2800

			(26)	(26)	(26)	(22)	(22)	(22)
<b>q<sub>F</sub></b>	-	-0.2307 (23)	-	-	-	-0.2424 (35)	-0.2396 (59)	-0.2388 (56)
<b>q<sub>c</sub></b>	-0.3493 (1)	-0.3070 (1)	-0.3792 (1)	-0.3494 (1)	-0.3999 (1)	-0.3449 (1)	-0.3011 (1)	-0.3647 (1)
<b>q<sub>c</sub></b>	0.3901 (2)	0.3985 (2)	0.4077 (2)	0.4042 (2)	0.4160 (2)	0.4192 (2)	0.4367 (2)	0.4333 (2)
<b>q<sub>c</sub></b>	-0.3207 (3)	-0.2838 (3)	-0.3507 (3)	-0.3799 (3)	-0.3339 (3)	-0.3112 (3)	-0.3660 (3)	-0.2986 (3)
<b>q<sub>c</sub></b>	-0.3854 (4)	-0.3378 (4)	-0.3531 (4)	-0.4011 (4)	-0.3890 (4)	-0.3436 (4)	-0.3257 (4)	-0.3434 (4)
<b>q<sub>c</sub></b>	0.4563 (5)	0.3379 (5)	0.4588 (5)	0.4588 (5)	0.4549 (5)	0.3283 (5)	0.3292 (5)	0.3298 (5)
<b>q<sub>c</sub></b>	-0.3585 (6)	-0.3381 (6)	-0.3949 (6)	-0.3482 (6)	-0.3515 (6)	-0.3311 (6)	-0.3428 (6)	-0.3249 (6)
<b>q<sub>c</sub></b>	0.0850 (13)	0.0897 (12)	0.1127 (13)	0.1137 (13)	0.1373 (13)	0.1184 (12)	0.1441 (12)	0.1434 (12)
<b>q<sub>c</sub></b>	-0.1528 (14)	-0.1564 (13)	-0.1478 (14)	-0.1624 (14)	-0.1989 (14)	-0.1516 (13)	-0.2064 (13)	-0.2017 (13)
<b>q<sub>c</sub></b>	-0.2483 (15)	-0.2454 (14)	-0.2305 (15)	-0.2301 (15)	-0.2503 (15)	-0.2280 (14)	-0.2503 (14)	-0.2476 (14)
<b>q<sub>c</sub></b>	---	0.2175 (15)	0.3205 (16)	0.2959 (16)	0.3219 (16)	0.3223 (15)	0.2950 (15)	0.3222 (15)

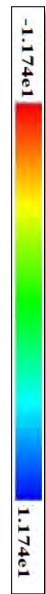
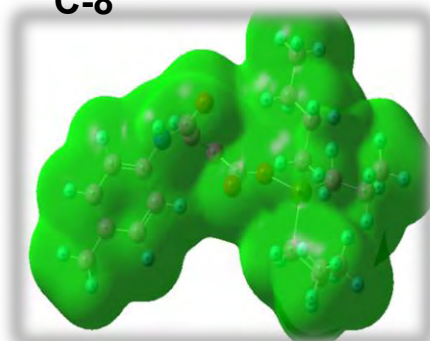
Molecular electrostatic potential (MEP) surfaces provide visual information about the relative polarity of a molecule and can be correlated to dipole moments, partial charges, and chemical reactivity of the investigated systems. The isodensity surfaces of all the compounds mapped with electrostatic potential are depicted in Figure 3.63. The dispersion of increasing electrostatic potential follows the order: red < orange < yellow < green < blue, where blue regions indicate the most positive and green depicts zero potential. It can be seen that while the ligands (IL<sup>3</sup>, IL<sup>4</sup>) are highly polar, the organotin carboxylates show a neutral nature, wherein no red or blue region is observed over the entire surface [164]. The more electronegative atoms of O and F in the two ligands IL<sup>3</sup> and IL<sup>4</sup> are depicted by the red and yellow electron-rich regions.



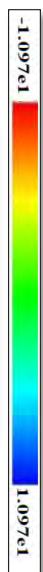
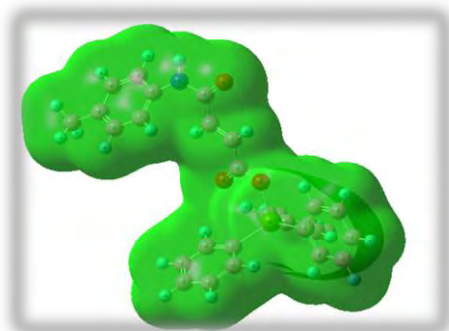
C-7



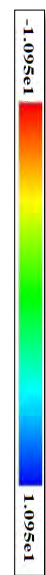
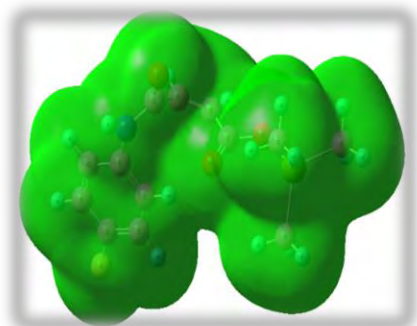
C-8



C-9



C-10



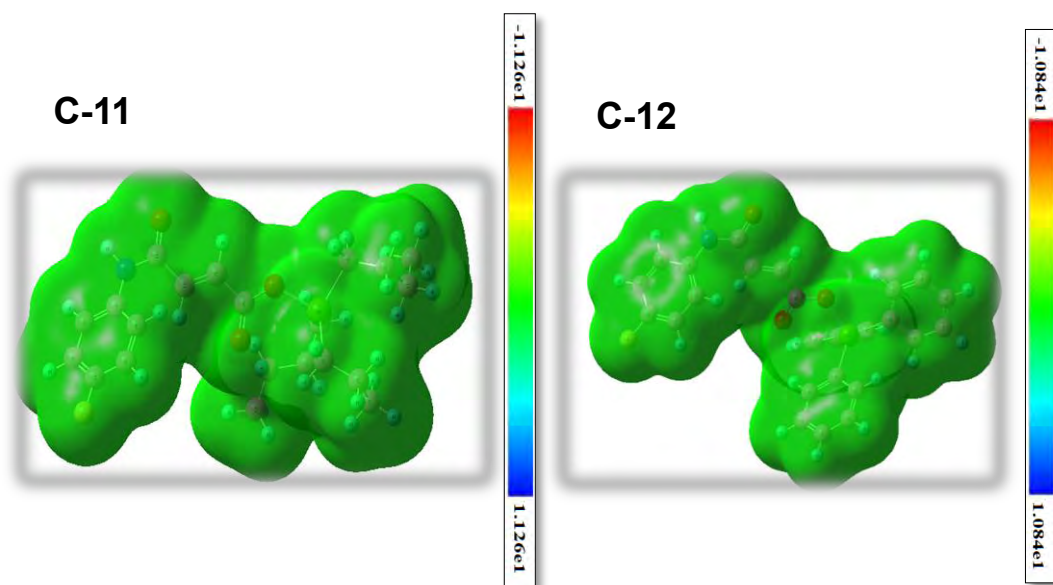


**Figure 3.63:** Electrostatic potential surfaces of the total SCF density (isovalue = 0.02) for the ligands (IL<sup>3</sup> and IL<sup>4</sup>) and organotin compounds (C7-C12). The color bars range from blue (electropositive) to green (neutral) to red (electronegative) potentials.

## Summary of Biological Assays

- The Ligands and trimethyltin(IV) complexes are least active while the tributyltin(IV) complexes are the most active anticancer agents followed by triphenyltin(IV) complexes. The tributyltin(IV) carboxylates **2** and **5** showed the most promising results against the anticancer cell lines and complex **2** revealed 20 times more activity against breast cancer cell lines as compared to normal cell lines which can further evaluated for in vivo study. It is noted that electron withdrawing substituents fluorine on benzene ring has profound effect on cancer cells because of the hydrogen bond interaction with the cancer cells. Similar the flexible nature of butyl moiety and their twisting nature to one side allowed the approach of negative DNA bases towards positive tin center.
- Studied complexes have revealed better antileishmanial activities as compared to the ligands. The triphenyltin(IV) complexes showed the best antileishmanial agents followed by tributyltin(IV) complexes and trimethyl(IV) complexes. Triphenyltin(IV) complexes **6,12** and **15** exhibited good antileishmanial agents than other complexes which can be evaluated for further study.
- Preliminary hemolytic activity has shown that these complexes are least toxic against the trimethyltin(IV) complexes followed by triphenyl(IV) complexes and trimethyltin(IV) complexes.
- The antimicrobial analysis carried out against three different bacterial and fungal strains indicated that the tributyltin(IV) complexes have most antibacterial and antifungal activity followed by triphenyltin(IV) complexes and then trimethyltin(IV) complexes. This strong antimicrobial activity may be

attributed to the strong lipophilic character of tributyltin(IV) complexes as compared to trip trimethyltin(IV) and triphenyl(IV) complexes.

- The synthesized ligands and complexes were also screened for cytotoxicity using the Brine shrimp (*Artemia salina*) bioassay lethality method and the results illustrate that all compounds are cytotoxic and the LD<sub>50</sub> values decreased in the following sequence. The complex **13** is the best compound which has LD<sub>50</sub> value comparable to the standard drug.



- Antioxidant study revealed that all the complexes exhibited least to highest antioxidant potential. Complexes **8**, **10** and **14** possessed the best antioxidant strength among the synthesized complexes. All these active complexes can be utilized as a free radical inhibitor after clinical trials and can further be evaluated for anti-tumor studies because of the effective antioxidants possess efficient anticancer potential as well. It is noted that electron withdrawing substituents fluorine pass a considerable effect on the antioxidant property by increasing complex lipophilic character and stability.

# **Chapter 4**

## **Crystallography**



## 4.1. Crystal structure of the free ligand

Crystal data along with structure modification parameters for **II**<sup>3</sup> with crystal system (monoclinic) and space group (P2<sub>1</sub>/n) is shown in Table 4.1 while the bond lengths along with bond angles are shown in Tables 4.2 & 4.3 respectively. The molecular structure having intramolecular hydrogen bonding OH---O is shown in Figure 4.1 while the molecular structure having both intramolecular OH---O and intermolecular hydrogen bonding NH---O is shown in Figure 4.2. The unit cell packing is shown in Figure 4.3. The benzene ring of the central plane (C1-C2) having a dihedral angle between them and the plane of the maleic acid group (C11-C8/O1-O2) is 8.1(3)°. The amide group –NHCO- and the aromatic ring mean plane are inclined at an angle of 31.3(3)°. The C=O and N-H conformations in the carbonyl amide part are *anti* to one another. The C-H bond is *syn* to the nearby carboxylic acid group C=O bond and the C-H bond is *anti* to the adjacent carbonyl amide C=O bond. The O-H and C=O bonds rare anti conformations in the segment of the acidic part is comparable to the one which is detected in N-(4-methoxyphenyl) maleamic acid [169]. There are intramolecular and intermolecular O-H---O and N-H---O connections that alleviate the packing assembly of the ligand (**II**<sup>3</sup>). The intermolecular N-H---O contact and C-H--- $\pi$  interaction linking the chain with each other into a three-dimensional network [170]. The details of intramolecular and intermolecular H-bonds showed in (Z)-4-(p-toluidino)-4-oxobut-2-enoic acid (**II**<sup>3</sup>) is given in Table 4.4.

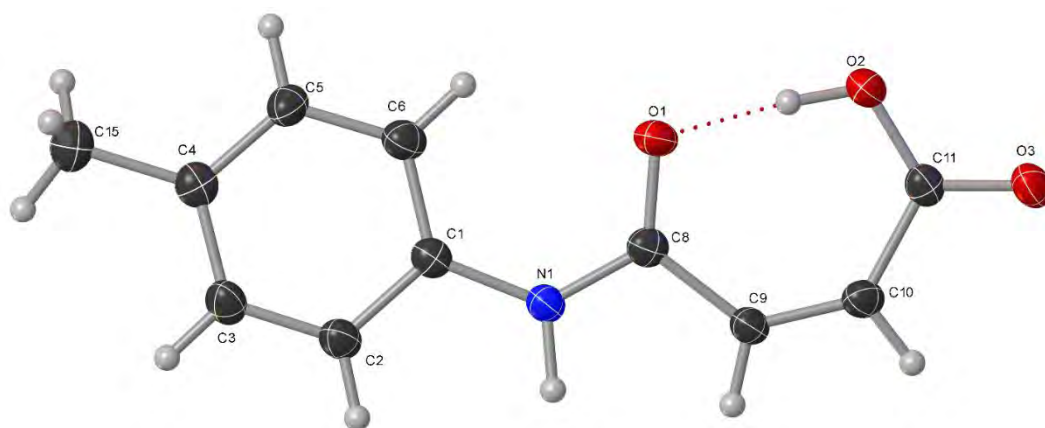


**Figure 4.1:** Outlook view of ligand IL<sup>3</sup> with intramolecular hydrogen bonding.

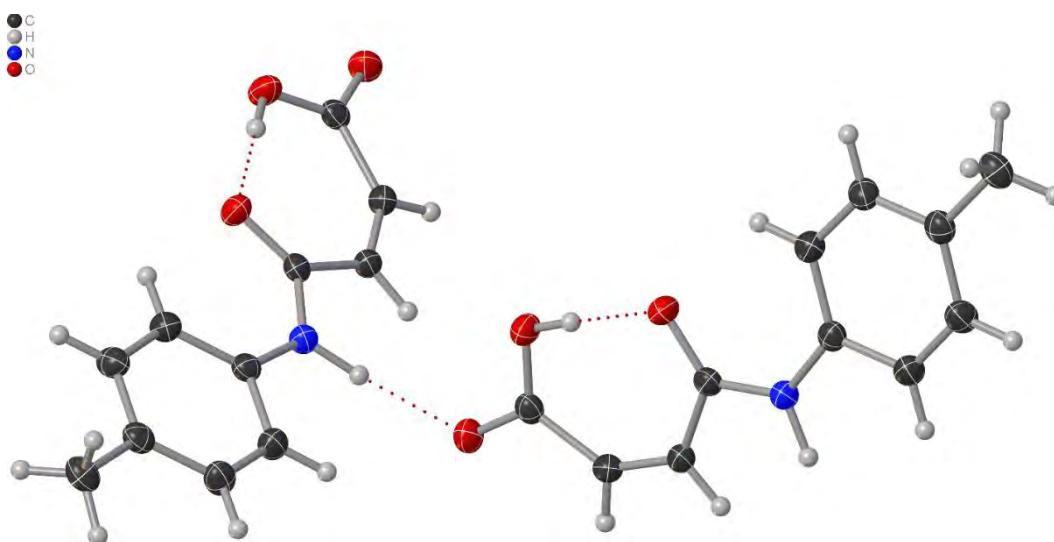


**Figure 4.2:** Outlook view of ligand IL<sup>3</sup> with intramolecular and intermolecular hydrogen bonding.

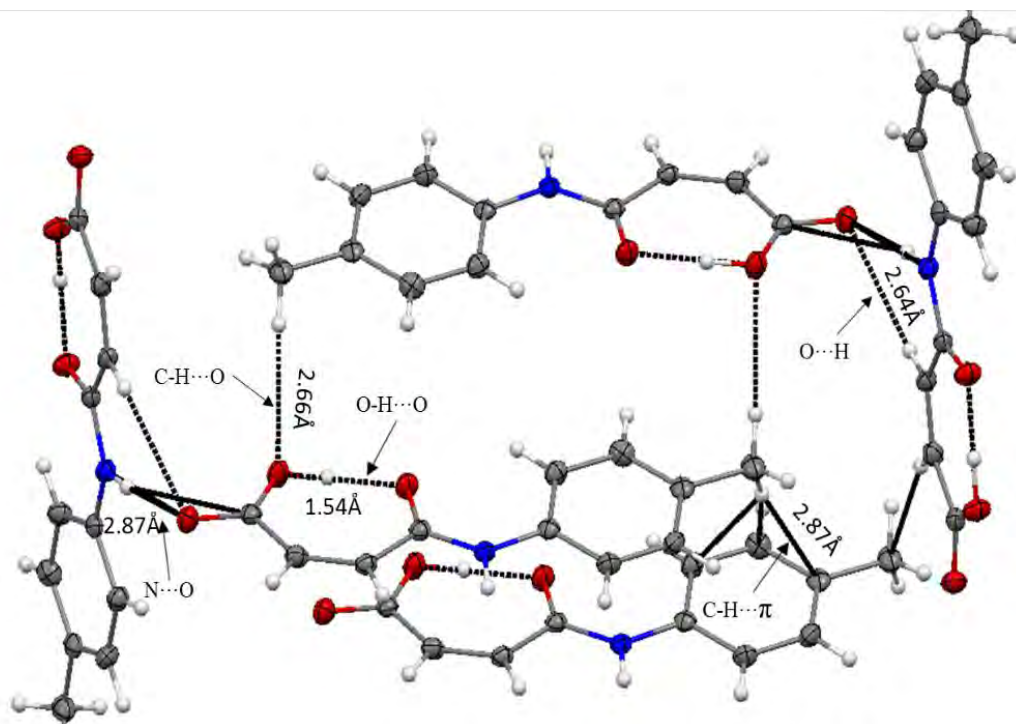


**Figure 4.3:** Outlook view of ligand **IL**<sup>3</sup> with packing diagram showing having hydrogen bonding and intermolecular secondary interactions.

**Table 4.1:** Crystal data and structure refinement parameters for ligand **IL**<sup>3</sup>

Parameters	<b>IL</b> <sup>3</sup>
Formula	C <sub>11</sub> H <sub>11</sub> NO <sub>3</sub>
<i>D</i> <sub>calc.</sub> / g cm <sup>-3</sup>	1.382
<i>μ</i> /mm <sup>-1</sup>	0.844
Formula Weight (g/mol)	205.21
Colour	colourless
Shape	needle
Size/mm <sup>3</sup>	0.41×0.15×0.11
<i>T</i> /K	100(2)
Crystal System	monoclinic
Space Group	P2 <sub>1</sub> /n
<i>a</i> /Å	4.6737(5)
<i>b</i> /Å	18.492(2)
<i>c</i> /Å	11.4286(10)
<i>α</i> <sup>°</sup>	90
<i>β</i> <sup>°</sup>	93.305(10)
<i>γ</i> <sup>°</sup>	90
<i>V</i> /Å <sup>3</sup>	986.07(18)
<i>Z</i>	4
<i>Z</i> '	1
Wavelength/Å	1.54184
Radiation type	CuK <sub>α</sub>
<i>θ</i> <sub>min</sub> <sup>°</sup>	4.554
<i>θ</i> <sub>max</sub> <sup>°</sup>	68.235
Measured Refl.	4256
Independent Refl.	1715
Reflections with <i>I</i> > 2σ( <i>I</i> )	1520
<i>R</i> <sub>int</sub>	0.0236
Parameters	145
Restraints	0
Largest Peak	0.232
Deepest Hole	-0.296
GooF	1.071
<i>wR</i> <sub>2</sub> (all data)	0.1252
<i>wR</i> <sub>2</sub>	0.1166
<i>R</i> <sub>1</sub> (all data)	0.0480
<i>R</i> <sub>1</sub>	0.0429

**Table 4.2:** Selected Bond Lengths (Å) for compound **IL**<sup>3</sup>

O1-C8	1.2522(17)	C1-C6	1.393(2)
O3-C11	1.2250(18)	C8-C9	1.479(2)
O2-C11	1.3090(18)	C9-C10	1.341(2)
N1-C1	1.4120(19)	C10-C11	1.4951(19)
N1-C8	1.3408(18)	C2-C3	1.380(2)
C1-C2	1.402(2)	C6-C5	1.390(2)
C4-C5	1.393(2)	C4-C15	1.501(2)

**Table 4.3:** Selected Bond Angles (°) for compound **IL**<sup>3</sup>

C8-N1-C1	129.18(12)	N1-C8-C9	113.17(11)
C2-C1-N1	116.37(12)	C10-C9-C8	128.79(12)
C6-C1-N1	124.72(13)	C9-C10-C11	131.69(13)
C6-C1-C2	118.87(13)	O3-C11-O2	121.31(13)
O1-C8-N1	123.19(13)	O3-C11-C10	118.23(13)
O1-C8-C9	123.64(13)	O2-C11-C10	120.45(13)

**Table 4.4:** Hydrogen bond information for ligand **IL**<sup>3</sup>

D-H----A	d(D-H)/Å	d(H-A)/Å	d(D-A)/Å	D-H-A/deg
C6-H6-O1	0.93	2.30	2.8930(18)	120.9
O2-H2-O1	0.95(3)	1.54(3)	2.4850(14)	174(2)
N1-H1- O3 <sup>1</sup>	0.918(19)	1.961(19)	2.8698(15)	170.3(16)

Symmetry codes: <sup>1</sup>1/2+X,3/2-Y,-1/2+Z

## 4.2 Single Crystal XRD structures of triorganotin carboxylates

### 4.2.1 Five coordinated trigonal bipyramidal geometry

The molecular structure of complexes **1**, **4**, **5**, **7**, **8**, **10**, **13**, **14**, and **22** with intermolecular and intramolecular interactions are given in Figures 4.4-4.27 below. The presence of bidentate ligands, (Z)-4-(4-methoxyphenylamino)-4-oxobut-2-enoic acid (**IL**<sup>1</sup>), (Z)-4-(3,5-bis(trifluoromethyl)phenylamino)-4-oxobut-2-enoic acid (**IL**<sup>2</sup>), (Z)-4-(p-toluidino)-4-oxobut-2-enoic acid (**IL**<sup>3</sup>), (Z)-4-(4-fluorophenylamino)-4-oxobut-2-enoic acid (**IL**<sup>4</sup>), 4-(1,3-dioxoisindolin-2-yl)butanoic acid (**IL**<sup>5</sup>), 4-(4-methoxyphenylamino)-4-oxobutanoic acid (**IL**<sup>6</sup>), 4-(3,5-bis(trifluoromethyl)phenylamino)-4-oxobutanoic acid (**IL**<sup>7</sup>), 4-(p-toluidino)-4-oxobutanoic acid (**IL**<sup>8</sup>), 4-(4-fluorophenylamino)-4-oxobutanoic acid (**IL**<sup>9</sup>) lead the compound to polymeric structure in solid state and seems distorted trigonal bipyramidal geometry around Sn atom [171].

Crystal data, as well as structure modification constraints for the selected complexes with crystal system having distorted five coordinated trigonal bipyramidal geometry, are displayed in the table, while the bond angles along with bond length are shown in Tables **4.5-4.13** respectively. The molecular structure is shown in the figures below while their unit cell packing is also displayed there in the figures.

The crystal structures of compounds **1**, **4** and **5** with intramolecular and intermolecular interactions are given in Figures **4.4-4.12** and particular symmetrical parameters, bond lengths along with bond angles are given in Tables **4.5-4.6**. While a related series of compounds (to be published elsewhere) refined well, the anisotropic refinement of the atoms of **4** and **5** here resulted in elongated temperature factors and disordered butyl

groups (for compound **5**) in sharp contrast to the other compounds. The inability of these compounds (**4** and **5**) to form well-ordered crystals is probably a consequence of the very weak intermolecular interactions between the CF<sub>3</sub> and CH<sub>2</sub> groups (with very weak H---H and H---F interactions). Compound **5** goes through a phase change on cooling (with the disintegration of the single crystal) and the data were collected at 173 K instead of 100 K. All the complexes in the solid-state are nature-wise polymeric and distorted trigonal bipyramidal with one elongated apical Sn-O bond. The three organic groups (methyl and butyl groups) are mutually equatorial and form the base of the bipyramid and the two oxygen atoms, one from carboxylate moiety and the other from amide carbonyl, occupy axial positions. It is the amide carbonyl that forms the weak bond to the Sn atom. The Sn atom has a 5s<sup>2</sup>5p<sup>2</sup>4d<sup>10</sup> configuration. The trigonal bipyramidal coordination geometries are best rationalized in terms of electron configuration and the relatively large radius of Sn atom. The four valence electrons are donated primarily to the three Sn-C bonds and the short Sn-O bond. The second Sn—O bond is considered to be a weak hypervalent interaction. Although higher coordination numbers are very rare in carbon and to a greater extent for silicon; higher coordination numbers are accessible to Sn due to its relatively large size. As in inorganic chemistry; the relative sizes of the cations and the anions perform a vital role in the coordination numbers in tin compounds. In an analysis of the coordination geometry in compounds **1** and **4**, the three methyl groups that are connected to tin form the basal plane with C2-Sn1-C1(118.7(2)°), C3-Sn1-C1(116.9(2)°), C3-Sn1-C2(123.2(2)°), C13-Sn1-C15(123.7(2)°), C13-Sn1-C14(115.9(2)°), C14-Sn1-C15(117.3(2)°). The two oxygen atoms from the 3-fold axis in an idealized D<sub>3h</sub> trigonal bipyramid arrangement one from carboxylate moiety and the other from amide carbonyl occupy axial positions with O1-Sn1-O3(176.48(11)°) and 179.19(11)° in compounds

**1** and **4**, respectively. The pivot atom that best describes the Berry pseudo rotation is C(1) in compound **1** and C(14) in compound **4** with a 9% transformation to square pyramidal geometry. In compound **5**, the large values for the anisotropic temperature factors for the butyl groups mean that there is large uncertainty in the ligand-Sn angles and this reflects the considerable flexibility of the L-Sn-L angles. The trigonal carbon atoms have bond angles ranging from 116.5(3)° to 120.0(3)° while two apical oxygen atoms, one from carboxylate moiety and the other from the amide group form angles of 176.48(11)° and 179.19(11)° with the tin atom. The five-coordination of Sn atom can also be calculated by using Tau value ( $\tau = (\beta - \alpha) / 60$ , where  $\beta$  is higher C-Sn-C basal angle and  $\alpha$  is the second higher basal angle [172]. The unitary value for tau indicates an exact trigonal bipyramid ( $\beta = 180^\circ$  and  $\alpha = 120^\circ$ ) while zero indicates an exact square pyramid ( $\alpha = \beta = 180^\circ$ ) [173]. For compound **1** the  $\tau$  value 0.89 ( $\beta = \text{O1-Sn1-O3}^1 = 176.48^\circ$  and  $\alpha = \text{C3-Sn1-C2} = 123.23^\circ$ ), for the compound **4** the  $\tau = 0.92$  ( $\beta = \text{O1-Sn1-O3}^1 = 179.19^\circ$  and  $\alpha = \text{C13-Sn1-C15} = 123.66^\circ$ ). There are two independent molecules in compound **5**. For molecule 1 the  $\tau = 0.97$  ( $\beta = \text{O1-Sn1-O3}^1 = 178.06^\circ$  and  $\alpha = \text{C12(2)-Sn1-C12(8)} = 116.5$ ). For Sn(2) the  $\tau = 0.93$  ( $\beta = \text{O1-Sn1-O3}^1 = 175.76^\circ$  and  $\alpha = \text{C12(2)-Sn1-C12(8)} = 119.86$ ) which designates a relatively undistorted trigonal pyramidal geometry [174]. The trend of shifting from trigonal bipyramidal to square planar geometry is associated with secondary intermolecular Sn $\cdots$ O interactions [175, 176]. One ligand carboxylate oxygen is attached with Sn atom in mono-dentate fashion with tin-oxygen covalent bond [(Sn(1)-O(1) = 2.118 Å and [(Sn(1)-O(1) = 2.169 Å respectively which is almost near to the covalent radii(2.13Å) and other amide linked oxygen of another carboxylate ligand coordinated with tin-oxygen bond by a coordinate covalent bond. The bond distance Sn(1)-O(3<sup>1</sup>) = 2.399 Å) and Sn(1)-O(3<sup>1</sup>) = 2.527 Å), are lesser than the totality of the Van der Waals radii of tin and oxygen (3.68 Å) and greater



than the totality of the covalent radii of tin and oxygen (2.13 Å) which is a feeble type of contact between these atoms [177]. The two ligands are interrelated with one another by oxygen atoms involving Sn moiety, thus making a 1D polymeric network. Although in these interactions one of the oxygens which covalent radii is (2.188 Å) is stronger than the coordinately bonded oxygen which bond length is (2.399 Å) because the solid-state geometry is five coordinated while four coordinated geometry in solution which showed that coordinate covalent bond break in solution form. The solid-state structure of **1** which is represented in Figures 4.4, 4.5 and 4.6 and interatomic factors are exhibited in Tables 4.5 and 4.6. The crystal structure of this complex is mediated by intramolecular O···H interactions. This interaction makes a seven-membered ring in the compound which is rarely seen in organotin(IV) amide-based carboxylate complexes in the polymer chain in solid-state. The polymeric chain is alleviated by C-H··· $\pi$  interactions and intramolecular hydrogen bond in a corkscrew style, which is associated into a 3-D linkage via C-H··· $\pi$  interactions [178, 179].

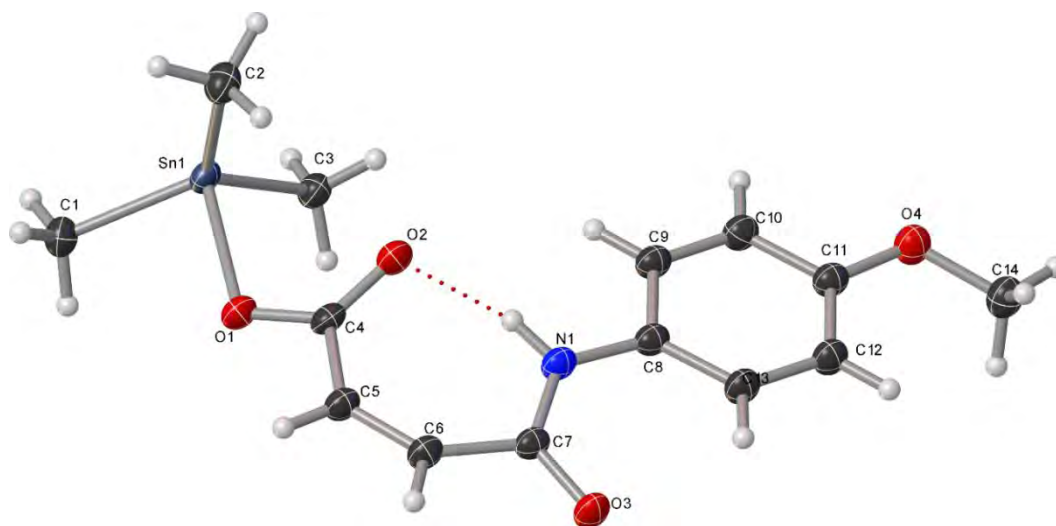


**Figure 4.4:** Perspective view of monomeric structural unit of complex **1**.

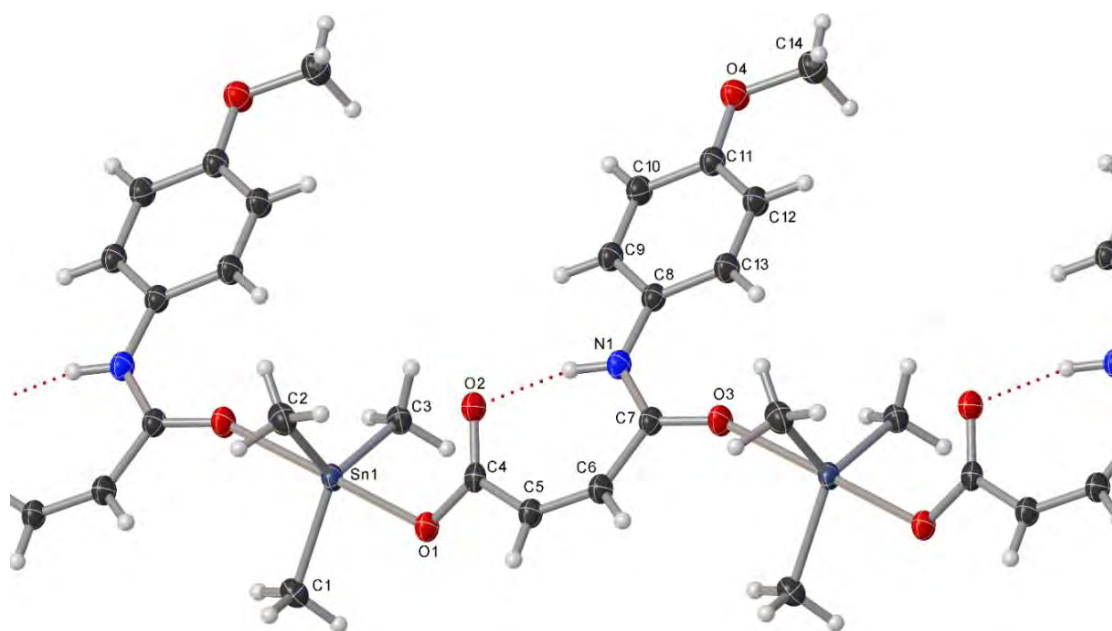


**Figure 4.5:** A perspective of one of the linear polymeric chains of compound **1**. The translation ellipsoids are haggard at the probability level of 50% and hydrogen atoms are presented as trifling spheres of arbitrary radii.1.

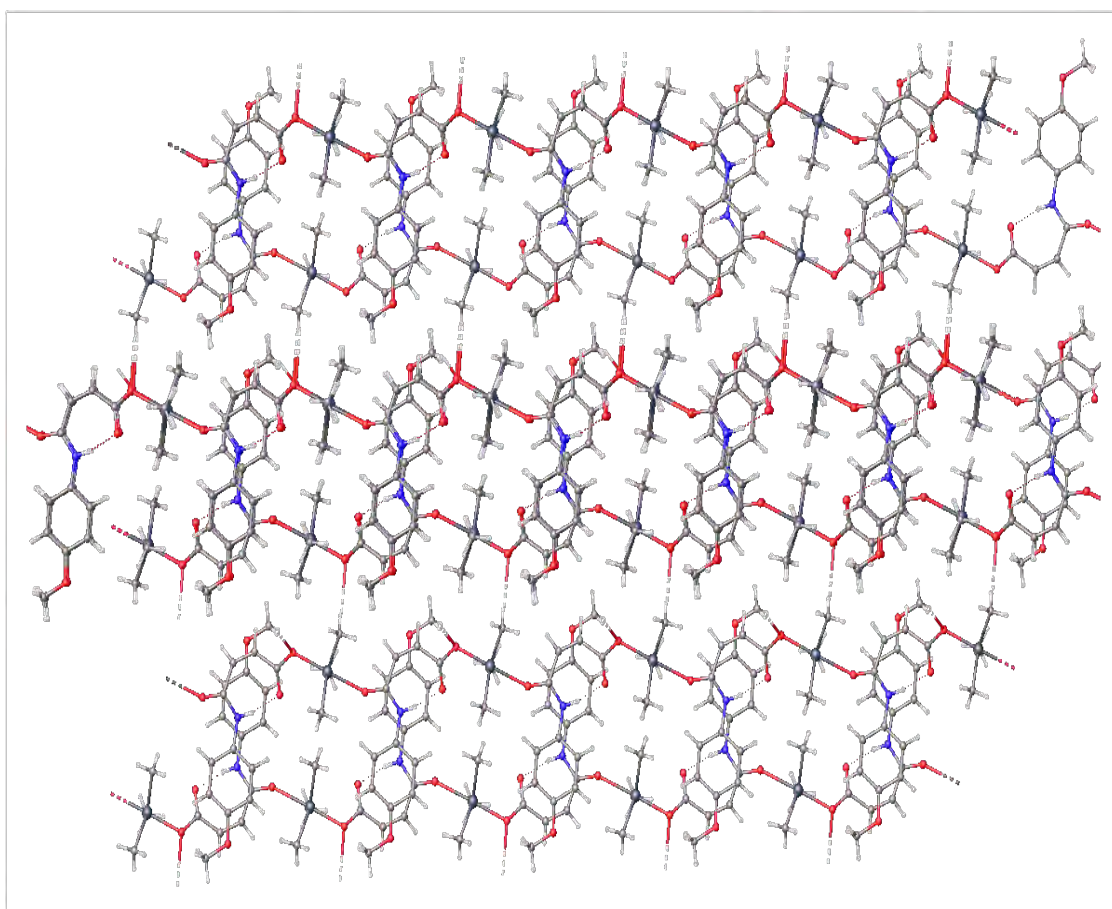


**Figure 4.6:** Perspective outlook of complex **1** with packing structure having intramolecular and intermolecular hydrogen bonding and Van der Waals interactions.

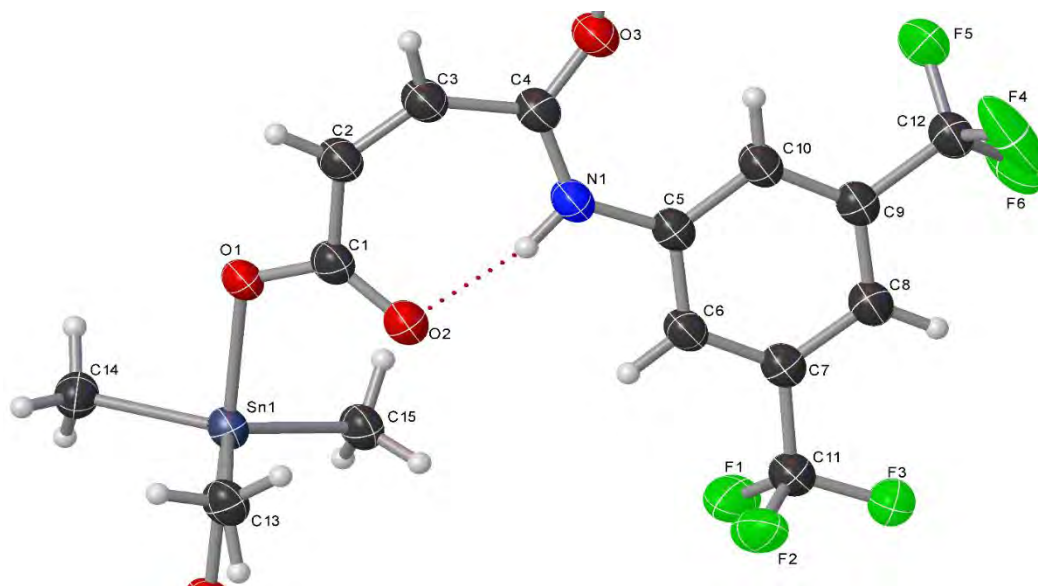


**Figure 4.7:** A perspective of the monomeric structural unit of compound 4.

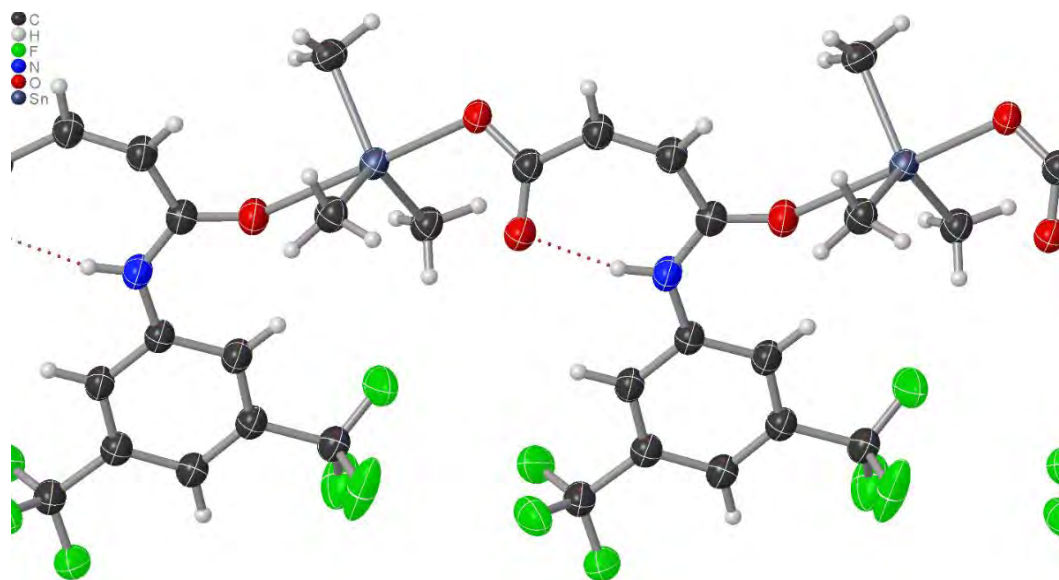


**Figure 4.8:** A perspective of one of the two crystallographically distinct one-dimensional polymeric chains of the crystal structure of compound 4.

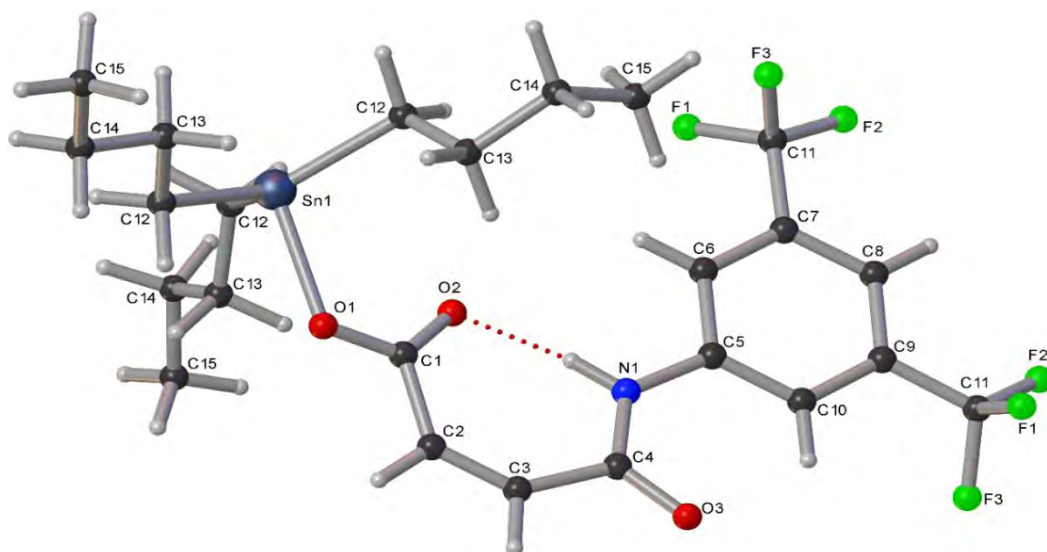


**Figure 4.9:** A perspective of one of the two crystallographically distinct monomeric structural units of compound **5**.

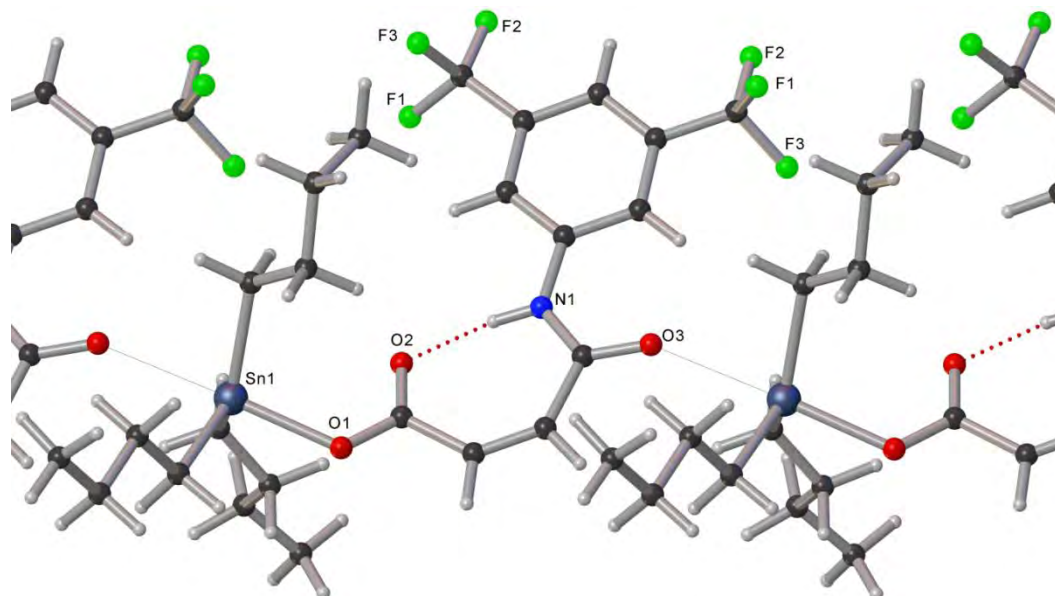


**Figure 4.10:** A perspective of one of the two crystallographically distinct one-dimensional polymeric chains of the crystal structure of complex **5**.

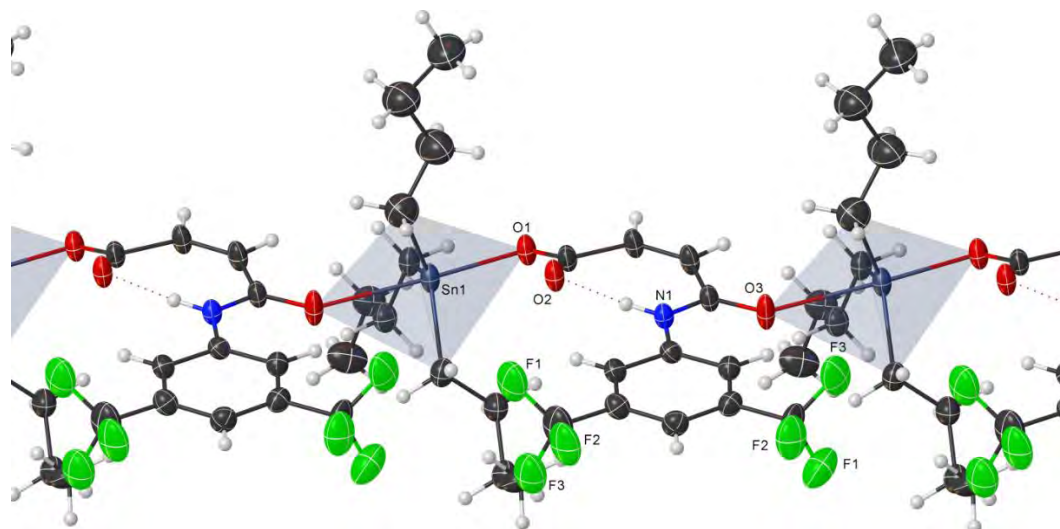


**Figure 4.11:** Perspective outlook of 1D monomeric structure of complex **5**.

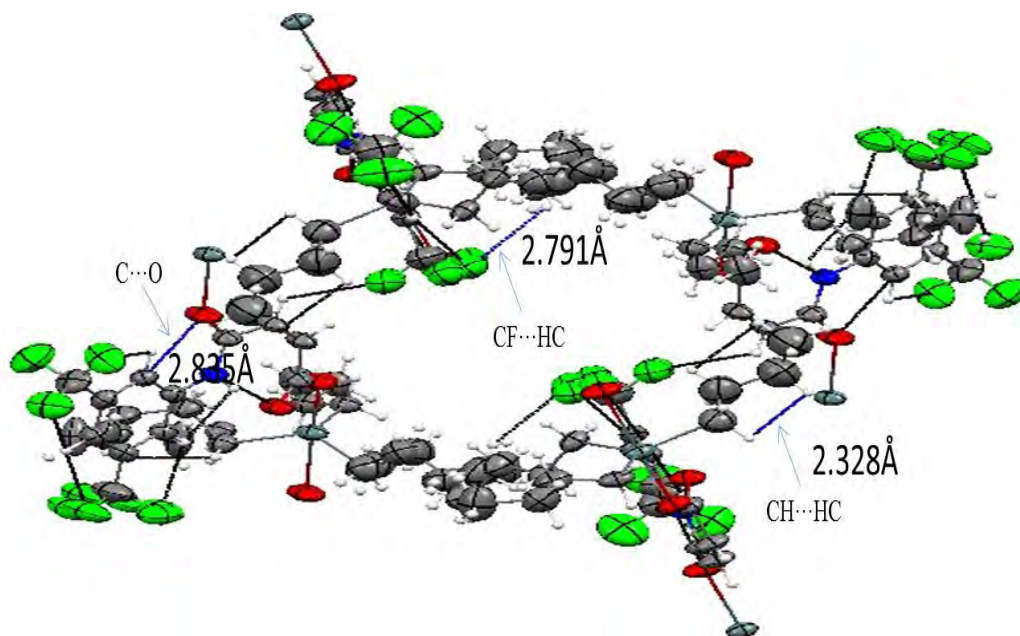


**Figure 4.12:** Perspective outlook of complex **5** with packing structure having intramolecular and intermolecular hydrogen bonding and Van der Waals interactions.

**Table 4.5:** Crystal data and structure refinement parameters for the complexes

Complex	1	4	5
Empirical Formula	C <sub>14</sub> H <sub>19</sub> NO <sub>4</sub> Sn	C <sub>15</sub> H <sub>15</sub> F <sub>6</sub> NO <sub>3</sub> Sn	C <sub>24</sub> H <sub>33</sub> F <sub>6</sub> NO <sub>3</sub> Sn
<i>D</i> <sub>calc.</sub> / g cm <sup>-3</sup>	1.657	1.851	1.467
$\mu$ /mm <sup>-1</sup>	13.321	12.291	0.979
Formula Weight	383.99	489.97	616.20
g/mol			
Colour	colourless	colourless	colourless
Shape	needle	prism	needle
Size/mm <sup>3</sup>	0.32×0.10×0.05	0.44×0.39×0.20	0.32 × 0.174 × 0.156
<i>T</i> /K	99.93(16)	100.00(10)	173.00(10)
Crystal System	monoclinic	monoclinic	triclinic
Space Group	P2 <sub>1</sub> /c	C2/c	P-1
<i>a</i> /Å	9.5424(3)	15.3177(5)	9.67709(14)
<i>b</i> /Å	6.9070(2)	10.9589(3)	14.1678(2)
<i>c</i> /Å	23.3651(8)	22.7379(7)	21.1430(3)
$\alpha$ /°	90	90	94.4266(13)
$\beta$ /°	91.774(3)	112.868(4)	94.1105(12)
$\gamma$ /°	90	90	104.0913(13)
<i>V</i> /Å <sup>3</sup>	1539.25(9)	3516.9(2)	2790.85(7)
<i>Z</i>	4	8	4
<i>Z'</i>	1	1	1
Wavelength/Å	1.54184	1.54184	0.710743
Radiation type	CuK $\alpha$	CuK $\alpha$	MoK $\alpha$
$\theta$ <sub>min</sub> /°	3.785	5.042	2.978
$\theta$ <sub>max</sub> /°	70.073	68.220	54.964
Measured Refl.	15835	16612	56312
Independent Refl.	2933	3197	12815
Reflections with <i>I</i> > 2 $\sigma$ ( <i>I</i> )	2770	3091	1248
<i>R</i> <sub>int</sub>	0.0667	0.0889	0.0339
Parameters	185	238	767
Restraints	120	129	544
Largest Peak	1.728	3.564	1.82
Deepest Hole	-1.150	-1.187	-1.42
GooF	1.077	1.084	1.054
<i>wR</i> <sub>2</sub> (all data)	0.1083	0.1575	0.1807
<i>wR</i> <sub>2</sub>	0.1067	0.1563	0.1731
<i>R</i> <sub>1</sub> (all data)	0.0418	0.0592	0.0695
<i>R</i> <sub>1</sub>	0.0402	0.0584	0.0601

**Table 4.6:** Selected Bond Lengths (Å) and Bond Angles ( $\theta$ ) for complexes **1**, **4** and **5**

Compound 1		Compound 4		Compound 5	
Bond lengths					
Sn1-O1	2.188(3)	Sn1-O1	2.169(3)	Sn1-O1	2.147(3)
Sn1-O3 <sup>1</sup>	2.399(3)	Sn1-O3 <sup>1</sup>	2.527(3)	Sn1 <sup>1</sup> -O3	2.556(3)
Sn1-C3	2.118(4)	Sn1-C13	2.123(5)	Sn1C12_2	2.092(7)
Sn1-C2	2.127(5)	Sn1-C14	2.128(4)	Sn1-C13_3	2.163(6)
Sn1-C1	2.131(4)	Sn1-C15	2.127(5)	Sn1-C12_8	2.138(4)
O1-C4	1.288(5)	F3-C11	1.335(3)	Sn1-C12_1	2.091(7)
O2-C4	1.235(4)	O1-C1	1.288(6)	Sn1-C12_4	2.146(5)
O4-C11	1.360(4)	F2-C11	1.336(3)	Sn2-O1B	2.154(3)
O4-C14	1.436(5)	F1-C11	1.336(3)	Sn2-C12_9	2.144(7)
O3-Sn1 <sup>2</sup>	2.399(2)	O2-C1	1.225(6)	Sn2-C12_13	2.127(4)
O3-C7	1.248(4)	O3-Sn1 <sup>2</sup>	2.527(3)	Sn2-C12_C14	2.122(4)
Bond angles					
O1-Sn1-O3 <sup>1</sup>	176.48(10)	O1-Sn1-O3 <sup>1</sup>	179.19(12)	O1-Sn1-O3 <sup>2</sup>	178.06(14)
C3-Sn1-O1	98.99(12)	C13-Sn1-O1	95.89(18)	C1-O1-Sn1	119.7(3)
C3-Sn1-O3 <sup>1</sup>	83.95(12)	C13-Sn1-O3 <sup>1</sup>	84.66(17)	C4-O3-Sn1 <sup>1</sup>	148.7(4)
C3-Sn1-C2	123.23(15)	C13-Sn1-C14	115.94(19)	O1-Sn1-C12_3	96.9(5)
C3-Sn1-C1	116.86(16)	C13-Sn1-C15	123.66(19)	C12_2-Sn1-O1	99.8(6)
C2-Sn1-O1	93.10(12)	C14-Sn1-O1	92.01(15)	C12_2-Sn1-C12_3	140.0(9)



C2-Sn1-O3 <sup>1</sup>	83.64(13)	C14-Sn1-O3 <sup>1</sup>	87.21(15)	C12_2-Sn1-C12_8	110.0(8)
C2-Sn1-C1	118.67(14)	C15-Sn1-O1	99.23(15)	C12_8-Sn1-O1	90.38(16)
C1-Sn1-O1	88.71(12)	C15-Sn1-O3 <sup>1</sup>	80.93(15)	C12_8-Sn1-O3 <sup>2</sup>	88.43(15)
C1-Sn1-O3 <sup>1</sup>	91.67(12)	C15-Sn1-C14	117.34(19)	C12_8-Sn1-C12_3	106.0(4)
C4-O1-Sn1	115.9(2)	C1-O1-Sn1	114.1(3)	C12_8-Sn1-C12_4	121.2(3)
C11-O4-C14	117.6(3)	C4-O3-Sn1 <sup>2</sup>	142.7(3)	C12_1-Sn1-O1	100.3(3)
C7-O3-Sn1 <sup>2</sup>	152.2(2)	C4-N1-O5	129.2(4)	C12_1-Sn1-O3 <sup>2</sup>	79.0(3)
C7-N1-C8	129.3(3)	C6-C7-C8	121.6(4)	C12_1-Sn1-C12_8	119.1(4)

Complexes **7** and **10** are shown in the figures below while the structure modification and data, the bond lengths along with bond angles are given in Table 4.7-4.9. The organotin(IV) amide based carboxylates compound **7** and **10** are polymeric in solid state in nature and revealed distorted trigonal bipyramidal geometry around a tin atom as well with two oxygen atoms of carboxylate moiety at the plane positions while the methyl and butyl groups are at the axial positions [180]. The value of  $\tau$  can be calculated by the formula  $\tau=(\beta-\alpha)/60$ , where  $\beta$  is the larger basal angle and  $\alpha$  is the second larger basal angle for Sn atom which show the exact geometry around the tin atom. For picture-perfect trigonal bipyramid geometry, the  $\tau$  value is unity ( $\alpha=120^\circ$ ) and for a perfect square, the pyramid is zero ( $\alpha=\beta=180^\circ$ ) [181, 182]. For compound **7** ( $\beta= \text{O1-Sn1-O3}^1=176.22^\circ$  and  $\alpha= \text{C3-Sn1-C2}=124.17^\circ$ ) the  $\tau$  value 0.87 and for the compound **10** the  $\tau=0.95$  which indicate that the geometry around the Sn atom is distorted trigonal pyramidal [179]. The tendency of going from trigonal bipyramidal to square planar geometry is associated with secondary

intermolecular Sn $\cdots$ O interactions [173]. The C–Sn–C angle is 124.2 and 119.5 respectively display that sufficient space is available around Sn to form additional coordination. One ligand carboxylate oxygen is attached with Sn atom in mono-dentate mode with tin-oxygen covalent bond [(Sn(1)–O(1)) = 2.181 Å and [(Sn(1)–O(1)) = 2.171 Å respectively which is almost near to the covalent radii (2.13 Å) and other amide linked oxygen of another carboxylate ligand coordinated with tin-oxygen bond by coordinate covalent bond [183]. Sn(1)–O(3<sup>1</sup>) = 2.421 Å) and Sn(1)–O(3<sup>1</sup>) = 2.500 Å) which showed a coordinate type of interaction that is larger than the sum of covalent radii of Sn and oxygen (2.13 Å) and much shorter than the sum of secondary interactions of Sn and oxygen (3.68 Å) which is a weak type of interaction between these atoms but still enough strong bond. The two oxygen atoms of the two ligands units are interconnected with Sn moiety in-plane positions to make a 1D polymeric network. Although in these interactions one of the oxygen which covalent radii is (2.118 Å) is stronger than the coordinately bonded oxygen of amide carbonyl- which bond length is (2.399 Å) because the solid-state geometry is five coordinated while four coordinated geometry in solution which showed that coordinate covalent bond break in solution form. The solid-state geometry of **7** and **10** is represented in Figures **4.13-4.17** and interatomic aspects are given in Tables 4.7, 4.8 and 4.9. The intramolecular O $\cdots$ H interactions mediate the molecular structures of these complexes. This interaction makes a seven-membered ring in the compound which is rarely seen in organotin(IV) complexes in the polymer chain in solid-state. The 1D polymeric chain stabilized by intramolecular and intermolecular hydrogen bonding via C–H $\cdots$  $\pi$  interactions in a corkscrew fashion, which lead to a three-D linkage via C–H $\cdots$ CH and CH $\cdots$ O interactions. The amide group NH- hydrogen atom takes part in intramolecular

hydrogen bonds (N1-H/O2). These organotin(IV) carboxylate complexes make self-assembly thru  $\text{CH}\cdots\pi$ ,  $\pi\cdots\pi$ , and amassing interactions [184, 185]. The protracted nets of CH-O,  $\text{CH}\cdots\pi$  and CH-O interactions are the main clues to accretion and supramolecular chemistry. There is three reason for intermolecular Sn-O coordinate covalent bond which are: (a) the small methyl group existence permits handy interaction of molecules;(b) the butyl and methyl assemblies exist squishy enough to twist to one side of the trigonal plane, which give adequate space to an oxygen atom to make a bond with tin atom; (c) Due to the presence of the respective d orbitals, the lone pair of electron of oxygen interacts with Sn to form a coordinate covalent bond[8]. This can be surely construed for all ligands and complexes. Here in this paper, we report that in complex **7** there is a weak or partial coordinate covalent bond between Sn(1)–O(3<sup>1</sup>) but in complex **10** it is a strong coordinate covalent bond it is due to the increase in reaction time from 6 hours to 18 hours for complex **10** which provide enough time to make a strong enough covalent bond between Sn and O atom [186].

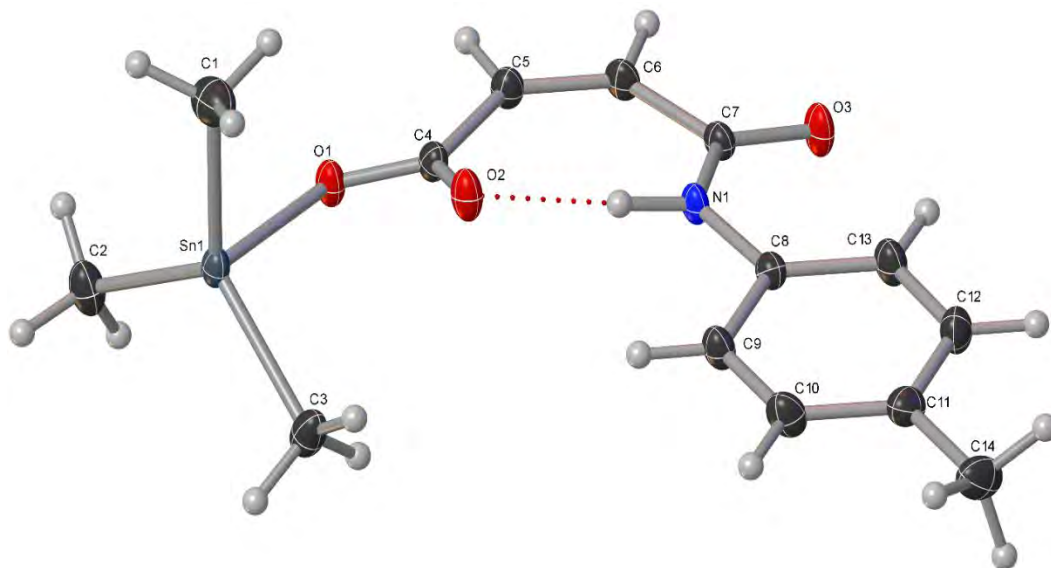


**Figure 4.13:** Perspective view of a monomeric structure of complex 7.

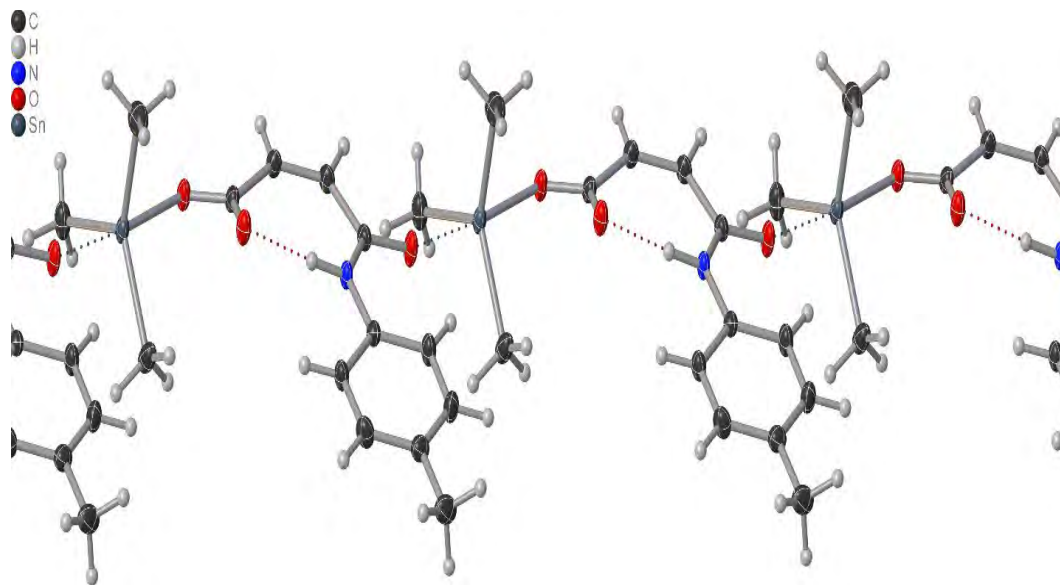


**Figure 4.14:** Perspective outlook of 1D Polymeric structure of complex 7.

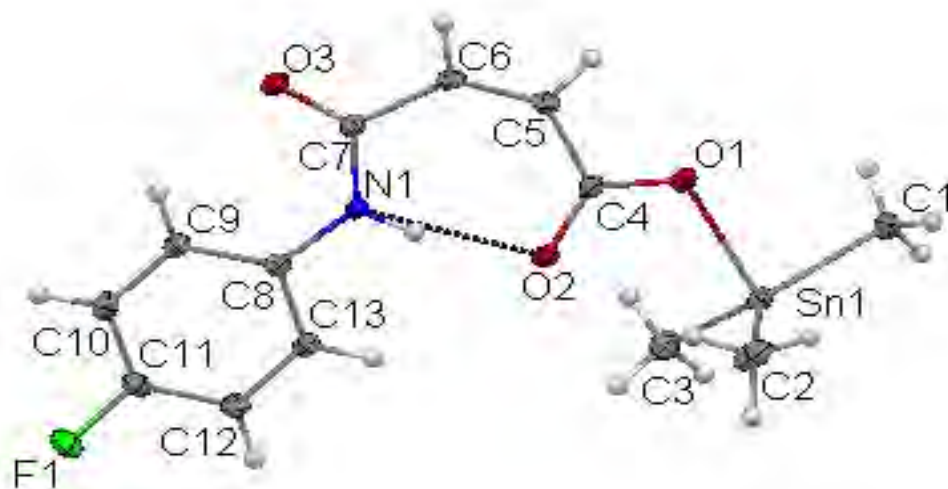


**Figure 4.15:** Perspective outlook of the monomeric structure of complex 7.

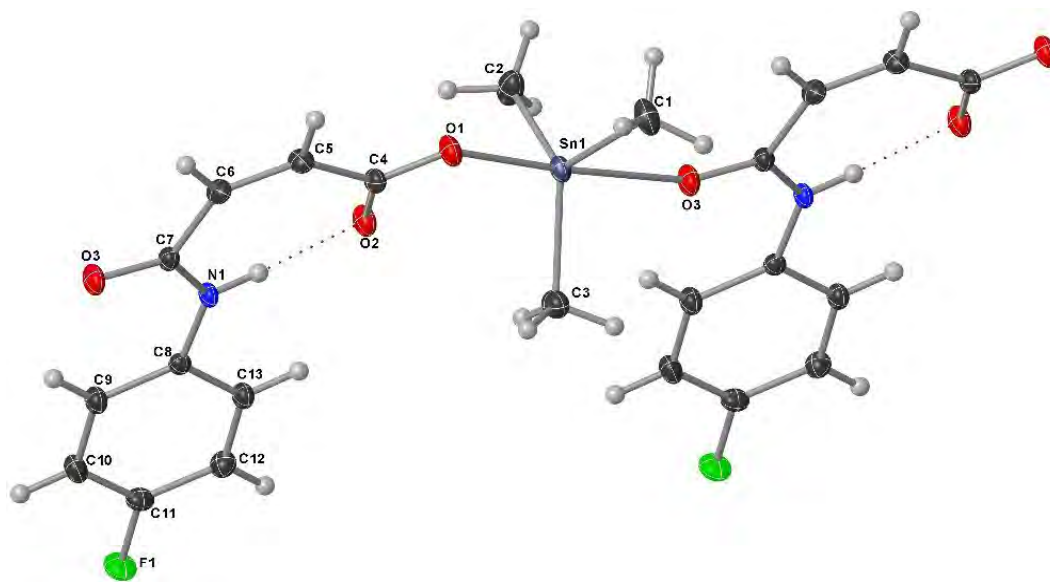


**Figure 4.16:** Perspective view of the dimeric structure of complex 10.

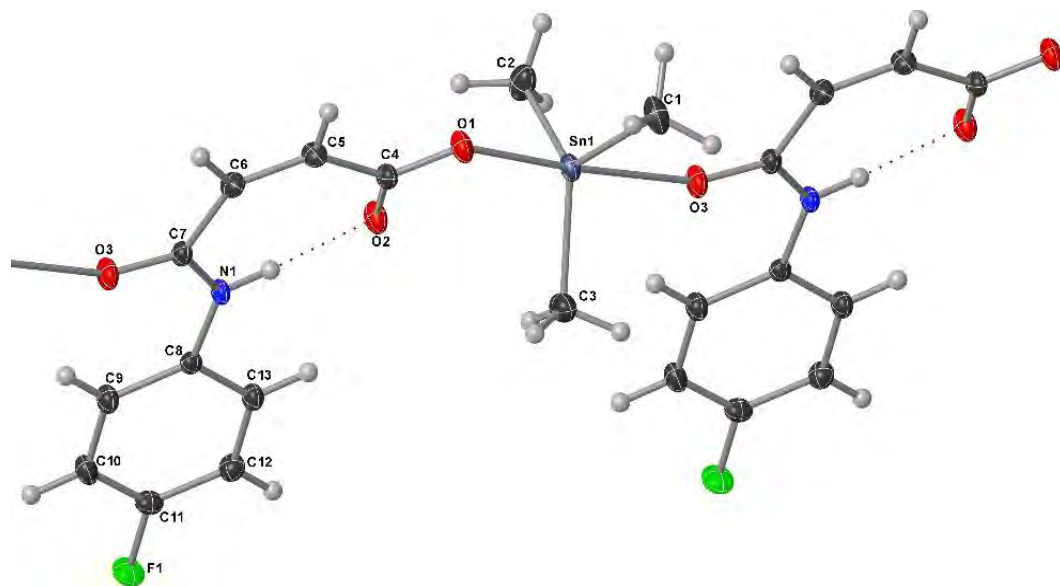


**Figure 4.17:** Perspective view of 1D Polymeric structure of complex **10**.

**Table 4.7:** Crystal data and structure refinement parameters for complexes (7) and (10).

Formula	C <sub>56</sub> H <sub>76</sub> N <sub>4</sub> O <sub>12</sub> Sn (7)	C <sub>13</sub> H <sub>16</sub> FNO <sub>3</sub> Sn (10)
<i>D</i> <sub>calc.</sub> / g cm <sup>-3</sup>	1.621	1.743
<i>μ</i> /mm <sup>-1</sup>	1.698	1.817
Formula Weight	1471.96	371.96
Colour	colourless	colorless
Shape	needle	plate
Size/mm <sup>3</sup>	0.25×0.06×0.06	0.34×0.27×0.09
<i>T</i> /K	100(2)	100(2)
Crystal System	monoclinic	monoclinic
Space Group	P2 <sub>1</sub> /n	P2 <sub>1</sub> /c
<i>a</i> /Å	9.4941(4)	9.7104(3)
<i>b</i> /Å	6.9657(3)	6.8388(2)
<i>c</i> /Å	22.8048(10)	21.3462(6)
<i>α</i> <sup>°</sup>	90	90
<i>β</i> <sup>°</sup>	91.541(4)	90.467(2)
<i>γ</i> <sup>°</sup>	90	90
<i>V</i> /Å <sup>3</sup>	1507.60(12)	1417.51(7)
<i>Z</i>	1	4
<i>Z'</i>	0.25	1
Wavelength/Å	0.71073	0.71073
Radiation type	MoK <sub>α</sub>	MoK <sub>α</sub>
<i>θ</i> <sub>min</sub> <sup>°</sup>	1.787	2.097
<i>θ</i> <sub>max</sub> <sup>°</sup>	30.996	29.575
Measured Refl.	17557	15512
Independent Refl.	4754	3956
Reflections with <i>I</i> > 2σ( <i>I</i> )	4328	3645
<i>R</i> <sub>int</sub>	0.0234	0.0277
Parameters	180	175
Restraints	1	0
Largest Peak	0.893	0.761
Deepest Hole	-0.522	-0.667
GooF	1.047	1.052
<i>wR</i> <sub>2</sub> (all data)	0.0559	0.0529
<i>wR</i> <sub>2</sub>	0.0547	0.0521
<i>R</i> <sub>1</sub> (all data)	0.0267	0.0219
<i>R</i> <sub>1</sub>	0.0230	0.0197

**Table 4.8.** Selected bond lengths (Å) for compounds **7** and **10**.

Bond Lengths			
Sn1-O1	2.1806(12)	Sn1-O1	2.1715(11)
Sn1- O3 <sup>1</sup>	2.4211(12)	Sn1- O3 <sup>1</sup>	2.5004(11)
Sn1-C2	2.1323(18)	Sn1-C1	2.1237(18)
Sn1-C1	2.114(2)	Sn1-C3	2.1225(18)
Sn1-C3	2.1177(18)	Sn1-C2	2.1228(19)
O2-C4	1.233(2)	F1-C11	1.3596(17)
O1-C4	1.289(2)	O1-C4	1.294(2)
O3- Sn1 <sup>2</sup>	2.4211(12)	O2-C4	1.2368(19)
O3-C7	1.2477(19)	O3- Sn1 <sup>2</sup>	2.5004(11)
N1-C7	1.331(2)	O3-C7	1.2483(18)
N1-C8	1.409(2)	N1-C8	1.4086(19)

**Table 4.9.** Selected Bond Angles (°) for compounds **7** and **10**

Bond angles			
O1-Sn1- O3 <sup>1</sup>	176.22(5)	O1-Sn1-O3 <sup>1</sup>	176.50(4)
C2-Sn1-O1	89.15(6)	C1-Sn-O1	89.66(6)
C2-Sn1- O3 <sup>1</sup>	90.65(6)	C1-Sn-O3 <sup>1</sup>	88.52(5)
C1-Sn1-O1	93.28(6)	C3-Sn1-O1	100.09(6)
C1-Sn1- O3 <sup>1</sup>	83.50(6)	C3-Sn1-O3 <sup>1</sup>	83.40(5)
C1-Sn1-C2	118.53(8)	C3-Sn1-C1	118.66(8)
C1-Sn1-C3	124.17(8)	C3-Sn1-C2	119.65(7)
C3-Sn1-O1	100.60(6)	C2-Sn1-O1	95.80(5)
C3-Sn1- O3 <sup>1</sup>	82.89(6)	C2-Sn1- O3 <sup>1</sup>	82.51(5)
C3-Sn1-C2	115.50(8)	C2-Sn1-C1	119.25(8)
C4-O1-Sn1	113.73(10)	C4-O1-Sn1	116.49(10)
C7-O3- Sn1 <sup>2</sup>	150.90(11)	C7-O3- Sn1 <sup>2</sup>	152.75(11)



The crystal structure and refinement parameters for complexes **13** and **14** are shown in Table **4.10**. The designated bond lengths along with bond angles are given in Table **4.11** and the monomeric and polymeric structures are given in Figures **4.18-4.23**. The asymmetric unit in figure **4.18** contains a single monomeric structure. The Figure **4.19** and **4.20** indicated the 1D polymeric and 2D Polymeric structure of the compound **13** which is linked through the oxygen of carboxylate through a covalent bond and the other oxygen is linked to another Sn atom to give a coordinate covalent bond which gives rise to a 2D dimensional assembly of the complex **13**.

The structural features of complex **13** are different from the other compounds, together with bond angles and bond distances. The O1-Sn1-O2<sup>1</sup> angle in complex **13** is 171.63° which is the biggest basal angle and the angle between C1-Sn1-C2 is the second biggest basal angle is 126.07°. The  $\tau$  value calculated for this compound is 0.76 which confirmed that the synthesized compound is distorted trigonal bipyramidal structure. The O1-Sn1-O2<sup>1</sup> angle is 171.63° and C4-O2-Sn1<sup>2</sup> Sn1 is 141° which are pointedly dissimilar from one another [187, 188].

The summation of the C-Sn-C bond angle in complex **13** is (358.61°) which is very near to the perfect value of 360°. The Sn-O bond lengths in complex **13** range from 2.12 to 2.35Å and the unevenness in Sn-O bonding is similar to other compounds. The polymeric structure of **13** is relatively flat, much like other complexes.

Organotin carboxylates with cyclic these types of polymeric structures are not very common, and to the greatest of our information, the two structures reported here of triorganotin(IV) amide-based carboxylates complexes are novel examples with 2D polymeric structure bearing varied organic substituents bound to Sn atom. Importantly,

these triorganotin (IV) carboxylate complexes with such a polymeric structure are very rare. The cause for the espousal of these polymeric structures by **13** and **14** is very little known at the current time, though an extra effort is a prerequisite for a deeper understanding of these novel developed structures [189].

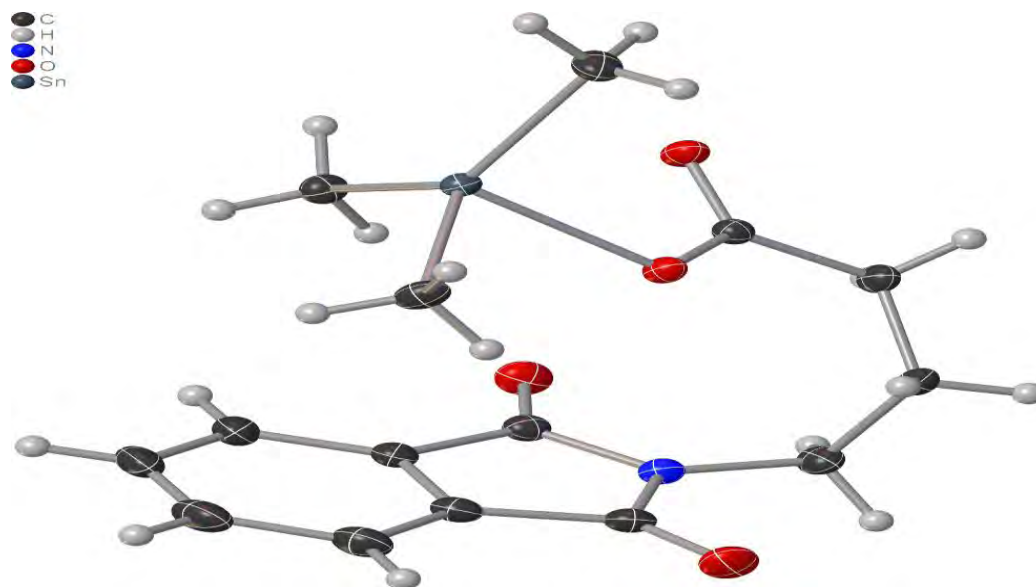


**Figure 4.18:** Plot of the asymmetric unit of monomeric compound **13**.

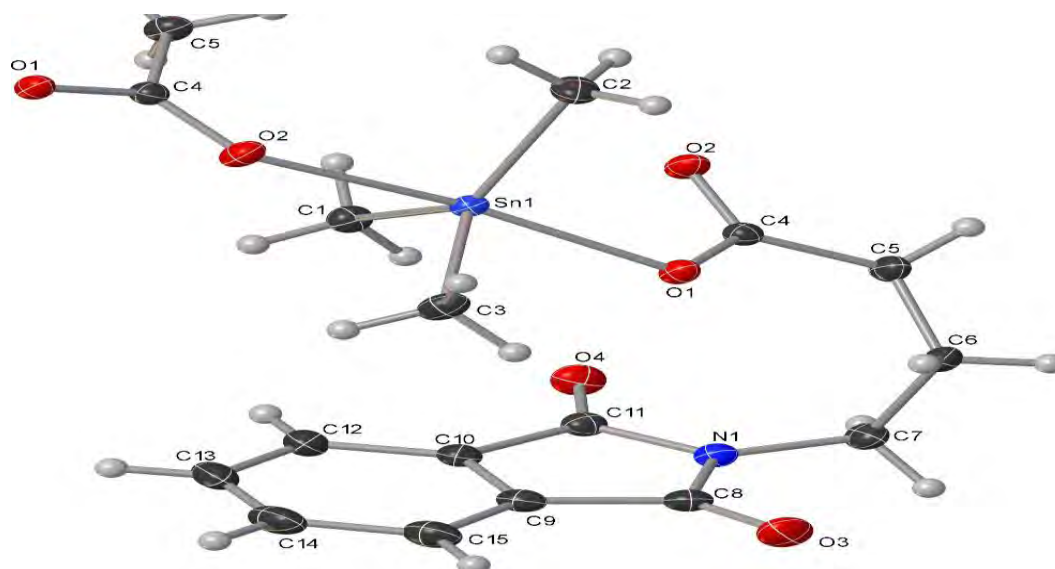


**Figure 4.19:** A perspective of one of the linear polymeric chains of compound **13**.

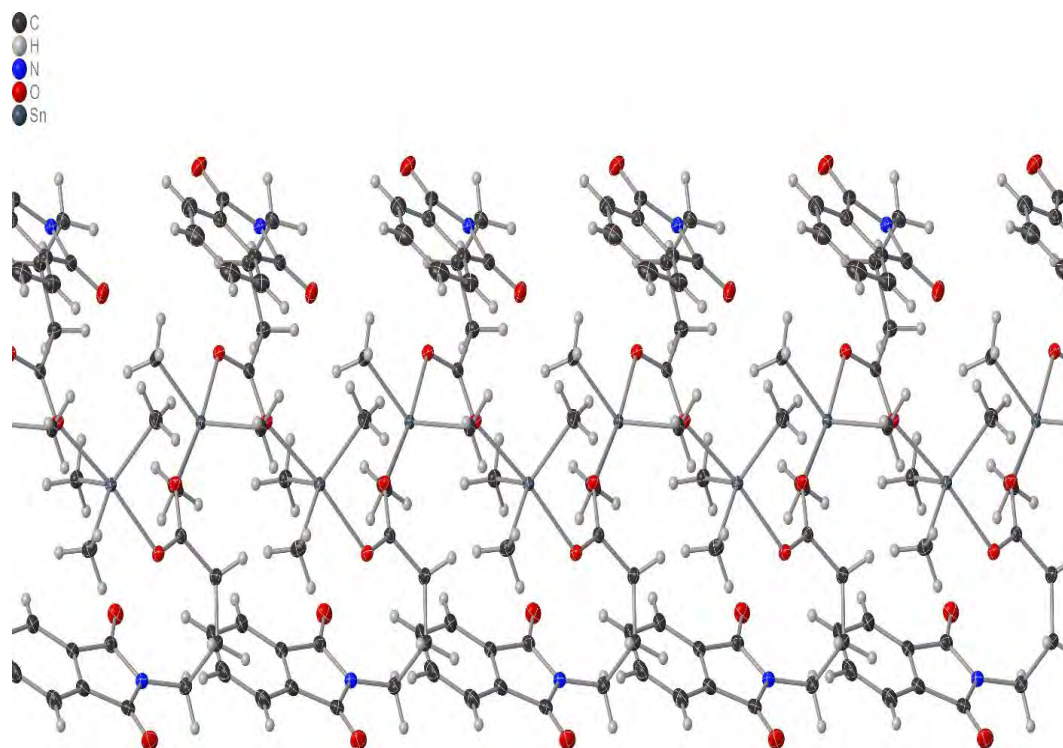


**Figure 4.20:** A perspective of one of the linear 2D polymeric chains of compound **13**.

The translation ellipsoids are haggard at the probability level of 50% and hydrogen atoms are presented as trifling spheres of arbitrary radii.1.

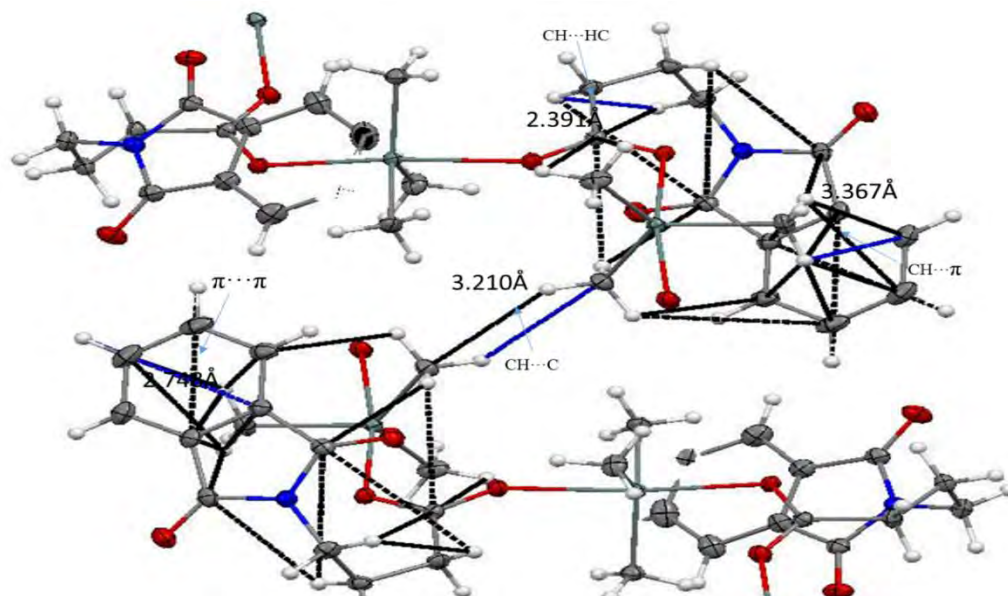


**Figure 4.21:** Packing diagram showing hydrogen bonding and secondary interactions of complex 13.

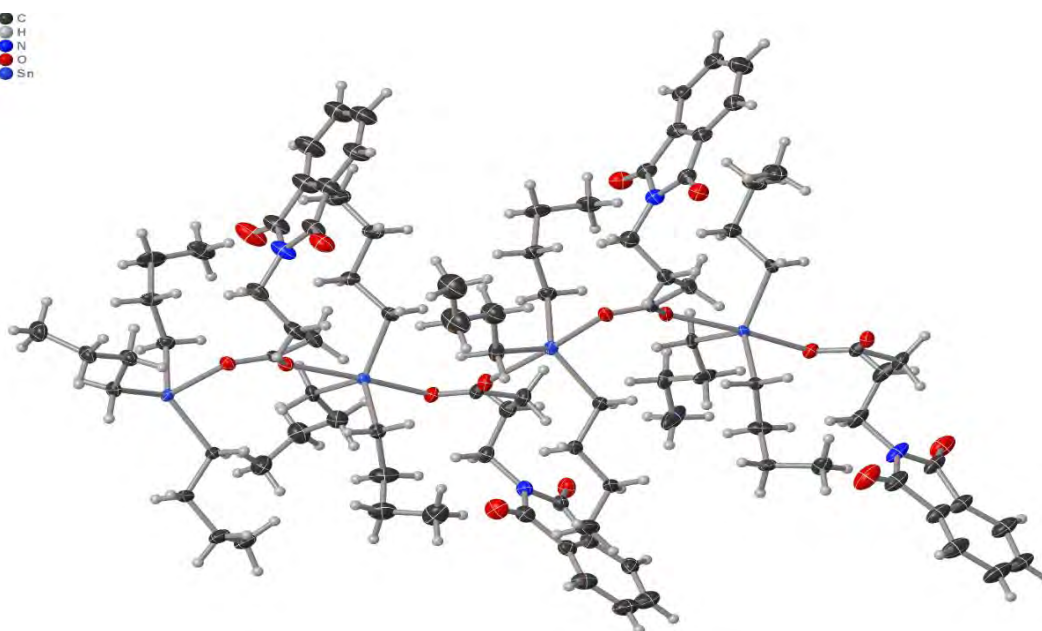


**Figure 4.22:** Perspective view of the monomeric structure of complex 14.

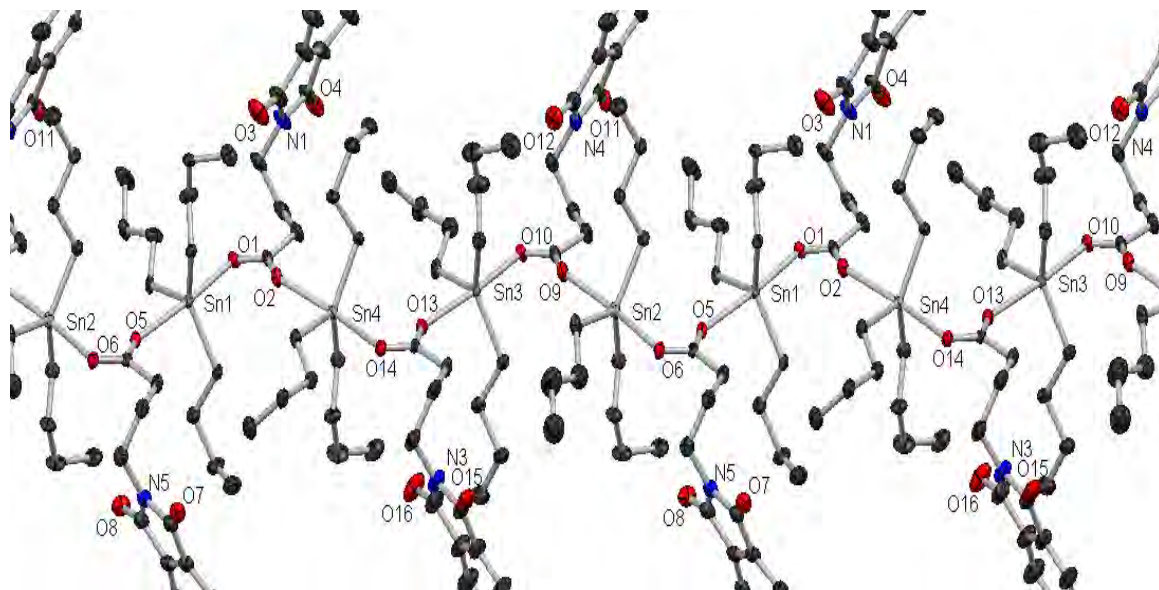


**Figure 4.23:** Perspective view of 2D Polymeric structure of complex 14.

**Table 4.10.** Crystal data and structure refinement parameters for complexes (13) and (14)

Formula	C <sub>15</sub> H <sub>19</sub> NO <sub>4</sub> Sn (13)	C <sub>24</sub> H <sub>37</sub> NO <sub>4</sub> Sn (14)
<i>D</i> <sub>calc.</sub> / g cm <sup>-3</sup>	1.658	1.403
μ/mm <sup>-1</sup>	1.625	1.061
Formula Weight	396.00	522.25
Colour	colourless	colourless
Shape	plate	needle
Size/mm <sup>3</sup>	0.43×0.30×0.08	0.45×0.26×0.09
<i>T</i> /K	100(2)	100(2)
Crystal System	monoclinic	monoclinic
Space Group	P2 <sub>1</sub> /c	Cc
<i>a</i> /Å	13.4156(4)	17.4939(4)
<i>b</i> /Å	9.5868(2)	19.9606(4)
<i>c</i> /Å	12.9762(4)	29.1536(8)
α/°	90	90
β/°	108.099(3)	103.709(3)
γ/°	90	90
<i>V</i> /Å <sup>3</sup>	1586.33(7)	9890.1(4)
<i>Z</i>	4	16
<i>Z</i> '	1	4
Wavelength/Å	0.71073	0.71073
Radiation type	MoK <sub>α</sub>	MoK <sub>α</sub>
Θ <sub>min</sub> /°	1.597	1.438
Θ <sub>max</sub> /°	36.315	30.507
Measured Refl.	33118	59723
Independent Refl.	7565	26454
Reflections with I > 2σ(I)	6629	22734
<i>R</i> <sub>int</sub>	0.0482	0.0321
Parameters	193	1094
Restraints	0	986
Largest Peak	1.093	1.096
Deepest Hole	-0.794	-0.857
GooF	1.050	1.038
<i>wR</i> <sub>2</sub> (all data)	0.0630	0.1015
<i>wR</i> <sub>2</sub>	0.0604	0.0950
<i>R</i> <sub>1</sub> (all data)	0.0295	0.0524
<i>R</i> <sub>1</sub>	0.0242	0.0422

**Table 4.11** Selected Bond Lengths (Å) and Bond Angles ( $\theta$ ) for compounds **13** and **14**

Bond lengths			
Sn1-O1	2.2285(8)	Sn1-O1	2.199(6)
Sn1- O2 <sup>1</sup>	2.3508(9)	Sn4- O2 <sup>1</sup>	2.349(6)
Sn1-C2	2.1305(13)	Sn1-C85	2.152(8)
Sn1-C1	2.1263(12)	Sn3-C39	2.149(8)
Sn1-C3	2.1295(12)	Sn4-C16	2.126(10)
O2-C4	1.2555(13)	Sn2-C62	2.137(10)
O1-C4	1.2780(13)	Sn1-O4	2.199(6)
O2- Sn1 <sup>2</sup>	2.3507(9)	Sn1-O5	2.351(6)
O3-C8	1.2148(14)	O2- Sn4 <sup>2</sup>	2.349(6)
N1-C7	1.4571(16)	O3-C5	1.225(10)
N1-C8	1.3952(16)	N1-C4	1.468(9)
Bond angles			
O1-Sn1- O2 <sup>1</sup>	171.63(3)	O10-Sn3-O13 <sup>1</sup>	173.1(2)
C2-Sn1-O1	96.15(4)	C39-Sn3-O13	83.9(3)
C2-Sn1- O2 <sup>1</sup>	88.19(4)	O14-Sn4-O2 <sup>1</sup>	172.6(2)
C1-Sn1-O1	96.88(4)	C1-Sn1-O5	173.5(2)
C1-Sn1- O2 <sup>1</sup>	86.23(4)	O6-Sn2-O9	171.8(2)
C1-Sn1-C2	126.07(5)	C16-Sn4-C20	123.6(4)
C1-Sn1-C3	117.53(5)	C62-Sn2-C70	124.0(4)
C3-Sn1-O1	88.03(4)	C66-Sn2-O6	88.7(3)
C3-Sn1- O2 <sup>1</sup>	83.64(4)	C20-Sn4- O2 <sup>1</sup>	91.3(3)
C3-Sn1-C2	115.01(6)	C66-Sn2-C62	119.2(4)
C4-O1-Sn1	113.40(7)	C13-O5-Sn1	138.2(5)
C4-O2- Sn1 <sup>2</sup>	140.92(8)	C1-O2- Sn4 <sup>2</sup>	135.4(5)

For Complexes **8** and **22** the structural data and refinement parameters are given below in table 4.12. The bond angle and bond length of these compounds are also given in Table 4.13 below. The solid-state structure of **8** and **22** and is depicted in Figures below from 24-28.

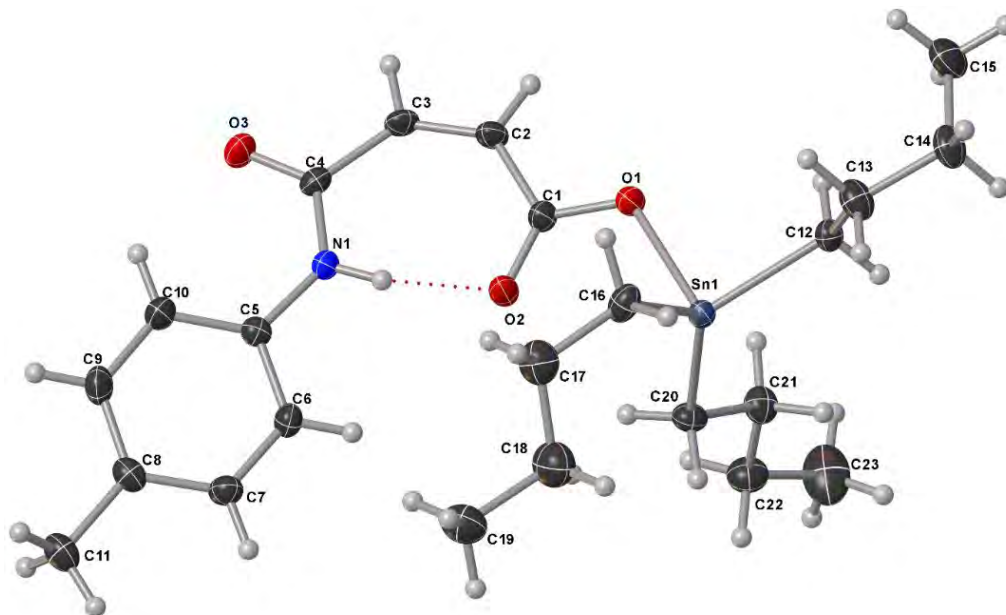


**Figure 4.24:** Outlook view of the monomeric structure of compound **8**.



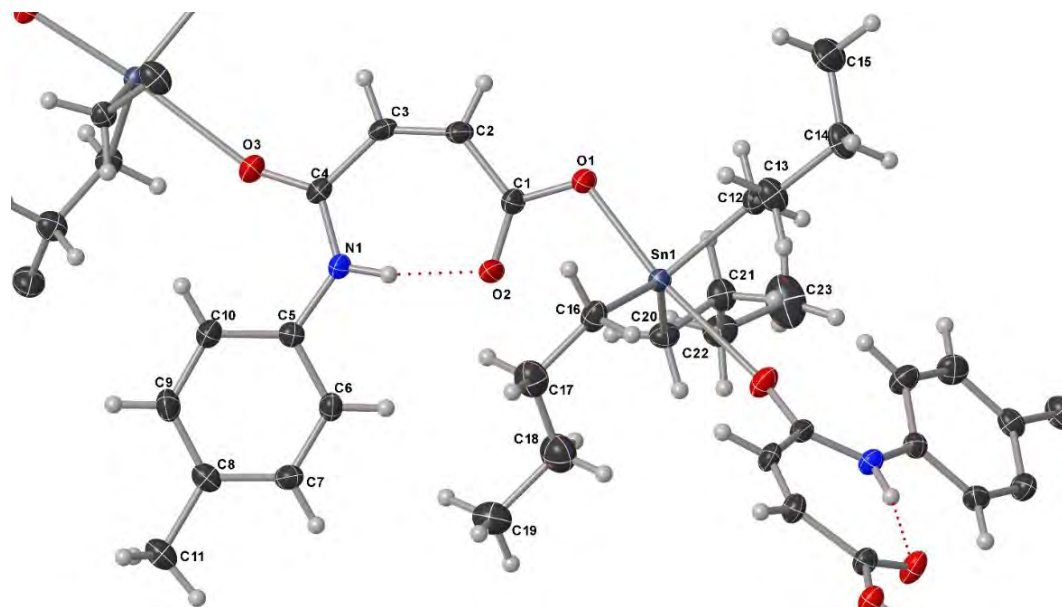


**Figure 4.25:** Outlook view of 1D Polymeric structure of compound **8**.

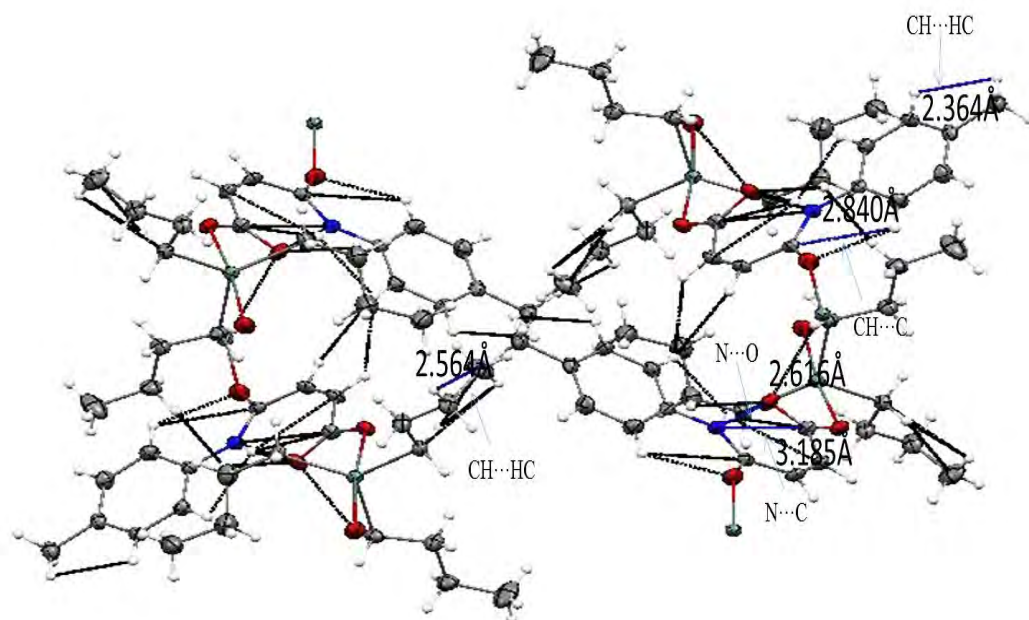


**Figure 4.26:** Packing diagram showing hydrogen bonding and Van der Waals interactions of complex **8**.

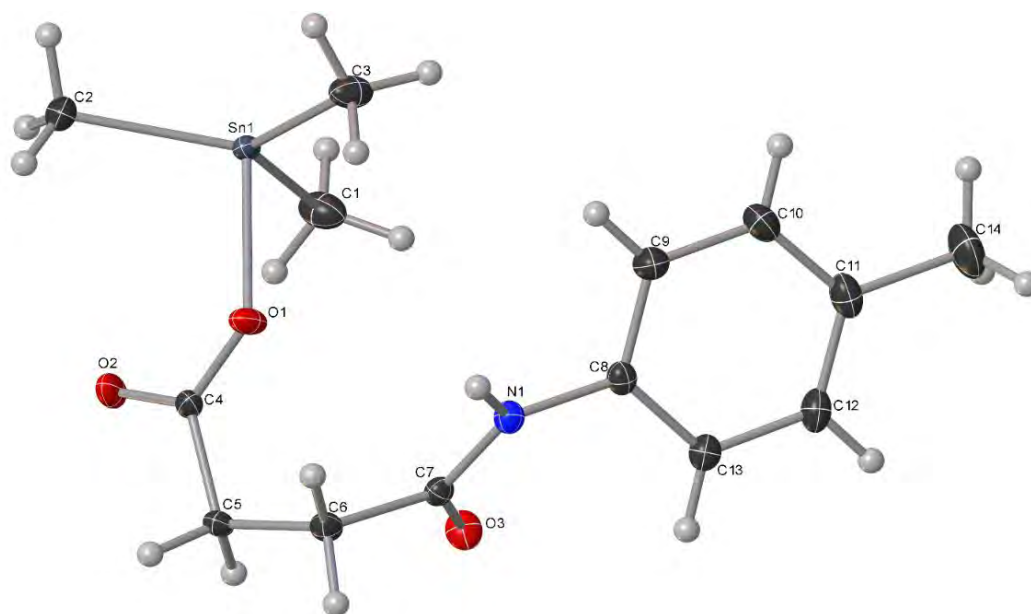


**Figure 4.27:** Perspective view of the monomeric structure of compound 22.

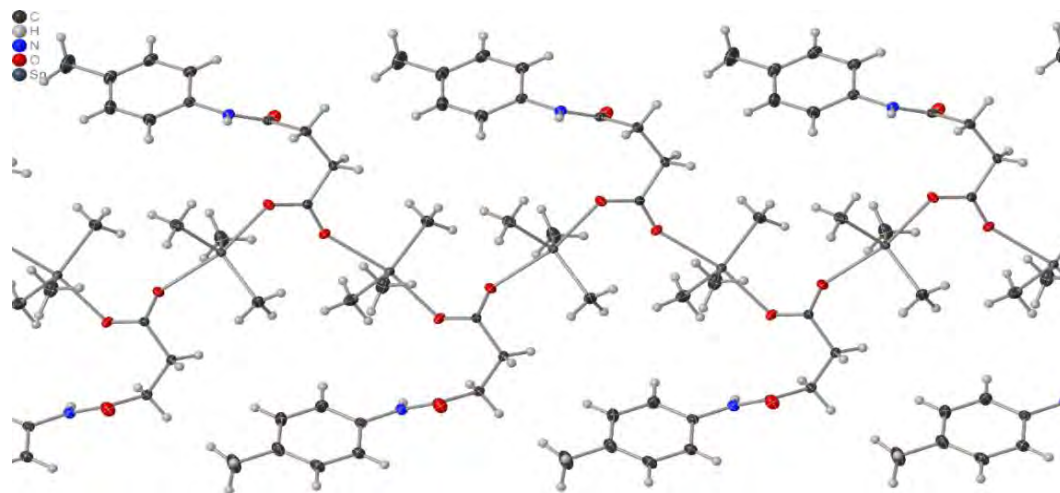


**Figure 4.28:** Perspective view of 2D Polymeric structure of compound 22.

**Table 4.12:** Crystal data and structure refinement parameters for complexes (8) and (22).

Compound	8	22
Formula	C <sub>56</sub> H <sub>76</sub> N <sub>4</sub> O <sub>12</sub> Sn <sub>4</sub>	C <sub>14</sub> H <sub>21</sub> NO <sub>3</sub> Sn
<i>D</i> <sub>calc.</sub> / g cm <sup>-3</sup>	1.621	1.559
$\mu$ /mm <sup>-1</sup>	1.698	1.624
Formula Weight (g/mol)	1471.96	370.01
Colour	colourless	colorless
Shape	needle	block
Size/mm <sup>3</sup>	0.25×0.06×0.06	0.50×0.38×0.32
<i>T</i> /K	100(2)	100(2)
Crystal System	monoclinic	orthorhombic
Space Group	P2 <sub>1</sub> /n	P2 <sub>1</sub> 2 <sub>1</sub> 2 <sub>1</sub>
<i>a</i> /Å	9.4941(4)	8.9446(2)
<i>b</i> /Å	6.9657(3)	10.0496(2)
<i>c</i> /Å	22.8048(10)	17.5352(4)
$\alpha$ /°	90	90
$\beta$ /°	91.541(4)	90
$\gamma$ /°	90	90
<i>V</i> /Å <sup>3</sup>	1507.60(12)	1576.23(6)
<i>Z</i>	1	4
<i>Z'</i>	0.25	1
Wavelength/Å	0.71073	0.71073
Radiation type	MoK $\alpha$	MoK $\alpha$
$\theta$ <sub>min</sub> /°	1.787	2.323
$\theta$ <sub>max</sub> /°	30.996	36.316
Measured Refl.	17557	29646
Independent Refl.	4754	7621
Reflections with <i>I</i> > 2 $\sigma$ ( <i>I</i> )	4328	7504
<i>R</i> <sub>int</sub>	0.0234	0.0371
Parameters	180	185
Restraints	1	1
Largest Peak	0.893	0.573
Deepest Hole	-0.522	-0.821
GooF	1.047	1.051
<i>wR</i> <sub>2</sub> (all data)	0.0559	0.0457
<i>wR</i> <sub>2</sub>	0.0547	0.0456
<i>R</i> <sub>1</sub> (all data)	0.0267	0.0194
<i>R</i> <sub>1</sub>	0.0230	0.0189
<i>R</i> <sub>1</sub>	0.0189	0.0189

**Table 4.13:** Selected Bond Lengths (Å) and Bond Angles ( $\theta$ ) for compounds **8** and **22**.

Complex 8		Complex 22	
Bond lengths			
Sn1-O1	2.1806(12)	Sn1-O1	2.1959(12)
Sn1-O3 <sup>1</sup>	2.4211(12)	Sn1-O2 <sup>1</sup>	2.3514(13)
Sn1-C2	2.1323(18)	Sn1-C2	2.1259(18)
Sn1-C3	2.1177(18)	Sn1-C3	2.1184(18)
Sn1-C1	2.114(2)	Sn1-C1	2.1200(19)
O2-C4	1.233(2)	O3-C7	1.2363(19)
O1-C4	1.289(2)	O2-C4	1.249(2)
O3-Sn1 <sup>2</sup>	2.4211(12)	O2-Sn1 <sup>2</sup>	2.3514(13)
O3-C7	1.2477(19)	O1-C4	1.2737(19)
N1-C7	1.331(2)	N1-C7	1.351(2)
Bond angles			
O1-Sn1-O3 <sup>1</sup>	176.22(5)	O1-Sn1-O2 <sup>1</sup>	166.86(5)
C2-Sn1-O1	89.15(6)	C2-Sn1-O1	99.59(7)
C2-Sn1-O3 <sup>1</sup>	90.65(6)	C2-Sn1-O3 <sup>1</sup>	93.02(7)
C1-Sn1-O1	93.28(6)	C3-Sn1-C1	88.75(6)
C1-Sn1-O3 <sup>1</sup>	83.50(6)	C3-Sn1-C2 <sup>1</sup>	82.17(6)
C1-Sn1-C2	118.53(8)	C3-Sn1-C2	117.36(9)
C1-Sn1-C3	124.17(8)	C3-Sn1-C1	122.52(8)
C3-Sn1-O1	100.60(6)	C1-Sn1-O1	90.71(7)
C3-Sn1-O3 <sup>1</sup>	82.89(6)	C1-Sn1-O2 <sup>1</sup>	86.25(7)
C3-Sn1-C2	115.50(8)	C1-Sn1-C2	119.34(9)
C4-O1-Sn1	113.73(10)	C4-O1-Sn1	122.76(11)
C7-O3-Sn1 <sup>2</sup>	150.90(11)	C4-O2-Sn1 <sup>2</sup>	145.22(12)
C7-N1-C8	128.51(14)	C7-N1-C8	124.92(14)
O3-C7-N1	123.53(15)	O3-C7-N1	123.54(15)

## Conclusions/Future Perspectives

New ligands and their novel amide-based triorganotin(IV) carboxylates have been synthesized and characterized by different analytical techniques, namely elemental analysis, FT-IR, multinuclear ( $^1\text{H}$ ,  $^{13}\text{C}$ ,  $^{119}\text{Sn}$  and  $^{19}\text{F}$ ) NMR and X-ray single crystal analysis. In FT-IR spectra, the presence of peaks namely Sn-O in the range of 400-600  $\text{cm}^{-1}$  indicated the attachment of carboxylate oxygen ligands in the complexes. In complexes, absence of acidic OH peak (10-13 ppm) has confirmed the coordination of carboxylate anion to organotin(IV) moieties while a downfield shift of  $^{13}\text{C}$ NMR signal for COO- moiety in complexes than the free ligand have also confirmed the coordination of carboxylate ligands with Tin. Furthermore, the  $^{119}\text{Sn}$  NMR confirmed the geometry of the complexes in solution. The presence of fluorine was confirmed by  $^{19}\text{F}$  NMR signal for each ligands and their complexes.

X-ray single crystal analysis has confirmed the distorted trigonal bipyramidal geometry of these complexes in solid state. The molecules are self-assembled in solid state via non covalent and van der Waals forces to form a fascinating supramolecular architectures.

The biological action of organotin(IV) carboxylates depends on their geometry and types ligands coordinated to tin atom. It is well documented fact that triorganotin(IV) compounds are being more active than their di-analogues owing to more lipophilic character enabling them to cross lipid layer of the cell membrane of microbes with more ease. For complexes the better antimicrobial, antioxidant, anti-leishmanial, hemolytic and anticancer activity, despite of few exceptions, are due to more lipophilic organic groups and presence of electronegative substituent i.e. fluoro. The latter enable the complexes to bind strongly with

cell vital components altering their structural and functional chemistry-ultimately resulting in cell death.

The anticancer and antileishmanial screening results indicated that the complexes **2**, **5**, **8**, and **11** have shown good anticancer results and complexes **6**, **12** and **15** having best antileishmanial activity respectively. Tributyl tin moiety plays important role for the safe access of these complexes to the target DNA. Presence of fluoro moiety in the ligand not only increases the lipophilicity of these complexes to get into the cells, but also stabilizes the complex-DNA adduct through H-bonding.

Biological activity data shows that all the complexes are biologically active with few exceptions and they having a great biological significance. Promising *in vitro* antimicrobial (**2**, **3**, **5**, **6**, **7**, **8**, **9**, **12**, **14**) and antioxidants (**8**, **10**, **14**) activities of these compounds contend an *in vivo* study in the upcoming times. Triorganotin(IV) derivatives were more active than diorganotin(IV) analogues due to greater lipophilicity and permeability through cell membrane.

DFT studies of compounds **1**, **2**, **7**, **8**, **9**, **10**, **11**, **12** showed an excellent correlation with the structural parameters obtained from XRD crystallographic data.

We have plans in future to synthesize some new triorganotin(IV) derivatives of amide-based carboxylates having different electron-donating and electron-withdrawing substituents on benzene ring of carboxylates moieties to tune their structure for biological and material applications.

It is our programme to test the synthesized complexes against different cancer cell lines and send the best complexes for *in vivo* studies. We will also study the mechanism of action of these complexes in biological systems with the help of molecular docking.

## References

- [1] E. Frankland, XXVII.—On the isolation of the organic radicals. *Quarterly Journal of the Chemical Society of London*, 2(3) (1850) 263-296.
- [2] C. Alzieu, J. Sanjuan, J. Deltreil, M. Borel, Tin contamination in Arcachon Bay: effects on oyster shell anomalies. *Marine Pollution Bulletin*, 17(11) (1986) 494- 498.
- [3] W.T. Piver, Organotin compounds: industrial applications and biological investigation. *Environmental Health Perspectives*, 4 (1973) 61-79.
- [4] J.B. Graceli, G.C. Sena, P.F.I. Lopes, G.C. Zamprogno, M.B. da Costa, A.F.L. Godoi, D.M. Dos Santos, M.R.R. de Marchi, M.A. dos Santos Fernandez, Organotins: a review of their reproductive toxicity, biochemistry, and environmental fate. *Reproductive Toxicology*, 36 (2013) 40-52.
- [5] X. Shang, X. Meng, E.C. Alegria, Q. Li, M.F.C. Guedes da Silva, M.L. Kuznetsov, A.J. Pombeiro, Syntheses, molecular structures, electrochemical behavior, theoretical study, and antitumor activities of organotin(IV) complexes containing 1-(4-chlorophenyl)-1-cyclopentanecarboxylato ligands. *Inorganic chemistry*, 50(17) (2011) 8158-8167.
- [6] J. Devi, J. Yadav, Recent advancements in organotin(IV) complexes as potential anticancer agents. *Anti-Cancer Agents in Medicinal Chemistry (Formerly Current Medicinal Chemistry-Anti-Cancer Agents)*, 18(3) (2018) 335-353.
- [7] A.G. Hadi, K. Jawad, D.S. Ahmed, E. Yousif, Synthesis and biological activities of organotin(IV) carboxylates: a review. *Systematic Reviews in Pharmacy*, 10(1) (2019) 26- 31.
- [8] E. Yousif, Triorganotin(IV) complexes photo-stabilizers for rigid PVC against

- photodegradation. *Journal of Taibah University for Science*, 7(2) (2013) 79-87.
- [9] E. Yousif, B.I. Mehdi, R. Yusop, J. Salimon, N. Salih, B.M. Abdullah, Synthesis, structure and antibacterial activity of some triorganotin(IV) complexes with a benzamidoalanine ligand. *Journal of Taibah University for Science*, 8(3) (2014) 276-281.
- [10] Y. Farina, A. Graisa, E. Yousif, M. Kassim, Synthesis and structure of some diorganotin(IV) with *N*-methyl-*m*-nitrobenzohydroxamic acid. *Australian Journal of Basic and Applied Sciences*, 3(1) (2009) 291-294.
- [11] A. Graisa, Y. Farina, E. Yousif, M. Kassem, Synthesis and characterization of some diorganotin(IV) complexes of *N*-Tolyl-*m*-nitrobenzohydroxamic acid. *ARPJN Journal of Engineering and Applied Sciences*, 3(6) (2008) 47-50.
- [12] E. Yousif, Synthesis, spectroscopic studies and fungicidal activity of some diorganotin(IV) with 2-[(phenylcarbonyl) amino] propanoate. *Journal of King Saud University-Science*, 24(2) (2012) 167-170.
- [13] A. Graisa, Y. Farina, E. Yousif, M. Kassim, Preparation and spectroscopic studies of diorganotin(IV) complexes of *N*-methyl-*M*-methoxybenzohydroxamic acid. *Prosiding Seminar Kimia Bersama UKM-ITB VIII*, (9) (2009) 11.
- [14] D.A. Najeeb, N. Shalan, H. Ibraheem, Y. Farina, E. Yousif, Synthesis and fungicidal activity of some diorganotin(IV) with benzamidocysteine. *Al-Nahrain Journal of Science*, 12(1) (2009) 24-28.
- [15] E.R. Tieckink, Structural chemistry of organotin carboxylates: a review of the crystallographic literature. *Applied Organometallic Chemistry*, 5(1) (1991) 1-23.
- [16] N. Rabiee, M. Safarkhani, M.M. Amini, Investigating the structural chemistry of



- organotin(IV) compounds: recent advances. *Reviews in Inorganic Chemistry*, 39(1) (2019) 13-45.
- [17] C. Ma, Q. Jiang, R. Zhang, Synthesis and structure of a novel trinuclear 18-membered macrocycle of diphenyltin complexes with 2-mercaptopyridine-3-thiol. *Journal of Organometallic Chemistry*, 678(1-2) (2003) 148-155.
- [18] T.S. Cameron, P.K. Bakshi, R. Thangarasa, T.B. Grindley, The crystal structure of methyl 4,6-O-benzylidene-2,3-O-dibutylstannylene- $\alpha$ -D-glucopyranoside. *Canadian Journal of Chemistry*, 70(6) (1992) 1623-1630.
- [19] A. Jancsó, L. Nagy, E. Moldrheim, E. Sletten, Potentiometric and spectroscopic evidence for co-ordination of dimethyltin(IV) to phosphate groups of DNA fragments and related ligands. *Journal of the Chemical Society: Dalton Transactions*, (10) (1999) 1587-1594.
- [20] R. Barbieri, A. Silvestri, V. Piro, Tin-119 'Mössbauer titration' of dimethyl- and trimethyl-tin(IV) hydroxides with model ligands mimicking nucleic acid phosphate sites, and with deoxyribonucleic acid. *Journal of the Chemical Society: Dalton Transactions*, (12) (1990) 3605-3609.
- [21] Q. Li, P. Yang, H. Wang, M. Guo, Diorganotin(IV) antitumor agent.  $(C_2H_5)_2SnCl_2$  (phen)/nucleotides aqueous and solid-state coordination chemistry and its DNA binding studies. *Journal of Inorganic Biochemistry*, 64(3) (1996) 181-195.
- [22] J. Cashion, G. Domazetis, B. James, Mössbauer spectra of organotin amino-acid and glutathione derivatives. *Journal of Organometallic Chemistry*, 185(3) (1980) 433-441.
- [23] S. Shahzadi, S. Ali, Structural chemistry of organotin(IV) complexes. *Journal of*

*the Iranian Chemical Society*, 5(1) (2008) 16-28.

- [24] G. Arena, A. Gianguzza, L. Pellerito, S. Musumeci, R. Purrello, E. Rizzarelli, Coordination properties of dialkyltin(IV) in aqueous solution. Thermodynamics of complex formation with carboxylic acids. *Journal of the Chemical Society: Dalton Transactions*, (8) (1990) 2603-2608.
- [25] P.G. Harrison, N.W. Sharpe, Model studies of trialkyltin–protein interactions: <sup>13</sup>C NMR analysis of solution equilibria of the complex between trimethyltin and methyl N-benzoyl-L-leucyl-L-histidinate. *Applied Organometallic Chemistry*, 3(2) (1989) 141-150.
- [26] H. Preut, M. Vornefeld, F. Huber, Bis [diethyl (glycylhistidinato) tin]–methanol (1/1). *Acta Crystallographica Section C: Crystal Structure Communications*, 47(2) (1991) 264-267.
- [27] P. Surdy, P. Rubini, N. Buzás, B. Henry, L. Pellerito, T. Gajda, Interaction of dimethyltin(IV) <sup>2+</sup> cation with Gly-Gly, Gly-His, and some related ligands. A new case of a metal ion able to promote peptide nitrogen deprotonation in aqueous solution. *Inorganic Chemistry*, 38(2) (1999) 346-352.
- [28] A.G. Davies, P.J. Smith, Recent advances in organotin chemistry. *Advances in Inorganic Chemistry and Radiochemistry*, 23 (1980) 1-77.
- [29] S. Nesci, V. Ventrella, F. Trombetti, M. Pirini, A.R. Borgatti, A. Pagliarani, Tributyltin (TBT) and dibutyltin (DBT) differently inhibit the mitochondrial Mg-ATPase activity in mussel digestive gland. *Toxicology in Vitro*, 25(1) (2011) 117-124.
- [30] M. Hanif, M. Hussain, S. Ali, M.H. Bhatti, M.S. Ahmed, B. Mirza, H.S. Evans,

- Synthesis, spectroscopic investigation, crystal structure, and biological screening, including antitumor activity, of organotin(IV) derivatives of piperonylic acid. *Turkish Journal of Chemistry*, 31(3) (2007) 349-361.
- [31] M. Helliwell, S. Ali, S. Shahzadi, (4-Chloro-3, 5-dinitrobenzoato) triphenyltin(IV). *Acta Crystallographica Section E: Structure Reports Online*, 62(7) (2006) 1656-1657.
- [32] G. Eng, X. Song, A. Zapata, A.C. de Dios, L. Casabianca, R.D. Pike, Synthesis, structural and larvicidal studies of some triorganotin 2-(p-chlorophenyl)-3-methylbutyrates. *Journal of Organometallic Chemistry*, 692(6) (2007) 1398-1404.
- [33] M. Parvez, S. Ali, M. Mazhar, M. Bhatti, M. Choudhary, (N-maleoylmethioninato) trimethyltin(IV). *Acta Crystallographica Section C: Crystal Structure Communications*, 55(9) (1999) 1429-1431.
- [34] M.N. Tahir, D. Ülkü, M. Danish, S. Ali, A. Badshah, M. Mazhar, {2-[(2, 3-Dimethylphenyl) amino] benzoato-O: O'}-trimethyltin(IV). *Acta Crystallographica Section C: Crystal Structure Communications*, 53(2) (1997) 183-185.
- [35] S. Ali, M. Najam-ul-Haq, S. Shahzadi, K. Wurst, {4-[1-(4-Hydroxyphenyl)-1-methylethyl] phenoxy} trimethyltin(IV). *Acta Crystallographica Section E: Structure Reports Online*, 62(3) (2006) 451-453.
- [36] M.T. Masood, S. Ali, M. Danish, M. Mazhar, Synthesis and characterization of tri-, di-, and chlorodiorganotin(IV) derivatives of 3-benzoyl- $\alpha$ -methylphenylacetic acid and 3-(2-thienyl) acrylic acid. *Synthesis and Reactivity in Inorganic and Metal-Organic Chemistry*, 32(1) (2002) 9-23.
- [37] S. Ali, M. Helliwell, S. Shahzadi, (3-Amino-4-chlorobenzoato) trimethyltin(IV).

- Acta Crystallographica Section E: Structure Reports Online*, 62(8) (2006) 1778-1779.
- [38] M. Parvez, S. Ali, M.H. Bhatti, M.N. Khokhar, M. Mazhar, S.I. Qureshi, Tri-n-butyl (N-maleoyl- $\beta$ -alaninato) tin. *Acta Crystallographica Section C: Crystal Structure Communications*, 55(9) (1999) 1427-1429.
- [39] A. Ahmad, A. Khan, S. Ali, M. Parvez, catena-Poly [[tri-n-butyltin(IV)]- $\mu$ -cyclopent-2-enylacetato- $\kappa$ 2O: O']. *Acta Crystallographica Section E: Structure Reports Online*, 62(6) (2006) 1192-1194.
- [40] M. Danish, S. Ali, M. Mazhar, A. Badshah, T. Masood, E.T. Tiekink, Crystal and molecular structures of two polymeric triorganotin 2-(2-thiophenyl)-ethylene-1-carboxylate derivatives. *Main Group Metal Chemistry*, 18(1) (1995) 27-34.
- [41] S. Ali, M. Mazhar, A. Badshah, M. Parvez, Synthesis, spectroscopic characterization, and biological activity studies of organotin(IV) derivatives of (E)-3-(3-fluorophenyl)-2-phenyl-2-propenoic acid. Crystal and molecular structure of  $\text{Et}_2\text{Sn} [\text{OCOC}(\text{C}_6\text{H}_5)=\text{CH}(3\text{-FC}_6\text{H}_4)]$ . *Heteroatom Chemistry: An International Journal of Main Group Elements*, 17(5) (2006) 420-432.
- [42] S.W. Ng, V.K. Das, G. Pelizzi, F. Vitali, Synthesis and crystal structures of the triphenylstannyl esters of N-phthaloyl-glycine and-leucine. *Heteroatom Chemistry*, 1(6) (1990) 433-438.
- [43] M. Gielen, A. El Khouloufi, M. Biesemans, F. Kayser, R. Willem, B. Mahieu, D. Maes, J.N. Lisgarten, L. Wyns, Tri-n-butyltin 2, 6-difluorobenzoate, a unique macrocyclic tetramer containing a 16-membered  $\text{Sn}_4\text{C}_4\text{O}_8$  ring, and other related compounds. *Organometallics*, 13(7) (1994) 2849-2854.
- [44] T.S. Basu Baul, K.S. Singh, X. Song, A. Zapata, G. Eng, A. Lycka, A. Linden,

- Synthesis and characterization of tributyltin(IV) complexes of 2-[(E)-2-(3-formyl-4-hydroxyphenyl)-1-diazenyl] benzoic acid and 4-[(E)-1-{2-hydroxy-5-[(E)-2-(2-carboxyphenyl)-1-diazenyl] phenyl} methylidene) amino] aryls: crystal structures of polymeric (Bu<sub>3</sub>Sn [O<sub>2</sub>CC<sub>6</sub>H<sub>4</sub> {N= N (C<sub>6</sub>H<sub>3</sub>-4-OH-5-CHO)}-o]) and (Bu<sub>3</sub>Sn [O<sub>2</sub>CC<sub>6</sub>H<sub>4</sub> (N= N (C<sub>6</sub>H<sub>3</sub>-4-OH (C (H)= NC<sub>6</sub>H<sub>4</sub>Cl-4)))-o]) n-toxicity studies on the second instar of *Aedes aegypti* mosquito larvae. *Journal of Organometallic Chemistry*, 689(25) (2004) 4702-4711.
- [45] A. Linden, T.S. Basu Baul, K.S. Singh, catena-Poly [[tri-n-butyltin(IV)]-μ-2-{(E)-4-hydroxy-3-[(E)-4-methylphenyliminomethyl] phenyldiazenyl} benzoato-κ<sup>2</sup>O: O']. *Acta Crystallographica Section E: Structure Reports Online*, 61(12) (2005) 2711-2713.
- [46] T.S. Basu Baul, K.S. Singh, M. Holcapek, R. Jirasko, E. Rivarola, A. Linden, Synthesis, characterization and crystal structures of polymeric and dimeric triphenyltin(IV) complexes of 4-[(E)-1-{2-hydroxy-5-[(E)-2-(2-carboxyphenyl)-1-diazenyl] phenyl} methylidene) amino] aryls. *Journal of Organometallic Chemistry*, 690(19) (2005) 4232-4242.
- [47] T.S.B. Baul, K.S. Singh, A. Linden, X. Song, G. Eng, Synthesis, spectroscopic characterization of tribenzyltin(IV) complexes of polyaromatic carboxylic acid ligands: Crystal and molecular structures of Bz<sub>3</sub>Sn[O<sub>2</sub>CC<sub>6</sub>H<sub>4</sub> {N=N (C<sub>6</sub>H<sub>3</sub>-4-OH (C(H) NC<sub>6</sub>H<sub>4</sub>X-4))}-o](OH<sub>2</sub>)(X=Cl, -OCH<sub>3</sub>). *Polyhedron*, 25(17) (2006) 3441-3448.
- [48] Sadiq-ur-Rehman, H. Vienly, S. Ali, A. Badshah, M. Parvez, *Acta Crystallographica Section E*, 60 (2004) 1144.

- [49] B.O. Leung, S. Ali, A. Badshah, M. Parvez, Bis [2, 3-bis (4-chlorophenyl) propenoato- $\kappa^2$ O, O'] dimethyltin(IV). *Acta Crystallographica Section E: Structure Reports Online*, 60(7) (2004) 984-986.
- [50] G.D. Van Kerk, J. Luijten, Investigations on organo-tin compounds. III. The biocidal properties of organo-tin compounds. *Journal of Applied Chemistry*, 4(6) (1954) 314-319.
- [51] G.J.M. van der Kerk, J.G.A. Luijten, Investigations on organo-tin compounds. V The preparation and antifungal properties of unsymmetrical tri-n-alkyltin acetates. *Journal of Applied Chemistry*, 6(2) (1956) 56-60.
- [52] X. Song, A. Zapata, G. Eng, Organotins and quantitative-structure activity/property relationships. *Journal of Organometallic Chemistry*, 691(8) (2006) 1756-1760.
- [53] G.L. Grady, J.R. Saucier, W.J. Foley III, D.J. O'hern, W.J. Weidmann, A hammett correlation for the addition of organotin hydride to benzaldehydes. *Journal of Organometallic Chemistry*, 35(2) (1972) 307-313.
- [54] S. Doctor, D. Fox, Effects of organotin compounds on maximal electroshock seizure (MES) responsiveness in mice. I. Tri (n-alkyl) tin compounds. *Journal of Toxicology and Environmental Health: Part A Current Issues*, 10(1) (1982) 43-52.
- [55] P. Mushak, M. Krigman, R. Mailman, Comparative organotin toxicity in the developing rat: somatic and morphological changes and relationship to accumulation of total tin. *Neurobehavioral Toxicology and Teratology*, 4(2) (1982) 209-215.
- [56] A.J. Kuthubutheen, R. Wickneswari, V.G. Kumar Das, Efficacy of selected

- triorganotin(IV) compounds on leaves against *Phytophthora palmivora* (Butler) Butler isolated from black pepper and cocoa. *Applied Organometallic Chemistry*, 3(3) (1989) 243-248.
- [57] M. Bouâlam, J. Meunier-Piret, M. Biesemans, R. Willem, M. Gielen, Organotin(IV) compounds of 2-thiopyridine. Crystal and molecular structure of dicyclohexyltin (IV) bis (2-pyridylthiolate). *Inorganica Chimica Acta*, 198 (1992) 249-255.
- [58] N. Cardarelli, B. Cardarelli, E. Libby, E. Dobbins, Organotin implications in anticarcinogenesis. Effects of several organotins on tumour growth rate in mice. *Australian Journal of Experimental Biology and Medical Science*, 62(2) (1984) 209-214.
- [59] L.C. Miller, Efficacy of a Series of Organometallic Polymers as Anti-cancer and Antiviral Agents (doctoral dissertation). 2017.
- [60] C.E. Carraher Jr, G.A. Scherubel, Production of organometallic polymers by the interfacial technique. XX. Synthesis of polyoxystannyloxyalkylenes. *Journal of Polymer Science Part A-1: Polymer Chemistry*, 9(4) (1971) 983-989.
- [61] S. Hussain, S. Ali, S. Shahzadi, M.N. Tahir, M. Shahid, Synthesis, characterization, biological activities, crystal structure and DNA binding of organotin(IV) 5-chlorosalicylates. *Journal of Coordination Chemistry*, 68(14) (2015) 2369-2387.
- [62] C.J. Evans, Organotin compounds in modern technology. *Journal of Organometallic Chemistry Library*, 16 (1985).
- [63] Y.F. Win, S.G. Teoh, S.T. Ha, T.S. Tengku-Muhammad, E. Yousif, Preliminary

- in vitro cytotoxic assay on HepG2 and antibacterial screening activity: synthesis and characterization of organotin(IV) complexes derivatives of 2-methyl-3-nitrobenzoic acid. *Asian Journal of Chemistry*, 25(6) (2013) 3376.
- [64] F.W. van Der Weij, The action of tin compounds in condensation-type RTV silicone rubbers. *Die Makromolekulare Chemie: Macromolecular Chemistry and Physics*, 181(12) (1980) 2541-2548.
- [65] D. Van, F. Van Der Weij, The action of tin compounds in condensation-type rtv silicone rubbers. *Die Makromolekulare Chemie: Macromolecular Chemistry and Physics*, 181(12) (1980) 2541-8.
- [66] S.H. Iftikhar, S.R. Gilani, B.M. Taj, A. Raheel, S.A. Termizi, M. Al-Shakban, H.M. Ali, Design, synthesis and biological evaluation of organotin(IV) complexes of flumequine and cetirizine. *Journal of the Serbian Chemical Society*, 83(4) (2018) 425-437.
- [67] C.E. Tan, V. Luona, T. Tirri, C.E. Wilen, The synthesis of low-viscosity organotin-free moisture-curable silane-terminated poly (urethane-urea)s. *Polymers*, 10(7) (2018) 781.
- [68] A. Mahmoud, A. Shaaban, M. Azab, N. Messiha, Organotin polymers—XVI. Synthesis of p-acryloyloxybenzoic acid and n-methacryloyloxytetrabromophthalimide and copolymerizations with tri-n-butyltin acrylate and methacrylate. *European Polymer Journal*, 28(5) (1992) 555-559.
- [69] C.A. Harper, Handbook of plastics technologies: the complete guide to properties and performance. McGraw-Hill Education, 2006.
- [70] E. Yousif, A. Ahmed, R. Abood, N. Jaber, R. Noaman, R. Yusop, Poly (vinyl



- chloride) derivatives as stabilizers against photodegradation. *Journal of Taibah University for Science*, 9(2) (2015) 203-212.
- [71] E. Yousif, J. Salimon, N. Salih, A. Jawad, Y.-F. Win, New stabilizers for PVC based on some diorganotin(IV) complexes with benzamidoleucine. *Arabian Journal of Chemistry*, 9 (2016) 1394-1401.
- [72] E. Yousif, J. Salimon, N. Salih, New photostabilizers for PVC based on some diorganotin(IV) complexes. *Journal of Saudi Chemical Society*, 19(2) (2015) 133-141.
- [73] L. Pellerito, L. Nagy, Organotin(IV) n+ complexes formed with biologically active ligands: equilibrium and structural studies, and some biological aspects. *Coordination Chemistry Reviews*, 224(1-2) (2002) 111-150.
- [74] K. Shahid, S. Ali, M.H. Bhatti, M. Parvez, Organotin esterification of (E)-3-(3-fluoro-phenyl)-2-(4-chlorophenyl)-2-propenoic acid: synthesis, spectroscopic characterization and in vitro biological activities. Crystal structure of  $[\text{Ph}_3\text{Sn}(\text{OC}(\text{O})\text{C}(4\text{-ClC}_6\text{H}_4)=\text{CH}(3\text{-FC}_6\text{H}_4))]$ . *Journal of Organometallic Chemistry*, 690(5) (2005) 1396-1408.
- [75] G. Arena, R. Calì, A. Contino, A. Musumeci, S. Musumeci, R. Purrello, Coordination properties of dialkyltin(IV) in aqueous solution. Thermodynamic study of dimethyltin (IV) complexes with l-amino acids. *Inorganica Chimica Acta*, 237(1-2) (1995) 187-191.
- [76] M. Gielen, Tin-based antitumour drugs: new developments. *Metal-based drugs*, 2(2) (1995) 99-103.
- [77] W. Li, Z.W. Zhang, S.M. Ren, Y. Sibiril, D. Parent Massin, T. Jiang, Synthesis

- and antitumor activity of novel dibutyltin carboxylates of aminoglucosyl derivatives. *Chemical Biology & Drug Design*, 73(6) (2009) 682-686.
- [78] W. Kang, X. Wu, J. Huang, Synthesis, crystal structure and biological activities of four novel tetranuclear di-organotin (IV) carboxylates. *Journal of Organometallic Chemistry*, 694(15) (2009) 2402-2408.
- [79] K. Shahid, M. Mazhar, S. Ali, M. Danish, Synthesis and In Vitro Antitumour Studies of Trimethyltin (IV) trans-M-Methylcinnamate. *Journal of The Chemical Society of Pakistan*, 26(4) (2011) 140.
- [80] A. Attanzio, M. Ippolito, M.A. Girasolo, F. Saiano, A. Rotondo, S. Rubino, L. Mondello, M.L. Capobianco, P. Sabatino, L. Tesoriere, Anti-cancer activity of di- and tri-organotin (IV) compounds with D-(+)-Galacturonic acid on human tumor cells. *Journal of Inorganic Biochemistry*, 188 (2018) 102-112.
- [81] W.A. Wani, S. Prashar, S. Shreaz, S. Gomez-Ruiz, Nanostructured materials functionalized with metal complexes: In search of alternatives for administering anticancer metallodrugs. *Coordination Chemistry Reviews*, 312 (2016) 67-98.
- [82] V. Cepeda, M.A. Fuertes, J. Castilla, C. Alonso, C. Quevedo, J.M. Pérez, Biochemical mechanisms of cisplatin cytotoxicity. *Anti-Cancer Agents in Medicinal Chemistry (Formerly Current Medicinal Chemistry-Anti-Cancer Agents)*, 7(1) (2007) 3-18.
- [83] P. Yang, M. Guo, Interactions of organometallic anticancer agents with nucleotides and DNA. *Coordination Chemistry Reviews*, 185 (1999) 189-211.
- [84] M.K. Amir, S. Khan, A. Shah, I.S. Butler, Anticancer activity of organotin(IV) carboxylates. *Inorganica Chimica Acta*, 423 (2014) 14-25.

- [85] M. Sirajuddin, S. Ali, A. Badshah, Drug–DNA interactions and their study by UV–Visible, fluorescence spectroscopies and cyclic voltametry. *Journal of Photochemistry and Photobiology B: Biology*, 124 (2013) 1-19).
- [86] (<http://triplesteptowardthecure.org/understanding.php>).
- [87] (<https://www.dr.dineshmg.com/types-of-cancer.html>).
- [88] J. Devi, J. Yadav, Recent advancements in organotin(IV) complexes as potential anticancer agents. *Anti-Cancer Agents in Medicinal Chemistry*, 18(3) (2018) 335–353).
- [89] M. Lind, Principles of cytotoxic chemotherapy. *Medicine*, 39(12) (2011) 711-716.
- [90] L.H. Hurley, DNA and its associated processes as targets for cancer therapy. *Nature Reviews Cancer*, 2(3) (2002) 188-200.
- [91] M. Polat, H. Polat, Recent Advances in Chitosan-Based Systems for Delivery of Anticancer Drugs. *Functional Chitosan*, (2019) 191-228.
- [92] D. Waseem, A.F. Butt, I.-u. Haq, M.H. Bhatti, G.M. Khan, Carboxylate derivatives of tributyltin (IV) complexes as anticancer and antileishmanial agents. *DARU Journal of Pharmaceutical Sciences*, 25(1) (2017) 1-14.
- [93] P. Desjeux, Leishmaniasis: current situation and new perspectives, Comparative immunology. *Microbiology and Infectious Diseases*, 27(5) (2004) 305-318.
- [94] H.W. Murray, Clinical and experimental advances in treatment of visceral leishmaniasis. *Antimicrobial Agents and Chemotherapy*, 45(8) (2001) 2185-2197.
- [95] E. Rosenthal, P. Marty, Treatment of visceral leishmaniasis: a review of current treatment practices. *Expert Opinion on Pharmacotherapy*, 3(8) (2002) 1101-1108.

- [96] P.J. Guerin, P. Olliaro, S. Sundar, M. Boelaert, S.L. Croft, P. Desjeux, M.K. Wasunna, A.D. Bryceson, Visceral leishmaniasis: current status of control, diagnosis, and treatment, and a proposed research and development agenda. *The Lancet Infectious Diseases*, 2(8) (2002) 494-501.
- [97] Pearson, D. Richard Mary E. Wilson. "Host defenses against prototypical intracellular protozoans, the Leishmania." *Parasitic Infections in the Compromised Host*. CRC Press, (2020) 31-81).
- [98] H. Yoshida, K. Inaba, N. Sato, X-ray diffraction reciprocal space mapping study of the thin film phase of pentacene. *Applied Physics Letters*, 90(18) (2007) 181930.
- [99] A.D. Becke, Density-functional thermochemistry. IV. A new dynamical correlation functional and implications for exact-exchange mixing. *The Journal of Chemical Physics*, 104(3) (1996) 1040-1046.
- [100] C. Lee, W. Yang, R.G. Parr, Development of the Colle-Salvetti correlation-energy formula into a functional of the electron density. *Physical Review B*, 37(2) (1988) 785.
- [101] L. Touafri, A. Hellal, S. Chafaa, A. Khelifa, A. Kadri, Synthesis, characterisation and DFT studies of three Schiff bases derived from histamine. *Journal of Molecular Structure*, 1149 (2017) 750-760.
- [102] W. Armarego, C. Chai, Purification of Laboratory Chemicals, *Butesworth, Heinemann: Oxford*, 2003.
- [103] N. Muhammad, S. Ali, A. Meetsma, F. Shaheen, Organotin(IV) 4-

- methoxyphenylethanoates: synthesis, spectroscopic characterization, X-ray structures and in vitro anticancer activity against human prostate cell lines (PC-3). *Inorganica Chimica Acta* 362(8) (2009) 2842-2848.
- [104] O.V. Dolomanov, L.J. Bourhis, R.J. Gildea, J.A. Howard, H. Puschmann, OLEX2: a complete structure solution, refinement and analysis program. *Journal of applied crystallography* 42(2) (2009) 339-341.
- [105] M. Chahkandi, M.H. Bhatti, U. Yunus, S. Shaheen, M. Nadeem, M.N. Tahir, Synthesis and comprehensive structural studies of a novel amide based carboxylic acid derivative: Non-covalent interactions. *Journal of Molecular Structure*, 1133 (2017) 499-509.
- [106] A. Shah, A. Rauf, A. Ullah, A. Munir, R. Qureshi, I. Ahmad, M.T. Soomro, Z.U. Rehman, Engineering, Electrochemical investigations of unexplored anthraquinones and their DNA binding. *Journal of Electrochemical Science and Engineering*, 3(1) (2013) 19-27.
- [107] N. Muhammad, S. Ali, A. Meetsma, F. Shaheen, Organotin(IV) 4-methoxyphenylethanoates: synthesis, spectroscopic characterization, X-ray structures and in vitro anticancer activity against human prostate cell lines (PC-3). *Inorganica Chimica Acta*, 362 (2009) 2842-2848.
- [108] A. Shah, N. Muhammad, S. Ali, R. Qureshi, I.S. Butler, Synthesis, characterization and DNA binding studies of penta-and hexa-coordinated diorganotin(IV) 4-(4-nitrophenyl) piperazine-1-carbodithioates. *Journal of Organometallic Chemistry*, 694(13) (2009) 1998-2004.
- [109] K.N. de Oliveira, V. Andermark, L.A. Onambele, G. Dahl, A. Prokop, I. Ott,

Organotin complexes containing carboxylate ligands with maleimide and naphthalimide derived partial structures: TrxR inhibition, cytotoxicity and activity in resistant cancer cells. *European Journal of Medicinal Chemistry*, 87 (2014) 794-800.

- [110] T. Mosmann, Rapid colorimetric assay for cellular growth and survival: application to proliferation and cytotoxicity assays. *Journal of Immunological Methods*, 65(1-2) (1983) 55-63.
- [111] A.A. Alrajhi, E.A. Ibrahim, E.B. De Vol, M. Khairat, R.M. Faris, J.H. Maguire, Fluconazole for the treatment of cutaneous leishmaniasis caused by *Leishmania major*. *New England Journal of Medicine*, 346(12) (2002) 891-895.
- [112] A. Nadhman, S. Nazir, M.I. Khan, A. Ayub, B. Muhammad, M. Khan, D.F. Shams, M. Yasinzai, Visible-light-responsive ZnCuO nanoparticles: benign photodynamic killers of infectious protozoans. *International Journal of Nanomedicine*, 10 (2015) 6891.
- [113] A. Ihsan-Ul-Haq, I. Ahmed, I. Hussain, M. Jamil, B. Mirza, Antibacterial activity and brine shrimp toxicity of *Artemisia dubia* extract. *Pakistan Journal of Botany* 44(4) (2012) 1487- 1490.
- [114] U.A. Khan, A. Badshah, M.N. Tahir, E.J.P. Khan, Gold(I), silver(I) and copper(I) complexes of 2, 4, 6-trimethylphenyl-3-benzoylthiourea; synthesis and biological applications. *Polyhedron*, 181 (2020) 114485.
- [115] S. Tabassum, M. Ahmed, B. Mirza, M. Naeem, M. Zia, Z.K. Shanwari, G.M. Khan,

- Appraisal of phytochemical and in vitro biological attributes of an unexplored folklore: *Rhus Punjabensis* Stewart. *BMC Complementary Medicine and Therapies*, 17(1) (2017) 1-13.
- [116] S. Naz, F. Shams, S. Tabassum, M. Ashraf, M. Zia, Kinnow peel extract as a reducing and capping agent for the fabrication of silver NPs and their biological applications. *Journals of the Institution of Engineering and Technology*, 11(8) (2017) 1040-1045.
- [117] P. Hohenberg, W. Kohn, Inhomogeneous electron gas. *Physical Review Journal Archive*, 136(3B) (1964) B864.
- [118] W. Kohn, L.J.J.P.r. Sham, Self-consistent equations including exchange and correlation effects. *Physical Review Journal Archive*, 140(4A) (1965) A1133.
- [119] P. Giannozzi, S. Baroni, N. Bonini, M. Calandra, R. Car, C. Cavazzoni, D. Ceresoli, G.L. Chiarotti, M. Cococcioni, I. Dabo, A. Dol Corso, QUANTUM ESPRESSO: a modular and open-source software project for quantum simulations of materials. *Journal of Physics: Condensed Matter*, 21(39) (2009) 395502.
- [120] J. Perdew, K. Burke, M. Ernzerhof, Perdew, burke, and ernzerhof reply. *Physical Review Letters*, 80(4) (1998) 891.
- [121] H.J. Monkhorst, J.D. Pack, Special points for Brillouin-zone integrations. *Physical Review B*, 13(12) (1976) 5188.
- [122] D. Moitra, S. Dhole, B.K. Ghosh, M. Chandel, R.K. Jani, M.K. Patra, S.R. Vadera, N.N. Ghosh, Synthesis and microwave absorption properties of BiFeO<sub>3</sub> nanowire-RGO nanocomposite and first-principles calculations for insight of electromagnetic

- properties and electronic structures. *Journal of Physical Chemistry C*, 121(39) (2017) 21290-21304.
- [123] I. Ahmad, A. Waseem, M. Tariq, C. MacBeth, J. Bacsa, D. Venkataraman, A. Rajakumar, N. Ullah, S. Tabassum, Organotin(IV) derivatives of amide-based carboxylates: Synthesis, spectroscopic characterization, single crystal studies and antimicrobial, antioxidant, cytotoxic, anti-leishmanial, hemolytic, noncancerous, anticancer activities. *Inorganica Chimica Acta*, 505 (2020) 119433.
- [124] S. Shujah, S. Ali, N. Khalid, M.J. Alam, S. Ahmad, A. Meetsma, Synthesis, spectroscopic characterization, X-ray structure, DFT calculations, and antimicrobial studies of diorganotin(IV) complexes of monotopic oxygen nitrogen donor Schiff base. *Chemical Papers*, 72(4) (2018) 903-919.
- [125] Z.U. Rehman, A. Shah, N. Muhammad, S. Ali, R. Qureshi, A. Meetsma, I.S. Butler, Synthesis, spectroscopic characterization, X-ray structure and evaluation of binding parameters of new triorganotin(IV) dithiocarboxylates with DNA. *European Journal of Medicinal Chemistry*, 44(10) (2009) 3986-3993.
- [126] M. Yousefi, M. Safari, M.B. Torbati, V.M. Kazemiha, H. Sanati, A. Amanzadeh, New mononuclear diorganotin(IV) dithiocarboxylates: synthesis, characterization and study of their cytotoxic activities. *Applied Organometallic Chemistry*, 26(8) (2012) 438-444.
- [127] N. Muhammad, Z.U. Rehman, S. Ali, A. Meetsma, F. Shaheen, Organotin (IV) 4-methoxyphenylethanoates: synthesis, spectroscopic characterization, X-ray structures and in vitro anticancer activity against human prostate cell lines (PC-3). *Inorganica Chimica Acta*, 362 (2009) 2842-2848.



- [128] M. Sirajuddin, V. McKee, M. Tariq, S. Ali, Newly designed organotin(IV) carboxylates with peptide linkage: synthesis, structural elucidation, physicochemical characterizations and pharmacological investigations. *European Journal of Medicinal Chemistry*, 143 (2018) 1903-1918.
- [129] A. Uusiku, Synthesis and characterization of metal complexes 2-Benzoylpyridine and di-2-pyridyl ketone schiff base ligands derived from s-methyldithiocarbazate fragment and its application to biological activity toward P. Falciparum (Doctoral dissertation, University of Namibia) (2015) 44-45.
- [130] M.A. Ali, A.H. Mirza, R.J. Butcher, P.V. hardt, M.R. Karim, Self-assembling dicopper (II) complexes of di-2-pyridyl ketone Schiff base ligands derived from S-alkyldithiocarbazates. *Polyhedron*, 30(9) (2011) 1478-1486.
- [131] Y.Y. Zhang, R.F. Zhang, S.L. Zhang, S. Cheng, Q.L. Li, C.L. Ma, Syntheses, structures and anti-tumor activity of four new organotin(IV) carboxylates based on 2-thienylselenoacetic acid. *Dalton Transactions*, 45(20) (2016) 8412-8421.
- [132] D. Kovala-Demertzi, V.N. Dokorou, J.P. Jasinski, A. Opolski, J. Wiecek, M. Zervou, M.A. Demertzis, Organotin flufenamates: synthesis, characterization and antiproliferative activity of organotin flufenamates. *Journal of Organometallic Chemistry*, 690(7) (2005) 1800-1806.
- [133] Y. Han-Dong, G. Zhong-Jun, W. Chuan-Hua, Synthesis, Characterization and Properties of Organotin Complexes Dibutyltin(IV) Bis (heteroaromatic carboxylate) and Crystal Structure of Dibutyltin (IV) Bis (2-thiazolylcarboxylate). *Chinese Journal of Chemistry*, 23(7) (2005) 928-932.
- [134] G. Eng, X. Song, A. Zapata, A.C. de Dios, L. Casabianca, R.D. Pike, Synthesis,

- structural and larvicidal studies of some triorganotin 2-(p-chlorophenyl)-3-methylbutyrates. *Journal of Organometallic Chemistry*, 692(6) (2007) 1398-1404.
- [135] T.P. Lockhart, W.F. Manders, E.M. Holt, Solution and solid-state molecular structures of  $\text{Me}_2\text{Sn}(\text{OAc})_2$  and its hydrolyzate,  $([\text{Me}_2\text{Sn}(\text{OAc})]_2\text{O})_2$ , by solution and solid-state carbon-13 NMR. X-ray diffraction study of the hydrolyzate. *Journal of American Chemical Society*, 108(21) (1986) 6611-6616.
- [136] B. Wrackmeyer, Application of  $^{119}\text{Sn}$  NMR parameters. *Annual Reports on NMR Spectroscopy*, 38 (1999) 203-264.
- [137] V. Torocheshnikov, A. Tupčiauskas, Y.A. Ustynyuk, A  $^{119}\text{Sn}$  NMR study of tin derivatives of cyclopentadiene. *Journal of Organometallic Chemistry*, 81(3) (1974) 351- 356.
- [138] M. Iqbal, S. Ali, N. Muhammad, M. Parvez, P. Langer, A. Villinger, Synthesis, characterization, crystal structures and electrochemical studies of organotin(IV) carboxylates. *Journal of Organometallic Chemistry*, 723 (2013) 214-223.
- [139] W.F. Howard Jr, R.W. Crecely, W.H. Nelson, Octahedral dialkyltin complexes: a multinuclear NMR spectral solution structural study. *Inorganic Chemistry*, 24(14) (1985) 2204-2208.
- [140] M. Gielen, A.E. Khloufi, M. Biesemans, F. Kayser, R. Willem, Diorganotin 2-fluorocinnamates and 4-fluorophenylacetates: Synthesis, characterization and in vitro antitumour activity. *Applied Organometallic Chemistry*, 7(3) (1993) 201-206.
- [141] T. Mosmann, Rapid colorimetric assay for cellular growth and survival: application to proliferation and cytotoxicity assays. *Journal of Immunological Methods*, 65(1-2) (1983) 55-63.

- [142] M.S. Ahmad, M. Hussain, M. Hanif, S. Ali, M. Qayyum, B. Mirza, d. design, Di- and Triorganotin(IV) Esters of 3, 4-Methylenedioxyphenylpropenoic Acid: Synthesis, Spectroscopic Characterization and Biological Screening for Antimicrobial, Cytotoxic and Antitumor Activities. *Chemical Biology and Drug Design*, 71(6) (2008) 568-576.
- [143] M.S. Ahmad, M. Hussain, M. Hanif, S. Ali, B. Mirza, Synthesis, chemical characterization and biological screening for cytotoxicity and antitumor activity of organotin(IV) derivatives of 3, 4-methylenedioxy 6-nitrophenylpropenoic acid. *Molecules*, 12(10) (2007) 2348-2363.
- [144] I. Ahmad, A. Waseem, M. Tariq, C. MacBeth, J. Bacsa, D. Venkataraman, A. Rajakumar, N. Ullah, S. Tabassum, Organotin(IV) derivatives of amide-based carboxylates: Synthesis, spectroscopic characterization, single crystal studies and antimicrobial, antioxidant, cytotoxic, anti-leishmanial, hemolytic, noncancerous, anticancer activities. *Inorganica Chimica Acta*, 505 (2020) 119433.
- [145] M.S. Ahmad, M. Hussain, M. Hanif, S. Ali, M. Qayyum, B. Mirza, Di-and Triorganotin(IV) esters of 3, 4-methylenedioxyphenylpropenoic acid: synthesis, spectroscopic characterization and biological screening for antimicrobial, cytotoxic and antitumor Activities. *Chemical Biology & Drug Design*, 71(6) (2008) 568-576.
- [146] M. Ahmad, M. Hussain, M. Hanif, S. Ali, B. Mirza, Synthesis, chemical characterization and biological screening for cytotoxicity and antitumor activity of organotin(IV) derivatives of 3, 4-methylenedioxy 6-nitrophenylpropenoic acid. *Molecules*, 12(10) (2007) 2348-2363.
- [147] A. Ihsan-Ul-Haq, I. Ahmed, I. Hussain, M. Jamil, B. Mirza, Antibacterial activity

- and brine shrimp toxicity of *Artemisia dubia* extract. *Pakistan Journal of Botany*, 44(4) (2012) 1487- 90.
- [148] J. Adeyemi, D. Onwudiwe, Organotin (IV) dithiocarbamate complexes: chemistry and biological activity. *Molecules*, 23(10) (2018) 2571.
- [149] M. Gielen, C.C. Camacho, M. Kemmer, R. Willem, E. Horn, E.R. Tiekink, The crystal structure of bis [(3,4-(methylene-dioxyphenylacetato)-di-n-butyltin] oxide. *Main Group Metal Chemistry*, 23(12) (2000) 797-798.
- [150] S. Tabassum, M. Ahmed, B. Mirza, M. Naeem, M. Zia, Z.K. Shanwari, G.M. Khan, a. medicine, Appraisal of phytochemical and in vitro biological attributes of an unexplored folklore: *Rhus Punjabensis* Stewart. *BMC Complementary Medicine and Therapies*, 17(1) (2017) 1-13.
- [151] M. Tariq, S. Ali, N.A. Shah, N. Muhammad, M.N. Tahir, N. Khalid, M.R. Khan, Catalytic, biological and DNA binding studies of organotin(IV) carboxylates of 3-(2-fluorophenyl)-2-methylacrylic acid: Synthesis, spectroscopic characterization and X-ray structure analysis. *Polyhedron*, 57 (2013) 127-137.
- [152] C.C. Camacho, D. de Vos, B. Mahieu, M. Gielen, M. Kemmer, M. Biesemans, R. Willem, Organotin (IV) derivatives of 3, 4-(methylenedioxy) phenylacetic acid: synthesis, spectroscopic characterization and in vitro antitumour properties. *Main Group Metal Chemistry*, 23(7) (2000) 381-386.
- [153] S. Tabassum, M. Ahmed, B. Mirza, M. Naeem, M. Zia, Z.K. Shanwari, G.M. Khan, Appraisal of phytochemical and in vitro biological attributes of an unexplored folklore: *Rhus Punjabensis* Stewart, BMC complementary and alternative medicine. *BMC Complementary Medicine and Therapies*, 17(1) (2017) 146.

- [154] S. Naz, M. Rezgui, R. Rehman, F. Nadeem, Pomegranate an Ancient Seed for Modern Cure—A Review of Potential Applications. *International Journal of Chemical and Biochemical Sciences*, 8 (2015) 78-84.
- [155] H. Yoshida, K. Inaba, N. Sato, X-ray diffraction reciprocal space mapping study of the thin film phase of pentacene. *Applied Physics Letters*, 90(18) (2007) 181930.
- [156] A.D. Becke, Density-functional thermochemistry. IV. A new dynamical correlation functional and implications for exact-exchange mixing. *The Journal of Chemical Physics*, 104(3) (1996) 1040-1046.
- [157] C. Lee, W. Yang, R.G. Parr, Development of the Colle-Salvetti correlation-energy formula into a functional of the electron density. *Physical Review B*, 37(2) (1988) 785.
- [158] H. Ferjani, R. Bechaieb, W. Abd El-Fattah, M. Fettouhi, Broad-band luminescence involving fluconazole antifungal drug in a lead-free bismuth iodide perovskite: Combined experimental and computational insights. *Spectrochimica Acta Part A: Molecular and Biomolecular Spectroscopy*, 237 (2020) 118354.
- [159] P.J. Hay, W.R. Wadt, Ab initio effective core potentials for molecular calculations. Potentials for the transition metal atoms Sc to Hg. *The Journal of Chemical Physics*, 82(1) (1985) 270-283.
- [160] F.S. Legge, G.L. Nyberg, J.B. Peel, DFT calculations for Cu-, Ag-, and Au-containing. *Molecules*, 105(33) (2001) 7905-7916.
- [161] S.R. Wang, M. Arrowsmith, J. Böhnke, H. Braunschweig, T. Dellermann, R.D. Dewhurst, H. Kelch, I. Krummenacher, J.D. Mattock, J.H. Müssig, T. Thiess, Engineering a Small homo–lumo Gap and Intramolecular C–H Borylation by

- Diborene/Anthracene Orbital Intercalation. *Agwewandte Chemie*, 56(27) (2017) 8009-8013.
- [162] C.J. Cramer, D.G. Truhlar, Density functional theory for transition metals and transition metal chemistry. *Physical Chemistry Chemical Physics*, 11(46) (2009) 10757-10816.
- [163] I.T. Lima, L. Sousa, R.D.S. Freitas, L.A.R. Junior, R.T. de Sousa Júnior, D.A. da Silva Filho, A DFT study of a set of natural dyes for organic electronics. *Journal of Molecular Model*, 23(12) (2017) 343.
- [164] A.F. Butt, M.N. Ahmed, M.H. Bhatti, M.A. Choudhary, K. Ayub, M.N. Tahir, T. Mahmood, Synthesis, structural properties, DFT studies, antimicrobial activities and DNA binding interactions of two newly synthesized organotin(IV) carboxylates. *Journal of Molecular Structure*, 1191 (2019) 291-300.
- [165] F. Javed, M. Sirajuddin, S. Ali, N. Khalid, M.N. Tahir, N.A. Shah, Z. Rasheed, M.R. Khan, Organotin(IV) derivatives of o-isobutyl carbonodithioate: Synthesis, spectroscopic characterization, X-ray structure, homo/lumo and in vitro biological activities. *Polyhedron*, 104 (2016) 80-90.
- [166] A. Tarahhomi, A. Van Der Lee, A new six-coordinate organotin(IV) complex of OP [NC<sub>5</sub>H<sub>10</sub>]<sub>3</sub>: A comparison with an analogous five-coordinate complex by means of X-ray crystallography, Hirshfeld surface analysis and DFT calculations. *Journal of Coordination Chemistry*, 71(10) (2018) 1575-1592.
- [167] R.G. Pearson, Absolute electronegativity and hardness correlated with molecular orbital theory. *Proceeding of the National Academy of Sciences of USA*, 83(22) (1986) 8440-8441.

- [168] S. Fliszár, Conclusion and assessment, charge distributions and chemical effects. Springer science and business media, (1983) 181-189.
- [169] M. Chahkandi, M.H. Bhatti, U. Yunus, S. Shaheen, M. Nadeem, M.N. Tahir, Synthesis and comprehensive structural studies of a novel amide based carboxylic acid derivative: Non-covalent interactions. *Journal of Molecular Structure*, 1133 (2017) 499-509.
- [170] T.J. Mooibroek, P. Gamez, J. Reedijk, Lone pair- $\pi$  interactions: a new supramolecular bond. *Crystal Engineering Community*, 10(11) (2008) 501-1515.
- [171] X. Xiao, Y. Li, Y. Dong, W. Li, K. Xu, N. Shi, X Liu, J. Xie, P. Liu P, "S" shaped organotin(IV) carboxylates based on amide carboxylic acids: syntheses, crystal structures and antitumor activities. *Journal of Molecular Structure*, 1130 (2017) 901-908.
- [172] A.W. Addison, T.N. Rao, J. Reedijk, J. van Rijn, G.C. Verschoor, Synthesis, structure, and spectroscopic properties of copper (II) compounds containing nitrogen-sulphur donor ligands; the crystal and molecular structure of aqua [1,7-bis (N-methylbenzimidazol-2'-yl)-2,6-dithiaheptane] copper (II) perchlorate. *Journal of Chemical Society, Dalton Transactions*, 7 (1984) 1349-1356.
- [173] S. Shujha, A. Shah, N. Muhammad, S. Ali, R. Qureshi, N. Khalid, A. Meetsma, Diorganotin(IV) derivatives of ONO tridentate Schiff base: synthesis, crystal structure, in vitro antimicrobial, anti-leishmanial and DNA binding studies. *European Journal of Medicinal Chemistry*, 45(7) (2010) 2902-2911.
- [174] M. Tariq, S. Ali, N.A. Shah, N. Muhammad, M.N. Tahir, N. Khalid, Catalytic, biological and DNA interaction studies of 3-(4-cyanophenyl)-2-methylacrylate

- organotin (IV) carboxylates derivatives: Synthesis, spectroscopic characterization and X-ray structures. *Inorganica Chimica Acta*, 405 (2013) 444-454.
- [175] H. Masood, S. Ali, M. Mazhar, S. Shahzadi, K. Shahid,  $^1\text{H}$ ,  $^{13}\text{C}$ ,  $^{119}\text{Sn}$  NMR, Mass, Mössbauer and biological studies of tri-, di- and chlorodiorganotin(IV) carboxylates. *Turkish Journal of Chemistry*, 28(1) (2004) 75-86.
- [176] M. Hussain, M. Hanif, M. Altaf, S. Ali, K.J. Cavell, Structural studies of diethyltin(IV) derivatives and their biological aspects as potential antitumor agents against *Agrobacterium tumefaciens* cells. *Applied Organometallic Chemistry*, 25(6) (2011) 412-419.
- [177] M. Hussain, M. Hanif, S. Ali, M. Altaf, H. Stoeckli-Evans, (E)-3-(6-Nitrobenzo[d][1,3] dioxol-5-yl)-2-phenylacrylic acid. *Acta crystallographica Section E*, 62(11) (2006) o5020-o5021.
- [178] N. Muhammad, Z.U. Rehman, S. Shujah, S. Ali, A. Shah, A. Meetsma, Synthesis and structural characterization of monomeric and polymeric supramolecular organotin(IV) 4-chlorophenylethanoates. *Journal of Coordination Chemistry*, 67(6) (2014) 1110-1120.
- [179] M.S. Ahmad, M. Hussain, M. Hanif, S. Ali, B. Mirza, Synthesis, chemical characterization and biological screening for cytotoxicity and antitumor activity of organotin(IV) derivatives of 3, 4-methylenedioxy 6-nitrophenylpropenoic acid. *Molecules*, 12(10) (2007) 2348-2363.
- [180] R. Willem, A. Bouhdid, M. Biesemans, J. Martins, D. de Vos, E.R. Tiekink, M. Gielen, Synthesis and characterization of triphenyl- and tri-n-butyltin



- pentafluorobenzoates,- phenylacetates and -cinnamates. X-ray structure determination of tri-n-butyltin pentafluorocinnamate. *Journal of organometallic chemistry*, 514(1-2) (1996) 203-212.
- [181] X. Xiao, D. Du, M. Tian, X. Han, J. Liang, D. Zhu, L. Xu, Organotin(IV) carboxylates based on benzenedicarboxylic acid derivatives: Syntheses, crystal structures and characterizations. *Journal of organometallic chemistry*, 715 (2012) 54-63.
- [182] D. Du, Z. Jiang, C. Liu, A.M. Sakho, D. Zhu, L. Xu, Macrocyclic organotin(IV) carboxylates based on benzenedicarboxylic acid derivatives: Syntheses, crystal structures and antitumor activities. *Journal of organometallic chemistry*, 696(13) (2011) 2549-2558.
- [183] S. Kundu, V. Chandrasekhar,  $\eta^6$ -Benzene (tricarbonyl) chromium and cymantrene assemblies supported on an organostannoxane platform. *Crystal Growth & Design*, 15(11) (2015) 5437-5450.
- [184] M. Roy, S.S. Devi, S. Roy, C.B. Singh, K.S. Singh, Synthesis, characterization, crystal structures and in vitro antimicrobial activities of triorganotin(IV) complexes of azo-dicarboxylates. *Inorganica Chimica Acta*, 426 (2015) 89-98.
- [185] G. Prabusankar, R. Murugavel, Hexameric organotin carboxylates with cyclic and drum structures. *Organometallics*, 23(23) (2004) 5644-5647.
- [186] T.S.B. Baul, A. Paul, A. Linden, Synthesis, characterization and crystal structures of 2-[(E)-2-(4-hydroxy-3,5-dimethylphenyl)-1-diazenyl] benzoic acid and its polymeric and monomeric triorganotin(IV) complexes. *Journal of Organometallic Chemistry*, 696(26) (2012) 4229-4235.

- [187] R. Zhang, J. Sun, C. Ma, Structural chemistry of mononuclear, tetranuclear and hexanuclear organotin(IV) carboxylates from the reaction of di-n-butyltin oxide or diphenyltin oxide with rhodanine-N-acetic acid. *Journal of Organometallic Chemistry*, 690(19) (2005) 4366-4372.
- [188] S. Ali, S. Shahzadi, M. Parvez, Di-n-butylbis [(E)-2-(4-chlorophenyl)-3-(3-fluorophenyl) prop-2-enoato- $\kappa^2$ O, O] tin(IV). *Acta Crystallographica Section E, Structure Reports Online* 62(4) (2006) m910-m911.
- [189] T.S.B. Baul, K.S. Singh, M. Holčapek, R. Jirásko, E. Rivarola, A. Linden, Synthesis, characterization and crystal structures of polymeric and dimeric triphenyltin(IV) complexes of 4-[(E)-1-{2-hydroxy-5-[(E)-2-(2-carboxyphenyl)-1-diazenyl] phenyl} methylidene) amino] aryls. *Journal of Organometallic Chemistry*, 690(19) (2005) 4232-4242.

## List of Publications

- [1] **I. Ahmad**, A. Waseem, M. Tariq, C. MacBeth, J. Bacsá, D. Venkataraman, A. Rajakumar, N. Ullah, S. Tabassum, *Inorganica Chimica Acta*, 505 (2020) 119433.
- [2] H. Nawaz, R. Abbasi, M. Nafees, Z. ur Rehman, **I. Ahmad**, M.N. Arshad, A.M. Asiri, A. Waseem, *Journal of Molecular Structure*, 1225 (2021) 129058.
- [3] S.Z. Khan, Z. Khan, **I. Ahmad**, S. Khan, S. Khan, M. Ahmed, M. Inam, F. Bélanger-Gariépy, Z. ur Rehman, *Inorganic Chemistry Communications*, 123 (2021) 108316.
- [4] M.U. Rahman, H. Gul, Z.U. Rahman, S. Zulfiqar, R. Khan, B. Ullah, **I. Ahmad**, A. Saeed, K. Alamgir, M. Ullah, J.Fan, *Materials Today Communications*, (2021) 102882.
- [5] G. Shah, A. Ullah, M. Arshad, R. Khan, B. Ullah, **I. Ahmad**, *Journal of Materials Science: Materials in Electronics*, 31 (2020) 3557-3563.
- [6] S. Hassan, B. Ahmad, S.U. Khan, H. Linfang, S.I. Anjum, M.J. Ansari, K. Rahman, **I. Ahmad**, W.U. Khan, R. Qamar, *Saudi journal of biological sciences*, 26 (2019) 1602-1606.
- [7] S. Hassan, B. Ahmad, J. Shah, **I. Ahmad**, A. Rauf, E. Elsharkawy, Phytochemicals profile, antimicrobial and antioxidant properties of *Ziziphus nummularia* roots, *Journal of Medicinal and Spice Plants* (2019) 166.
- [8] A. Shah, A. Rauf, A. Ullah, A. Munir, R. Qureshi, **I. Ahmad**, M.T. Soomro, Z.-U. Rehman, *Journal of Electrochemical Science and Engineering*, 3 (2013) 19-27.
- [9] Biological Evaluation and Single Crystal Studies of Triorganotin(IV) Carboxylates (Submitted) *Applied organometallic chemistry*.
- [10] Comparative First-Principle and Experimental Study of Structural and Electronic

Properties of the organotin(IV) amide based carboxylates complexes (Ready for submission).

[11] Anticancer and Antileishmanial activities of Novel Synthesized Triorganotin(IV) Carboxylates Complexes. (Ready for submission).

## Appendices

Lockhart and coworkers have found a relationship between the magnitude of

$^2J(^{119}\text{Sn}, ^1\text{H})$  and Me-Sn-Me angle

$$\theta = 0.0161|^2J(^{119}\text{Sn}, ^1\text{H})|^2 - 1.32|^2J(^{119}\text{Sn}, ^1\text{H})| + 133.4 \quad (\text{In non-coordinating solvents})$$

$$\theta = 0.0105|^2J(^{119}\text{Sn}, ^1\text{H})|^2 - 0.799|^2J(^{119}\text{Sn}, ^1\text{H})| + 122.4 \quad (\text{In coordinating solvents})$$

By substituting value of  $\theta$  in the Lockhart's equation,  $^1J[^{119}\text{Sn}, ^{13}\text{C}]$  can be calculated for methyl derivatives

$$^1J[^{119}\text{Sn}, ^{13}\text{C}] = 11.4\theta - 875$$

For *n*-butyl- derivatives

Howard et al.,

$$^1J[^{119}\text{Sn}, ^{13}\text{C}] = [(9.99 \pm 0.73)\theta - [746 \pm 100]]$$

For phenyltin(IV)

Howard et al.,

$$^1J[^{119}\text{Sn}, ^{13}\text{C}] = [(15.56 \pm 0.84)\theta - [1160 \pm 101]]$$

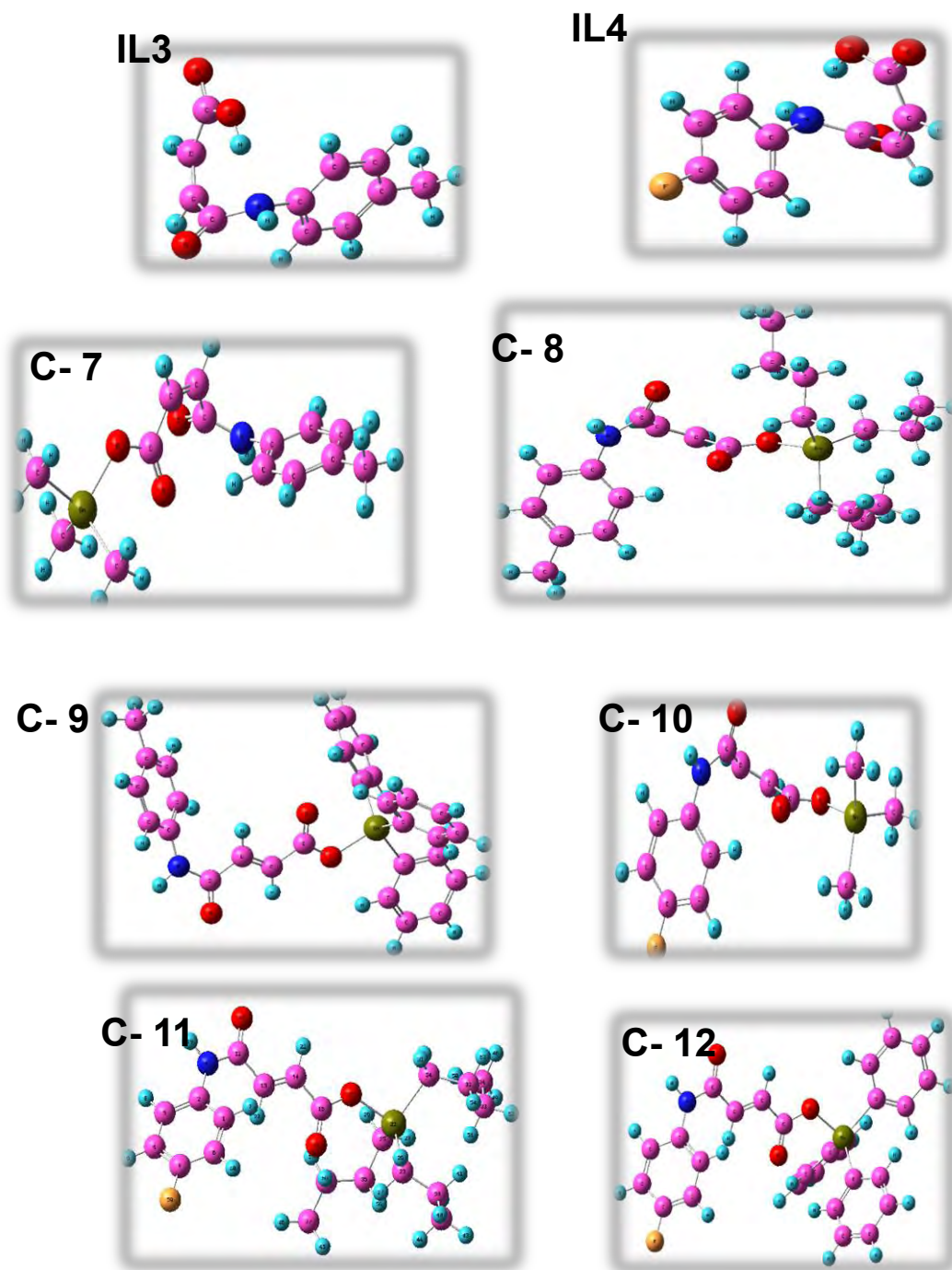


**Fig S1.** Optimized structural view of compounds HL1, C1, C2 and C3 obtained from DFT simulations in the Gaussian software package at the B3LYP/LANL2DZ level.

The global reactivity parameters of global hardness ( $\eta$ ), electronegativity ( $\chi$ ), chemical potential ( $\mu$ ), and softness  $\sigma$  were evaluated by using the following equations.

$$I = -E_{\text{HUMO}} \quad (1)$$

$$A = -E_{\text{LUMO}} \quad (2)$$

$$E_g = E_{\text{LUMO}} - E_{\text{HUMO}} \quad (3)$$

$$\eta = \frac{I-A}{2} = \frac{E_{\text{LUMO}} - E_{\text{HOMO}}}{2} \quad (4)$$

$$\chi = \frac{(I+A)}{2} = \frac{-(E_{\text{LUMO}} + E_{\text{HOMO}})}{2} \quad (5)$$

$$\mu = \frac{-(I+A)}{2} = \frac{(E_{\text{LUMO}} + E_{\text{HOMO}})}{2} \quad (6)$$

$$\sigma = \frac{1}{\eta} \quad (7)$$

